Simulation of cyclic variability in gasoline engine under cold start conditions

Suyabodha, Apiwat

Award date:
2012

Awarding institution:
University of Bath

Simulation of cyclic variability in gasoline engine under cold start conditions

Apiwat Suyabodha

A thesis submitted for the degree of Doctor of Philosophy

University of Bath

Department of Mechanical Engineering

March 2012

Abstract

Emissions from gasoline engines remain an important issue worldwide as they are both harmful to health and contribute to green house effects especially under cold start conditions. A major challenge of the automotive industry is to reduce harmful emissions as much as possible whilst continuing to reduce CO_2 emissions.

Three-way-catalytic converters have been used very successfully to convert the harmful gases before release to the environment but these devices have to reach their light-off temperature in order to activate the chemical reactions. Therefore, the conversion time is delayed and during the pre light-off period, high levels of emissions are released. An investigation into methods capable of increasing catalyst temperature under cold start conditions has been carried out. The most beneficial technique used in this research was the secondary air method. The method introduced extra air into the exhaust manifold which allowed the engine to run rich and then the residual unburned fuel to be oxidised in the exhaust before approaching the converter. An experiment following a *Box-Behnken* design was used to study the effect of engine speed, spark angle, load, relative air/fuel ratio (lambda) and secondary air flow on pre-catalyst temperature. The study suggested the best result for the engine studied was to achieve fast catalytic light-off time was to run engine at 1225 rpm, spark angle of 0 degree BTDC, lambda of 0.82 and load of 0.5 bar BMEP. These settings allowed the remaining fuel to be burned with 5.87 kg/hr of secondary air in the exhaust manifold to achieve a pre-catalytic temperature of 631.1^{o}C and achieve light-off for all emissions within 17.2 seconds. The results were also used to build a temperature prediction model using the Matlab MBC toolbox and the best available model gave an R^2 of 0.9997 by using radial base functions (RBF). However, the optimum conditions still produced cyclic variation in the combustion, giving an average COV_{imep} of 14.8% during the pre-catalytic heating period which caused problems concerning engine smoothness.

To derive a greater insight into the mechanisms governing the cyclic variability observed a simulation study was undertaken. The study used a simulation using Ricardo WAVE and Matlab Simulink to allow a detailed representation of some of the principle mechanisms giving rise to cyclic variability under cold start conditions. The study included combustion under rich and lean mixtures and considered the effect of variations of air/fuel ratios and residual gas fraction. As a result, the simulation showed a similar characteristic variability of heat release to that observed experimentally. The validation of the model for heat release showed that the predictions were under estimated by 0.49 % while under lean combustion, there was an under estimation of 2.07%. Both predictions had normally distributed residuals. The model suggested that the residual gas fractions were higher than the limit of 8.8% (under rich fuelling) or 8.0% (under lean fuelling) that was predicted to cause ignition delay to increase significantly and therefore contribute to high cyclic variability.

An optimisation was carried out by varying camshaft angle in the simulation. The results suggest that retarding the exhaust camshaft position by 4 degrees (EVC 12 degrees BTDC) could reduce COV_{imep} by 63.2% under rich combustion. In contrast, advancing the intake camshaft position suggested that the COV_{imep} can be reduced but more experimental data is required to validate the results because variation of intake camshaft positions had a larger impact on pumping work than varying exhaust camshaft positions. These additional pumping losses result in higher air and fuel flow requirements.

In summary, this thesis describes a detailed investigation into the effects of engine calibration on catalyst heating performance. One of the limiting factors in achieving rapid light-off is combustion variability. Extensions have been introduced to an industry standard 1D engine simulation to allow realistic cyclic variability to represented and developed. These tools could allow cyclic variability to be considered more rigorously during a calibration exercise.

Contents

Chapter 5

Engine Simulation

List of figures

Chapter 2

Literature Reviews

Chapter 3

Test Facilities and Design of Experimental

Chapter 4

Experimental Results

Chapter 5

Engines Simulation

Chapter 6

Analysis data for simulation

Chapter 7

Result from Simulation

Chapter 8

Model optimisation by using simulation

List of tables

Chapter 4

Experimental Results

Chapter 5

Engines Simulation

Chapter 6

Analysis data for simulation

List of abbreviations

A_{eff}	=	effective area [m^2]
ABDC	=	after bottom dead centre
ATDC	=	after top dead centre
BBDC	=	before bottom dear centre
BDUR	=	user-entered 10-90% burn duration in crank degrees
BTDC	=	before top dead centre
^oC	=	degree Celsius
C_D	=	discharge co-efficient
C_F	=	valve flow co-efficient forward flow
CO	=	carbon monoxide
COV	=	coefficient of variation [%]
C_R	=	valve flow co-efficient backward flow
D_i , D_e	=	inner seat diameters of the intake and exhaust valve [mm]
D_v	=	valve inner seat diameter [mm]
ECU	=	electronic control unit
EGR	=	exhaust gas recirculation
EVC	=	exhaust valve close
FID	=	flame ionisation detector
GDI	=	gasoline direct injection
GFR	=	gas/fuel ratio [%]
GMEP	=	gross mean effective pressure [bar]
HC	=	hydrocarbon
HR	=	heat release
IC	=	internal combustion
IMEP or imep	=	indicated mean effective pressure [bar]
IVO	=	intake valve open
L_i , L_e	=	lift of intake and exhaust valve [m]
$L_{v,\max}$	=	maximum valve lift [m]
m_a	=	trapped mass of air [kg]
m_b	=	mass of burned gas in mixture during compression [kg]
m_f	=	trapped mass of fuel [kg]

m_r	=	residual gas mass [kg]
N	=	engine speed [rpm]
NEDC	=	New European Drive Cycle
NO_x	=	oxides of nitrogen
P	=	pressure [bar]
p_i , p_e	=	absolute pressure of intake and exhaust gas respectively [bar]
PFI	=	port fuel injection
PM	=	particulate matter
r_c	=	compression ratio [-]
Re	=	Reynolds number [-]
RMSE	=	root mean square error
SA	=	secondary air
Sh	=	Sherwood number [-]
SI	=	spark ignition
SMD	=	sauter mean diameter
TDC	=	top dead centre
u_f , u_g	=	velocities of gas flow and liquid fuel droplet [m/s]
U_{inj}	=	fuel injected speed [m/s]
V	=	volume [m^3]
V_d	=	displacement volume of the engine [m^3]
V_s	=	swept volume [m^3]
W	=	cumulative mass fraction burned
We	=	Weber number [-]
WEXP	=	user-entered Wiebe exponent
σ	=	standard deviation [-]
ϕ	=	equivalence ratio [-]
$\Delta\theta$	=	valve overlap angle [Crank angle]
ϕ_u	=	Equivalence ratio where combustion efficiency is 90% [-]
ϕ_l	=	Equivalence ratio where combustion efficiency is 10% [-]
ϕ_m	=	critical equivalence ratio = $(\phi_l + \phi_u)/2$
γ	=	ratio of specific heats [-]
θ	=	crank angle
ρ_f , ρ_g	=	fuel and gas density [kg/ m^3]
μ_f , μ_g	=	dynamic viscosity of fuel and gas respectively [Pa.s]

Acknowledgements

I firstly thank Rangsit University for supporting me with the scholarship during this research. I also thank my supervisor, Dr. Chris Brace, who gave me the directions and all the support throughout this work. A big thank you to Dr. Chris Bannister for his help on the cold start testing, which gave me opportunity to really enjoy and be excited under extreme test conditions.

I would like to thank Dr. Sam Akehurst, Allan Cox, Andy Lewis, Sam Hurley and Vijay Rajput for their support on the test facility and instrumentation.

I would also like to thank my colleagues at PVRC for all their advice and support throughout my research: Peter Dowell, Joe Moyers, Richard Burke, Mitch Piddock, Adrian Hunt, Adam Rose, Hasan Ali, Kai Zhang, Shifei Ye, Tomasz Duda, Huayin Tang and Nic Zhang. In particular, Roger Tily, who carefully read and corrected this thesis, thank you so much.

Finally, I give a billion thanks for my family who have always been beside me during my time studying in Bath. Especially I thank my lovely wife who not only looked after our family but also took good care of my daughter.

Thank you very much indeed.

Chapter 1

Introduction

1.1 Introduction

The internal combustion (IC) engine is a device for converting energy from fuel into mechanical work. The most common form of the IC engine, for automotive use, uses the four stroke cycle. This arrangement divides the working cycle into four strokes (a stroke is the travel of the piston from one end of the bore to the other): the induction, compression, expansion and exhaust strokes. Modern engines are designed to achieve not only high levels of fuel efficiency and low emissions but also exceptional reliability and smoothness. The term *emissions*, in regards to IC engines, has come to be associated with two different aspects of engine exhaust products. Firstly, the collection of harmful products of incomplete combustion that have adverse local or regional heath affects. These include oxides of nitrogen (NO_x), particulate matter (PM), carbon monoxide (CO) and unburned hydrocarbons (HC). Legislation has been introduced across the world since the 1970s (Stone, 1999) to control these harmful emissions and they are now reduced to very low levels. Secondly, the term *emissions* is used to describe the CO_2 output of engines while they operate burning hydrocarbon fuels in air to create CO_2 and H_2O while releasing heat. The CO_2 output is of concern as it has been shown to be a major contributory factor to the greenhouse effect, a global issue that will become increasingly important as time progresses. Legislation and taxation regimes have been introduced to encourage lower CO_2 production and further limitations are planned (ref. EU CO_2 levy). This is much more problematic for engine designers since an efficient engine produces CO_2 roughly in proportion to its power output, and there is no easy way to remove it from the exhaust gasses in the way that has been achieved with other harmful emissions.

Therefore, the most pressing challenge for automotive engineers today is to reduce CO_2 emissions while still complying with the very tight limits on harmful emissions, imposed by regulatory authorities, and without sacrificing reliability or smoothness. In normal operation, emissions from spark ignition (SI) engines are controlled by using a three way catalytic converter, which in turn requires that the engine is operated under stoichiometric conditions. There are, however, some conditions where lean operation can be tolerated (for example, during idle speed and cruising on motorway) and some occasions when rich operation is necessary, typically at wide open throttle in order to reduce component temperatures.

Plans for ever tighter regulation of emissions (Table 1-1) will force engines to operate with low emissions to achieve Euro 6 in 2014. Cold start conditions play an important role in emissions production even though the catalytic converter has been introduced. The reason is that the emissions are reduced by the catalytic converter only when its catalyst has reached its light-off temperature. In the short time before full catalyst operation is achieved a sufficient quantity of emissions can be produced to cause the vehicle to fail the type approval test. Thus, a range of techniques to encourage rapid heating of the catalytic converter have been investigated.

For SI engines, air and fuel are mixed before combustion occurs. Commonly this is implemented to give a homogeneous mixture, and ideally the quantity of heat released when this mixture burns would be constant from one cycle to the next. In a conventional SI engine, this will be an ideal situation and will never occur because there are many phenomena which vary from one cycle to the next and which affect the mechanism of combustion. This effect of combustion changes from one cycle to the next is called “cyclic variability”.

Cyclic variability in gasoline engines has been studied for many decades. Most of this research has concentrated on the understanding of the mechanism of combustion, especially under extremely lean conditions, in order to improve fuel consumption.

Table 1-1: Emission limits for cars sold in Europe (Miller J.M., 2010). All figures are for vehicles tested using the New European Drive Cycle (NEDC).

Regulation	Euro 3 (Jan 2000) (g/km)		Euro 4 (Jan 2005) (g/km)		Euro 5 (Jan 2009) (g/km)		Euro 6 (Jan 2014) (g/km)	
	Diesel	Gasoline	Diesel	Gasoline	Diesel	Gasoline	Diesel	Gasoline
CO	0.64	2.30	0.50	1.00	0.50	1.00	0.50	1.00
HC	-	0.20	-	0.10	-	0.10	-	0.10
HC + NO_x	0.56	-	0.3	-	0.23	-	0.17	-
NO_x	0.50	0.15	0.25	0.08	0.18	0.06	0.08	0.06
PM	0.05	-	0.025	-	0.005	0.005	0.005	0.005

The work described in this thesis seeks to investigate a range of operating conditions that can improve catalyst light-off time by using a range of measures, including the secondary air injection technique. Cyclic variability is also taken into account to ensure smoothness of the engine during the catalyst heating period. To derive a greater insight into the mechanisms governing the cyclic variability observed, a simulation study was undertaken. The study used combination of Ricardo Wave and Matlab Simulink software to provide a detailed representation of some of the principal mechanisms giving rise to cyclic variability under cold start conditions. The study also investigates combustion under rich and lean fuel mixtures, since these offer alternative strategies to manage catalyst heating. Finally, opportunities for reducing cyclic variability and areas for future research are introduced.

1.2 Objectives

The main aim of this research is to investigate the cyclic variability of gasoline engines and in particular its role in constraining the cold start optimisation of the engine and catalyst system. The main tools used in the study are an experimental engine test facility and a commercial engine simulation software package extended in a co-simulation environment.

In order to achieve the main aim there are a number of objectives, which include;

- A review of previous research in the field, including:
  - Previous research into cold start optimisation.
  - The causes and effects of cyclic variability in gasoline engines.
  - Understanding the effect and the mechanisms associated with the variations in the air/fuel ratio in gasoline engines.
  - Understanding the effect and mechanism of variations in the proportion of residual gases in the combustion chamber.
- To carry out an experimental design to determine the influence of key calibration factors on the cold start performance of a port fuel injected SI engine and subsequently to:
  - Determine the effect on catalyst light-off time of different engine operating conditions.
  - Develop a method for the analysis of raw data (i.e. pressure pegging (measurement equipment calibration), smoothing data, determination of top dead centre and gamma (heat capacity ratio) selection).
- The construction of an engine model using Ricardo Wave engine simulation software in combination with Matlab Simulink.
- Describe some of the key mechanisms causing variation in SI engines by using the Wave and Simulink modelling environments.
- To calibrate the engine model to a level where it is capable of representing cyclic variability in a similar manner to a real engine.
- To use the simulation to attempt a calibration task with represented to cyclic variability.

1.3 Structure of the thesis

In the remainder of the thesis, the chapters are organised as follows:

Chapter 2 presents a review of literature in the field of gasoline engine operation under cold start conditions and highlights the emissions problem. This leads on to a review of the use of catalytic converters on passenger vehicles and the challenge of ensuring rapid

light-off. Regarding the main target of this thesis, namely a focus on the area of cyclic variability in gasoline engines, a review of cyclic variability including causes and effects is presented. Later in the thesis an engine simulation software package is used in order to study cyclic variation. Accordingly, the review also includes previous work on engine simulation in order to understand the strengths and limitations of the tools. In the past, investigations into cyclic variability in engines have been focused primarily on lean conditions in order to improve fuel consumption. This thesis will use the review to gain an insight into cyclic variability during cold start conditions that encompass both rich and lean mixtures.

Chapter 3 describes the engine test facilities used for the research and develops an experimental design for cold start conditions. The engine setup and test procedures are also described in this chapter.

Chapter 4 presents the results from the experimental programme and their effect on catalyst light-off time at each test point. A subset of the test points have been selected to show the effect of engine speed, spark angle, load, lambda (air/fuel ratio) and secondary air flow. Finally, the best test configuration for early catalytic converter light-off time is selected for further analysis of the cyclic variation using the engine simulation.

In Chapter 5, an engine model is created using the Ricardo Wave software, using the basic engine design data as a starting point. In order to allow an investigation into cyclic variability effects seen in the experimental work, Matlab Simulink has been used in a co-simulation environment which allows Ricardo Wave to produce varying combustion results cycle by cycle by representing the variation in key operating parameters. Information detailing the building of the engine model and its calibration and subsequent use in simulation are also presented in this chapter.

In Chapter 6, the experimental results of the test engine running under rich and lean fuelling conditions are selected and analysed for use within an engine model. The analysis includes a selection of simulation times and characteristic combustion profiles. The profiles of combustion are focused on ignition delay, combustion duration, and the efficiency of combustion, which is used to build a look-up table in the simulation environment.

In Chapter 7, the cyclic variability of the engine under cold start conditions is simulated. The results from the experimental work are analysed to yield data required for the simulation model inputs. The results include simulations of both rich and lean mixtures in order to explain the different mechanisms contributing to engine variations. The simulation results are then compared with the experimental data.

For Chapter 8, an optimisation method for reducing cyclic variability in the engine is introduced using the engine simulation model. The method is based on camshaft position. The exhaust camshaft position is shifted to advanced and retarded positions while the intake camshaft position is kept constant. Also, experiments where the intake camshaft position is varied are discussed and results given and compared.

In Chapter 9, conclusions from the research are presented and areas requiring further work to improve the experimental work and engine model are detailed.

Chapter 2

Literature Review

The purpose of the literature reviews in this chapter is to gain an understanding of existing research within the areas associated with this thesis. The reviews are mainly focused on three topics:

- Engine cold start conditions.
- Cyclic variability.
- Engine simulation.

2.1 Cold start in gasoline engines

The review in this section will discuss engine cold start conditions and emission problems. The two major topics are explained, they are:

- Engine cold start conditions.
- The catalytic converter.

2.1.1 Cold start condition

The cold start condition is defined as the engine operational period before the coolant temperature of the engine reaches about 80 ^{o}C (Lee et al., 2002). When the engine is started from cold there are two states to be considered. In the first state, the system has to compensate for the fuel that could not easily evaporate for mixture preparation. This state is called the after start condition. In order to ensure the starting state, a rich mixture is always used, thus unburned fuel is emitted to the exhaust manifold in the form of unburned hydrocarbons (HC). Cheng et al. (2001) stated that 60% to 80% of unburned HC emissions are presented during cold start. Jeong et al. (1998) claimed

that those HC emissions are present during the first 100 to 150 seconds following engine start. The second state is where the engine is operated under warm-up conditions and the lambda sensor (i.e. the oxygen sensor) is inactive. In order to operate the engine during these periods, the control strategies are run in an open-loop mode and use look-up tables to control the air/fuel ratio (Lee et al. 2002). Therefore, carbon monoxide (CO) and oxides of nitrogen (NO_x) are presented during this period.

2.1.2 Catalytic converter light-off strategies

A common device for converting the emissions before release in to the atmosphere is a catalytic converter. Catalytic converters have been used in the automotive industrial for many years. The converters are mainly used to reduce unburnt HC, CO and NO_x so they are called three-way catalytic converters.

The converters consist of a stainless steel container which is mounted on the exhaust pipe of the engine. Inside the container, there is a ceramic honeycomb structure that allows gas flow. The most common materials for catalytic converters are: platinum, palladium and rhodium (Pulkrabek, 1997). Platinum and palladium are used to convert unburnt HC and CO where rhodium is used to convert NO_x. The catalytic converters are ineffective until their temperature has risen above 250 to 300^{o}C (Heywood, 1988). The time at which 50% of emissions are being converted is called the light-off time. Stone (1999) also observed that the catalytic converter can be damaged by operating at too high a temperature over a period of time or contaminated by HC emissions from a series of misfire cycles.

Although catalytic converters have been introduced to reduce unwanted emissions, the converters still take time to activate. In addition, the new emission regulations require a further decrease in harmful emissions. Therefore, the automotive industry has to find solutions to meet those requirements. There are many techniques for increasing the catalytic converter's temperature to achieve light-off time as soon as possible (Borland et al., 2002). Each technique has its advantages and disadvantages depending on the operating conditions. In this current research, a second air injection technique has been used and the relevant techniques for heating the converter are discussed.

1) Location of catalytic converters

One method for heating a catalytic converter is to install the converter near the exhaust port. The exhaust temperature of a SI engine, during idle speed, can vary between 200 to 500 ^{o}C, and can increase up to 900 ^{o}C during high power output conditions (Heywood, 1988). Because of the limit on the temperature of the converter, as mentioned above, most SI engines have to locate the converter away from the exhaust port. On a diesel engine, the catalytic converter can be located near the exhaust port because the exhaust gas temperatures of diesel engines are generally lower. When the converter is located far from the exhaust port, the gas temperature is released to the ambient air during transportation before reaching the converter. Thus, this technique may take time to heat the converter so it is not practical in SI engines.

2) Retard spark angle

Regards the above method, the procedure of retarding the spark angle is introduced to raise the temperature at the exhaust port. This technique makes the catalytic converter activate faster than it would with an advanced spark angle which is used to produce high torque output. Retarding the spark angle causes the engine to consume more fuel to achieve the same output. Russ et al. (1999) argued that fuel consumption was a small problem compared with the variation in in-cylinder pressure that could lead to engine roughness. Cheng et al. (2001) concluded that retarded spark timing resulted in incomplete combustion and an increase in HC emissions in the exhaust pipe, especially during cold start conditions which need a rich fuel mixture. These situations can lead to a failure of the catalytic converter to meet the requirements of HC emissions. The retarded spark method incurs no extra cost and only requires a change in the engine management system to provide a retarded spark angle during the catalytic converter's warm up period.

3) Electric heating

This method uses resistance heating to pre-heat the converter before starting the engine. The typical values of electrical energy for this system are 24 volts and 500 to 700 amperes (Pulkrabek, 1997). The advantage of this technique is to reduce power

consumption to the 2 to 3 kW level (Sendilvelan et al., 2001). The problem with this system is that the electrical power requirement may exceed that which can be provided by the battery. Increasing the size of battery or alternator is a solution but it is not practical in commercial vehicles because the weight and load could lead to a rise in fuel consumption. A further problem is that a battery in a vehicle that is used for short trips, so that the battery has less time to charge, will run flat quickly with this technique. Sendilvelan et al. (2001) also claimed that to provide 2 to 3 kW from 12-volt battery requires large wire diameters and has an impact on battery life.

4) Secondary air injection

Regarding the previous methods that have been discussed, the benefits from each of the techniques are different depending on how the systems are used. Considering the problem of the cold start condition, where an engine's HC emission could degrade the catalytic converter, a new technique has been used to make use of the unburnt HC and introduce secondary air into the exhaust manifold. The idea of this method is to allow unburnt HC emissions to burn with extra air and generate heat. Borland et al. (2002) concluded that the system could improve catalytic light-off performance but that there were some parameters that had to be considered. Firstly, mixing of the gases in the exhaust pipe is the key to optimising the secondary air flow. Secondly, a retarded spark angle may be required to initialise the reaction. In this thesis, the variation in the combustion is also taken into account to ensure engine smoothness during cold start conditions.

2.2 Cyclic variability

Cyclic variability in SI engines has been studied for many years. Cyclic variability is defined as the unintended variations of one combustion event to the next while all engine controls remain constant. The main undesirable effect of these variations is the fluctuation in engine work output, especially at extreme operating conditions. Soltau (1960) explained the cyclic variability in SI engines by plotting the P-V diagram of an engine operating under lean and rich fueling conditions as can be seen in Figure 2-1.

Under lean fuelling conditions, the variations of peak pressure were present more than with the engine running under rich fuelling conditions.

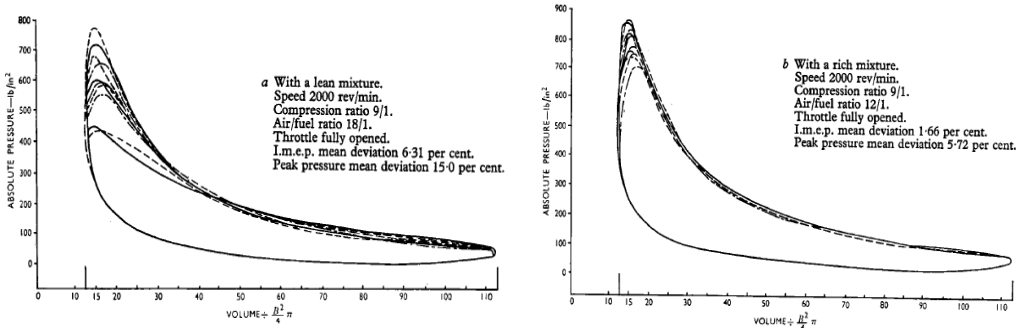

a) Lean mixture *b) Rich mixture*

Figure 2-1: P-V diagrams of rich and lean mixtures over 10 consecutive cycles (Soltau, 1960)

Heywood (1988) explained the cyclic variability in term of COV_{imep} by *Equation 2-1* below.

$$COV_{imep} = \frac{\sigma_{imep}}{imep} \times 100 \quad \text{.....Equation 2-1}$$

Heywood (1988) stated that problems in vehicle drivability are observable when COV_{imep} is higher than 10%. Thus, researchers have concentrated on studying the mechanisms behind those variations under lean mixture fuelling conditions, because power output would be improved by approximately 10% if cyclic variations could be substantially reduced (Soltau, 1960).

Recently, phase lag plots (sometimes called return maps) were introduced as a technique to illustrate cyclic variability in an engine and help explain its behaviour. The plot is used to illustrate a relationship between a current event and the next event.

Scholl et al. (1999) applied return maps to GMEP data from their test results (Figure 2-2). Under stoichiometric fuelling (Figure 2-2a), the GMEP values are located within a small area, which means that every combustion event resulted in a similar GMEP output.

When the mixture became leaner, the GMEP values started to spread and form an angular or boomerang shape. A chaotic cyclic behaviour was indicated by the GMEP data when the mixture was extremely lean (Figure 2-2d). These results suggest that there is an operational limit connected with lean fuelling after which combustion cycles display cyclic variability which appears to be random in nature.

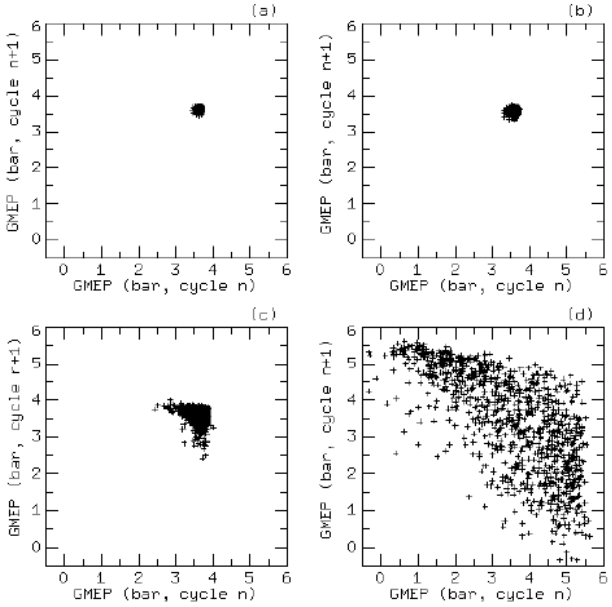

a) air/fuel ratio = 14.6:1
b) air/fuel ratio = 20.0:1
c) air/fuel ratio = 22.0:1
d) air/fuel ratio = 25.0:1

Figure 2-2: Phase lag plot for GMEP (Scholl et al., 1999)

Tily et al. (2008) applied phase lag plots to heat release data obtained from a V8 GDI engine (Figure 2-3). The plots started to spread and form an angular shape like those described by Scholl et al. (1999) when the fuel mixture became increasingly lean. Tily et al. (2008) explained that the combustion events appear to be a combination of strong-weak or weak-strong combustion events. In additional, the result for each cylinder, of the multi-cylindered engine, shows a different data distribution which suggests a variation in the combustion characteristics for each cylinder was present.

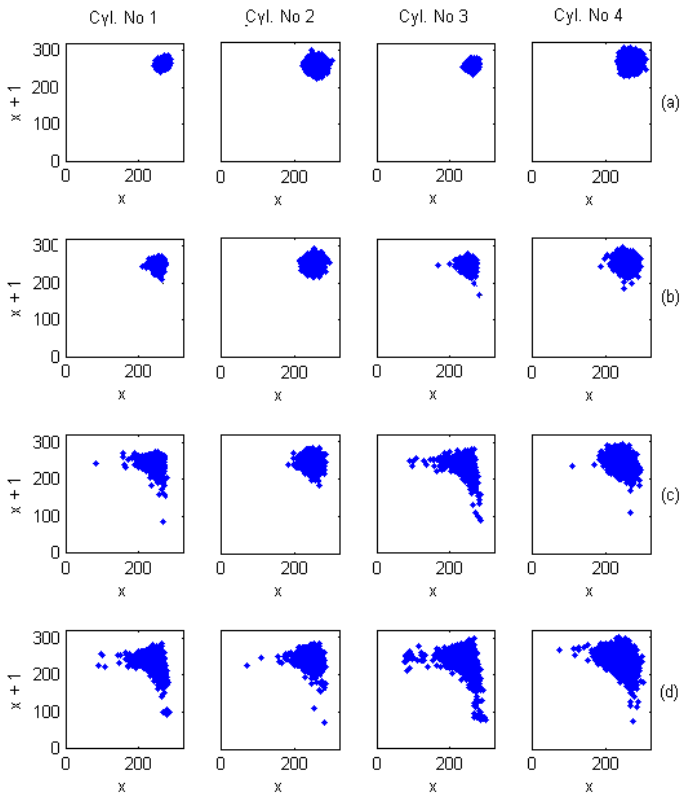

a) air/fuel ratio = 14.50:1
b) air/fuel ratio = 18.05:1
c) air/fuel ratio = 19.84:1
d) air/fuel ratio = 20.47:1

Figure 2-3: Phase lag plot for heat release (Tily et al., 2008)

In the past, researchers have studied engines running under lean mixture fuelling in order to improve fuel consumption while maintaining smooth operation. Phase lag plots of different sets of engine parameter data have been used to help explain the mechanisms behind cyclic variability. IMEP data can provide a measure of engine smoothness whereas heat release data can indicate energy consumption.

This section reviews work in the field of cyclic variability in spark ignition engines. The causes and the effects observed during experimental and simulation work are used to explain the phenomenon of cyclic variation. Moreover, the opportunities for improving cyclic variability and future research are explained.

2.2.1 Causes of variation

Dai et al. (2000) classified the causes of cyclic variations into two major groups.

- Prior-cycle effects
- Same-cycle effects

The prior-cycle effects are mainly a result of a variation in residual gas in the combustion chamber, whereas the same-cycle effects are a result of variations in air/fuel mixtures in the cylinder. The mechanisms of these effects are discussed below.

2.2.1.1 Prior-cycle effects

Prior-cycle effects consist primarily of the effect of residual gas in the combustion chamber, which causes different rates of burning and may even cause engine misfire. In spark ignition engines, the residual gases consist of exhaust gases that have not been expelled during the exhaust stroke and gases that are returned to the chamber by internal exhaust gases recirculation. These gases are mainly N_2, CO_2, H_2O and either O_2 when the mixture is lean or CO and H_2 when the mixture is rich (Heywood, 1988).

Schwarz et al. (2003) have studied the flow in gasoline engines as can be seen in Figure 2-4.

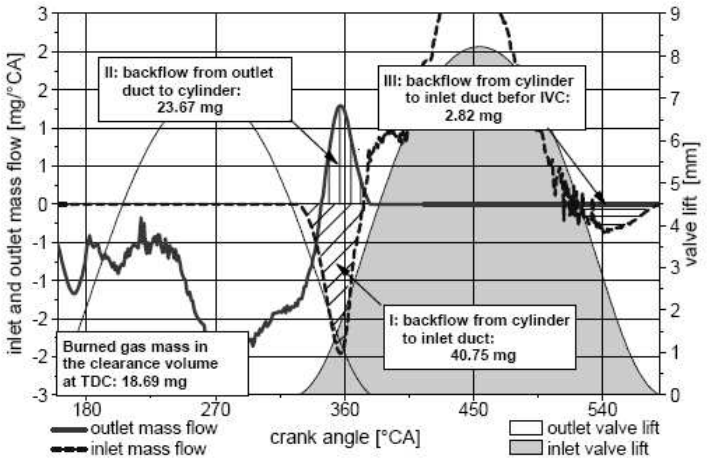

Figure 2-4: Inlet and outlet mass flow phenomena on a BMW/Rotax 650 engine (Schwarz et al., 2003)

The flows of burned gases were classified into four parts:

1) Backflow of burned gases from the cylinder that enter the inlet manifold during the valve overlap period and mix with the fresh mixture during the next cycle.

2) Backflow of exhaust gases from exhaust manifold into the cylinder during valve overlap.

3) Backflow of the in-cylinder charge that contains fresh air, fuel and residual gases into the intake manifold ready to mix during the next cycle.

4) Partially burned gases remaining in the clearance volume during valve overlap.

Leroy et al. (2008) suggested that the mechanism above is associated with valve timing and engine condition. Their research was focused on the gas flow rates through the intake and exhaust valves using different valve timing and engine configurations. The results proved that the levels of residual gases were greater during large valve overlap operation than they were during small value overlap operation.

According to the mass flow analysis above, the mechanism shows that the remains of burnt gas in cylinder can vary depending on the flow rate which in turn is affected by the engine's characteristics. In addition, the mass flow analysis showed a limitation on valve overlap time. Figure 2-5 shows the mass flow during long valve overlap that made a small pressure difference across the intake and exhaust valves. Thus, the undefined flow situation is presented. In this case, it is very difficult to identify the different residual gas sources (Schwarz et al., 2003).

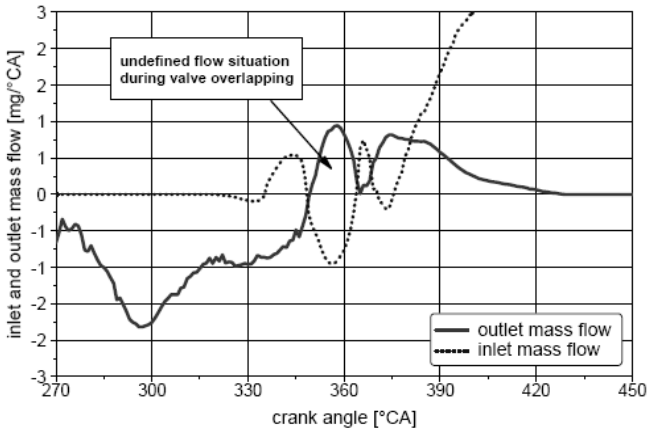

Figure 2-5: Inlet and outlet mass flow rate during long valve overlapping (Schwarz et al., 2003)

Mass flow analysis indicates that the majority of residual gases are the gases that remain in the clearance volume which depends on valve profile, flow coefficients and speed of the engine. In addition, the gases exchanged during valve overlap are caused by the gas dynamics in the port (Schwarz et al., 2003). The pressure oscillations during valve overlap period can lead to variations in the fresh charge and exhaust gas backflow. These mechanisms lead to variations in residual gas in the combustion chamber that can affect the next combustion event.

When turbocharged engines are taken into account, the mechanism, as discussed above, is changed. Under turbocharged conditions, the inlet manifold pressure is normally higher than the exhaust manifold pressure, so the flow of gases are forced to move forward, resulting in no backflow in the system (Leroy et al., 2008). Thus, the residual gases are only those in-cylinder gases that remain, which are relatively low.

The mechanism of residual gas, as seen from the review, show that there are many factors involving the amount of residual gases. Those factors include pressure difference across the valves, valve characteristic, pressure, engine speed and the gas dynamics during valve overlap (Winterbone et al., 2000). Another factor is in the quantity of burned gas from combustion which is caused by variations in mixture preparation for each combustion cycle.

1) Measurement technique

The residual gas in the cylinder contains many species of gas but the availability of measurement devices for individual species limits the choices to CO_2 and HC for such a technique (Prucka et al., 2008). Table 2-1 and Table 2-2 show an advantage and disadvantage of the species selection and experimental method on residual gas.

Prucka et al. (2008) studied details of residual gas based on the measured HC and CO_2 concentrations in the cylinder of a 2.4L I-4 engine. The engine's spark plug was located centrally and the combustion chamber was of a pent-roof type. The researchers used fast response equipment to measure the concentration of the sample gases. The sensors were installed in the cylinder and used to measure HC and CO_2. Another sensor was installed

in the exhaust system to measure CO_2. The data from the experiment were calculated by using the wet molar fraction equations.

Table 2-1: Residual gas fraction tracer species selection criteria (Prucka et al., 2008)

Tracer Species	CO_2	CO	HC	NO	H_2O
Primary Origin	Exhaust	Exhaust	Intake Mixture	Exhaust	Exhaust
Secondary Origin	Ambient (0.04%)	Ambient(Very Low)	Residual Gas (Higher than Exhaust levels)	Ambient (Very Low)	Ambient (Humidity)
Physical State	Gaseous	Gaseous	Liquid/Gaseous	Gaseous	Liquid/Gaseous
Level of Mixing (Pre-Combustion)	Nearly Homogenous	Nearly Homogenous	Stratified	Nearly Homogenous	Unknown
Relative Concentration (Pre-Combustion)	High (1-4%)	Medium (<1%)	High (2-5%)	Low (<500 ppm)	High (1-4%)
Measurement Technique	NDIR inaccuracy with pressure fluctuations	NDIR (inaccuracy with pressure fluctuations)	FID (inaccuracy with pressure fluctuations)	CLD	Optical
Other Considerations			Air-to-fuel ratio fluctuations from cycle-to-cycle induce RGF calculation error	Concentration drops significantly at high residual gas levels	

Table 2-2: Residual gas fraction experimental method selection criteria (Prucka et al., 2008)

Experimental Configuration for Pre-Combustion Gas Measurement	Fast response analyzer directly measuring in-cylinder gases	Fast response analyzer behind a fast sample valve measuring in-cylinder gases	Single Fast response analyzer mounted in the exhaust port	Standard analyzer or gas chromatograph used with a fast sample valve	Optical or Laser based technique
Measurement Type	Single Point	Single Point	Exhaust Port	Single Point	Spatial Resolution
Cycle-by-cycle Measurements	Yes (Up to ~1500rpm)	Yes (All Engine Speeds)	No (misfire required)	No	Yes (All Engine Speeds)
Engine Modification	Minimal (Sparkplug mounting)	Dependant on sample valve design	Minimal (Mount analyzer probe in the exhaust port)	Dependant on sample valve design	Varies by method
System Complexity	Low	Medium	Low	Medium	High
Additional Considerations	1. Response time limits make misfires necessary at high engine speeds. 2. Pressure fluctuations can reduce analyzer accuracy	1. Sample valve timing must be closely controlled. 2. Measurement pressure can be controlled, improving analyzer accuracy	1. A model is required to account for over-expansion backflows that can occur during the misfire cycle	1. Low sample flow rates can complicate use of standard analyzers. 2. Gas chromatograph analysis will occur off-line	1. Optical access can require severe engine modification. 2. Can provide very high accuracy. 3. Spatial measurement is highly desirable

For CO_2, the wet molar fraction in residual gas is assumed to be equal to the previous exhaust cycle, so the equation is

$$\chi_{RGF}^{Molar} = \frac{\chi_{CO_2}^{\Pr e-Comb}}{\chi_{CO_2}^{RGF}} \quad \text{.....Equation 2-2}$$

where; $\chi_{CO_2}^{\Pr e-Comb}$ = wet molar of CO_2 in pre-combustion

$\chi_{CO_2}^{RGF}$ = wet molar of CO_2 in residual gas

For HC, the *Equation 2-3* used to computed the wet molar fraction is

$$\chi_{RGF}^{In-CylinderHC} = 1 - \frac{\chi_{HC}^{Pre-Combustion}}{\chi_{HC}^{reference}} \quad \text{.....Equation 2-3}$$

where; $\chi_{HC}^{Pre-Combustion}$ = wet molar of HC in pre-combustion

$\chi_{HC}^{reference}$ = reference wet molar HC

The results show the variation in residual gas fraction and show that the HC based method gave more variation than the CO_2 based method, as shown in Figure 2-6. Prucka et al. (2008) pointed out that the HC concentration is more susceptible to variation because it depends on the air/fuel ratio and the residual gas but CO_2 concentration does not depend on the air/fuel ratio.

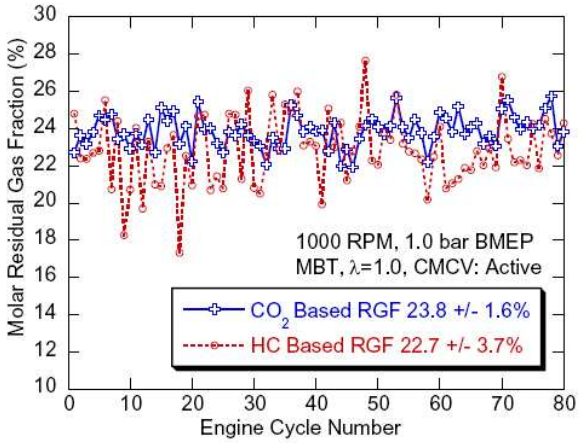

Figure 2-6: Measurement of residual gas fraction by the HC based method and the CO_2 based method (Prucka et al., 2008)

The quantities of HC and CO_2 present during the experiments were changed by varying the pressure in the intake and exhaust manifolds. Varying the camshaft timing lead to different valve overlaps and this caused the two species of gases to change.

Prucka et al. (2008) changed the pressure ratio between the intake and exhaust manifolds and calculated the residuals using the equation that they introduced. The results showed that increasing the exhaust pressure resulted in a low pressure ratio (Pint/Pexh) caused by residual gas increases due to a high magnitude of backflow. Figure 2-7 shows the measurements of in-cylinder CO_2 are related to this mechanism but that other measurements do not display a consistent trend.

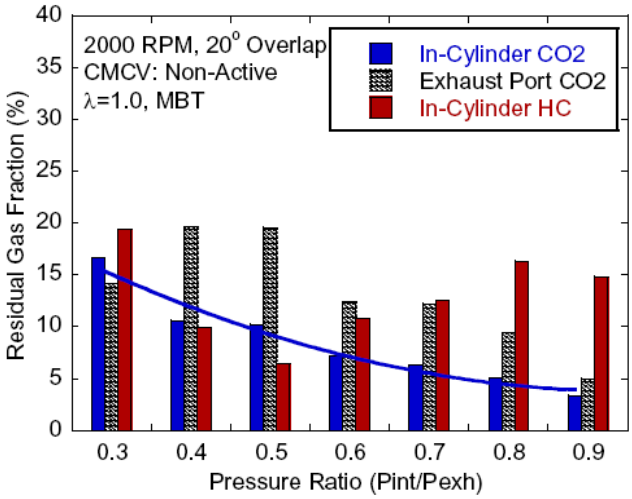

Figure 2-7: Residual gas fraction against pressure ratio (Prucka et al., 2008)

The next parameter was valve overlap, and the results show that positive overlap increases residual gas because the backflow duration was extended. The residual gas is increase when the valve overlap is set in negative mode because the exhaust valve closes early so that more burnt gas remains in the cylinder. The minimum residual gas occurs around zero valve overlap as can be seen in Figure 2-8. The measurements also show that the in-cylinder CO_2 method shows lower variability compared with others.

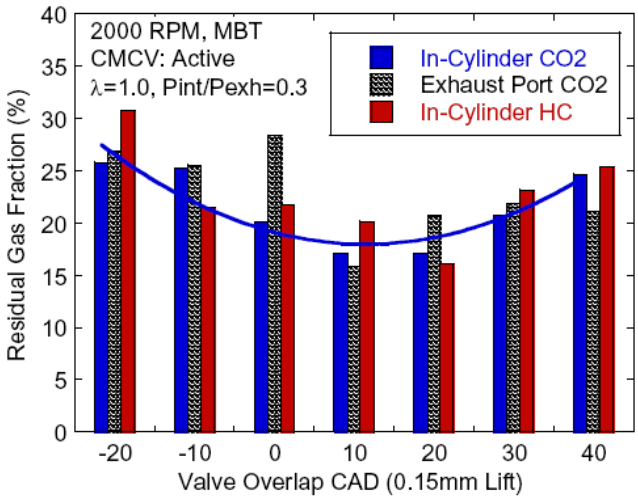

Figure 2-8: Residual gas fraction against valve overlap (Prucka et al., 2008)

The effect of residual gas is caused by changing the overlap centerline as shown in Figure 2-9. Prucka et al. (2008) stated that the overlap centerline's location influences

the residual gas by altering the phasing of the overlap with the piston movement. Thus, moving the centerline to the exhaust stroke decreases the fresh charge because the exhaust gases flow into the intake manifold during the valve overlap and piston motion. The fresh charge increase by the centerline is shifted into the intake stroke, but the residual gas also increase because piston motion during intake stroke pulls exhaust from exhaust port into the cylinder. The measurement of the in-cylinder CO_2 shows the least variability.

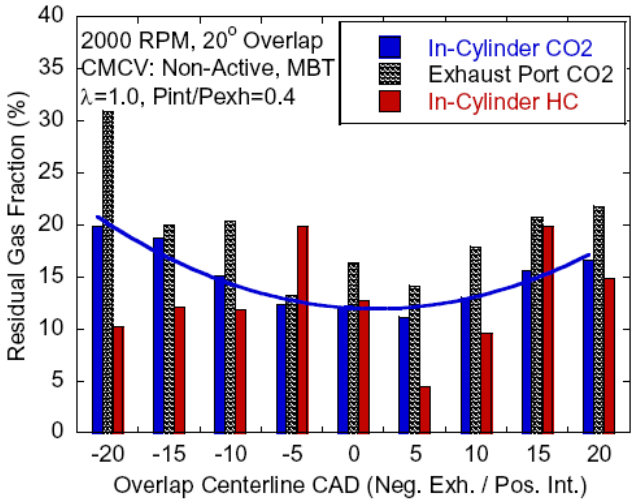

Figure 2-9: Residual gas fraction against overlap centreline (Prucka et al., 2008)

The results from the research above show that the concentration of in-cylinder CO_2 is the best indicator of the remaining residual gas in the combustion chamber. The measurement of CO_2 method needs special equipment that can provide a fast response.

2) Calculation of residual gas

For the mass flow mechanism, Fox et al. (1993) stated that the residual gas mass (m_r) is a combination between two components as the *Equation 2-4* below shows.

$$m_r = \int_{IVO}^{EVC} \dot{m}_e dt + m_{IVO} \quad \text{.....Equation 2-4}$$

The first term represents the backflow of burned gases from the exhaust port to the cylinder during the valve overlap period ($\int_{IVO}^{EVC} \dot{m}_e dt$). The second term represents the trapped gas in the cylinder before the intake valve is opened (m_{IVO}). Fox et al. (1993) developed the equation above, thus the residual gas fraction can be calculated by the *Equation 2-5* below.

$$x_r = 1.266 \frac{OF}{N} \left[\frac{p_i}{p_e} \right]^{-0.87} \sqrt{|p_e - p_i|} + 0.632\phi \frac{(p_i / p_e)^{-0.74}}{r_c} \quad \text{.....Equation 2-5}$$

p_e and p_i are absolute pressure in [bar], ϕ is the fuel equivalence ratio, N is the engine speed in [rpm], r_c is the compression ratio and the overlap factor (OF) is obtained by *Equation 2-6*;

$$OF = \frac{(D_i A_i + D_e A_e)}{V_d} \quad \text{.....Equation 2-6}$$

where D_i and D_e are the inner seat diameters of the intake and exhaust valve and V_d is the displacement volume of the engine. A_i and A_e can obtain by *Equation 2-7* and *Equation 2-8*;

$$A_i = \int_{IVO}^{IV=EV} L_i d\theta \quad \text{.....Equation 2-7}$$

$$A_e = \int_{IV=EV}^{EVC} L_e d\theta \quad \text{.....Equation 2-8}$$

In order to calculate the residual gas fraction using this equation, the lift values of the intake and exhaust valves (L_i , L_e) are required. Shayler et al. (2004) found that the lift profile is not known precisely so a new equation was formulated to estimate the OF and is shown below.

$$OF = \frac{1.45}{B} \left(107 + 7.8\Delta\theta + \Delta\theta^2\right) \frac{L_{v,\max} D_v}{B^2} \quad \text{.....Equation 2-9}$$

where $\Delta\theta$ is the valve overlap in crank angle degrees [°CA], B is the bore, $L_{v,\max}$ is the maximum valve lift and D_v is the valve inner seat diameter. $L_{v,\max}$ and D_v are the averaged values for the intake and the exhaust valves. The equation for the calculation of residual gas enables researchers to use existing sensors.

2.2.1.2 Same-cycle effects

The same-cycle effects are the variations in the flow of the air/fuel mixture, which, in turn, is partially based on the type of fuel injection system being used. For SI engines, there are port fuel injection (PFI) engines where the injectors are installed so that they inject fuel into the intake manifold, and direction injection engines where fuel is injected directly into the combustion chamber. Both these systems are commonly used in commercial vehicles. In each type of engine, the fuel and air has to ideally fully mixed before combustion occurs.

In spark ignition engines, the air/fuel mixture is changed by the way the gases flow through the intake system during transportation to the combustion chamber, especially in port fuel injection (PFI) engines. Thus, the mixture in the combustion chamber can vary from one cycle to the next and cause cyclic variability. Many researchers have investigated the air/fuel ratio in the spark ignition engines using both direct and indirect injection.

Batteh et al. (2003) studied the physics of the mixture preparation in PFI engines. The authors point out that there are four puddles of fuel located in the engines, which made the air and fuel mixture change from cycle to cycle. The puddles are located on the valves, downstream in the intake port near the valve, upstream near the injector, and on the cylinder wall, as shown in Figure 2-10. Batteh et al. (2005) extended the research to difference types of fuel, and found that the fuel properties had an influence on puddles because of the differences in evaporation.

Heywood (1988) explained that the fuel transportation process of PFI engines depends significantly on the timing and duration of the fuel injector pulse. For some systems, the fuel is injected onto the back of the intake valve when the valve is closed or partially open. Therefore, the vaporization of liquid fuel off the valve and wall occur by the

backflow of hot residual gas during part load. In some cases, although the engine is running under fully warm conditions, the fuel is drawn into the chamber as a liquid drop.

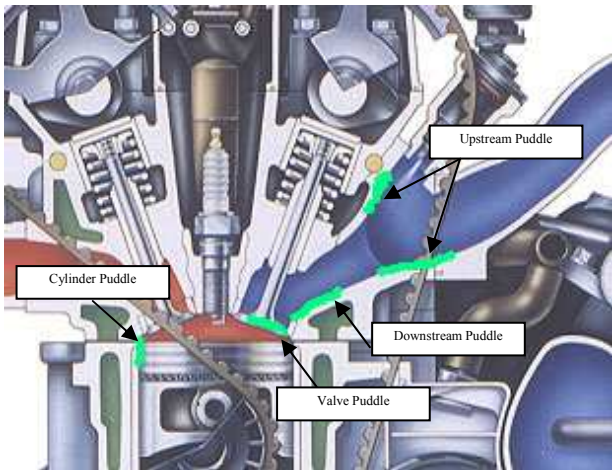

Figure 2-10: Location of fuel puddles in engines (Batteh et al., 2003)

The mechanism of fuel transportation along the manifold has been illustrated by Bai et al. (1995). The impingement regimes were classified in to seven categories which are:

(1) “Stick”
(2) “Spread”
(3) “Rebound”
(4) “Rebound with break-up”
(5) “Boiling-induced with break-up”
(6) “Break-up”
(7) “Splash”

These regimes are governed by a number of fuel and manifold wall parameters. The parameters from fuel include droplet velocity, size, temperature, angle when hitting the wall, and fuel properties. For the wall, the factors are temperature, surface roughness and remaining fuel droplets. These effects have a significant impact on variation in the air/fuel ratio before ignition. More details in these categories is given in Chapter 5.

Regarding the puddles in cylinder, these puddles can remain in the cylinder as an unburnt fuel. The puddles can also evaporate and flow out to the exhaust system. Therefore, some of hydrocarbon (HC) can return to the cylinder as a residual gas.

Heywood (1988) believed that there are four possible mechanisms that cause HC variation in the cylinder, they are:

1) Flame quenching at the combustion chamber walls, leaving a layer of unburnt air/fuel mixture adjacent to the wall.
2) The filling of crevice volumes with unburnt fuel mixture.
3) Absorption of fuel vapor into the oil layers on the cylinder wall during the intake and compression strokes, followed by fuel evaporation into the cylinder during expansion and exhaust stroke.
4) Incomplete combustion during the engine's operating cycles, which includes partial burning and misfire events.

In addition, the air that enters the engine's intake system may vary in temperature and also contain particles that are not useful for combustion. When the intake valves open, the air passes through the throttle valve and along the intake manifold to the combustion chamber and stops flowing when the intake valves close. Winterbone et al. (2000) explained that these factors can generate different pressures inside the intake manifold. Resonance can take place inside the inlet pipe which may vary for each combustion cycle.

Stone (1999) agreed with those physical mechanisms and concluded that the significant variations in pressure occur at low engine speeds. The density of the air is changed during its travel inside the inlet manifold because the temperature at the entrance is lower than at the inlet valve. Moreover, the geometry of the intake manifold and its diameter and length vary with different engines, and influence the variation of the air charge (Winterbone et al., 2000).

Maftouni et al. (2006) showed the effect of the intake manifold on the volumetric efficiency by using 3-D computational fluid dynamics (CFD) model. The results from Table 2-3 shows the volumetric efficiency in each cylinder is not equal over a range of constant engine speeds.

Table 2-3: Comparison of volumetric efficiency from individual cylinders (Maftouni et al., 2006)

	1st cyl.	2nd cyl.	3rd cyl.	4th cyl.	Engine
2500 rpm	88%	89.1%	89.2%	87.5%	88.45%
3500 rpm	83.87%	84.11%	84.12%	83.9%	84%
4500 rpm	81.5%	81.47%	81.52%	81.55%	81.42%
5500 rpm	77.6%	78%	78.1%	77.8%	77.8%

The physical phenomena above have a direct influence on the air/fuel mixture when the values of the air/fuel ratio are kept constant. The effect on variation in volumetric efficiency leads to different fuel injected and causes fluctuation in in-cylinder pressure. In 1996, Sung et al. claimed that an optimum length for an intake manifold exists at a given speed and that the different air charges between cylinders are very small. Those results prove that each cylinder could have different combustion characteristic, which agrees with the results from Tily et al. (2008).

Although the fuel injection is typically controlled by an electronic engine control unit (ECU) the fuel injectors can still cause a variation in mixture preparation. Bedford et al. (2006) studied the fuel injectors when they injected fuel. The research involved applying voltages across a sample of injectors to control injection duration. In order to measure the mass of fuel injected, a laser doppler anemometer (LDA) system was used to measure a centreline velocity and take it into account. The results shown a variation in the mass of fuel injected although the duration was controlled. This is another factor that makes the air/fuel ratio change before it is burnt.

2.2.1.3 Additional causes of cyclic variation

Although the causes from prior-cycle effects and same-cycle effects are always present in the combustion, Dai et al. (2000) concluded that there were other factors that influence the cyclic variations. These include:

- Turbulence intensity in the combustion chamber.
- Mean flow speed and direction at the spark plug.
- A/F ratio at spark plug and in the combustion chamber.
- Variation in residual gas at the spark plug and in the combustion chamber.

- Variations in the spark discharge characteristics (breakdown energy, timing, type of spark plug, and spark orientation).
- Charge mass variations (fuel plus air).
- Leakage through valves; crevice effects.

2.2.1.4 Discussion

The causes of cyclic variation, listed above, have a strong relationship with each other. According to the review, various residual gases and air/fuel ratios are the causes of cyclic variability. Regards the factor of the air/fuel ratio, there are many parameters influencing the variation, especially with a port fuel injection system. The most influential factor came from the losses of fuel during transportation. For the causes of residual gas, the variation came from the mass transfer during the cycle. These variations came during the opening and closing periods of the intake and exhaust valves. However, the qualities of residual gases that remain in the cylinder are dependent on the previous combustion event. Thus, the residual gas can vary from cycle to cycle, although the mass transfer is kept constant.

2.2.2 Effects of variation

Ozdor et al. (1994) reviewed the effects of cyclic variability and divided it into four categories. Those were the parameters that are related to pressure, combustion, flame front, and exhaust gas. In this report, the effect of cyclic variability is focused on variations in the air/fuel mixture and residual gases.

2.2.2.1 Effects of cyclic variability on cylinder pressure

The effects on pressure include variations in the maximum in-cylinder pressure and IMEP based on the causes of variations in the air/fuel mixture and residual gases.

1) Variation in cylinder pressure and IMEP

In regard to the causes of various residual gases in the cylinder, Figure 2-11 shows variations in in-cylinder pressure with different valve overlaps (Leroy et al., 2008).

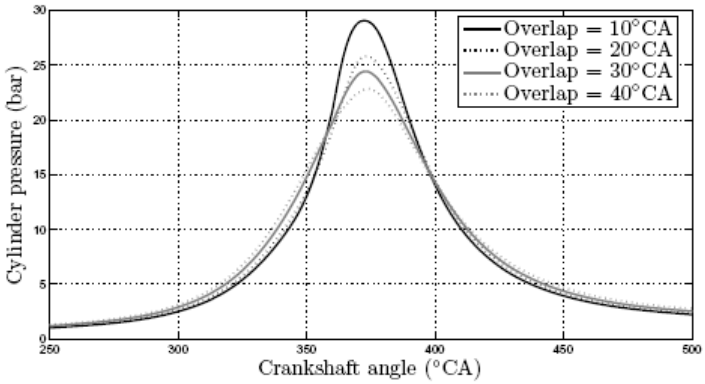

Figure 2-11: In-cylinder pressures from different valve overlap setting at 1000 rpm and 4 bar of BMEP (Leroy et al., 2008)

As can be seen, the maximum in-cylinder pressure decreases when valve overlap increases. Leroy et al. (2008) explained that the change in the in-cylinder pressure profile came from different fresh air charges dependent on valve overlap. At the same manifold pressure (P_{man}) in Figure 2-12, the volumetric efficiency decreased when the valve overlap increased, because the total fresh charge is replaced by residual gases. The residual gas increased when the intake valve opening (IVO) phase was advanced and exhaust valve closing (EVC) phase was retarded. When there was no valve overlap, the residual gases still remained in the cylinder in the clearance volume before the intake valve closed. Thus, improvements in fresh air change can obtained by increasing the manifold pressure or by using a turbocharger. According to Figure 2-11, in-cylinder pressure dropped when valve overlap increased; however, a fast burn rate early in the combustion process benefits from hot gases which improve fuel vaporization but slows down the combustion when more residual gases are introduced (Leroy et al., 2008).

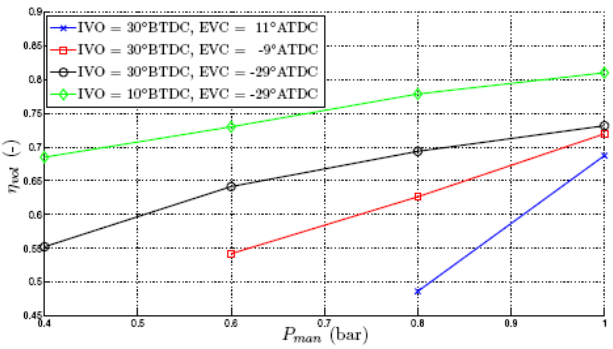

Figure 2-12: Effect of IEGR on volumetric efficiency at constant speed of 1500 rpm (Leroy et al., 2008).

Schwarz et al. (2003) showed IMEP with different residual gases, as can be seen in Figure 2-13. With the increasing IMEP, the backflow of burnt gas from the exhaust pipe to the cylinder and from the cylinder to the inlet manifold decreases due to the decreasing pressure difference between both valves. Schwarz et al. (2003) claimed that the backflow of gasses in the cylinder before the intake valve closes has no significance on the total residual gas mass as only a small fraction consists of burnt gas.

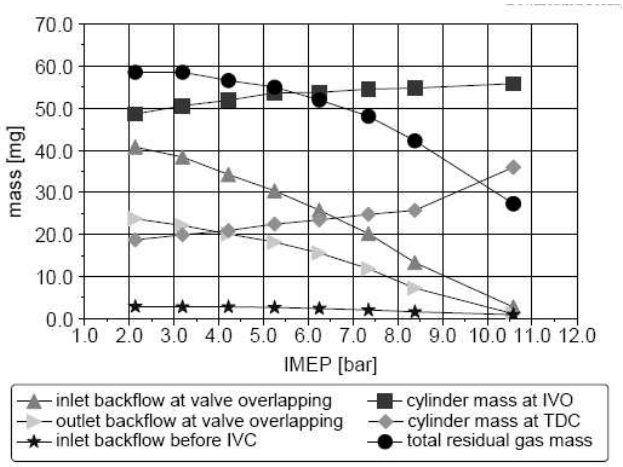

Figure 2-13: Mass flow analysis for different IMEPs at 2000 rpm (Schwarz et al., 2003)

When the engine speed increases, the graph in Figure 2-14 shows that the residual gas is reduced while the IMEP remains unchanged. The situation where the engine speed is kept constant shows variation in IMEP which is caused by different pressures across the intake and exhaust valves. In addition, the mass flow rates of the gases were affected by those mechanisms.

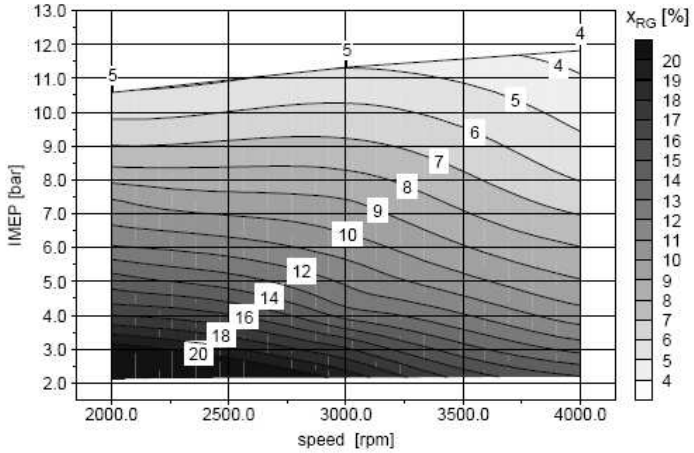

Figure 2-14: Effect of residual gas on IMEP at different engine speeds (Schwarz et al., 2003)

It is very important to understand how the residual gas affects the in-cylinder pressure and IMEP. Variations in in-cylinder pressure lead to variations in IMEP at the same engine speed. Figure 2-14 can be used to explain cyclic variability in combustion events. When the IMEP is high, the residuals contained in the combustion chamber, before the mixture is ignited, are relatively low.

2) Tolerance of the engine to residual gas fractions

Shayler et al. (2000) discusses the gas/fuel ratio (GFR) in spark ignition engines and explains the effect of residual gas on the IMEP. Ford SE 1.25L and 1.8L Zetec engines were used in the research. A NTK MB100 universal exhaust gas oxygen sensor was installed in the engines' exhaust manifolds. HC concentration was recorded from the exhaust manifolds by a flame ionisation detector (FID). The concentration of CO, CO_2 and O_2 emissions were measured by a Horiba MEXA 554LE.

A hot wire and gravimetric measurement equipment were used to measured air mass flow rates and fuel respectively. GFR is calculated by the following *Equation 2-10*;

$$GFR = \frac{(m_a + m_f + m_b)}{m_f} \quad \text{.....Equation 2-10}$$

Where m_a = Trapped mass of air [kg].
m_f = Trapped mass of fuel [kg].
m_b = Mass of burned gas in mixture during compression [kg].

Figure 2-15a, shows exhaust gas recirculation (EGR) and air/fuel ratio (AFR) data. Figure 2-15b shows COV_{imep} plotted against GFR (Shayler et al., 2000). When COV_{imep} was plotted against GFR, a single characteristic variation was present although AFR was changed. The trend shows that the limits of stable operation corresponds to a GFR value in the range of 26:1 to 28:1, as can be seen from the dispersion of the data values above 10% of COV_{imep}. The factors that effect COV_{imep} were described.

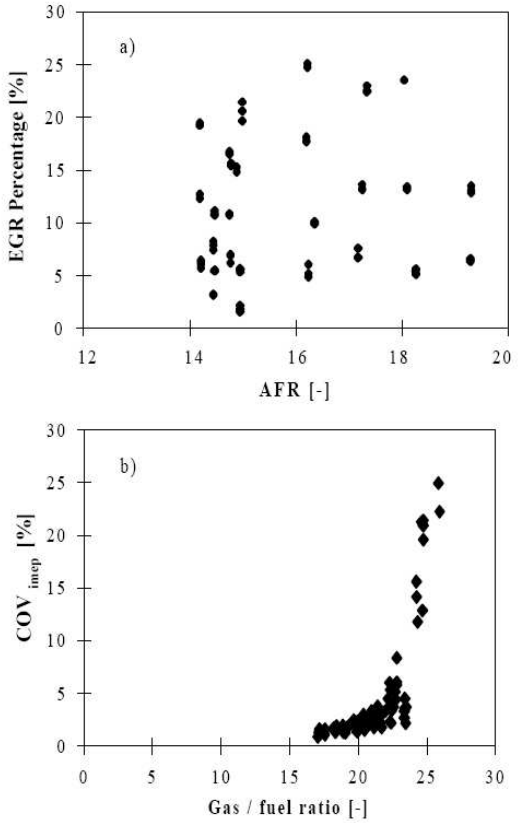

a) Variation of EGR with variation in AFR
b) GFR against COV_{imep}

Figure 2-15: Relationship between gas/fuel ratio (GFR) and AFR (Shayler et al., 2000).

Figure 2-16 shows the effect of spark timing at two different engine speeds during warm operation. Spark retarded from maximum brake torque (MBT) caused a COV_{imep} increase and became unstable at GFR between 26:1 and 28:1. Shayler et al. (2000) explained that a limitation on GFR was introduced when spark timing was retarded from MBT in order to maintain the same COV_{imep} as can be seen in Figure 2-17. Figure 2-18 shows the results when the engine was operated at -20˚ C coolant temperature, a significant rises in COV_{imep} is present and it reached an unstable limit when the GFR was about 24:1. During cool operation, Shayler et al. (2000) explained that the AFR value, observed during their research, can be significantly different from intake mixture, because of the loss of fuel to the crankcase had been ignored. Thus, the GFR ratio can be slightly unstable during low temperature operation, compared to fully warm operation.

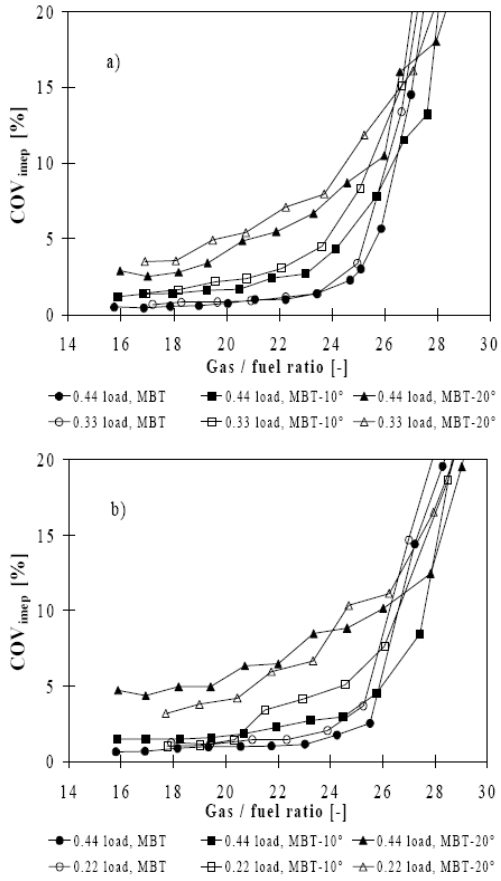

a) Engine speed 1000 rpm

b) Engine speed 2500 rpm

Figure 2-16: Variation of COV_{imep} in the GFR for the Zetec 1.8 engine at 90˚ C engine coolant temperature (Shayler et al., 2000).

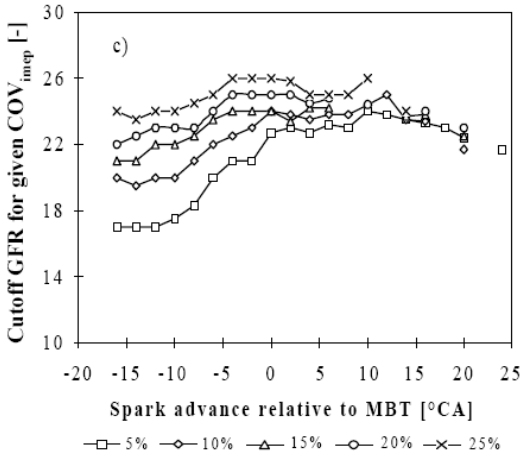

Figure 2-17: Limiting combination of GFR and spark timing relative to MBT of Zetec 1.25 engine for 5 values of COV_{imep} (Shayler et al., 2000).

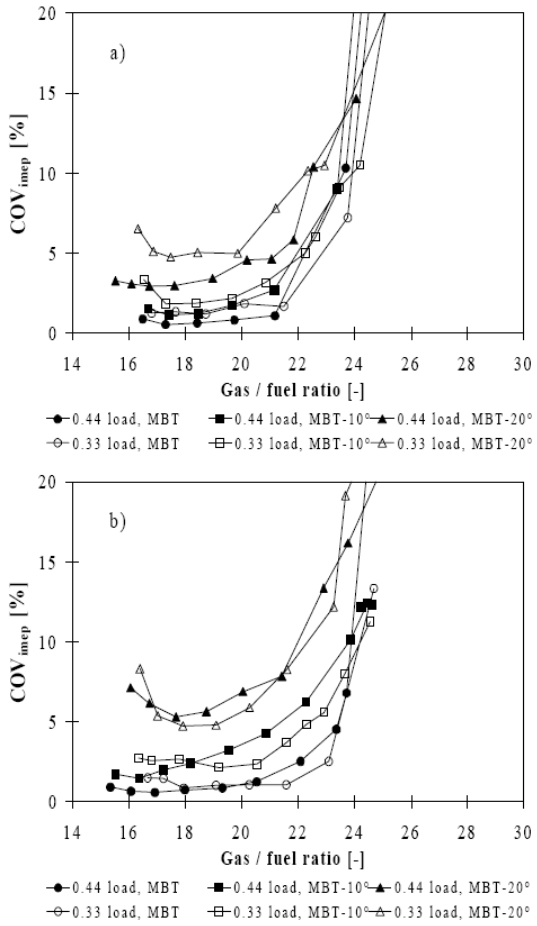

a) at 1000 rpm

b) at 2500 rpm

Figure 2-18: Variation of COV_{imep} with GFR of Zetec 1.8 engine at -20˚C engine coolant temperature (Shayler et al., 2000).

Shayler et al. (2004) carried out additional research to explain the limitations on charge dilution. A V8 engine with variable intake valve timing was used in the research. Residual gases can vary at any given speed and load while the duration was kept constant. The exhaust valve timing and duration of the engine were kept constant. In-cylinder pressures were measured by pressure transducers (Kistler model 6052A) which were installed on one cylinder from each bank of cylinders.

The experimental results were collected and illustrated in two diagrams. The first diagram shows a boundary of air/burnt gas mass ratio (m_a / m_b) and fuel/burnt gas mass ratio (m_f / m_b). The second diagram shows a boundary of the burnt gas fraction (x_b) and the air/fuel ratio (AFR).

The first diagram shows, in Figure 1-18, the ratio of m_a / m_b and m_f / m_b vary independently. The limits of GFR were calculated from the *Equation 2-11* below

$$\frac{m_a}{m_b} = (GFR - 1)\frac{m_f}{m_b} - 1 \quad \text{.....Equation 2-11}$$

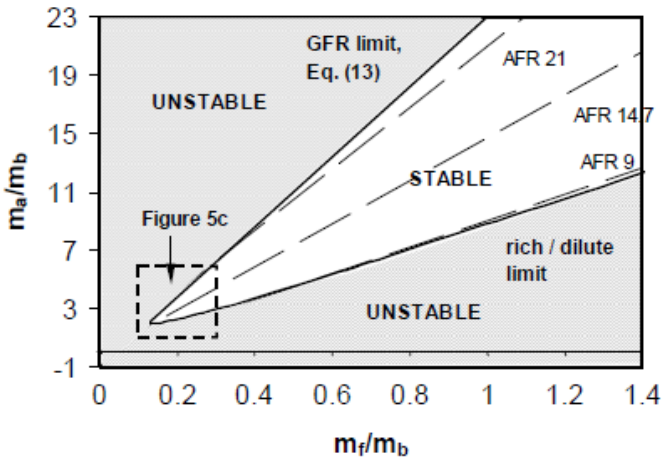

Figure 2-19: Boundary between stable and unstable combustion regions (Shayler et al., 2004).

Figure 2-19 shows that a large stable zone, which is referred to COV_{imep} below 10%, was present in the top right hand corner. The lines between the stable and unstable regions converge towards the left hand corner. Figure 2-20 shows the COV_{imep} in the stable zone was less than 10% whereas the values of COV_{imep} increased significantly when the engine operated in unstable zone which shows in vertical scale of COV_{imep} .

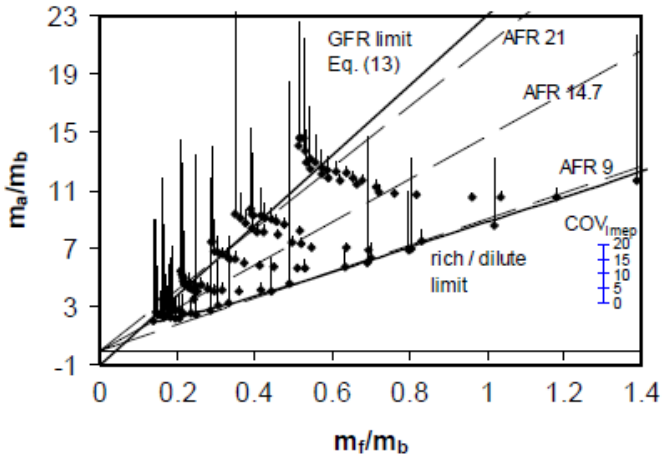

Figure 2-20: The height of the vertical attached to data points indicates the value COV_{imep} (Shayler et al., 2004).

Figure 2-21 shows the details of plots when they converge. The limits of GFR were restricted when m_a / m_b and m_f / m_b were reduced. If the mixture was diluted with burnt gas the m_a / m_b and m_f / m_b values became large. Shayler et al. (2004) explained that stable combustion required a minimum concentration of fuel to convert to GFR. In the research, the limit of GFR was approximately 25:1, that required a 4% of fuel concentration before COV_{imep} is greater than 10%.

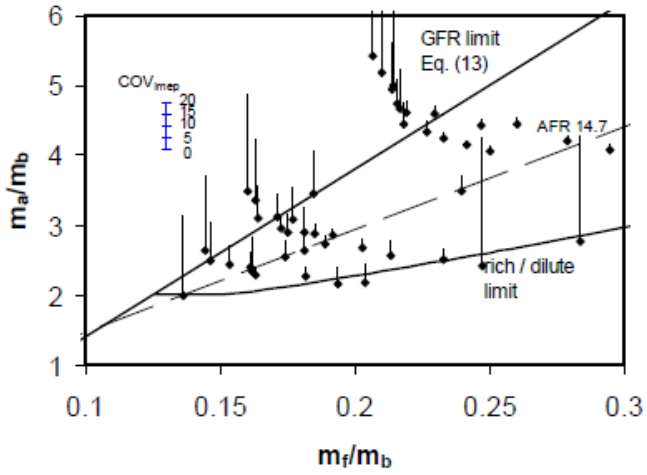

Figure 2-21: Large scale plot a section of Figure 2-19 around origin (Shayler et al., 2004).

Figure 2-22 shows the stable and unstable zones when the burnt gas fraction (x_b) was plotted against AFR. Shayler et al. (2004) proved that the burnt gas fraction was a related to AFR and GFR and is defined by the following *Equation 2-12*;

$$x_b = \frac{GFR - AFR - 1}{GFR} \quad \text{.....Equation 2-12}$$

Regards the above equation, when the residual gas is measured stable combustion can be achieved by varying the AFR.

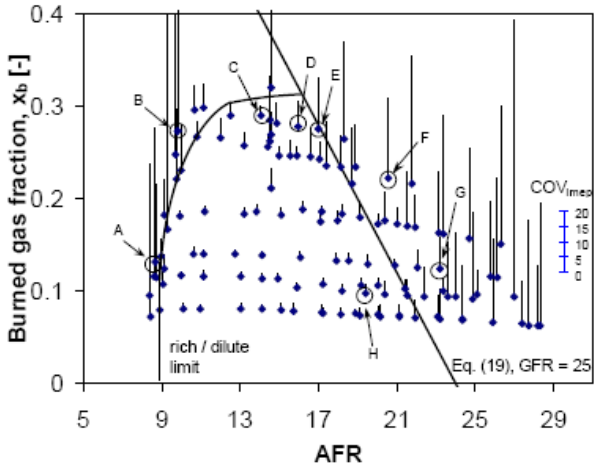

Figure 2-22: Variation of COV_{imep} with different burned gas fraction and AFRs (Shayler et al., 2004).

According to Figure 2-22, the stable boundary limit for rich mixture fuelling is approximately 9:1 AFR, and the maximum of burnt gas fraction is 0.15. Under lean fuelling conditions, the boundary was controlled by the GFR value of 25. Those two boundary lines were enclosed at about 0.3 of burned gas fraction (Shayler et al., 2004).

2.2.2.2 Effect of cyclic variability on combustion

The effect of variability in combustion is evidence of how the mixture is being burnt in the chamber. The effect includes combustion efficiency, mass burning rate and combustion duration. These factors vary depending on the amount of residual gas that is present.

According to the research from Shayler et al. (2000), the results from varying the engine's temperature shows a link to misfires. The results show that high engine temperatures lead to a reduction in misfire frequency. Figure 1-23a) shows the misfire frequency started increasing at GFR values between 25:1 and 28:1, which depended on the load and speed. At 20˚C coolant temperature, the misfiring started when GFR was approximately 23:1, and once the GFR exceeded the limit, the misfiring became constant. The effect on misfire frequency of partial burns, during fully warm and cold operating conditions, started when COV_{imep} exceeded 8% (Shayler et al., 2000).

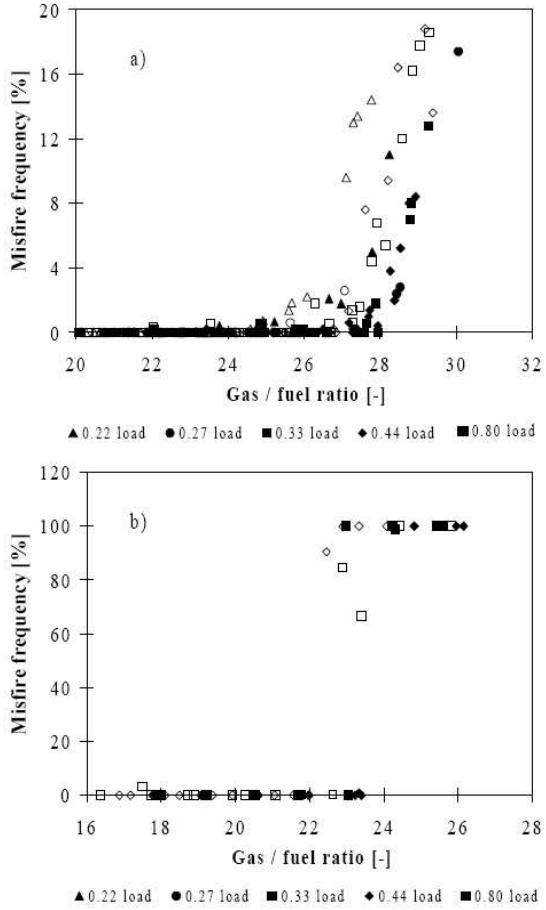

a) Coolant temperature 90˚C

b) Coolant temperature -20˚C

Figure 2-23: Relationship between misfire frequency and GFR from Zetec 1.8 engine (Shayler et al., 2000).

Related to the results shown in Figure 2-23, is the Table 2-4. Letters A to H are used to identify various conditions related to the variation in COV_{imep}. Misfire (as defined by a level of work output which was less than 5% of the mean), partial burn (as defined by a combustion event that produces less than 70% of mean IMEP) and burn duration were analysed against COV_{imep} as shown in Table 2-4 and Table 2-5.

Table 2-4: Correlation of COV_{imep} from different operating conditions (Shayler et al., 2004)

Condition	misfire [%]	partial burn [%]	COV_{imep} [%]
A	5.6	16.7	43.71
B	8.9	25.6	54.9
C	0	0	3.17
D	0	0	8.07
E	0	5.6	16.8
F	0	11.1	26.2
G	0	2.4	10.46
H	0	0	3.74

Table 2-4 shows the conditions labelled C, D and H that are related to stable regions of operation had no effect on misfiring or partial burns. Points F and G which are related to the lean mixture region and the burn gas fraction over its limit proved the variation in COV_{imep} is caused by partial burn while there were no misfires. For the rich fuelling limit, points A and B show the variation in COV_{imep} resulted from misfires and partial burns.

Table 2-5: Correlation coefficient between IMEP and burn duration from different operating conditions (Shayler et al., 2004)

Condition	Correlation coefficient between imep and burn duration		
	0-10% burn	10-90% burn	0-90% burn
A	0.247	0.969	0.977
B	0.550	0.658	0.432
C	0.215	0.035	0.120
D	0.349	0.605	0.505
E	0.457	0.767	0.697
F	0.095	0.759	0.722
G	0.063	0.821	0.752
H	0.170	0.699	0.682

Shayler et al. (2004) discuss the correlation coefficients for IMEP and burn duration as seen in Table 2-5. Points F and G, which refer to the engine operating under lean fuelling conditions with GFR over its normal limit, show that the COV_{imep} has a strong relationship with the 10-90% burn duration. Condition labelled C had the lowest COV_{imep} and provided no relationship on burn duration.

Daw et al. (1996) explained the details of misfire and partial burn in terms of combustion efficiency as shown in Figure 2-24.

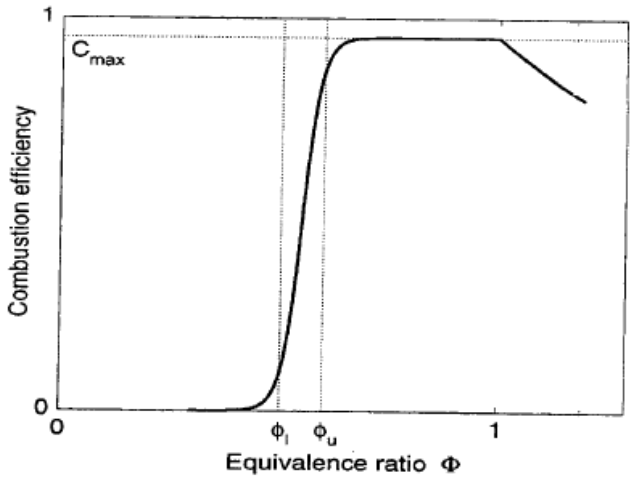

Figure 2-24: Relationship between combustion efficiency and equivalence ratio (Daw et al., 1996)

The combustion efficiency for a given air/fuel ratio is classified by Daw et al. (1996) using the equivalence ratio (ϕ) which is the inverse of lambda (λ). The equivalence ratio is the ratio of the actual fuel/air ratio to the stoichiometric ratio which commonly use in diesel study while the lambda generally use in gasoline study. The efficiency of combustion where equivalence ratio is more than 1 ($\phi > 1$) is defined by *Equation 2-13*;

$$C(\phi) = \frac{C_{\max}}{\phi} \quad \text{.....Equation 2-13}$$

When the equivalence ratio is less than 1 ($\phi < 1$), the combustion is defined by *Equation 2-14*

$$C(\phi) = \frac{C_{\max}}{1 + 100^{-\frac{\phi - \phi_m}{\phi_u - \phi_l}}} \quad \text{.....Equation 2-14}$$

where;

$C_{\max}$	=	Maximum combustion efficiency achieved at stoichiometric fuelling
ϕ_u	=	Equivalence ratio where combustion efficiency is 90%
ϕ_l	=	Equivalence ratio where combustion efficiency is 10%
ϕ_m	=	Critical equivalence ratio = $(\phi_l + \phi_u)/2$

Daw et al. (1996) stated that the combustion efficiency function is assumed to account for the residual gas effects, and that the critical equivalence ratio is typically about 0.5-0.6, but the ratio of residual gas was ignored. With variations in residual gas, the combustion efficiency itself can vary.

Research, on the effects on combustion, shows that residual gases have an impact on partial burning, misfire, and even auto ignition which depend on the quantity of residual gas contained in the combustion chamber before combustion takes place. This information can be used to explain the cyclic variability but experimental work needs to be done because different engines each have their own set of characteristics.

2.2.2.3 Effect of cyclic variability on flame front

The combustion flame front, during lean fuelling operation, can change according to variations in the air/fuel ratio. Aleiferis et al. (2004) discussed the effect of residual gas on the flame kernel radius during lean operation. A Honda engine with a single overhead camshaft, variable valve timing, and electronic lift control (VTEC), was used in the research. The in-cylinder pressure traces were collected, analyzed, and catagorised into three groups based on the mean IMEP value, as can be seen in Figure 2-25. These three groups are:

1) $0.9 < \text{IMEP}/\text{IMEP}_{\text{mean}} < 1.1$
2) $1.1 < \text{IMEP}/\text{IMEP}_{\text{mean}}$
3) $\text{IMEP}/\text{IMEP}_{\text{mean}} < 0.9$

From the in-cylinder pressure data the mass fraction burnt was calculated for each of the three groups of IMEP. Aleiferis et al. (2004) analyzed flame kernel radius at the crank angle of 5% mass fraction burnt point, as can be seen in Figure 2-26. The flame kernel radius data were divided into four groups dependent on the speed of combustion:

- Fastest lean cycles: $\theta_{x_b 5\%} \leq 355^{\circ} CA$
- Slowest lean cycles: $\theta_{x_b 5\%} > 365^{\circ} CA$
- Typical lean cycles (two grades): $355^{\circ} CA < \theta_{x_b 5\%} \leq 360^{\circ} CA$

  and $360^{\circ} CA < \theta_{x_b 5\%} \leq 365^{\circ} CA$

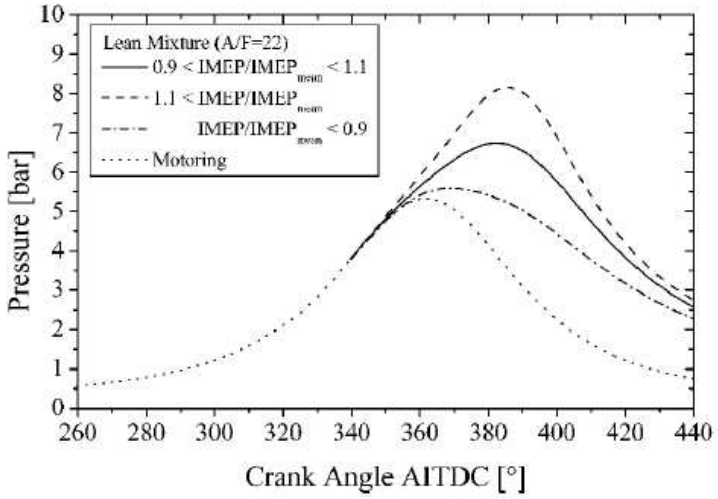

Figure 2-25: Classification of IMEP from different in-cylinder pressure (Aleiferis et al., 2004)

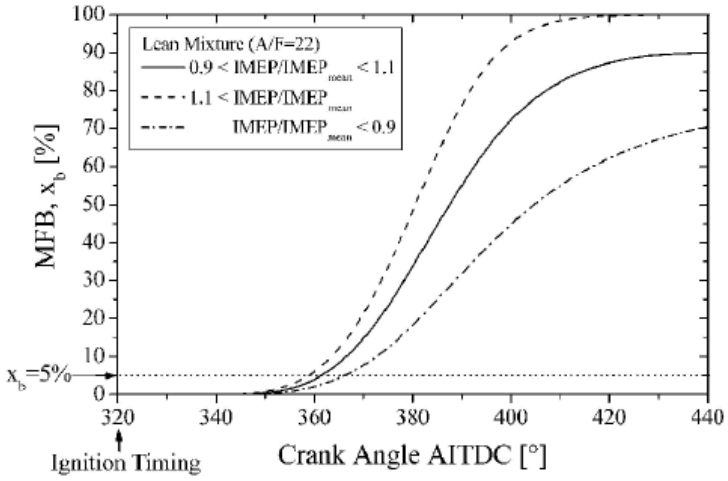

Figure 2-26: Mass fraction traces and the crank angle at 5% mass fraction burn (Aleiferis et al., 2004)

The results compared the flame kernel radius between stochiometric mixture (AFR = 15) and lean mixture (AFR = 22) fuelling. Lean mixture results show that the flame kernel grew slower than it did with a stochiometric mixture as observed. Aleiferis et al. (2004) carried out engine tests under lean fuelling conditions, and produced data showing flame kernel growth. Figure 2-27 shows that flame kernel grew faster when the in-cylinder pressure was high for the same mixture

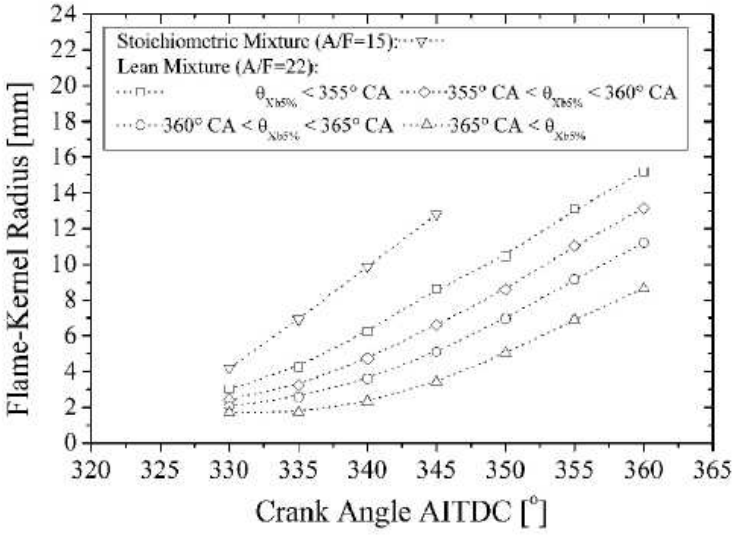

Figure 2-27: Flame kernel radius evolution (Aleiferis et al., 2004)

The mass fraction burnt with different residual gas amounts is explained by Bonatesta et al. (2008). A four cylinder 16V spark ignition engine was used in the research. The amount of residual gas can varied by using variable valve timing. The results are show in Figure 2-28.

The results supported the research from Chen et al. (2003) that showed that increased residual gas slows down the combustion and causes variations in cylinder pressure.

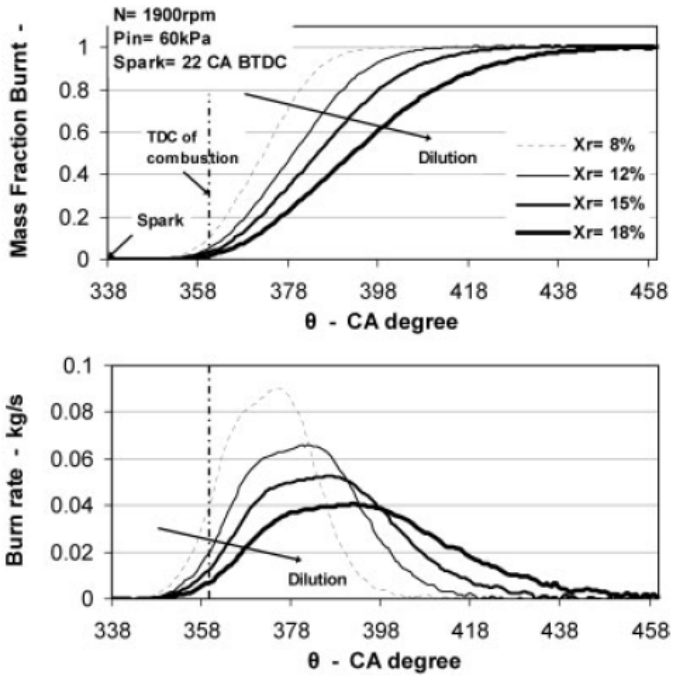

Figure 2-28: Charge in burn characteristic with variation in residual gas (Bonatesta et al., 2008).

Moon et al.'s (2005) research was focused on early combustion using three different injector's temperatures which were 25, 55 and 85 ^{o}C. The engine was operated with stochiometric fuelling under cold start conditions. Other tests were carried out with lean fuelling during the engine warm-up period. The results showing the mass fraction burnt under cold start conditions can be seen in Figure 2-29.

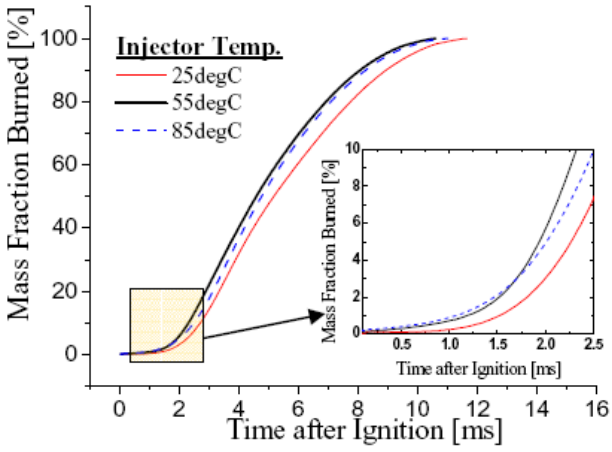

Figure 2-29: Mass fraction burned from cold start at 800 rpm, $\lambda = 1$ (Moon et al., 2005)

The results showed that the mass fraction burnt at injector temperature of 85 ^{o}C, during early combustion, was greater than with an injector temperature of 25 ^{o}C. These results suggest that high fuel temperatures provide an opportunity for evaporation more than cold fuel and lead to increased mass fraction burnt values during cold start conditions. Moon et al. (2005) showed the flame propagation of the three tests and the results from warm-up condition differed, as can be seen in Figure 2-30.

Moon et al. (2005) explained that during the first 10 degrees of crank angle movement after the start of ignition, the injector temperature of 85 ^{o}C gave the fastest flame propagation. However, at the later stage, the injector temperature of 55 ^{o}C shows faster flame propagation and larger flame area than with an injector temperature of 85 ^{o}C. The results suggest that during the burning process, the temperature increases because the remaining fuel was evaporated. Figure 2-30b shows that under warm-up conditions the flame propagation at 85 ^{o}C was slowed because of the lean mixture present near the spark plug which later became relatively rich. These findings require more information to explain because designs of fuel injection systems vary and may give different results. Moon et al. (2005) concluded that the injector temperature had an affect on fuel evaporation and droplet size. An increase in injector temperature had benefits in achieving faster combustion and an increase in IMEP. With cold start conditions, the observations showed an opposite value, thus stable combustion can be achieved by selecting an optimum injector temperature.

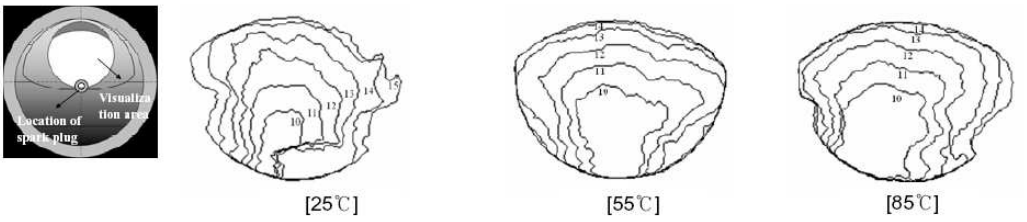

a) Under cold start condition, $\lambda = 1$

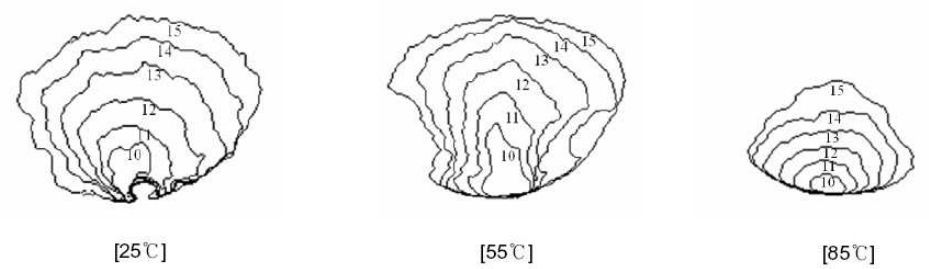

b) Under warming-up condition, $\lambda = 1.7$

Figure 2-30: Flame propagation during early combustion (Moon et al., 2005).

Moreover, the early combustions were affected by the orientation of the spark plug in the cylinder head. Aleiferis et al. (2000) studied the effect of the orientation of the spark plugs in the cylinder head by using a Honda VTEC-E engine with pent-roof shaped combustion chamber in a single-cylinder. The spark plug was installed in four different types of orientations named as “North”, “South”, “East” and “West” which are shown in Figure 31. The engine was run with an air/fuel ratio of 22. The authors showed that each orientation has cyclic variability, which results in the COV_{imep} value being equal to 14.2%, 15.6%, 17.0% and 19.2% for west, east, north and the south orientations respectively.

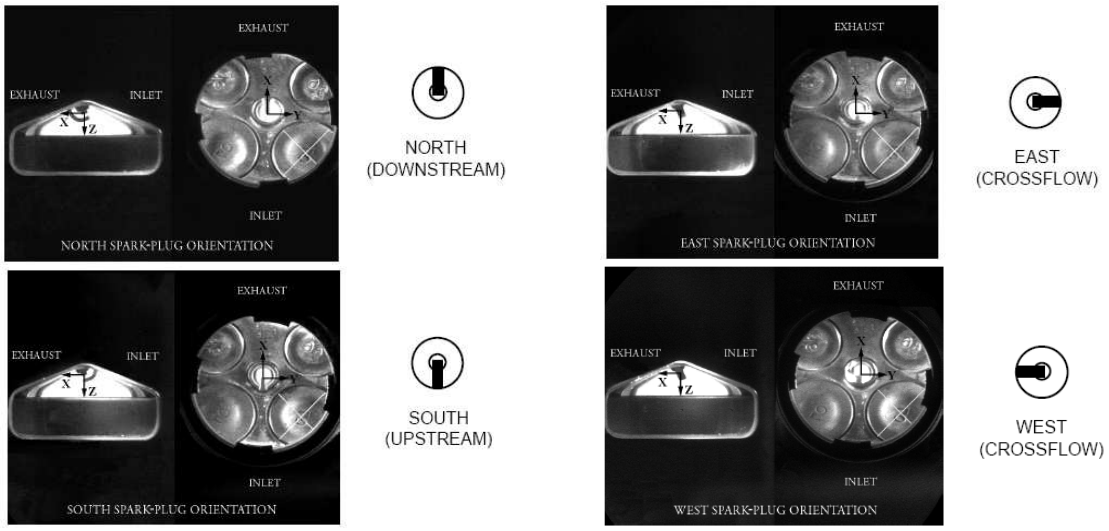

Figure 2-31: Orientation of Spark plug (Aleiferis et al., 2000)

According to the variation in COV_{imep}, the direction of spark-plug ground electrode can affect the flow of the mixture across the spark plug gap. In addition, the design of the intake and exhaust manifold also has an influence on those variations. Aleiferis et al. (2000) also showed a 5% of mass fraction burnt against IMEP for a west orientation, as can be seen in Figure 2-32. The early crank angle associated with 5% mass fraction burnt gave high IMEP.

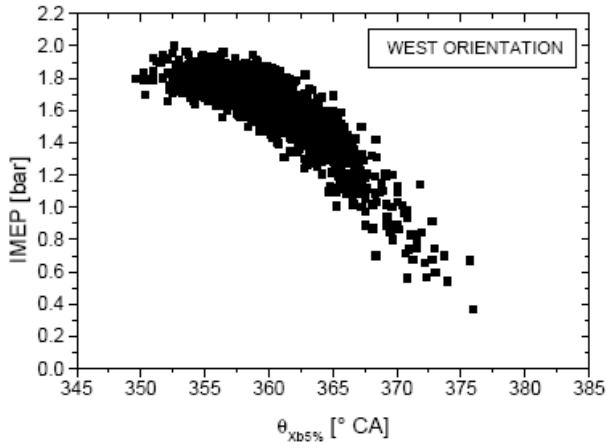

Figure 2-32: IMEP vs. Crank Angle of 5% Mass Fraction Burn (Aleiferis et al., 2000)

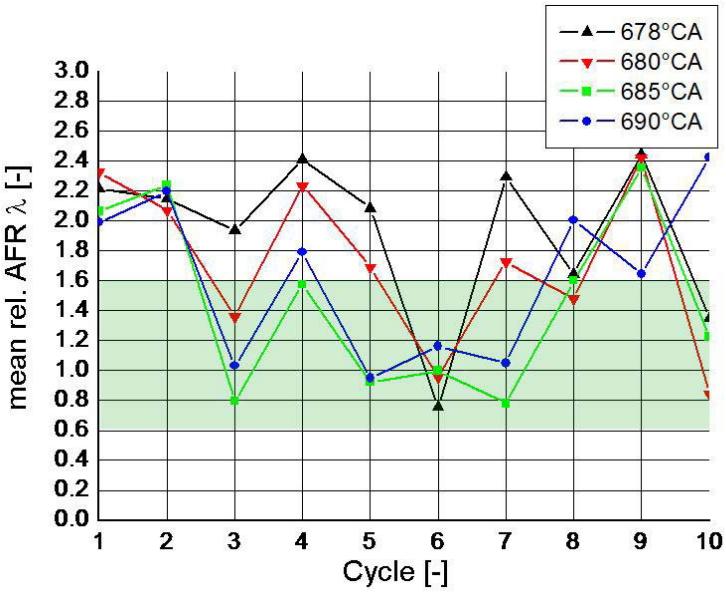

Figure 2-33: The mean relative AFR during ignition for 10 cycles (Adomeit et al., 2007).

Adomeit et al. (2007) observed the air/fuel mixture near the spark plug by controlling the speed of air using a tumble flap in an experimental. The results showed that a high air speed gave a better mixture distribution than a low air speed. Moreover, the results showed that the probability of misfires were high at low air speeds. In addition, a simulation of the variation of mixture near the spark plug was presented in Figure 2-33 with error below 0.05 (Adomeit et al., 2007).

2.2.2.4 Effect of cyclic variability on exhaust gas and engine torque output

The effect of cyclic variability can be seen on exhaust emissions including NO_x and HC, fuel consumption and engine torque output. From the previous topic it can be seen that variations in the level of residual gas in the cylinder can be related to changes in the degree of valve overlap (Leroy et al., 2008). Kramer et al. (2002) investigated the emissions and fuel consumption with different valve overlaps. In the research, a 1.6L Zetec SE twin cam with variable cam timing (VCT) engine from a Ford Focus was used.

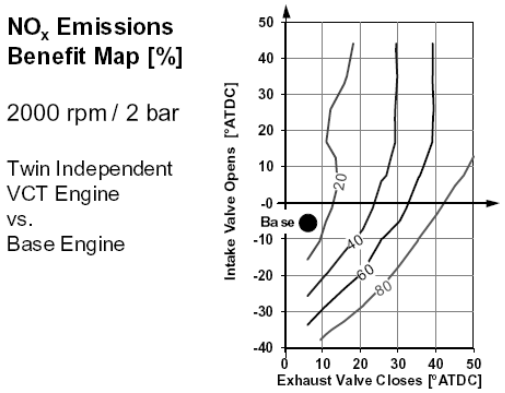

Figure 2-34: NO_x emissions with different valve overlap setting (Kramer et al., 2002)

Figure 2-34 shows that the benefit from an increased valve overlap is a significant reduction in NO_x emissions. Kramer et al. (2002) claimed that increasing amounts of internal EGR lead to a lower combustion temperature resulting in a reduction of NO_x emissions. Ghauri et al. (2000) stated that the most significant influences were intake phase, as shown in Figure 2-35, because by altering the intake valve's timing, whilst the exhaust valve timing is kept constant, leads to increased air with a resulting lowering of peak combustion temperature and lower NO_x emissions.

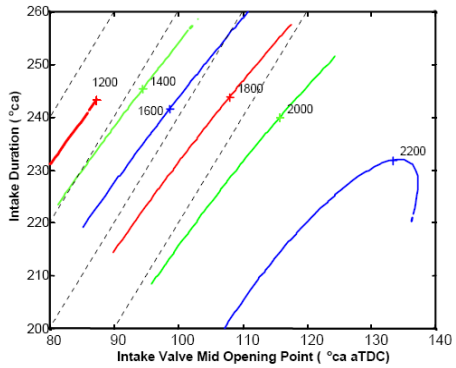

Values of NOx emissions in ppm
Dashed lines correspond to lines of constant valve overlap (highest overlap in top left hand corner reducing to zero overlap moving to the right across the dashed lines)

Figure 2-35: Effect of intake valve phasing and duration on NO_x (Ghauri et al., 2000)

Figure 2-36 illustrates HC emissions increase during high valve overlap. According to the base point, moving the intake valve timing had no effect on HC emissions, but a maximum of 10% improvement in the HC emissions was obtained by retarding the exhaust timing (Kramer et al., 2002). Ghauri et al (2000) explained that the later closing of exhaust valves gave a greater chance of the last exhaust gases leaving the cylinder being absorbed HC emissions before the exhaust valves closed. Retarded exhaust valve timing caused an increase in exhaust gas which helps the fuel to evaporate and burn more easily. Moreover, the HC emissions are dependent on many factors, for example, exhaust pressure, compression ratio and wall temperature etc (Heywood, 1988).

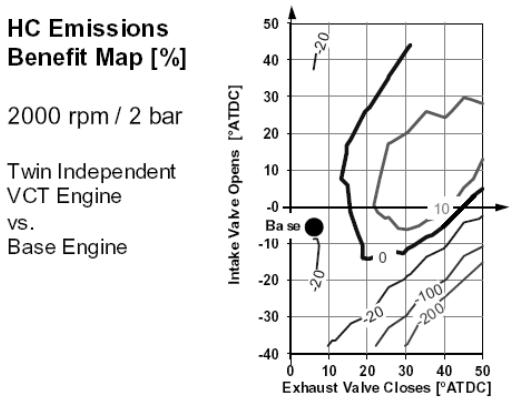

Figure 2-36: HC emissions with different valve overlap setting (Kramer et al., 2002).

In order to achieve the maximum fuel consumption, the exhaust valve timing retard is mechanically limited by the depth of the piston valve pockets. Thus, a combined strategy can be applied to obtain the best results.

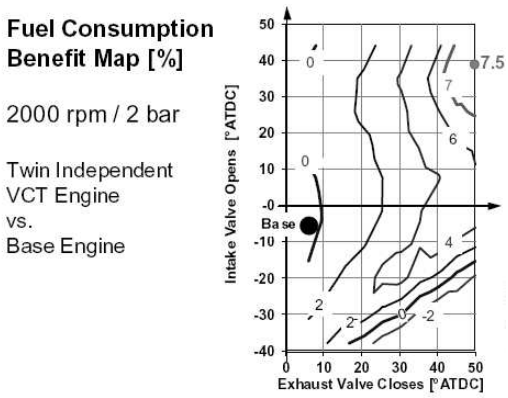

Figure 2-37: Fuel consumption with different valve overlap setting (Kramer et al., 2002).

Regards fuel consumption, Figure 2-37 shows a maximum improvement in fuel consumption of 7.5 was achieved by adjusting intake and exhaust valve timing. Kramer et al. (2002) concluded that there are three parameters that improve fuel consumption. Firstly, late intake valve closing allowed backflow to the intake manifold thus improving fuel evaporation. Secondly, late exhaust valve closure provided higher levels of residual gas which helps fuel evaporation when it flows back to the intake port. Finally, late exhaust valve opening increases the effective expansion ratio, resulting in increased work output. In additional, Kramer et al. (2002) also focused on the exhaust system's role regards engine efficiency. Figure 2-38 shows a torque improvement using two three-way catalysts (TWC). There was no torque benefit from a single TWC. These effects influence the design of the exhaust manifold and the pressure wave inside the pipe (Stone, 1999).

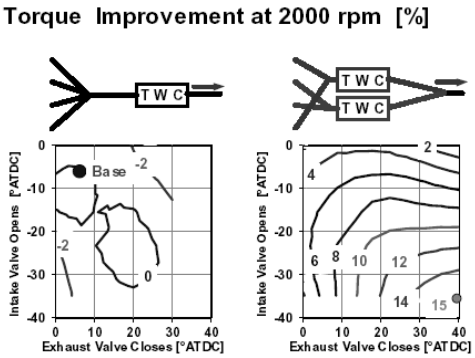

Figure 2-38: Torque improvements with different exhaust systems (Kramer et al., 2002)

The different types of exhaust system are compared in Figure 2-39.

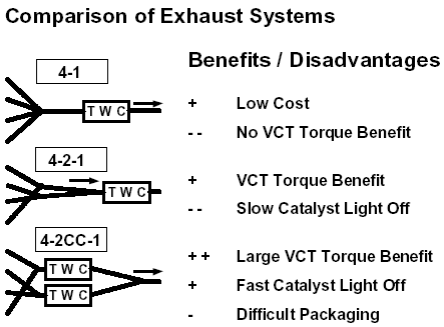

Figure 2-39: Applicability of different exhaust systems (Kramer et al., 2002)

As can be seen from the effects above, there is a trade off between the advantages and disadvantages of valve overlap. Understanding these factors can lead to the choice for the best operating point for the engine in a particular situation.

In 2004, Jung et al. investigated pumping work, which benefits from valve overlap. The research was focused on the variations in pumping with different valve timing. The test engine was run at 1200 rpm, 1.8 bar BMEP. Figure 2-40 shows an increase in pumping work caused by varying the intake valve closure (IVC) timing while the exhaust valve timing was kept constant. Jung et al. (2004) explain that moving the IVC close to top dead centre results in a smaller volume of fresh charge being drawn into the cylinder. Thus, the manifold absolute pressure was increased in order to maintain the same torque

output and this reduced pumping work. In comparison, when the exhaust valve closure (EVC) timing was varied and the IVC timing remained constant, pumping loop was smaller compared with the previous case (Figure 2-41). With the EVC timing retarded, the residual gas is increased so lowering pumping work and improving fuel consumption.

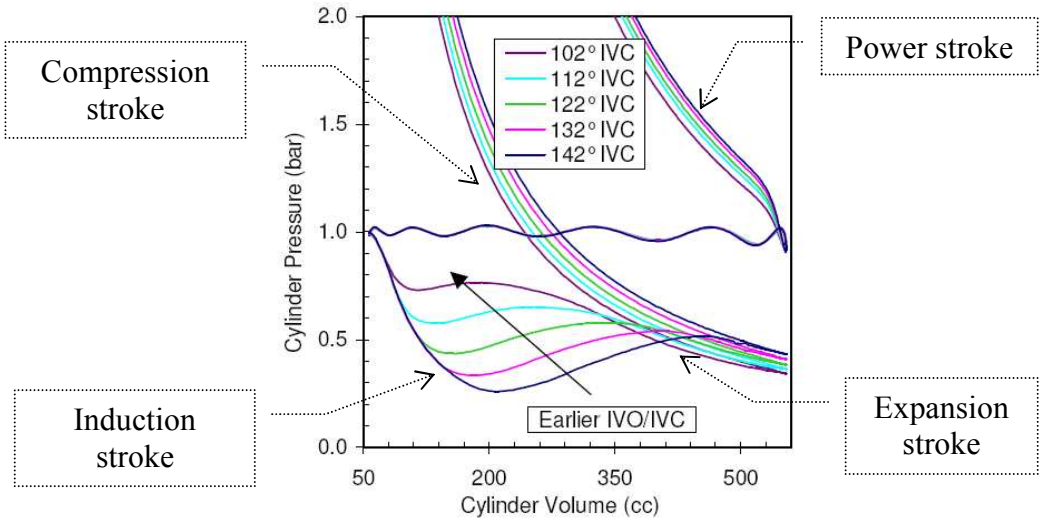

Figure 2-40: P-V diagram with constant exhaust valve closing angle of 30˚ ATDC (Jung et al., 2004)

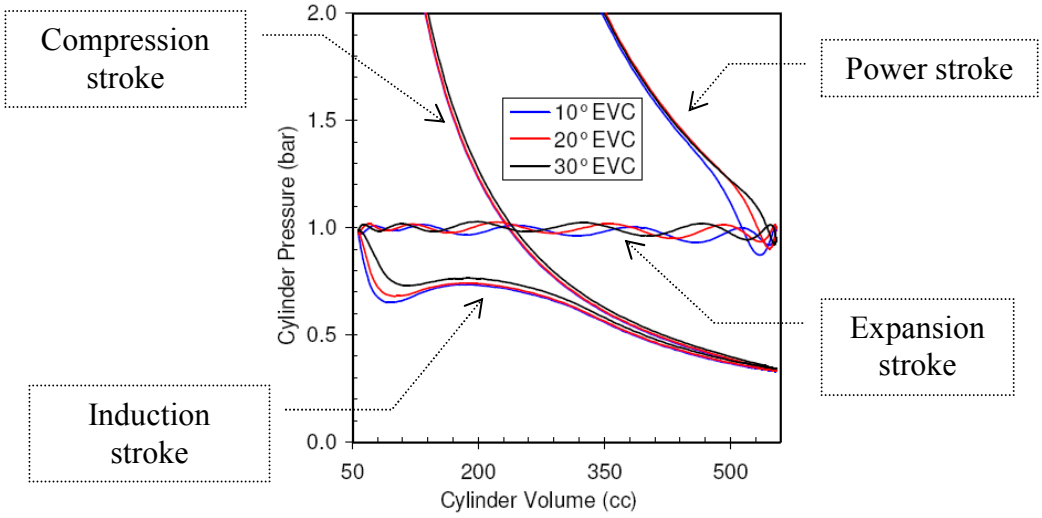

Figure 2-41: P-V diagram with constant intake valve closing angle of 102˚ ATDC (Jung et al., 2004)

Scharrer et al. (2004) stated that the use of variable valve timing had a strong affect on the intake manifold, pumping work of the engine, and residual gas after the intake valve was closed.

2.2.3 Ion current sensors

Some researches have experimented with an alternative technique called an ion current sensor which is used to observe behaviour in the combustion chamber. The evidence includes the air/fuel ratio, the physics of combustion, and the residual gases in the chamber. Wang et al. (2003) explained the fundamentals of ion current sensing using the spark plug as a sensor and adding a bias voltage to the ignition system. According to the chemical reactions in the combustion show by reaction below;

$$CH + O \rightarrow CHO^{+} + e^{-}$$

$$CHO^{+} + H_2O \rightarrow CO + H_3O^{+} + e^{-}$$

Ion and free electrons are produced during the ignition process and move in one direction under influence of a bias voltage between the spark gap. Wilstermann et al. (2000) explained that the large area will be able to collect amounts of ions during chemical reaction and also stay longer in contact with the propagating flame front

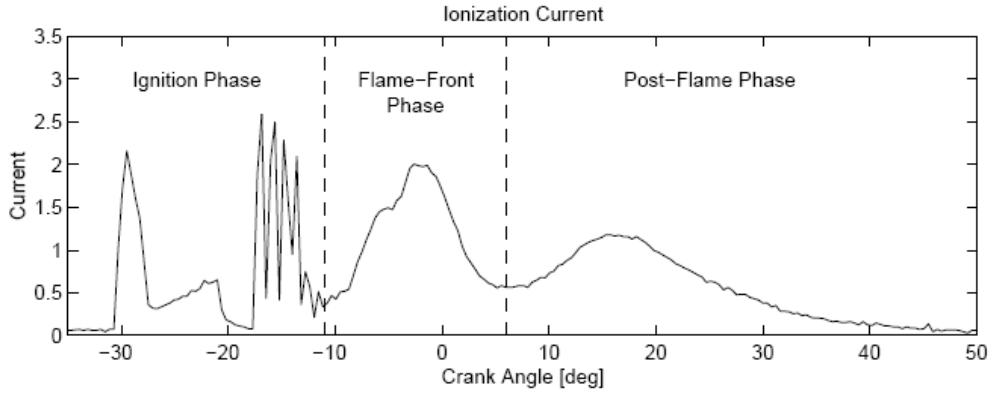

Figure 2-42: The signal from a typical ion current sensor (Wilstermann et al., 2000)

The results from ion current sensing are divided into three phases which are: ignition phase, flame-front phase and post-flame phase (Eriksson, 1999), as shown

in Figure 2-42. The first phase is called the *ignition phase* which is influenced by the ignition itself and the ignition circuitry. The second phase is called the *flame front phase* and is influenced by the ions that are generated in or nearby the flame front. The third phase is called the *post flame phase* which is influenced by pressure through its influence on the temperature. The third phase, that contains information about the pressure, is of special interest for ignition control.

The advantages of the ion current sensing are explained below.

Upadhyay et al. (1998) studied the signal of ion current with air/fuel ratio. The data from the ion current was recorded against crank angle, as can be seen in Figure 2-43. The ion current signal from rich mixture gave a higher current than with a lean mixture.

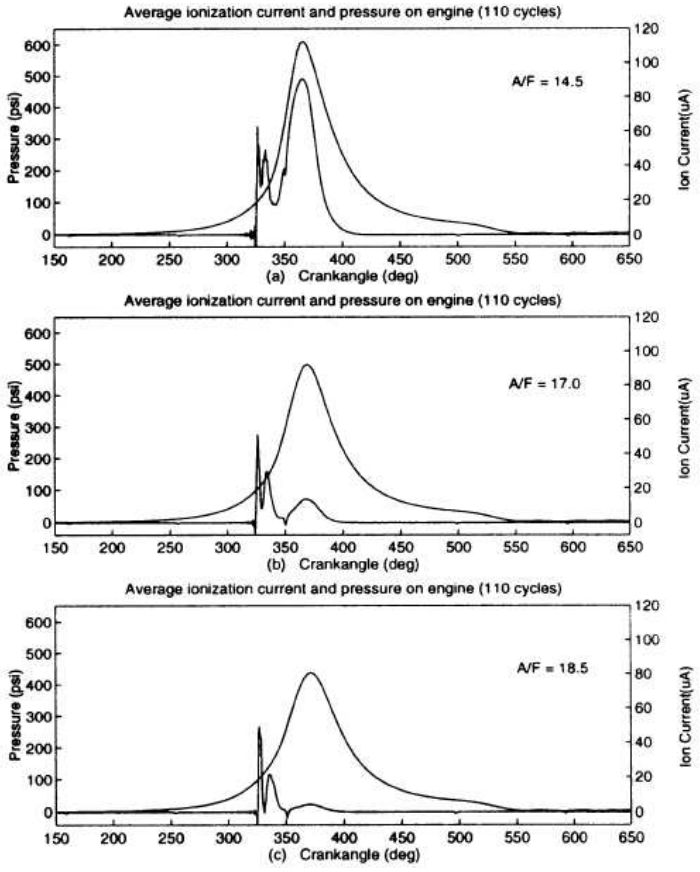

Figure 2-43: Ion current signal with different AFRs (Upadhyay et al., 1998)

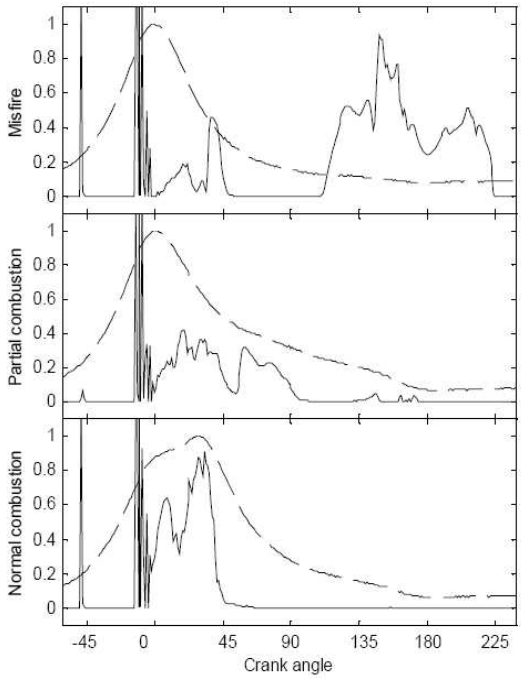

Figure 2-44: Ion current (solid) and cylinder pressure (dash) signal from misfire, partial combustion and normal combustion (Peron et al., 2000)

The ionization signals obtained by Peron et al. (2000) during misfire, partial combustion, and normal combustion operation are shown in Figure 2-44. During normal combustion, the ion current decreases to zero after combustion. For partial combustion, the ion current remained during the exhaust stroke. Thus, the signal can not be divided into 2 phases as shown in previous topic. During misfiring, the signal can be observed well after the exhaust valve opens.

The research also showed the ion signal when the EGR was changed, as shown in Figure 2-45. The early part of the curve corresponds to 0% of EGR, the middle to 2.5% and the lower to 5%. Peron et al. (2000) stated that the EGR rate influences greatly the flame front ionization, depending on the location of the sensor.

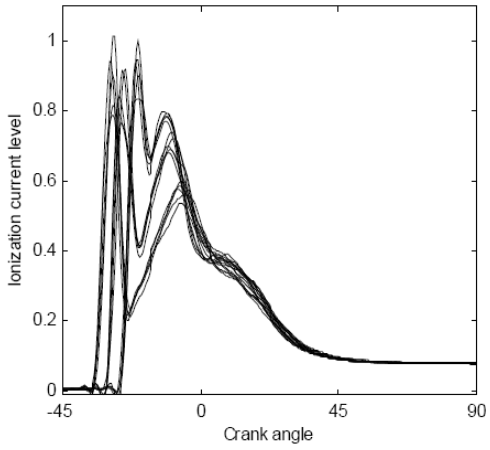

Figure 2-45: Ion current from different EGR levels (Peron et al., 2000)

Ion current sensors are a next step in engine sensor technology which can be used to optimise the combustion. In order to control combustion, information from the early combustion's state can be used. Therefore it is important for control system development to understand factors involving the combustion behaviour. Ion current sensors can help with this task.

2.3 Engine simulation

Computer simulations are useful tools for engineering. They help engineers solve complex problems and predict physical events. Heywood (1988) explained the benefits of engine modeling of:

- Developing a more complete understanding of the process under study from the discipline of formulating the model.
- Identifying key controlling variables to provide guidelines for a more rational and therefore less costly experimental development effort.
- Predicting engine behaviour over a wide range of design and operating variables to screen concepts prior to major hardware program.
- Determine behaviour and tradeoffs, and if the model is sufficiently accurate, to optimize design and control.
- Providing a rational basis for design innovation.

The simulation is divided into two types, they are:

1) One dimension (1D) simulation.
2) Two (2D) or three (3D) dimension simulation.

These two types of simulation are used for different purposes. 2D and 3D simulation software packages from ANSYS and FEA are mainly used for academic studies. The software is used to study data in both vector and scalar form. 1D simulation packages, such as Ricardo Wave and GT-Power are used for design and development in the automotive industry.

Maloney (2004) provided a diagram explaining the use of 1D simulation as shown in Figure 2-46. The engine model was built and run at a test point with Simulink. The results were then collected and analysed by the MBC toolbox before generating the code for a real engine controller.

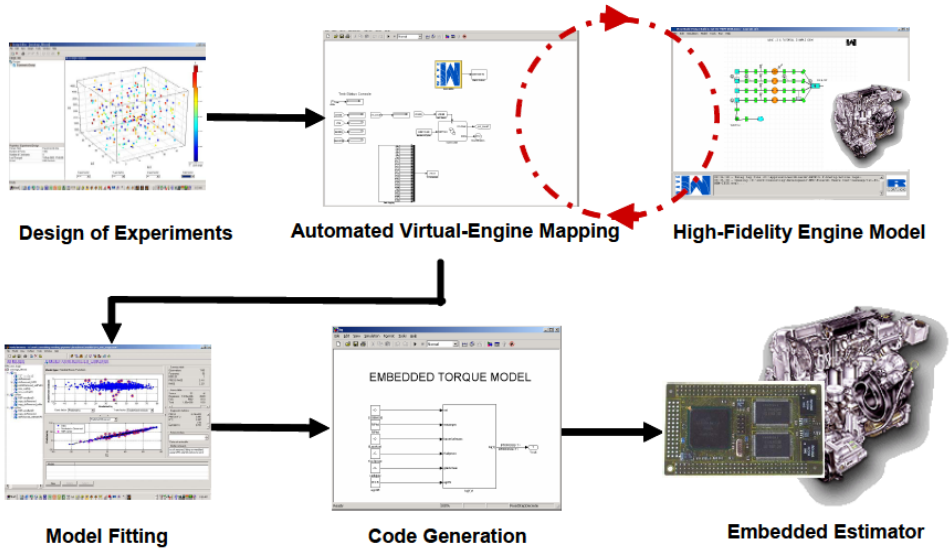

Figure 2-46: Flow diagram of 1D simulation (Maloney, 2004)

Considering cyclic variation, Tinaut et al. (2000) claimed that the phenomena is not easy to determine experimentally because the difficulty in controlling and measuring the changes of any one of the factors while keeping other factors constant. One way of tackling this problem is by using a computer simulation, which includes a sufficient description of the basic causes to check how these factors contribute to cycle to cycle variations.

2.4 Conclusion

The literature review was used to gain knowledge of cold start, cyclic variability and engine simulation which are relevant to the work in this thesis. The experimental work in this thesis is targeted towards cold start conditions in gasoline engines. The aims are to achieve a fast catalytic convertor light-off temperature, and reduced emissions and cyclic variations. Although researchers, in the past, have studied cyclic variations in combustion under lean mixture fuelling conditions, there has been less attention paid to rich mixture operating conditions. This thesis will use the experimental data from cold start condition which includes both rich and lean mixture fuelling to extend the knowledge of cyclic variability in gasoline engines. The research will aim to incorporate predictions of cyclic variability as a function of in cylinder air/fuel ratios and residual gas fractions as these are clearly major factors contributing to cyclic variability. The effect of turbulence and spark induced factors around early flame growth have also been shown to be important although these effects are not well represented in a 1D simulation and so are impractical to include in the current research. Future work may be able to address this by the use of an ion current sensor to obtain some qualitative data relating to turbulence and early flame growth, but this instrumentation was not available as part of the current research.

Chapter 3

Test Facilities and Design of Experimental

In order to understand the effect of engine control on catalyst light-off temperature, an experiment to investigate the effect of engine control parameters on cold start condition was introduced. The experiment was focused on improving catalytic light-off by using a secondary air technique. There were five parameters that had direct effect on catalyst temperature considered: engine speed, spark angle, load, lambda and secondary air. In this chapter, the details of the engine used in the research and the design of experiment are explained.

3.1 Test Facilities

The test facilities for this research were provided by the Powertrain and Vehicle Research Centre (PVRC) at the University of Bath and the work in partnership with Mahle powertrain. The details of engine and the test facilities are discussed below.

3.1.1 Engine

The engine was an Audi 1.8-litre engine (Figure 3-1) with a modified exhaust manifold that had been used in an earlier research project (Bannister, 2007). The engine's turbocharger had been removed, thus the engine operated as a naturally aspirated engine. The technical data of the engine is shown in Table 3-1 (Pfalzgraf et al., 2001).

Another modification on this engine was the addition of a secondary air pump. In order to control the secondary air flow to achieve 15 kg/hr at extreme test conditions, which involved operating the engine at 1500 rpm, 1 bar BMEP with a retarded spark angle of

15 degrees ATDC, the original pump had been replaced with a bigger pump. The pump was driven by an external power supply that provided an adjustable voltage for the air flow control rate.

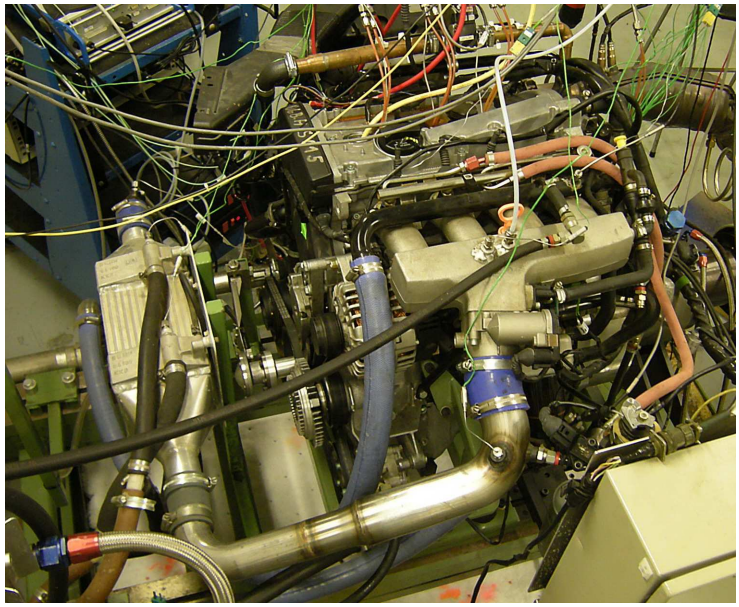

Figure 3-1: The Audi 1.8T research engine.

Table 3-1: Audi 1.8-litre engine technical data.

Characteristics	Audi 1.8-litre engine
Displacement	1781 cm^3
Bore	81 mm
Stroke	86 mm
Connecting rod Length	144 mm
Inlet valve lift	7.67 mm
Exhaust valve lift	9.3 mm
Intake valve spread angle	190 ^oCA
Exhaust valve spread angle	200 ^oCA
Compression ratio	9.3
Firing order	1-3-4-2
Valve timing measured at 1 mm valve lift	
Inlet valve opens	18 ^{o}ATDC
Inlet valve closes	28 ^{o}ABDC
Exhaust valve opens	28 ^{o}BBDC
Exhaust valve closes	8 ^{o}BTDC

3.1.2 Control data acquisition system

As can be seen from the diagram in Figure 3-2, the engine was directly coupled to an air-cooled 200kW AC dynamometer for measuring engine torque. According to the test conditions, the original lambda sensor would not activate until the sensor reached its operating temperature. Therefore, an additional lambda sensor was installed on the exhaust manifold near the inlet of the catalytic converter. As a result, the lambda was able to be measured from the very beginning of a cold start test until the end of the test period. The exhaust gases from the catalytic converter were drawn into Horiba MEXA-7000 emission analysers measuring the concentration of the gas species. Pre-catalytic and post-catalytic gases had been measured by analysers named "MEXA1" and "MEXA2" respectively.

A computer running Orisis software was used to record data by using a synchronised signal from an engine crank angle sensor and in-cylinder pressure from a Kistler spark plug. INCA software running on another computer was used for observing and editing engine parameters inside the engine control unit (ECU). Some important additional parameters were handled by a computer running the CADET software, for example, spark angle, mass air flow etc. The CADET computer was mainly used for data acquisition and test cell control.

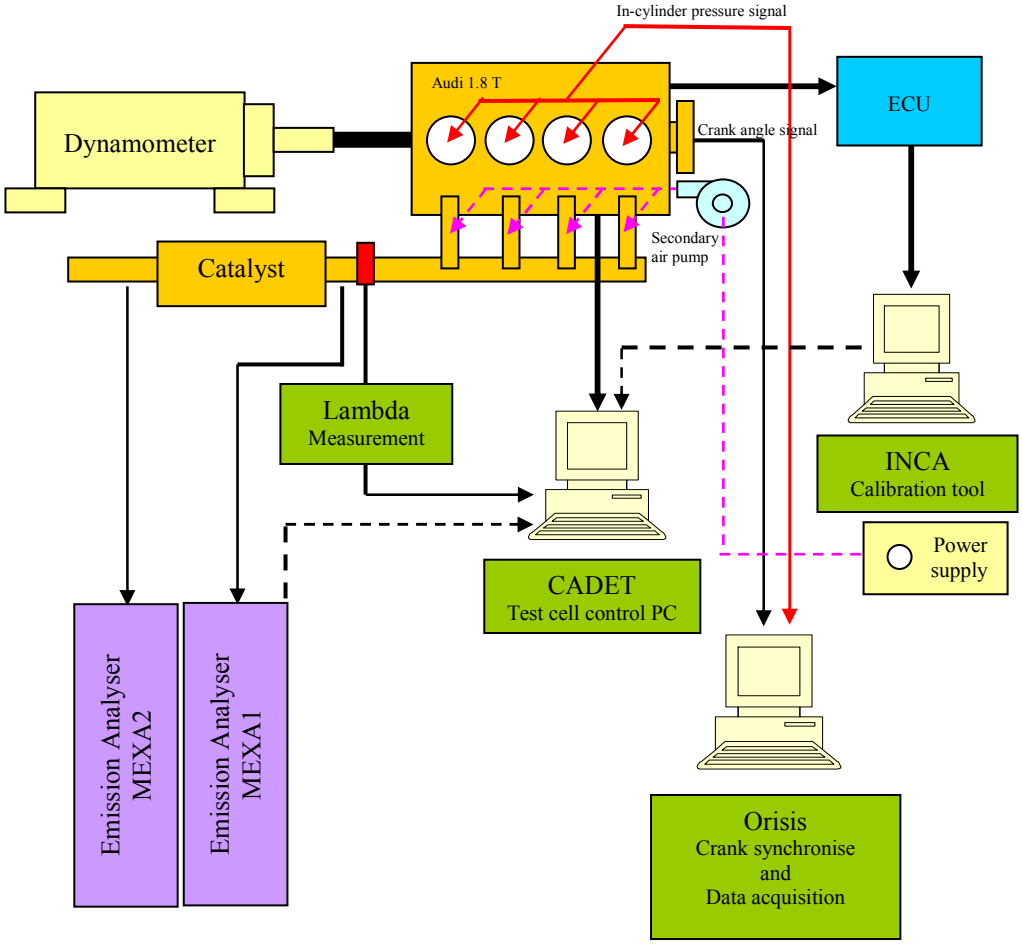

Note:

- *The CADET computer is used to record all the information from the installed sensors and some of selected data that had been sent from the INCA computer.*
- *The INCA computer is used to access the ECU of the engine and allow the user to modify parameters and the engine map.*
- *The Orisis computer is used to record in-cylinder pressure and crank angle data.*

Figure 3-2: Engine test system diagram

3.2 Design of experiments

Using an existing engine that has a secondary air pump system for reducing emissions, the aim is to understand the effects on the catalytic light-off time of different engine parameters. The five control parameters in this test are: engine speed, lambda, spark angle, load and air flow from the secondary air pump. Those control parameters are the factors that had direct effect on catalyst temperature. The *Box-Behnken designs* technique from the model based calibration (MBC) was used to determine the setting for each test points. The technique is suitable for a small number of factors and only three levels per factor are required (Matlab, 2008). This method gives a result that focuses on extreme factor combinations and the number at the corners are not required. Design points are targeted on the midpoints of the design space and at the centre, thus the design is always spherical in shape. The design used the five factors (i.e. the previously mentioned parameters) as inputs and the result from this design technique will suggest test points based on variations in the five parameters.

The maximum and minimum values of the five factors, mentioned previously, were selected by using personal knowledge from Mahle engineers and also aimed to cover the range of possible setting (see Table 3.2). Lambda was varied from rich to lean for comparison. Spark timing was focused on retarded operation because retarded spark timing can lead to increase gases temperature in the exhaust port. Engine speed was in the range from 900 rpm (which is slightly higher than normal idle of engine speed) to 1500 rpm (which is the slightly high for customer point of view). Secondary air flow was the most important aspect of this technique so the test covers the range from no air flow to a maximum flow rate that the pump can perform that is 15 kg/hr. Finally, load was taken in to account in the test, because during cold start conditions the engine load can vary depending on the amount of friction within in engine and engine accessories including alternator and heater. Considering the engine load from these conditions, the load is relatively low thus the tests only varied the load from 0 to 1 bar BMEP.

By applying the Box-Behnken design technique, the design test points formed a spherical shape as can be seen from Figure 3-3. Regarding to the design technique, most

of the test points covered the values in the middle range and to some of the extreme conditions, as shown in Table 3-3.

Table 3-2: Maximum and minimum value of MBC input parameter

Parameters	minimum	maximum
Lambda	0.78	1.1
Spark timing (^{o}ATDC)	0	15
Speed (rpm)	950	1500
Secondary air (kg/hr)	0	15
BMEP (bar)	0	1

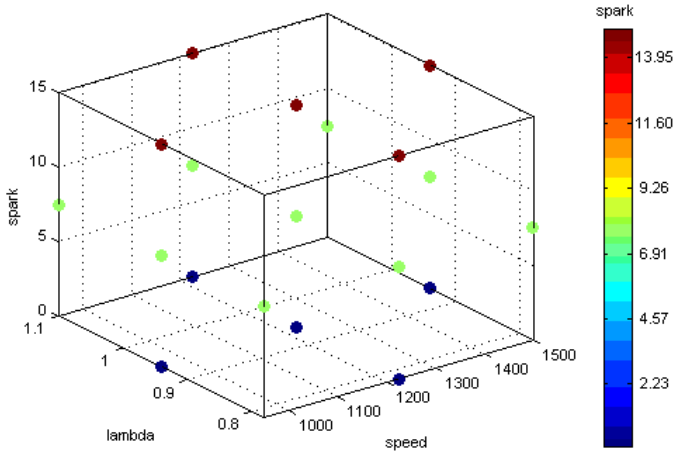

a) Distribution of the test points and target on the mid-range of the studied parameters

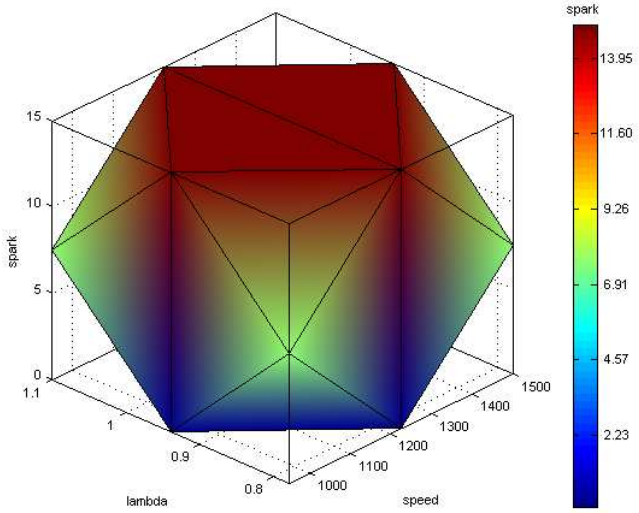

b) Overall shape of design test point by Box-Behnken designs technique which shows spherical in shape.

Figure 3-3: Test point selection by Box-Behnken designs

Table 3-3: Test points for the catalyst light-off experiment.

Test Point #	Lambda #	Spark (degree ATDC)	Speed (rpm)	2nd air injection (kg/hr)	Load (bar BMEP)
1	0.78	0	1225	7.5	0.5
2	0.78	15	1225	7.5	0.5
3	1.1	0	1225	7.5	0.5
4	1.1	15	1225	7.5	0.5
5	0.94	7.5	950	0	0.5
6	0.94	7.5	950	15	0.5
7	0.94	7.5	1500	0	0.5
8	0.94	7.5	1500	15	0.5
9	0.94	0	1225	7.5	0
10	0.94	0	1225	7.5	1
11	0.94	15	1225	7.5	0
12	0.94	15	1225	7.5	1
13	0.78	7.5	950	7.5	0.5
14	0.78	7.5	1500	7.5	0.5
15	1.1	7.5	950	7.5	0.5
16	1.1	7.5	1500	7.5	0.5
17	0.94	7.5	1225	0	0
18	0.94	7.5	1225	0	1
19	0.94	7.5	1225	15	0
20	0.94	7.5	1225	15	1
21	0.94	0	950	7.5	0.5
22	0.94	0	1500	7.5	0.5
23	0.94	15	950	7.5	0.5
24	0.94	15	1500	7.5	0.5
25	0.78	7.5	1225	0	0.5
26	0.78	7.5	1225	15	0.5
27	1.1	7.5	1225	0	0.5
28	1.1	7.5	1225	15	0.5
29	0.94	7.5	950	7.5	0
30	0.94	7.5	950	7.5	1
31	0.94	7.5	1500	7.5	0
32	0.94	7.5	1500	7.5	1
33	0.78	7.5	1225	7.5	0
34	0.78	7.5	1225	7.5	1
35	1.1	7.5	1225	7.5	0
36	1.1	7.5	1225	7.5	1
37	0.94	0	1225	0	0.5
38	0.94	0	1225	15	0.5
39	0.94	15	1225	0	0.5
40	0.94	15	1225	15	0.5
41	0.94	7.5	1225	7.5	0.5
42	0.94	7.5	1225	7.5	0.5
43	0.94	7.5	1225	7.5	0.5
44	0.94	7.5	1225	7.5	0.5
45	0.94	7.5	1225	7.5	0.5
46	0.94	7.5	1225	7.5	0.5

Low Middle High

3.3 Setup parameters

In order to run the tests and follow the design test points, the engine was prepared by modifying the parameters to constrain its behaviour. Therefore, the engine was operated with the same behaviour during each test period, which was 120 seconds, apart from the design factors that had to follow the condition from the design test point.

The factor to be modified can be changed via the INCA computer. The results from the default settings show that there are three signals that needed to be adjusted before performing the test. These are:

- *Camshaft position*

  Camshaft position was shifted after the engine had been started thus this position need to be controlled.

- *Catalytic heating time*

  According to the study in this thesis, the catalytic heating time has to be extended to 120 seconds.

- *Component protection*

  Component protection is linked with the smoothness and range of a studied parameter. This will be discussed later.

3.3.1 Camshaft position

During normal operation, the threshold temperature of the engine for switching camshaft position is low therefore the camshaft always shifted to another position during the test period. In order to prevent these mechanisms, the temperature threshold was adjusted to a value that the engine is unlikely to reach. According to the diagram in Figure 3-4, the camshaft position is controlled by a parameter called B_nwt, which is affected by three signals, which are:

- tmot - Engine temperature.
- TMNW - Engine temperature threshold for the camshaft adjustment,
- TMNWKH - Temperature threshold.

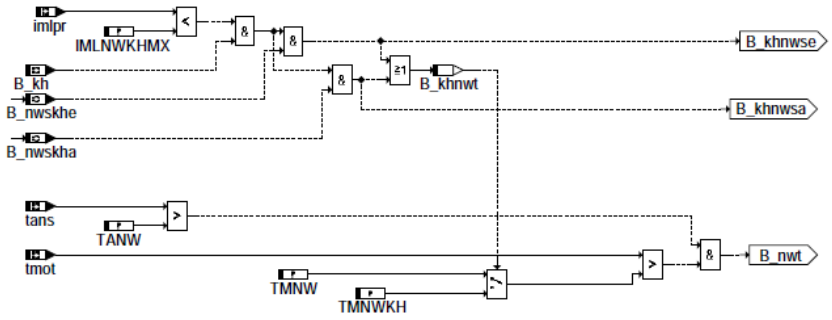

Figure 3-4: Strategy for control of camshaft position

B_nwt's value was made by comparing the tmot signal with the TMNW and TMNW signals. The default temperature on TMNW and TMNW were slightly higher than tmot. After the engine had been started and run for a few seconds, the temperature will reach the required temperature and change the camshaft position. However, the TMNW and TMNW signals are dependent on another signal, thus those two parameters need to be changed. Thus, the values of the TMNW and TMNW signals were set to 100 to ensure the correct camshaft position.

3.3.2 Catalytic heating time

The required test duration time for studying the catalytic light-off event using the secondary air technique was 120 seconds. The time was limited by the secondary pump that may damage when operate longer than those time. In addition, within the extended time, the catalyst light-off time expect to occur with secondary technique. In order to allow this the ECU limits determining the allowable catalyst heating time needed to be changed. Otherwise the pre-set catalyst heating period would expire and the engine settings would return to those defined by other controller features governing the warm-up condition. In order to extend the heating time, there were five parameters that needed to be changed, they were:

- TLMSSLMX – Maximum time for secondary air enrichment at idle.
- TKHLL - Cancelling time for catalyst heating at idle speed.
- TKHLLMX - Maximum time for increased catalyst heating idle speed.
- TKHMX - Maximum time for active catalyst heating.
- MLSUS - Reference of air mass flow integral.

The first four parameters were replaced with a new number of 120 and the last parameter, “MLSUS” was changed by multiplying by a factor of 3.

3.3.3 Component protection

Although the test had been extended to 120 seconds and the camshaft position was stable, during the test the spark angle was still out of control. The reason being was that the engine had another function to decide spark angle which is called “component protection”. This function is used to control the exhaust gas temperature by changing the spark ignition angle to avoid failure of the catalytic converter. According to the test, some conditions have to retard the spark angle by up to 15 degrees ATDC. With the component protection function active, the engine will prevent a component failure by adjusting the spark angle. To prevent these problems and achieve the required spark angle, there are three parameters that involve adjusting the spark angle, they are:

- KFFDLBTS - Factor delta nominal Lambda for component protection.
- KFLBTS - Nominal Lambda for component protection.
- KFDLBTS - Delta nominal Lambda for component protection.

The KFFDLBTS and KFLBTS are set to 1 where as KFDLBTS is set to 0 which enables the spark angle’s target value to be achieved. By deactivate the component protection setting may damage the catalytic converter by high exhaust temperature. However, the converter can resist temperatures up to 1700 Kelvin (Stone, 1999) but before achieve these temperatures the catalyst start to sintering. In addition, the test in this research only lasted for 120 seconds from a cold start condition thus the exhaust temperature is hardly likely to achieve such a temperature.

3.3.4 Discussion

By using the methods described above, the parameters, used in the test, were able to achieve a set point. However the signals of the studied parameters still presented variations but the range of variation was acceptable. Table 3-4 shows a conclusion of the ECU parameter settings as explained above.

The parameter values held in the ECU could be either a constant number or held in a look-up table. If the parameter is a constant, it can be updated with a new single value. If a parameter is held in a look-up table as multiple values, then all those values will need to be replaced in the appropriate manner if operational consistency is to be achieved.

Table 3-4: Final ECU parameters required to extend catalyst heating to 120 seconds

Parameter in ECU	Method of setting
Camshaft position	
TMNW	= 100
TMNWKH	= 100
Catalytic heating time	
TLMSSLMX	= 120
TKHLL	= 120
TKHLLMX	= 120
TKHMX	= 120
MLSUS	Multiply by 3
Component protection	
KFFDLBTS	= 1
KFLBTS	= 1
KFDLBTS	= 0

3.4 Test procedure

For the cold start test, the engine always starts from cold. Before starting the engine and achieving each individual test point, the test cell has to be ready by checking the following:

1. Check the engine's general condition, which includes checking for oil leaks and the coolant level.
2. Open water supply in the test cell and check that the water gauge reads 150 which means the water is at a safe level.
3. Turn on power supply to the ECU.
4. Turn the dynamometer on.
5. Turn the three computers on.

6. Change the ECU settings using the INCA computer to achieve the test point.
7. Press *record* on the Orisis software for capturing the pressure against crank angle data. The software will start to record the data when the engine starts cranking.
8. Turn the emission analysers on and calibrate the analyser before starting each test. Under some test conditions, the engine is operated under rich fuelling without secondary air, thus there are large amounts of emissions remaining in the exhaust. Before calibration, the exhaust can be cleaned by using the analyser to blow air through the exhaust for about 10 minutes. After calibration, monitor the emissions on the CADET computer until the emissions are stable, then start the test.
9. When the test is done, save all the data and turn everything off. Before starting each test, the engine has to be cooled down until the temperature of catalytic converter, engine coolant and engine oil are equal to the ambient temperature. Normally, the test can be preformed two times per day, that is morning and evening time. Therefore, increasing a number of tests per day was achieved by placing put two extra fans near the test engine and turning them on after the test had finished. The engine test cell temperature was set to a temperature of 5 ^{o}C which was a lot lower than ambient temperature. As a result, the engine was cooled by the circulated fresh air that was induced by the test cell. With those methods, the engine was ready for the next test within 3 to 4 hours depending on ambient temperature.

These are the processes had to be performed before each test. Each test has five different settings according to the studied parameters. Changing the engine speed, lambda and spark angle can be done by accessing the ECU via the INCA computer. Each parameter corresponds to a different factor in the ECU. Engine load is changed via the CADET computer and secondary air flow is controlled independently. The details of setting those parameters are explained below.

1. Engine speed

Engine speed during the catalytic converter's heating time is controlled by:

- KFNLLKHM - Nominal idling speed during catalytic heating.
- NSOLMX - Limit of target idle speed.

These two factors are set to the target speed according to the design test point.

2. Lambda

The engine's lambda value is limited to a range which allows the engine controller to decide the air flow and fuel flow rate by itself. Figure 3-5 shows the control network of engine lambda that is limited by an upper limit of lambda which is called *lamlgfmn* and lower limit of lambda which is called *lamlgm*.

The upper limit of lambda is controlled by:

- LAMLGMKT - Lean running limit during short test.
- LAMLGMTM - Lean lambda limit.

The lower limit of lambda is control by:

- LAMFLGS - Lambda enriched engine-running limit for secondary-air injection.

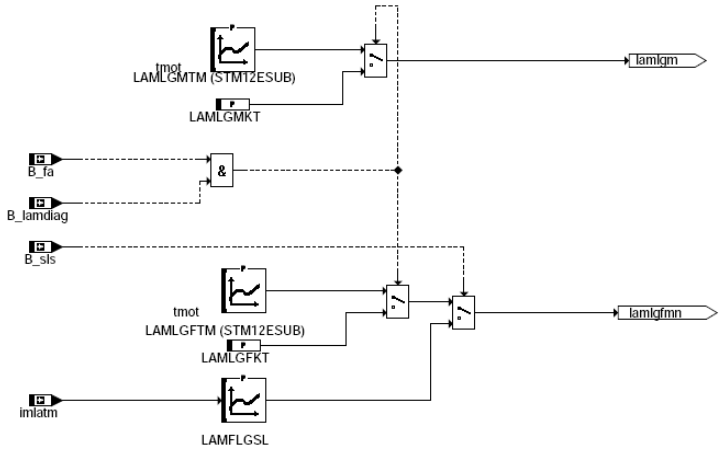

Figure 3-5: Strategy for control of lambda

The upper limit was set to the number of lambda of the design test point, whereas the lower limit was set to a slightly lower value. If the results were still outside of the permitted range, the tests were repeated by varying the range of lambda until the target lambda was obtained. Note that during the warm-up period lambda control was open loop only.

3. Spark angle

Spark angle can be changed by two control parameters in the ECU;

- KFZWMNKH - Map for minimal ignition angle catalyst warm-up.
- KFZWOP - The optimum ignition angle.

As discussed previously, spark angles were controlled by the component protection function, but the function had been disabled thus the spark angle will follow KFZWMNKH and KFZWOP using the look-up table, as can be seen from Figure 3-6.

KFZWMNKH and KFZWOP are dependent on engine speed (nmot) and air charge (rl or rl_w). As a result, the spark angle can change because during the test the engine speed and air charge are unstable. To avoid these variations, the same output number was applied to all boxes which makes the spark angle more stable.

a) KFZWMNKH b) KFZWOP

Figure 3-6: Strategy for control of spark angle

4. Load

Engine torque is controlled by setting the dynamometer via the CADET computer. There are two methods for setting load, they are:

- Control by percentage mode – open loop dynamometer demand.
- Control by torque mode – closed loop using torque feedback.

Using the percentage mode gave a more stable output torque compared to using the torque mode.

5. Secondary air flow rate

A secondary air pump was installed for pumping air into the exhaust manifold. The air pump is connected to a power supply, so that the flow rate is adjusted by adjusting its voltage supply. The rate of air flows were measured by the flow meter which located along the pipe before approach the exhaust manifold. For the test with secondary air technique, the power supply for the pump has to be turned on, before starting the engine.

3.5 Conclusion

The test facilities were introduced in this chapter. The five parameters that involved to pre-catalyst temperature including engine speed, lambda, spark angle, loads and secondary air pump were used for determine test points by *Box-Behnken* designs.

The setting of engine control parameters had been established to achieve the design test conditions. Even though the settings, as discussed previously, remained constant, the variables under investigation will still vary. Thus, an acceptable test was considered using an average value of each of the studied parameters. The average results were accepted if they were within 10% of the demanded value. Tests that had average results outside of this accepted tolerance, those test had to be repeated

Table 3-5 shows the settings of the ECU parameters that allow the engine to perform according to the design test point with the average error less than 10%.

Table 3-5: Final ECU parameters required to achieve target test condition

Test Point	KFNLLKHM & NSOLMX	LAMLGMKT & LAMLGMTM	LAMFLGSL	KFZWMNKH	KFZWOP	RESULTS			
#	(speed)	(upper limit for lambda)	(lower limit for lambda)	(spark angle)	(offset for spark)	Spark (°BTDC)	lambda	SA pump voltage (volt)	SA flow (kg/hr)
1	1230	0.78	0.77	-10	44	-0.65	1.02	8.5 - 9.1	7.04
2	1230	0.78	0.77	-17	25	-15.23	0.93	8.7 - 9.8	7
3	1230	1.2	1.1	-10	42	0.64	1.38	8.5 - 9.0	7.16
4	1230	1.2	1.1	-17	20	-11.74	1.28	8.8 - 9.7	7.07
5	950	0.95	0.94	-10	34.5	-7.533	0.948	-	-
6	950	0.95	0.94	-10	34.5	-7.862	1.594	13	14.03
7	1500	0.94	0.93	-10	32	-7.8	0.93	-	-
8	1500	0.94	0.93	-10	32	-7.89	1.33	16	15.51
9	1230	0.94	0.93	-10	44	-0.75	1.27	8.5	7.45
10	1225	0.95	0.94	-10	42	-0.08	1.19	8.5	7.29
11	1230	0.94	0.93	-17	25	-14.92	1.12	8.5	7.25
12	1225	0.95	0.94	-17	23	-14.34	1.08	8.6	7.21
13	950	0.79	0.77	-10	34.5	-8.33	1.042	8.3	7.01
14	1500	0.78	0.77	-10	32	-8.48	0.92	9	7.34
15	950	1.2	1.1	-10	29	-8.13	1.4	8.4	7.23
16	1500	1.2	1.1	-10	30	-7.11	1.25	9	7.76
17	1230	0.95	0.94	-10	31	-8.31	0.95	-	-
18	1225	0.94	0.93	-10	32	-7.58	0.93	-	-
19	1230	0.95	0.94	-10	31	-8.32	1.5	8.5	15.06
20	1225	0.94	0.93	-10	32	-7.67	1.36	14.5	15.04
21	950	0.95	0.94	-10	45	0.247	1.415	8.5	8.22
22	1500	0.94	0.93	-10	42	-0.64	1.17	9	7.78
23	950	0.95	0.94	-17	25	-14.95	1.182	8.5	7.29
24	1500	0.94	0.93	-17	23	-14.21	1.06	9	7.31
25	1230	0.78	0.77	-10	28	-8.24	0.8	-	-
26	1230	0.78	0.77	-10	28	-8.25	1.18	14.5 - 15.4	14.91
27	1230	1.2	1.1	-10	29	-8.23	1.07	-	-
28	1230	1.2	1.1	-10	29	-8.32	1.52	14.8	14.26
29	950	0.94	0.93	-10	32	-8.18	1.33	8.5	7.91
30	950	0.95	0.94	-10	32	-8.12	1.21	8.3	7.38
31	1500	0.94	0.93	-10	30	-8.38	1.14	9	7.7
32	1500	0.94	0.93	-10	32	-7.13	1.09	9	7.52
33	1230	0.77	0.76	-10	32	-8.37	0.96	8.5	7.12
34	1230	0.78	0.77	-10	32	-8.13	0.91	8.5	6.99
35	1230	1.2	1.1	-10	31	-8.5	1.32	8.5	7.13
36	1230	1.2	1.1	-10	30	-7.6	1.28	8.5	7.37
37	1230	0.95	0.94	-10	44	0.89	0.95	-	-
38	1230	0.95	0.94	-10	44	0.56	1.6	14.6	15.9
39	1230	0.95	0.94	-17	25	-14.13	0.93	-	-
40	1230	0.95	0.94	-17	25	-14.1	1.3	14.6	13.97
41	1230	0.95	0.94	-17	25	-8.13	1.15	8.5 - 9.5	7.25
42	1230	0.95	0.94	-17	25	-8.29	1.15	8.5 - 9.5	7.16
43	1230	0.95	0.94	-17	25	-8.3	1.16	8.5 - 9.5	7.37
44	1230	0.95	0.94	-17	25	-8.3	1.15	8.5 - 9.5	7.17
45	1230	0.95	0.94	-17	25	-8.31	1.16	8.5 - 9.5	7.28
46	1230	0.95	0.94	-17	25	-8.31	1.15	8.5 - 9.5	7.36

Chapter 4

Experimental Results

In this chapter, an analysis of the raw data from the experimental test programme described in Chapter 3 is described. Firstly, the accuracy of the cylinder pressure data has been examined by considering the effects of the cylinder pressure data smoothing method used, pressure pegging, real top dead centre (TDC) determination, and gamma's estimated value in the heat release calculations, and the COV_{imep} calculations. Secondly, the effects of the engine speed, spark angle, load, lambda and secondary air flow on the catalytic light-off time are presented and explained.

4.1 After start condition

For every test point, the engine had to start from cold and achieve a target load, lambda, and engine speed. Thus, the engine had to add extra energy by increasing air mass flow, the rate of fuel injected per cycle, and changing the spark angle during the "after start condition" period before moving on to the control period for each test point.

As can be seen, from the results of Test #1 shown in Figure 4-1, although the engine was set to run at 1225 rpm with the spark angle at TDC, the ECU tried to optimise the air flow rate and the spark angle to overcome all the friction in order to achieve the test condition after the engine had been started. The engine reached a maximum speed of 1373 rpm and the spark angle was advanced to 15 degrees BTDC before gradually reaching the setting value. According to the results, this stabilisation period lasted about 6 to 15 seconds depending on the test condition. The results suggested that during these periods there was another feature within control strategy active in the after start condition, before the ECU responsed to the setting parameters. At the end of the test,

the control strategy changed the condition (i.e. state) from the catalytic heating period to the warm-up mode so the data during this period was unstable.

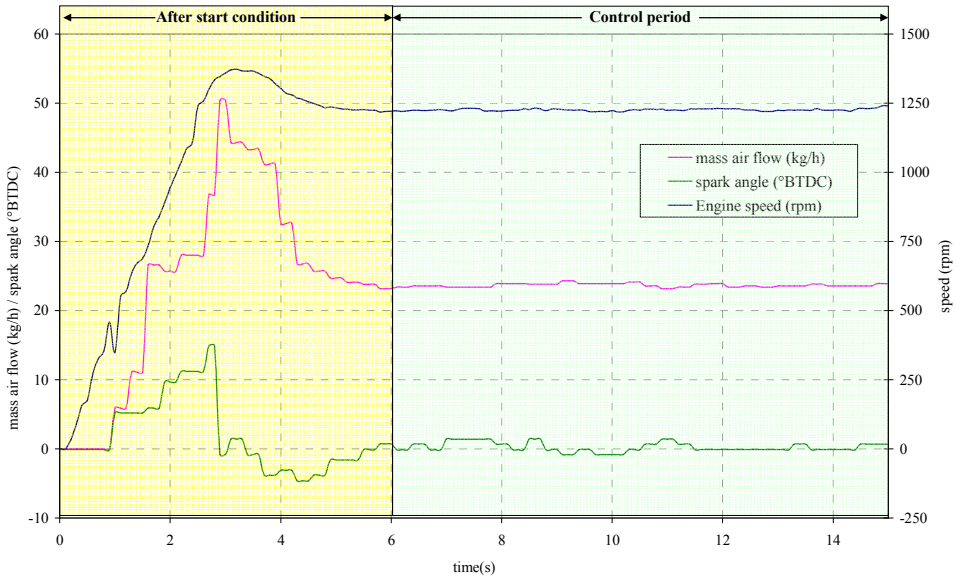

Figure 4-1: After start condition and control period of Test #1

Therefore, the results for speed, lambda, spark angle, secondary air flow, load, pre-catalytic temperature and COV_{imep}, that are presented in this chapter, use an average value from the 20th second to the 110th second period in order to avoid the unstable zone of each test point. For estimation catalytic light-off time which consider the time when 50% of emissions were converted as discussed in the review, the data from pre-catalyst and post-catalyst exhaust emissions had a lag time, thus they were shifted to align with the engine data before consideration.

4.2 Cylinder pressure data processing

A number of analysis techniques have been considered for processing the raw data from the cold start condition. The analysis had been focused on managing raw data before gross IMEP and gross heat release had been calculated.

4.2.1 Smoothing cylinder pressure data

In this experiment, in-cylinder pressure data was recorded for every crank angle degree. Data values that were outside of expected limits were considered as noise. There are several methods for filtering or smoothing data discussed in the literature. Some of these methods were reviewed and discussed before a suitable smoothing method was chosen to process the raw data, these include:

1) The *filtfilt* smoothing method (Tily, 2009).

The *filtfilt* smoothing methods perform zero-phase digital filtering by processing the input data in both the forward and reverse directions (Matlab help file, 2008). Then, the input goes into a lowpass digital Butterworth filter which was generated by specifying the order and cut-off frequency.

2) The *spline* smoothing methods (Zhong et al., 2004).

The *spline* smoothing methods are the smoothest functions that calculate the input data within the given tolerance (Matlab help file, 2008). A piecewise polynomial is calculated and the gradient of the current is matched at each junction

3) The *rloess* smoothing method (Matlab help file, 2008).

The *rloess* smoothing method use weighted linear least squares and a 2^{nd} degree polynomial model to smooth the input data (Matlab help file, 2008). The method assigns zero weight to data outside six mean absolute deviations. The method uses a span (refers to a percentage of the total number of data points, less than or equal to 1) to smooth the data.

Each smoothing function has parameters for varying the smooth curve to achieve the best fit. The *filtfilt* method has two parameters for changing: “order” and “cut-off frequency”. The *spline* method only has “tolerance” for tuning whereas the *rloess* method has “span” as a parameter. In order to compare these three smoothing methods, code was created in form of a Matlab M-file, and a sample of in-cylinder pressure data was used as can be seen below.

- *filtfilt* smoothing methods

```
%*********************************************************************
% an order n lowpass
NN = 5;
%cut-off frequency Wn
Wn = 0.5;
% Butterworth analog and digital filter design
[B,A] = butter(NN,Wn);
% smooth in-cylinder pressure data from D_11
smooth_1(:,2) = filtfilt(B,A,D_11(:,cycle));
%*********************************************************************
```

- *spline* smoothing methods

```
%*********************************************************************
angle = linspace(1,720,720);
%tolerance parameter
tolerance =0.9;
p_spline_1 = spaps(angle,D_11(:,cycle), tolerance);
% evaluate the "p_spline_1" into a the form of result per crank angle
smooth_1(:,3) = fnval(p_spline_1,angle)';
%*********************************************************************
```

- *rloess* smoothing methods

```
%*********************************************************************
%span parameter
span = 0.05;
smooth_1(:,4) = smooth(D_11(:,1),D_11(:,cycle),span,'rloess');
%*********************************************************************
```

The parameter for each method was changed to obtain the best fit before being compared. Figure 4-2 shows the results of smoothing the pressure data with the three methods. The *filtfilt* and *spline* methods show the line tends to follow the original data which could cause an error. The results from the *rloess* method showed that it tried to smooth the curve by ignoring the noisy point and produced a smooth line.

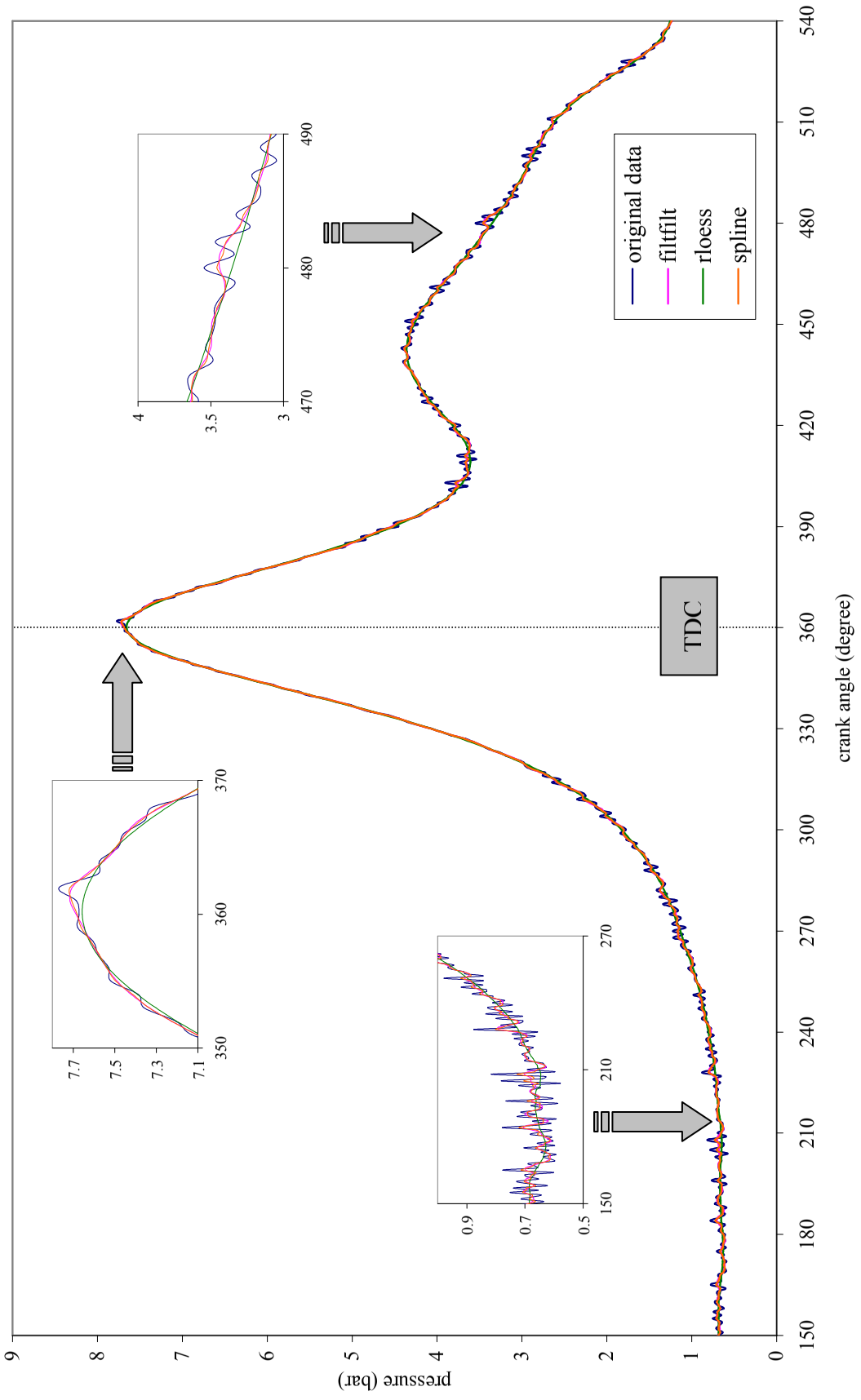

Figure 4-2: Results from different smoothing methods applied to cylinder pressure

In this research, the chosen smoothing method was used before calculating gross IMEP and gross heat release data because these two parameters are calculated directly from the in-cylinder pressure. The functions *filtfilt* and *spline* gave a good fit near TDC, but the signal after the mixture had been ignited and before the intake valves closed was still noisy. This becomes a problem when the rate of heat release had to be calculated because of the difficulty of defining the start of combustion. In summary, *rloess* method gave the best fit for in-cylinder pressure.

The rate of heat release was calculated using the equation shown in *Equation 4-1* (Stone, 1999).

$$\frac{dQ_n}{d\theta} = \frac{\gamma}{\gamma - 1} p \frac{dV}{d\theta} + \frac{1}{\gamma - 1} V \frac{dp}{d\theta} \quad \text{.....Equation 4-1}$$

By inspection of *Equation 4.1*, it can be seen that the rate of heat release depends on pressure (p) against volume of combustion chamber (V). It is also clear that the value of gamma (γ), used in the calculation, will have a significant effect on the result.

Figure 4-3a shows an example of the rate of heat release calculation during the fuel burn period. In this example, the spark timing was at TDC. Therefore, the rate of heat release suggested that *rloess* method gave a better smoothness compared to the other methods. Another problem was defining the end of combustion. Figure 4-3b shows some noise on the cumulative heat release data that causes the determination of the end of combustion to be problematic. The smoothing method could be applied again to the rate of heat release data in order to make the end of combustion easier to define but it can also contribute to further errors.

The main target of smoothing in-cylinder pressure data, in this research, is to obtain a smooth representation of the actual cumulative heat release since this is the beginning for the cyclic variation investigation. Thus, the *rloess* method, with a value for span of 0.05, has been used to smooth the raw in-cylinder pressure data.

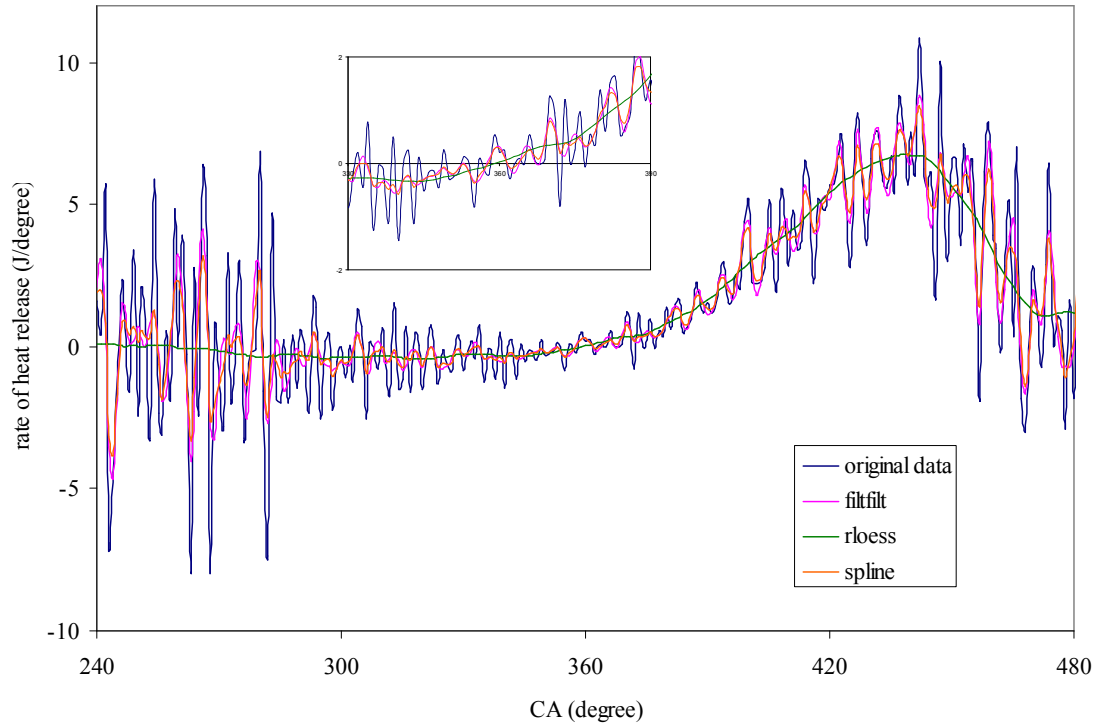

a) Rate of heat release calculated from a cylinder pressure curve filtered using three different smoothing techniques. The *rloess* method produced the best results.

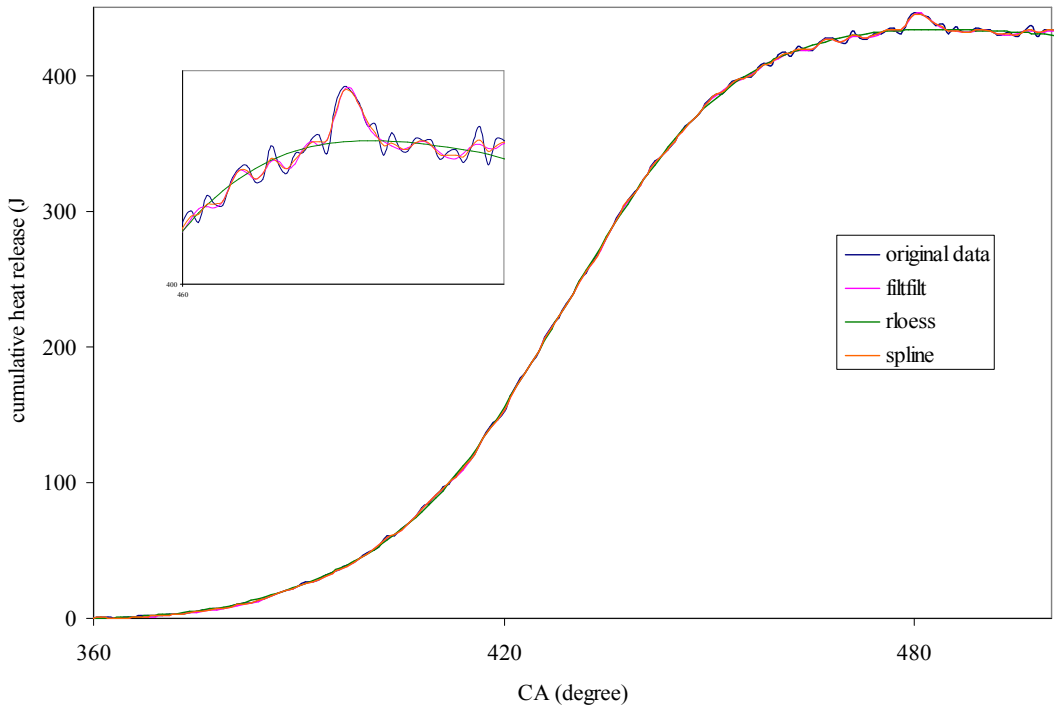

b) Cumulative heat release data showing different smoothing methods. The *rloess* method shows the end of combustion was smoothed and clearly defined.

Figure 4-3: Calculation of heat release using different smoothing techniques.

4.2.2 Cylinder pressure referencing

The raw data not only contained noise, but there was an additional problem with the measuring of the actual level of in-cylinder pressure. Figure 4-4 shows the pressure being shifted up and down. Randolph (1990) explained that this problem is caused by rapid changes in temperature in the pressure transducer's housing. The problem enhances measured cyclic variation by exaggerating the effects of actual cyclic variation in combustion. Randolph (1990) suggested several methods for referencing in-cylinder pressure to some absolute level which was named pressure pegging. According to the available test data, the relevant method, for the experimental data in this research, is pegging pressure by setting the cylinder pressure at inlet bottom dead centre equal to the intake manifold's absolute pressure. The manifold pressure was taken from ps_w (ps_w is the intake manifold's absolute pressure value held in the ECU) which had been sent from INCA to the CADET computer. The average of three points of pressure at inlet bottom dead centre was used to represent the manifold's pressure for an individual cycle. The pressure traces for all cycles in the experiment were shifted to the average value of ps_w.

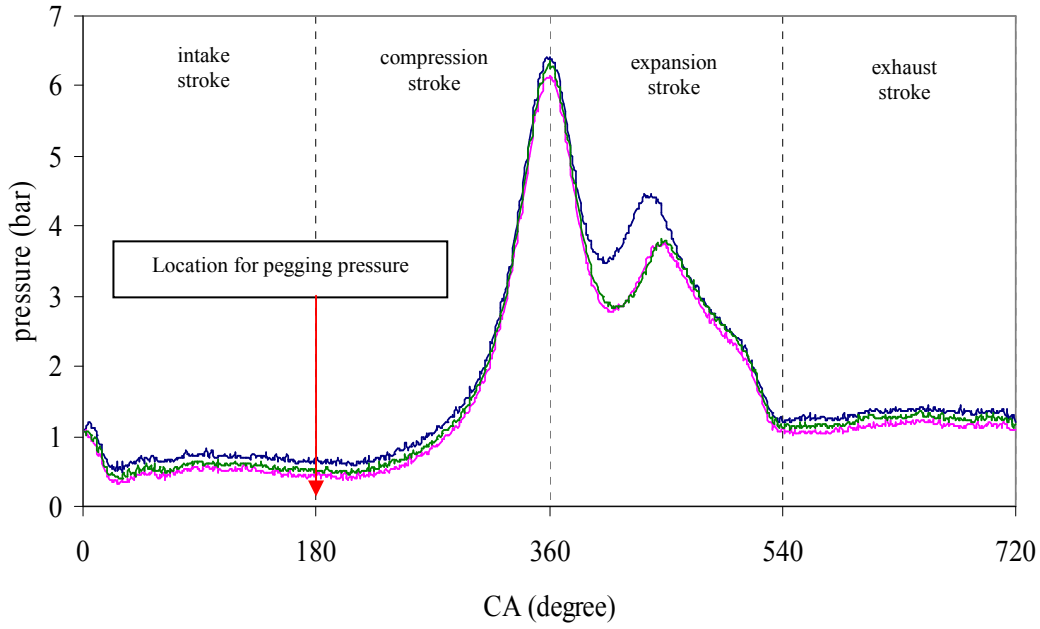

Figure 4-4: Illustration of effect of offsets in in-cylinder pressure.

4.2.3 Real top dead centre

In this section, the problem associated with the position of TDC is explained. Lapuerta et al. (2003) stated that in-cylinder pressure during the IVC to EVO period had a time lag between the peak pressure and the minimum volume because of heat transfer and mass leakage. Pipitone et al. (2008) claimed a calculation error of 10% for IMEP and 25% for heat release caused by the location of real TDC changes every 1 crank angle degree.

Calculations of the gross heat release and gross IMEP were carried out and compared to the results calculated with different locations of TDC. Gross IMEP was calculated by *Equation 4-2* (Taraza, 2000).

$$IMEP = \frac{1}{V_s}\int p.dV \quad \text{.....Equation 4-2}$$

According to *Equation 4-2*, pressure affects the IMEP calculation. Figure 4-5 shows the results for the calculation of gross heat release and gross IMEP from a sample of fifty consecutive combustion cycles with different locations of TDC. As a condition of the test, the mixture was ignited at TDC thus maximum compression pressures were shifted to TDC and were used as a reference values. In order to see the effect of TDC errors, those maximum pressures were shifted forwards and backwards by one degree before the calculations of gross heat release and gross IMEP were performed.

The values of HR increase when TDC is shifted to +1 degree and decrease when TDC shifted in the opposite direction. Within the shift, the difference of the gross heat release from one cycle to the next is small. The results for gross IMEP also show a similar behaviour when TDC was shifted.

The error in gross heat release and gross IMEP, when TDC was shifted, were less than 5% which contradicts with the results from Pipitone et al. (2008). The reason was that the combustion in the experiment was retarded and the mixture was burnt after TDC, thus the majority of additional pressure occurred after TDC. Considering the calculation of IMEP using *Equation 4-2*, the rate per crank angle has a negative value before TDC

and has a positive value after TDC. Thus, varying the location of TDC had less effect because the pressure near TDC of the test was relatively low compared with the normal combustion which has a high peak pressure at TDC. Therefore, when these values are considered with regards to cyclic variability, the results will be valid as long as the calculation uses a similar TDC. Thus, TDC located at 360 CA was used for the calculations in this research.

In addition, the errors from real TDC was low in this research but if the engine frictions are taken into account then the real TDC need to be corrected.

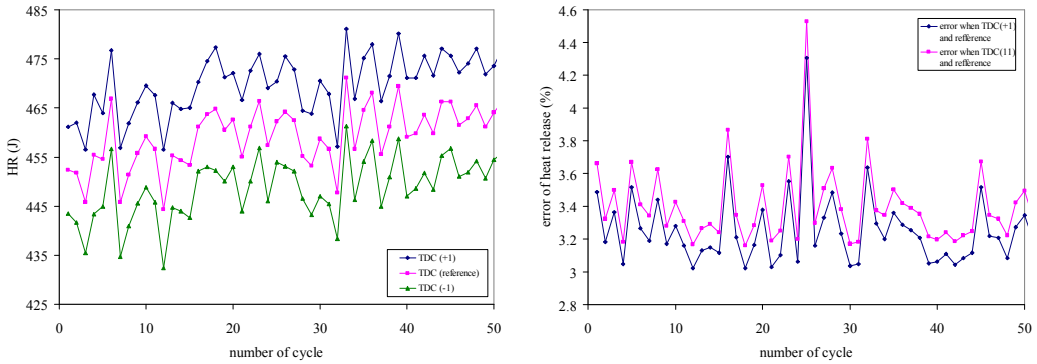

a) Comparison of heat release (left) and error from different TDC (right)

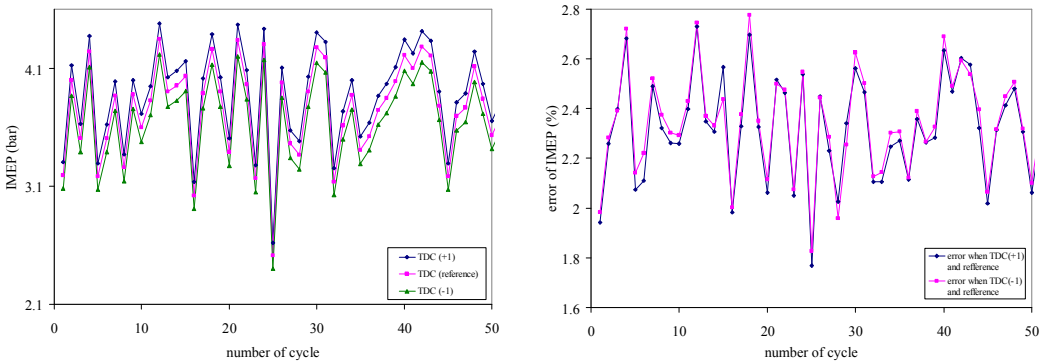

b) Comparison of IMEP (left) and error from different TDC (right)

Figure 4-5: Result of IMEP and HR from different TDC reference points

4.2.4 Gamma selections

Gamma, the ratio of the specific heat capacities, is another parameter that has an impact on the calculation of heat release. In an SI engine, gamma is dependent on the temperature of gases, equivalence ratio and the burnt gas fraction (Heywood, 1988). Kulzer et al. (2009) suggested a method to obtain an appropriate gamma value. He suggests that there are 3 steps in the analysis of a combustion process. Firstly, a deliberately high value of gamma is set in order to obtain the start of combustion. This will result in a distorted cumulative heat release curve with a dip below zero before the heat release phase. This is clearly not accurate but Kulzedr observes that the start of combustion will occur at the point where this distorted cumulative heat release curve has a point of inflection. However, the spark angle used for the tests in this research is known, therefore this process has been ignored. The second step is to, apply an artificially low value of gamma to obtain end of combustion, which will occur at the point of inflection observed the end of the combustion phase. Again this is an artificial artefact induced by the incorrect value of gamma. Once the start and end of combustion are identified the correct value of gamma can be estimated by iterating until a flat cumulative heat release curve is observed after the end of the combustion phase. As a result of the above procedure Kulzer selected a value of gamma of 1.25.

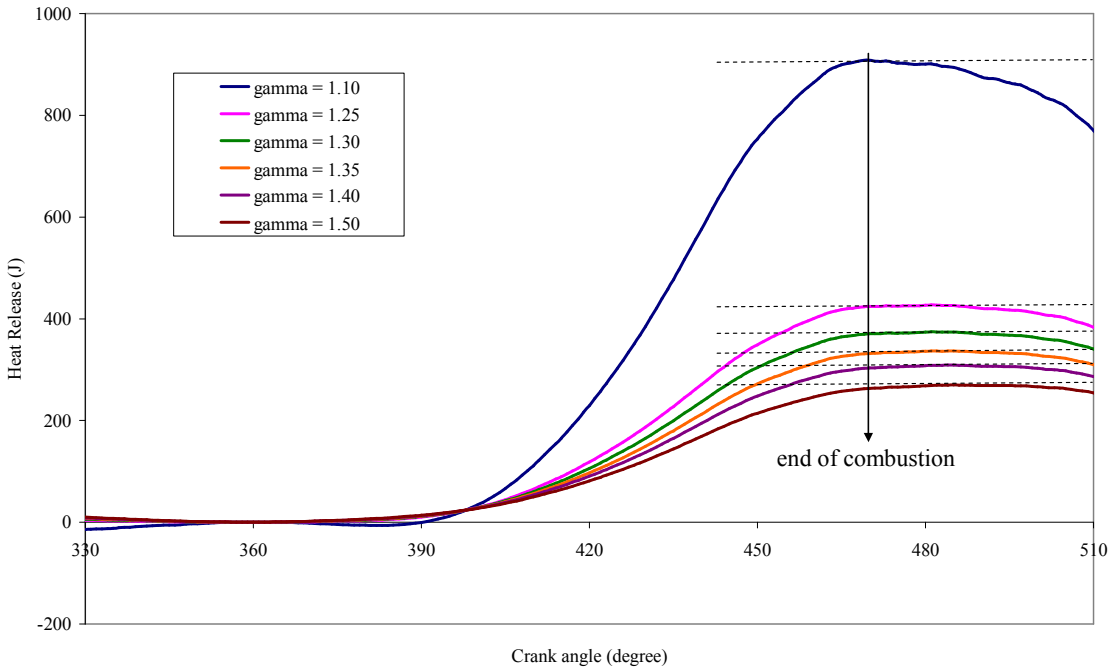

Figure 4-6: Effect on cumulative heat release of different value of gamma (C_p/C_v)

The technique was applied to the cold start test results with gamma varied in step sizes of 0.05 to locate a suitable value. Figure 4-6 shows the end of combustion is located using a low value of gamma at 471 degrees after TDC when a gamma value of 1.10 was applied. The criterion of flat cumulative heat release at the end of combustion specified by Kulzer is met by visual inspection with gamma values of 1.25, 1.30 and 1.35, whereas using other values for gamma indicates that the combustion is still in progress. Although three possible gamma values could be used, it was decided to use only one value for gamma used in this research. In order to find an appropriate value for gamma for the calculations, combustion efficiency was considered.

Two examples, from a series of tests, are used here to illustrate the effect of gamma's value on the combustion efficiency. Maximum heat release was calculated from the fuel mass injected per cycle. Table 4-1 shows the combustion efficiency using different values for gamma.

Table 4-1: Combustion efficiency from different assumption for the value of gamma

Test No.	Fuel consume (g/cycle)	Maximum HR (J) (by fuel)	Combustion efficiency (%)		
			Gamma = 1.25	Gamma = 1.30	Gamma = 1.35
1 (rich)	12.85	566.91	75.39	64.08	56.01
3 (lean)	11.27	497.20	97.95	84.08	74.17

Heywood (1988) claims the combustion efficiency for SI engines, using a lean fuel mixture, is usually in the range of 95% to 98%. The results in Table 4-1 show that a gamma value of 1.25 gave an efficiency within the range that Heywood claims. These results suggest that a value of gamma of 1.25 can be used to calculate heat release, and agree with the findings of Kulzer et al. (2009).

4.2.5 Discussion

Dependent on the pre-test results, the data acquisition system had been set to record in-cylinder pressure with a resolution of 1 degree crank angle over an engine speed range of 950 to 1500 rpm. In order to process the raw data, a Matlab file was created to carry out the following tasks:

- Apply an angular correction of 3 degrees of crank angle, this result in maximum compression pressure located at TDC.
- Smooth pressure data by using the *rloess* method with span value of 0.05.
- Pegging pressure by averaging three points of pressure at inlet bottom dead centre and shift to the average value of inlet manifold pressure from ECU which is presented in ps_w.
- Gross heat release calculated using a gamma value of 1.25.
- Calculation of gross IMEP.

4.3 Result of catalyst light-off time experiment using different engine calibration parameters

From the experimental design test point from the previous chapter, the effects from five factors were considered. According to the design of the test engine, the discussion will start with the effect of secondary air before continuing to assess other factors. Some of the tests have been selected for discussion and the full results can be seen in Table 4-7. The best test conditions for operation, that can be used to achieve a fast catalytic converter light-off time, are discussed at the end of this section.

4.3.1 Effect of secondary air flow on catalyst light-off

The idea of this system is to introduce extra air into the exhaust manifold which allows the remaining fuel from the combustion to be burnt in the exhaust manifold. Thus, the results from Test #25 and Test #26 are discussed first.

Table 4-2: Comparison of results with and without secondary air

Test	speed (rpm)	lambda Before 2^{nd} air	lambda After 2^{nd} air	spark angle (ATDC)	2^{nd} air flow (kg/hr)	load (bar)	maximum pre-cat temp (^oC)	light-off time (s)			average COV_{imep}
								NO_x	CO	HC	
#25	1228.3	0.80	-	8.3	-	0.5	403.4	20.7	-	-	15.3
#26	1228.3	0.80	1.2	8.3	13.8	0.5	649.5	-	11.4	15.8	15.2

Table 4-2 shows the result of the system with and without secondary air and Figure 4-7 shows a comparison between the emissions from these two cases. For the Test #25, the test without secondary air, shows that the HC and CO emissions were not converted during the test period, but NO_x had been converted within 20.7 seconds. The result suggested that under the condition where less oxygen was present in the process, the NO_x emissions were converted by the catalytic converter better than the condition where there was more oxygen, as can be seen from the results of Test #26. This is as expected since it is difficult to reduce NO_x in the presence of excess oxygen.

However, when the engine was operated under rich fuelling conditions (Test #25), the unburnt fuel was converted to high levels of HC and CO emissions. The pre-catalytic temperature from this test was higher than the light-off temperature but the emissions still sustain. The result suggests that not only temperature but also oxygen had an affect on the conversion. In the Test #26, secondary air was introduced and the results show that the CO and HC emissions had been converted within 11.4 and 15.8 seconds respectively.

In order to explain the mechanism of Test #26, the results suggest that under rich mixture fuelling, there was remaining fuel after the combustion had taken place. When the exhaust valves open, the unburned fuel was pushed to the exhaust manifold during the piston moves to TDC. The exhaust gases contain CO and HC that readily combine with air and release heat energy. The air was pumped into the exhaust manifold at the rate of 13.77 kg/hr, and resulted in increasing the pre-catalyst temperature from 403.4 ^{o}C to 649.5 ^{o}C. When the extra air was introduced, the lambda was increased to 1.2 which means that more air was pumped into the exhaust pipe than was needed to burn the fuel. This evidence shows that the air should be reduced to achieve a lambda value of approximately 1, so the unnecessary air can be eliminated. The temperature may increase due to there being no extra air to cool the system and NO_x emission could be converted. Therefore, the system could benefit by achieving a high temperature and reducing the electrical energy that was used to pump extra air.

The interesting results from Test #25 and Test #26 were the peak emission after the engine had been started and the conversion of NO_x emissions under second air was introduced. The peak of emissions during the first couple second caused by rich fuelling that engine tries to overcome the friction and achieve test condition. The engine also started from cold condition so the fuel may be in the liquid form and evaporate when the combustion occur so HC and CO emission increase significantly in the first place. In addition, the fuel cannot mix with air in the cylinder as the fuel was in the liquid form therefore the overall mixture become lean fueling and caused high NO_x emissions. The peak emission significantly dropped when the engine run a couple cycle as the temperature was high enough to evaporate the fuel. The conversion of NO_x emissions in Test #26 shows that the NO_x increased after passed the catalyst. The result may cause by an error of measurement or the efficiency of catalyst that had been used for a long time. Although the results as discuss look interesting but the aims of this research is to investigate the condition that the emission could reach light-off time faster. Therefore, those results could be investigated more in the future work.

Considering the smoothness of the engine based on the average COV_{imep} value, the tests gave similar results for COV_{imep} with secondary air as the tests did without it. Oscillations of pressure in the exhaust manifold could affect the combustion because the gases are able to flow back to the chamber. Potentially the magnitude of this effect could vary as a function of secondary air flow since the secondary air would dilute any back flow into the cylinder. However, the results confirm that secondary air had no affect on COV_{imep} .

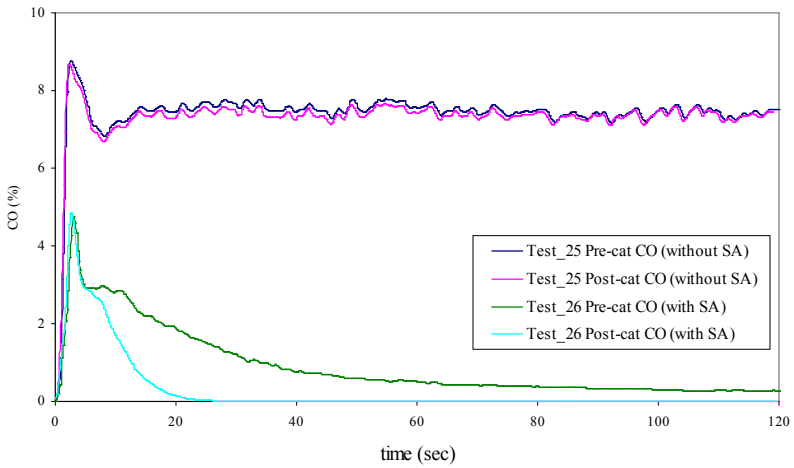

a) CO emissions

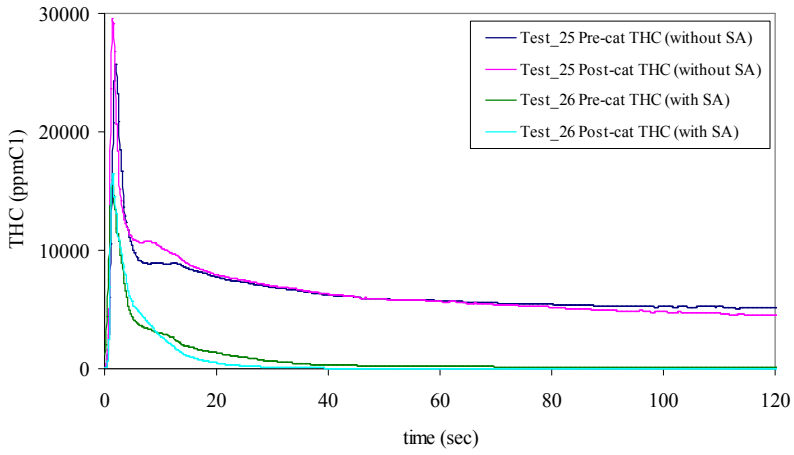

b) HC emissions

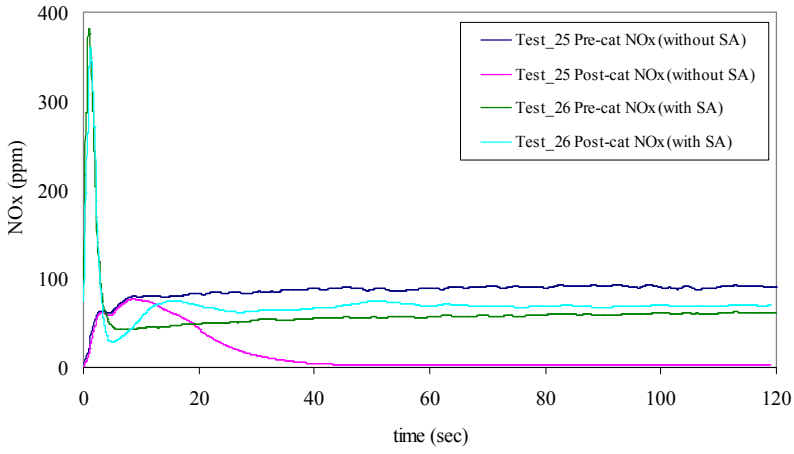

c) NO_x emissions

Figure 4-7: Comparison of CO, HC and NO_x emissions between Test #25 (without secondary air) and Test #26 (with secondary air)

In order to gain a deeper understanding of the burning process in the exhaust manifold, the temperatures from each of the sensors, that were located in different positions on the exhaust manifold (as shown in Figure 4-8), were recorded for comparison.

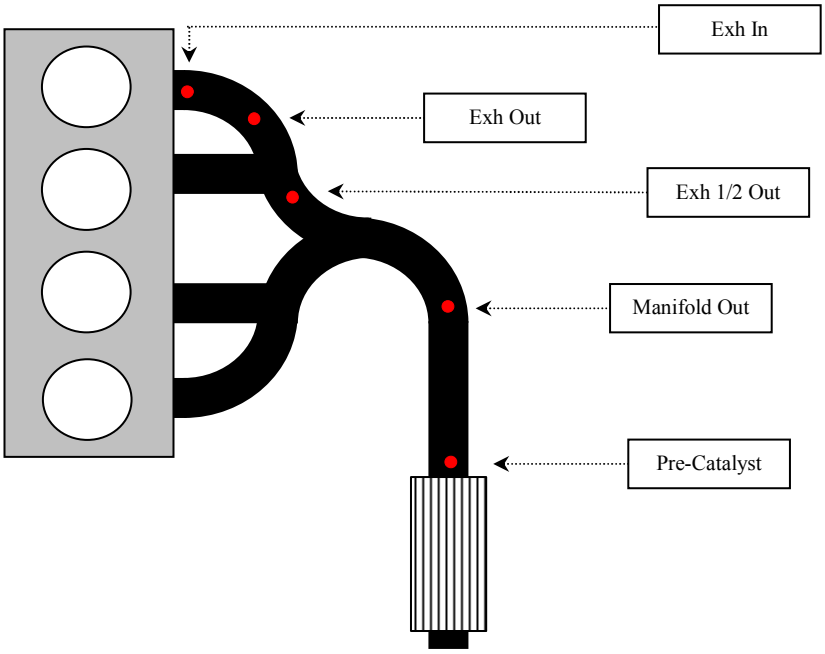

Definition;

Section #1 = distance between "Exh In" and "Exh Out"

Section #2 = distance between "Exh Out" and "Exh 1/2 Out"

Section #3 = distance between "Exh 1/2 Out" and "Manifold Out"

Section #4 = distance between "Manifold Out" and "Pre-Catalyst"

Figure 4-8: Location of sensors in the exhaust manifold

The heat was generated by burning the remaining fuel with extra air that was introduced into the exhaust manifold thus increasing the temperature. Figure 4-9 shows the temperature recorded from each sensor. Without secondary air in section #1, the temperature dropped, because of the heat released to the environment, and continued to drop until the catalytic converter. There was no extra heat energy produced in the exhaust pipe. With the secondary air condition from Test #26, the temperature increased in section #1 and section #2 but afterwards there was no further rise in temperature found. The temperatures from the first two sections suggested that the HC and CO emissions were oxidized with the oxygen from the extra air and released heat energy, as can be seen in the significant drop in HC and CO emissions, shown in Figure 4-7. Note that, heat losses through the pipe walls still continued, but the rate of heat being produced was greater than the loss rate.

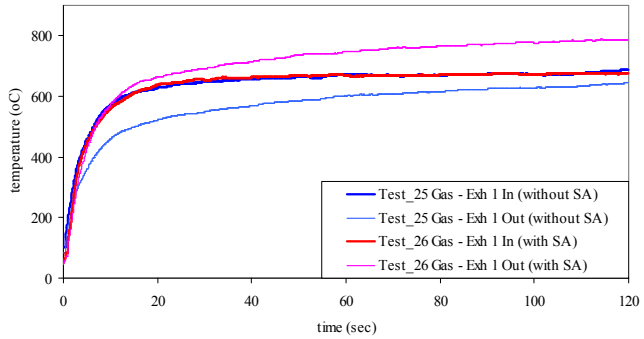

a) Temperature within section #1

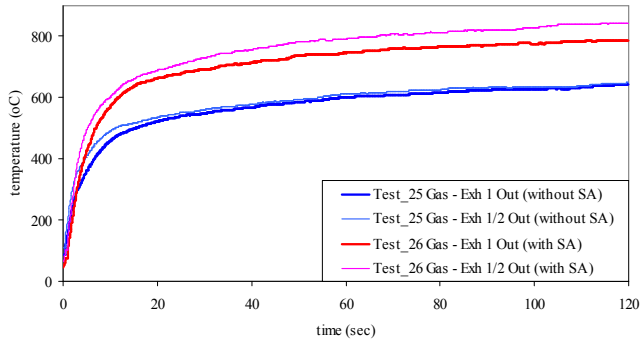

b) Temperature within section #2

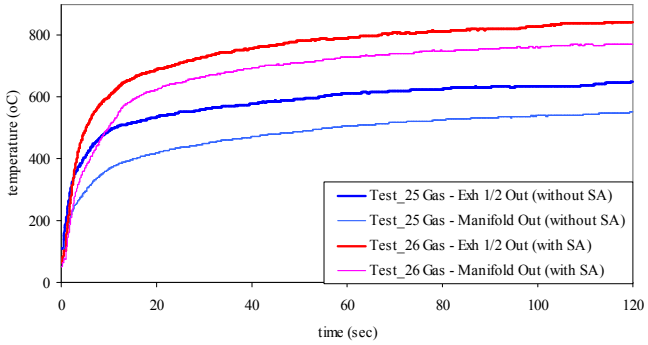

c) Temperature within section #3

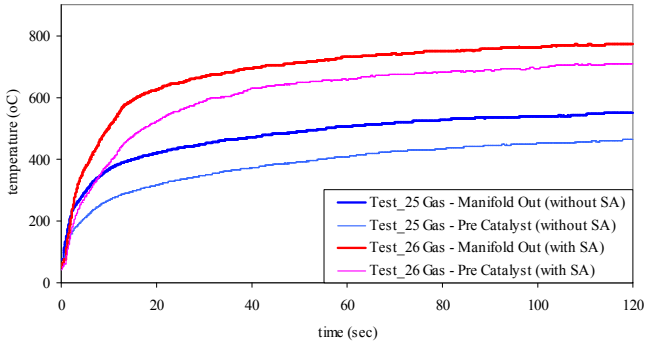

d) Temperature within section #4

Figure 4-9: Exhaust manifold temperatures from Test #25 (without secondary air) and Test #26 (with secondary air)

Considering the emissions in the case of lean fuelling, the emissions also dropped, but there are two possible reasons for this behaviour. Firstly, the emissions had been diluted with extra air, thus the concentration measured by the analyser will be low, although the mass of emissions still remains the same. Secondly, the remaining emissions in the exhaust pipe, especially the HC emissions, may be inhibited from condensing on the wall by the flow of extra air resulting in a high level reading.

These test points show that the fuel can be burnt in the exhaust manifold, but the electrical energy that had been used to drive the air into the manifold was high. A limitation of the air pump that was used is that it can only provide a 15 kg/hr maximum flow within 120 seconds, to protect the pump being damaged from heat and overload. This problem can be solved by using a bigger pump but the electrical energy requirement and cost also increases. In contrast, the small pump has less power to overcome the pressure inside the exhaust manifold and may cause back flow to the second air pipe. Therefore, the size of pump has to be optimised by considering the power consumption and the power required to force the air flow forward.

4.3.2 Effect of lambda on catalyst light-off

As previously stated, under the secondary air condition, engines have to run rich to enable fuel to be burnt in the exhaust manifold. Table 4-3 compares the results when the engine changed from rich to lean fuelling operation. For Test #27, the engine was operated under lean condition, and the pre-catalytic temperature was increased to 537.6 ^{o}C which was more than Test #25 because combustion events (Figure 4-10a) was slower than rich fuelling therefore the engine had to burn more fuel to maintain the same operating conditions. Figure 4-10b shows the calculation of heat releases from Test #27 were slightly higher than Test #25 which suggested the each combustion event release heat more than rich fuelling and resulted in high exhaust gases temperature. For CO and HC emissions from Test #27 were converted within 20.6 seconds. Those are a benefit from operating under lean fuelling but NO_x emissions remained at a constant rate although they passed through the converter. Another disadvantage of lean fuelling was that the average COV_{imep} increased significantly as can be seen in Figure 4-10c. The phase lag plot IMEP shows the IMEPs had a wide spread and caused engine roughness.

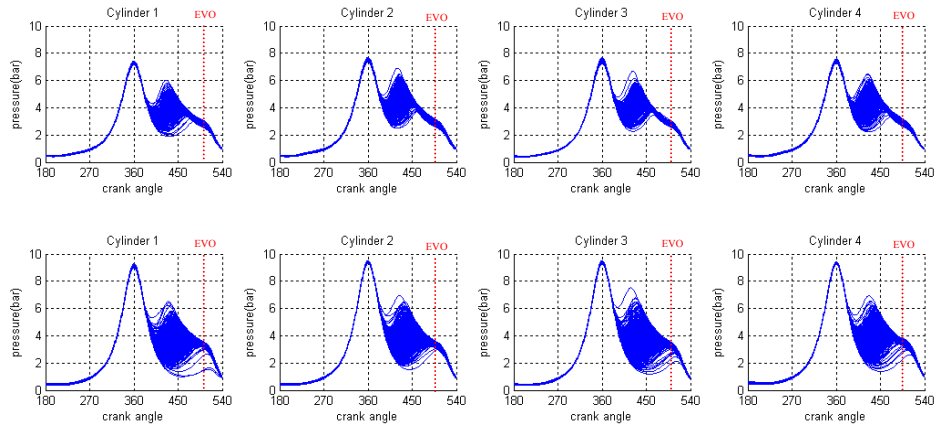

a) Comparison of in-cylinder pressure between Test #25 (top) and Test #27 (bottom)

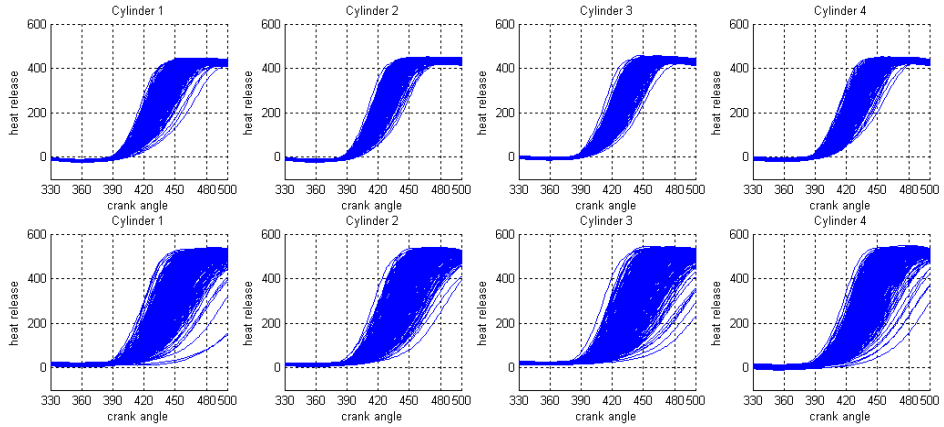

b) Comparison of cumulative heat release between Test #25 (top) and Test #27 (bottom)

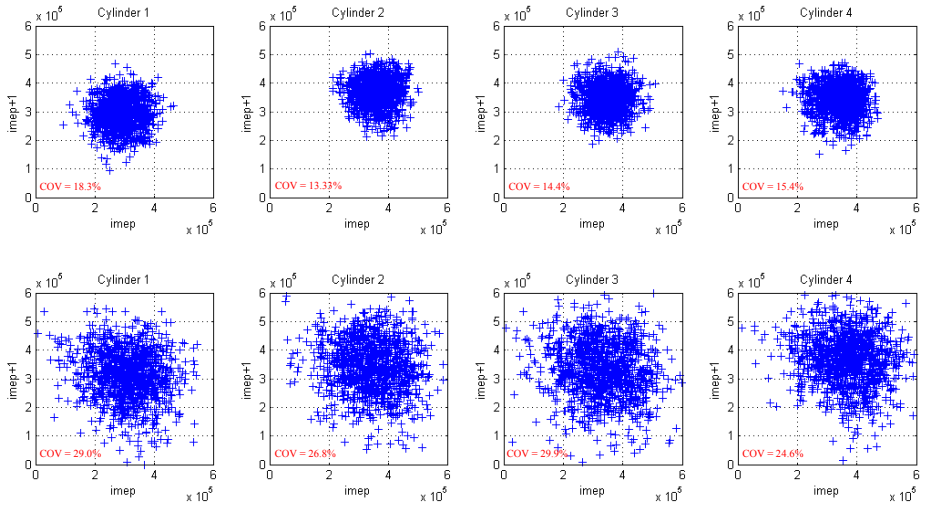

c) Comparison of phase lag plot imep between Test #25 (top) and Test #27 (bottom)

Figure 4-10: Comparison of the results of in-cylinder pressure, cumulative heat release and phase lag plot IMEP between Test #25 (with lambda = 0.8) and Test #27 (with lambda = 1.1).

Table 4-3: Comparison of results from different lambda setting

Test	speed (rpm)	lambda Before 2nd air	lambda After 2nd air	spark angle (BTDC)	2nd air flow (kg/hr)	load (bar)	maximum pre-cat temp (^oC)	light-off time (s)			average COV_{imep}
								NOx	CO	HC	
#25	1228.3	0.8	-	-8.3	-	0.5	403.4	20.7	-	-	15.3
#26	1228.3	0.8	1.2	-8.3	13.8	0.5	649.5	-	11.4	15.8	15.2
#27	1221.7	1.1	-	-8.2	-	0.6	537.6	-	17.8	20.6	27.6
#28	1223.4	1.1	1.5	-8.3	13.0	0.5	502.2	-	17.8	20.2	28.8

When secondary air was used in Test #28, there was no remaining fuel in the exhaust manifold therefore the extra air became a cooling air that caused the pre-catalytic temperature to decrease to 502.2 ^oC. This result proved that the extra air had affected the pre-catalytic temperature, and confirmed the result from Test #26 that the rate of secondary air had to be optimised in order to obtain a maximum pre-catalytic temperature. Once the extra air had been optimised, NO_x emissions could be converted when they passed through the converter.

4.3.3 Effect of spark angle on catalyst light-off

The spark angle in this test was changed from 0 to 15 degrees after TDC. Table 4-4 shows the result of a series of tests with different spark angles. Test #37 and Test #39 proved that a retarded spark angle resulted in a higher temperature at the exhaust port and lead to an increase in the pre-catalytic temperature. Figure 4-11a shows the combustion events were shifted from TDC which required more fuel to burn as can be seen in Figure 4-11b that the calculation of heat release increased significantly. Moreover, the pressures near EVO were higher under retarded spark ignition therefore when the gases release to the exhaust port the temperatures were higher (according to the gas law) than advanced spark ignition. Those contribute to increase exhaust gas temperature. The lambdas from those tests were slightly rich thus the HC and CO emissions could not convert during the test period. The reason was that there were unburnt fuel remains in the exhaust manifold but no extra air. In order to convert the emissions, extra air has to be pumped into the exhaust manifold at a rate which was enough for a reaction to take place. According to COV_{imep} results, a retarded spark angle caused an increase in COV_{imep} as can be seen from phase lag plot IMEP from Figure 4-11c.

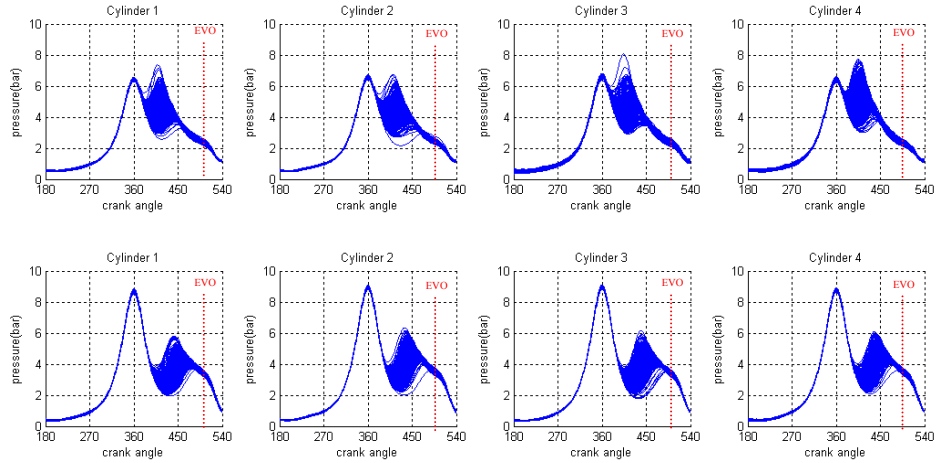

a) Comparison of in-cylinder pressure between Test #37 (top) and Test #39 (bottom)

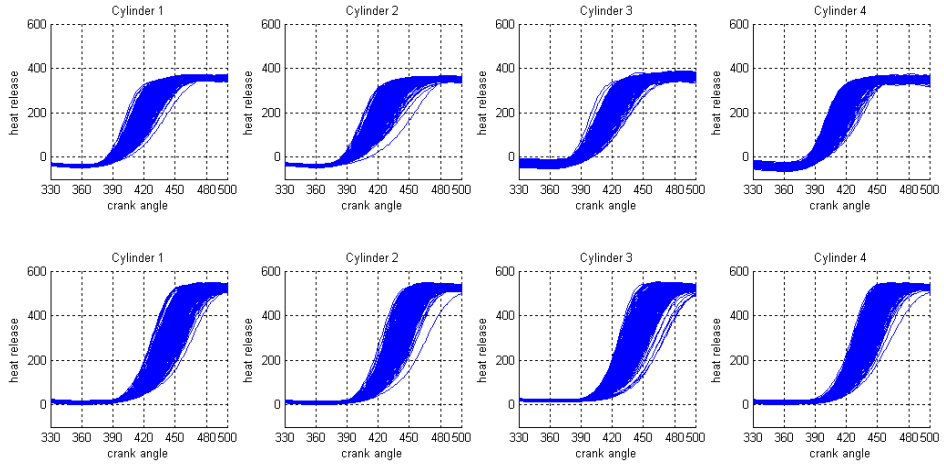

b) Comparison of cumulative heat release between Test #37 (top) and Test #39 (bottom)

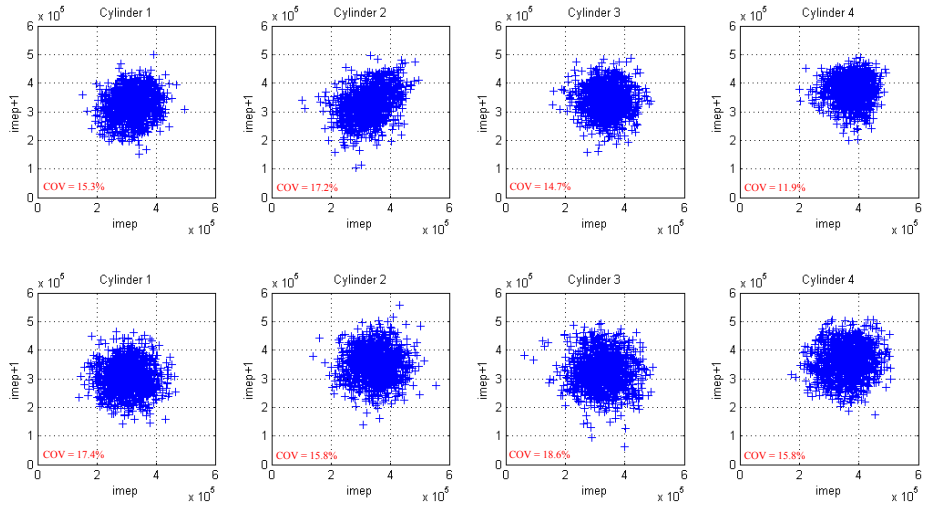

c) Comparison of phase lag plot imep between Test #37 (top) and Test #39 (bottom)

Figure 4-11: Comparison of the results of in-cylinder pressure, cumulative heat release and phase lag plot IMEP between Test #37 (spark at TDC) and Test #39 (spark at 14.2 degree ATDC).

Considering the rich fuelling conditions from Test #1 and Test #2, the retarded spark angle resulted in a high pre-catalyst temperature because when the spark is retarded, the engine has to burn more fuel to maintain speed and load. In some combustion event, the burn was incomplete before EVO, therefore the ratio of remaining fuel that normally presents in HC and CO emissions is higher than when the engine was operated with an advanced spark angle.

For Test #1, the lambda achieved a near stoichiometric value by the pumping of extra air at 5.9 kg/hr, and shows that all emissions were converted within 17.2 seconds. When the spark angle had been retarded (Test #2) while the secondary air was kept at similar rate, the lambda became rich because the engine needed to consume more fuel to maintain the test condition. However, the emissions were still converted but took a longer time, especially the CO emissions. This suggests that a limit on secondary air results in a slower conversion of CO emissions.

Test #3 and Test #4, where the engine operated under lean fuelling conditions, gave an opposite result. The retarded spark angle operations resulted in a faster catalyst light-off. The lambda value shows that Test #4 had less remaining unburnt fuel than Test#3 as the air was pumped at the same rate.

These results suggest that the value of measured lambda, after the secondary air had been introduced, can be used to explain the catalyst light-off time. Under lean measuring, where the measured lambda was greater than 1, the HC and CO emissions light-off time increased. In contrast, under rich measuring, HC emissions achieved light-off time before CO emissions. NO_x emissions reach light-off time early when measured lambda was near stoichiometric ratio and the time increased when measure lambda less then 1 and never achieve light-off time if the lambda greater than 1. The conversion of each emission base on the efficiency of catalytic converter which will be discussed later.

Table 4-4: Comparison of results from different spark angle setting

Test	speed (rpm)	lambda Before 2nd air	lambda After 2nd air	spark angle (BTDC)	2nd air flow (kg/hr)	load (bar)	maximum pre-cat temp (°C)	light-off time (s)			average COV_{imep}
								NO_x	CO	HC	
#1	1228.3	0.82	1.02	-0.7	5.9	0.6	631.1	5.3	11.9	17.2	14.8
#2	1228.3	0.80	0.93	-15.3	5.8	0.5	718.8	14.0	82.2	18.1	16.2
#3	1228.2	1.10	1.39	0.6	6.0	0.5	422.7	-	26.6	35.6	27.4
#4	1192.9	1.09	1.25	-12.7	6.1	0.5	590.8	-	18.1	21.1	28.0
#37	1228.3	0.95	-	0.9	-	0.5	375.3	29.3	-	-	14.8
#39	1228.3	0.94	-	-14.2	-	0.6	510.4	23.3	-	102	16.9

4.3.4 Effect of engine speed on catalyst light-off

Engine speed is another factor that was taken into account in this test. Table 4-5 shows the results of the engine speed tests. Test #14 was expected to achieve an earlier light-off time compared with Test #15, because the engine was operated under rich fuelling conditions and secondary air was pumped into the exhaust system. HC emissions were converted within 19.6 seconds and CO emissions were converted after engine had started and run for 61.4 seconds. These results suggest that the exhaust gases had less air and were slightly rich. The benefit from the rich mixture was in reducing NO_x emissions within 13.5 seconds. The problem of high CO emissions can be solved by pumping in more air into the exhaust pipe which then provides more oxygen for oxidation and can also raise the temperature. The flow has to be limited to that necessary to achieve a lambda of 1 because extra air could cause an increase in NO_x emissions.

Although higher engine speeds give faster catalytic light-off times, the average COV_{imep} also increases proportionality to the speed. Table 4-5 shows the result of the engine operated under lean fuelling conditions on Test #16 with a speed of 1482.8 rpm. This test had a light-off time close to that of the low engine speed in Test #13. The results prove that there was no benefit operating the engine at higher speeds because it not only increased COV_{imep} but also consumed more fuel. In Test #16, the result for the light-off time could be improved by switching off the secondary air pump and increasing the pre-catalyst temperature, but the COV_{imep} will remain at a similar value.

Table 4-5: Comparison of results from different engine speeds.

Test	speed (rpm)	lambda Before 2nd air	lambda After 2nd air	spark angle (ATDC)	2nd air flow (kg/hr)	load (bar)	maximum pre-cat temp (°C)	light-off time (s)			average COV_{imep}
								NO_x	CO	HC	
#13	948.2	0.81	1.04	-8.3	5.9	0.5	529	-	16.1	21.1	14.8
#14	1498.3	0.80	0.92	-8.5	6.1	0.5	706.3	13.5	61.4	19.6	16.2
#15	948.1	1.08	1.41	-8.1	6.1	0.5	387.4	-	28.0	36.8	22.3
#16	1482.8	1.08	1.26	-7.2	6.5	0.5	608.6	-	14.1	16.8	30.7

The results of the engine operating at high speed show that the catalytic converter could achieve a faster light-off time than at low speed. The main reason of this was that at higher engine speeds the engine consumed more fuel to overcome friction and produced more heat than at lower speeds. However, extra air has to be pumped to achieve a lambda value of 1 otherwise emissions will be high again.

4.3.5 Effect of load on catalyst light-off

Varying the load during the test was used to represent the condition of the engine during the initial start operation. Engine load can be changed by friction from different sources such as the alternator or compressor unit. In order to maintain target speed, the engine has to generate more power to overcome these loads by increasing the fuel.

Table 4-6 shows a comparison between the results for the engine operating under different loads. With load of 0.1 bar BMEP, Test #33 shows the pre-catalytic converter temperature was increased to 678.2 °C. In Test #34, the load was increased to 1.0 bar but the pre-catalytic converter temperature was lower than in Test #33 because the remaining fuel from those tests are different, as show in the lambda values, when the secondary air was introduced. In Test #34, the air was pumped to the exhaust pipe at the same rate, as in Test #33, but the lambda value was lower than in Test #33. The lambda value explained the amount of unburnt fuel in Test #34 was more than in Test #33 and caused lower combustion efficiency. These phenomena behave like the combustion of different mixtures that was explained by combustion efficiency.

The light-off time in regard to variations in engine load was slightly different but the average COV_{imep} was different for both rich and lean fuelling conditions. The results show that the COV_{imep} decreased significantly when the load increased. The evidence

shows that there was more air and fuel to be burned at the same condition. Thus, the mixture with same lambda is burned faster when the load increases.

Table 4-6: Comparison of results with different accessory loads

Test	speed (rpm)	lambda Before 2^{nd} air	lambda After 2^{nd} air	spark angle (ATDC)	2^{nd} air flow (kg/hr)	load (bar)	maximum pre-cat temp (°C)	light-off time (s)			average COV_{imep}
								NO_x	CO	HC	
#33	1228.3	0.80	0.97	-8.4	5.9	0.1	678.2	16.6	25.4	19.5	22.9
#34	1228.4	0.80	0.92	-8.2	5.8	1.0	579.3	20.1	24.0	22.6	12.9
#35	1228.6	1.09	1.33	-8.5	6.0	0.1	511.2	-	19.3	23.0	40.6
#36	1217.7	1.07	1.28	-7.7	6.2	1.0	529.4	-	20.3	23.3	22.0

Table 4-7: Results of catalyst light-off from each design test point

Test point	idle speed (rpm)	lambda before SA	lambda after SA	Spark (BTDC)	SA flow (kg/hr)	BMEP (bar)	Maximum Pre-Cat Temp (°C)	light-off time (s)			COV_{imep} each cylinder				average COV
								NO_x	CO	HC	Cy #1	Cy #2	Cy #3	Cy #4	
#1	1228.29	0.82	1.02	-0.73	5.87	0.57	631.11	5.3	11.9	17.2	22.5	12.1	13.2	11.3	14.8
#2	1228.33	0.80	0.93	-15.26	5.84	0.55	718.84	14.0	82.2	18.1	18.7	13.8	15.3	17.2	16.2
#3	1228.20	1.10	1.39	0.62	6.00	0.52	422.71	119.9	26.6	35.6	28.2	27.0	33.8	20.8	27.4
#4	1192.86	1.09	1.25	-12.74	6.06	0`.47	590.78	-	18.1	21.1	29.4	26.1	32.5	23.9	28.0
#5	948.10	0.95	0.95	-7.62	0.00	0.49	337.32	33.6	-	-	13.6	14.1	14.7	13.6	14.0
#6	948.15	0.95	1.59	-7.94	12.85	0.49	339.50	119.3	25.9	34.2	12.9	13.7	15.1	12.1	13.5
#7	1498.37	0.94	0.94	-7.86	-0.04	0.53	527.03	16.6	-	83.2	20.7	18.9	19.1	15.4	18.5
#8	1498.32	0.94	1.34	-7.93	14.35	0.51	564.65	-	12.4	15.9	20.2	18.4	19.8	14.8	18.3
#9	1228.40	0.96	1.28	-0.82	6.32	0.11	391.80	-	21.9	30.5	23.1	19.4	27.9	18.4	22.2
#10	1228.27	0.96	1.19	-0.15	6.14	0.99	415.90	-	24.0	31.2	11.8	11.3	10.7	9.2	10.7
#11	1228.46	0.93	1.13	-14.97	6.11	0.10	589.67	-	16.7	17.5	23.9	20.8	21.9	22.4	22.3
#12	1221.40	0.93	1.09	-14.38	6.08	0.97	641.48	-	16.6	20.2	14.2	12.8	13.7	13.1	13.5
#13	948.16	0.81	1.04	-8.34	5.86	0.52	528.96	-	16.1	21.1	16.2	13.5	15.9	13.8	14.8
#14	1498.31	0.80	0.92	-8.51	6.14	0.52	706.33	13.5	61.4	16.4	19.6	15.5	14.1	15.4	16.2
#15	948.09	1.08	1.41	-8.08	6.09	0.48	387.44	-	28.0	36.8	21.9	22.9	25.0	19.4	22.3
#16	1482.83	1.08	1.26	-7.23	6.51	0.49	608.63	-	14.1	16.8	34.9	30.0	35.1	23.0	30.7
#17	1228.35	0.95	0.95	-8.30	0.52	0.11	441.01	26.6	-	-	23.2	25.3	24.9	18.7	23.0
#18	1228.36	0.93	0.93	-7.62	-0.02	0.99	450.99	24.0	-	-	13.4	11.8	12.6	12.0	12.5
#19	1228.41	0.95	1.51	-8.32	13.92	0.12	446.72	-	18.6	23.2	25.5	21.8	28.5	19.8	23.9
#20	1228.39	0.93	1.37	-7.71	13.90	1.00	485.57	-	18.8	24.7	12.4	11.4	11.7	11.6	11.8
#21	948.04	0.96	1.42	0.22	7.11	0.50	300.72	-	45.8	59.5	12.9	14.4	15.0	13.7	14.0
#22	1498.35	0.95	1.18	-0.68	6.61	0.53	500.17	-	14.7	21.5	17.4	15.6	22.1	13.1	17.1
#23	948.10	0.93	1.18	-15.00	6.12	0.49	450.01	-	23.1	29.6	14.4	13.3	15.1	13.7	14.1
#24	1488.34	0.93	1.06	-14.25	6.09	0.51	718.86	-	11.4	13.5	22.6	18.8	20.5	16.4	19.6
#25	1228.20	0.81	0.81	-8.26	-0.01	0.53	403.36	20.7	119.2	-	18.3	13.3	14.4	15.4	15.3
#26	1228.34	0.81	1.19	-8.27	13.77	0.54	649.52	119.9	11.4	15.8	16.0	15.1	14.8	14.9	15.2
#27	1221.70	1.07	1.07	-8.20	-0.04	0.55	537.60	-	17.8	20.6	29.0	26.8	29.9	24.6	27.6
#28	1223.40	1.07	1.53	-8.32	13.02	0.51	502.23	119.9	17.8	20.2	28.1	29.7	32.7	24.7	28.8
#29	948.22	0.95	1.34	-8.19	6.78	0.11	348.99	2.0	28.8	37.4	19.6	25.3	21.6	16.8	20.8
#30	948.17	0.93	1.22	-8.16	6.23	0.98	371.07	-	28.4	37.0	10.5	9.8	14.9	9.9	11.3
#31	1498.37	0.94	1.14	-8.38	6.51	0.09	584.80	-	13.5	18.3	25.4	25.3	26.6	18.8	24.0
#32	1498.43	0.94	1.09	-7.17	6.32	0.96	618.92	-	13.2	16.8	16.1	14.2	16.4	12.2	14.7
#33	1228.26	0.80	0.97	-8.38	5.89	0.07	678.23	16.6	25.4	19.5	24.8	24.9	20.4	21.4	22.9
#34	1228.41	0.80	0.92	-8.15	5.79	0.97	579.25	20.1	24.0	22.6	14.4	11.5	12.2	13.5	12.9
#35	1228.59	1.09	1.33	-8.51	5.98	0.12	511.19	-	19.3	23.0	39.5	43.9	50.0	29.0	40.6
#36	1217.73	1.07	1.28	-7.67	6.24	0.98	529.41	-	20.3	23.3	21.9	20.8	26.9	18.3	22.0
#37	1228.26	0.95	0.95	0.86	0.56	0.53	375.32	29.3	120.0	-	15.3	17.2	14.7	11.9	14.8
#38	1228.28	0.95	1.61	0.53	14.74	0.54	366.05	-	24.6	34.3	14.3	13.7	17.6	12.8	14.6
#39	1228.29	0.94	0.94	-14.17	-0.04	0.56	510.40	23.3	-	102.7	17.4	15.8	18.6	15.8	16.9
#40	1228.22	0.94	1.31	-14.13	12.84	0.55	577.74	-	15.2	17.3	18.0	16.0	18.5	16.2	17.2
#41	1228.35	0.94	1.15	-8.32	6.13	0.53	507.31	-	18.6	24.0	17.5	15.1	17.2	14.8	16.1
#42	1228.31	0.94	1.16	-8.29	6.02	0.53	506.45	120.0	19.8	24.4	16.9	15.8	17.2	15.2	16.3
#43	1228.44	0.94	1.16	-8.31	6.19	0.57	505.39	-	20.0	24.3	18.1	14.3	16.6	14.1	15.8
#44	1228.41	0.94	1.16	-8.29	6.02	0.53	506.90	-	19.0	24.9	17.0	15.1	17.8	14.6	16.1
#45	1228.35	0.94	1.16	-8.32	6.14	0.50	503.59	-	20.3	23.9	16.6	15.6	17.9	15.8	16.5
#46	1228.37	0.94	1.16	-8.29	6.22	0.51	509.20	120.0	19.5	24.9	16.9	15.3	17.2	15.0	16.1

4.4 Discussion of experimental results

According to the experiment base on secondary air technique, there are two essential parameters that have to consider for engines operating under cold start conditions. Those are unburned fuel in the exhaust manifold and flow rate of the secondary air. Both of them have a significant effect on the pre-catalytic temperature and emissions.

The rate of unburned fuel in the exhaust manifold depends on the engine's operating conditions. Under rich fuelling conditions, the unburnt fuel increases proportional to engine speed, load and spark angle. Therefore, a similar engine lambda could result in different unburnt fuel amounts.

The rate of secondary air is the factor controlling the burning mechanism in the exhaust manifold. The exhaust gases that contained unburnt fuel from rich combustion events were expected to oxidize with additional fresh air and release energy in the form of heat. It is important that fresh air is pumped into the exhaust manifold at a rate that achieves a lambda value of 1, in order to enable the emissions to be converted by the catalytic converter and for all unburnt fuel to be burned.

According to the results, NO_x emissions were converted earlier than the HC and CO emissions for fuel rich exhaust gases. In contrast, NO_x emissions were not converted with lean exhaust gases, while CO emissions were converted faster than HC emissions. These results suggest that the mechanism, of the burning process in the exhaust manifold, behaves in a similar way to combustion, as can be seen from Figure 4-12.

However, there were no differences in COV_{imep} with and without the secondary air system. The results suggest that the variation in COV_{imep} from each test comes from the mechanism of combustion and is not affected significantly by back flow from the exhaust manifold into the combustion chamber.

The mechanism of combustion is dependent on the exhaust gas lambda, spark angle, engine load and speed. Although lean combustion could increase pre-catalytic converter temperature it also contributes to high COV_{imep}. Retarded spark angle and increasing

engine speed resulted in high COV_{imep} which occurred during the expansion stroke. In contrast, increasing the engine load resulted in low COV_{imep} because under high load the engine had to increase the ratio of air and fuel mixture which increases flame speed in the combustion chamber.

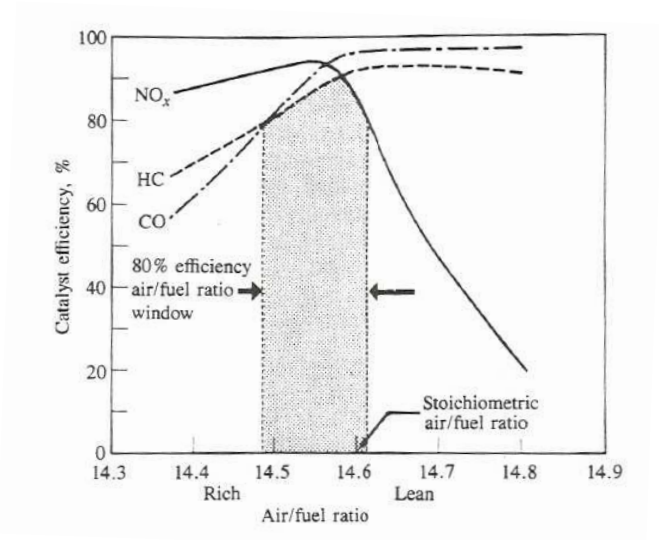

Figure 4-12: Conversion efficiency of catalytic converter (Heywood, 1988)

In accord with the secondary air technique, the remaining unburnt fuel in the exhaust is important, thus a rich mixture is used in this technique. With a rich mixture, retarded spark angle, increasing engine speed or load leads to an increase in unburnt fuel in the exhaust manifold. Due to the secondary air technique, a high flow rate could result in a low temperature because the extra air becomes a cooling gas and dilutes the exhaust gases. Each parameter has advantages and disadvantages depending on the condition thus there are trade-offs on using these factors.

In order to selected the best test point, there are a number of factors that need to be taken into account, they are:

1) Achieving a fast light-off time.
2) Consuming less fuel.
3) Achieving a high temperature in order to heat the catalytic converter and the engine oxygen sensor.
4) Low secondary air flow rate that can reduce electrical power demands and protect the air pump from being damage.
5) Smoothness with low COV_{imep}.

Figure 4-13 shows the results for the COV_{imep} for each test point. There are a number of test points that give a low average COV_{imep} but none of test points have an average COV_{imep} of less than 10%. The percentage was a limit demand from subjective customer acceptance level. Therefore, the values observed seem high and is a reflection of the old port fuel injection technology used with incomplete calibration. Each cylinder had a different COV_{imep} value, which suggests that the mechanism of combustion for each cylinder differed. The results of COV_{imep} for each cylinder could be a result of variations in the amount of fuel injected into each cylinder. Also, variations in air flow, especially under rich fuelling conditions, and in the spark angle that is unstable during the test period, could also be factors.

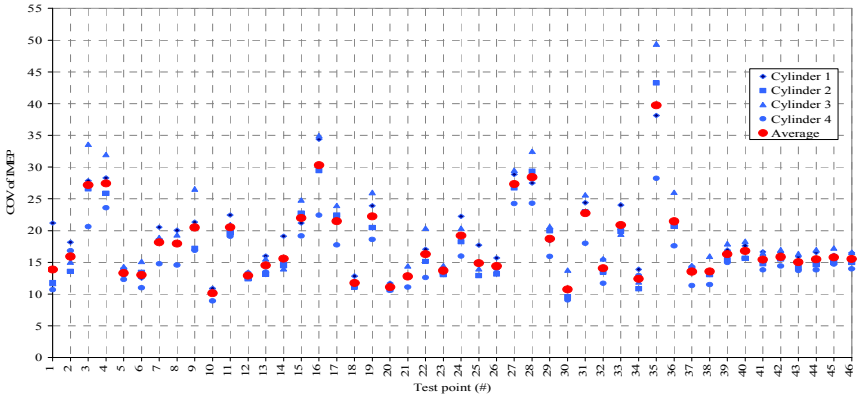

Figure 4-13: Experimental results on an individual COV_{imep} and average COV_{imep} from each test point.

The decision of the best test condition was made by considering the parameters. Therefore, the best test condition for heating the catalytic converter is to focus on the light-off time of emissions and take the average COV_{imep} value into account. Test #35 is the worse condition which has average COV_{imep} of 40.6%. The engine was run under lean condition and had no load which contributed to a high COV_{imep}. Test #10 and Test #30 shows average COV_{imep} of 10.7% and 11.3% respectively which are the lowest values compared with the other test points. However, NO_x emissions from those two tests were not achieved the light-off times. For CO and HC emissions, those two tests took 31.2 and 37.0 seconds respectively (Table 4-7) to achieve light-off times which were longer than Test #1 that used 17.2 seconds to convert all emissions.

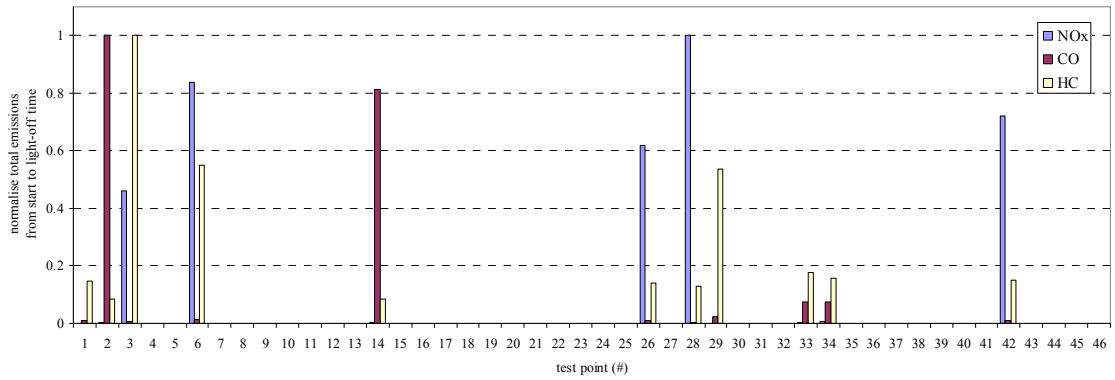

a) Normalisation of total emissions since engine which were calculated since engine had been started until achieves the light-off time of each emission species.

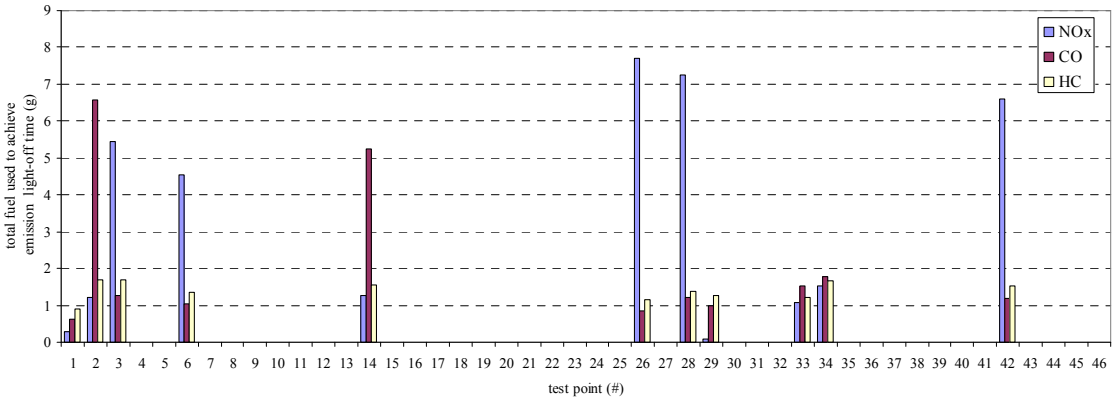

b) Total fuel used which was calculated from the time of engine start to the time of achieving light-off time of each emission species.

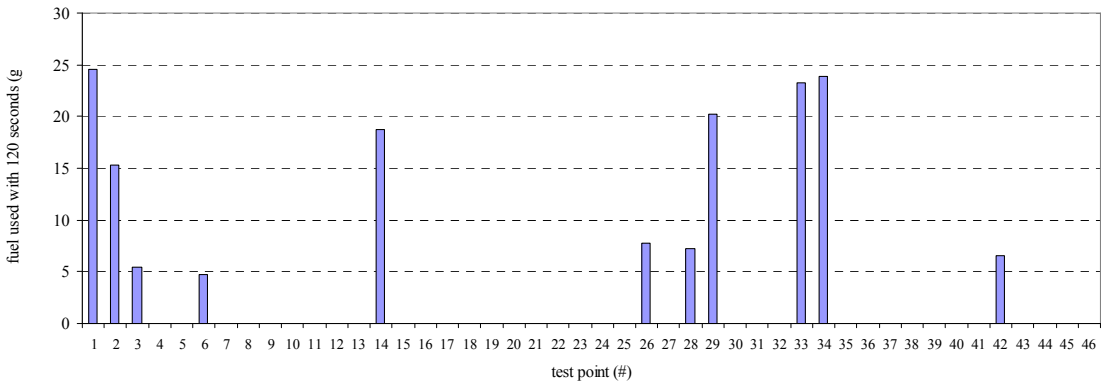

c) Total fuel consumed over the 120 second test period estimated by adding fuel burnt prior to light-off to the fuel that could be used at the operating condition from Test #21 which had the lowest fuel consumption

Figure 4-14: Comparison of fuel that consumed to achieve light-off time of each emission with total emission since engine started achieve light-off time with the only successful tests are presented here.

Figure 4-14a shows the total emissions since the engine had been started until successfully achieving light-off of each emission species and the total fuel that was used to achieve light-off for each emission species (Figure 4-14b). Test #1 shows the fuel that was used to achieve fast light-off was 0.63 grams which was the lowest fuel value from any test that could achieve light-off. However, Test #33 and Test #34 resulted in relatively low emissions level but these two tests had CO emissions higher than Test #1. Moreover, Test #33 resulted in high value of COV_{imep} when compare with Test #1 (22.9% compared with 14.8%). In additional analysis, Figure 14-4c shows the total of fuel used over a two minute period by adding the fuel used up to light-off to the fuel that would be used after this time. This value was taken from the tested condition that had the lowest fuel consumption of 0.23 grams per second, that was Test #21 and Test #29. However, Test #21 (lambda = 0.94, spark angle at TDC, 950 rpm, load = 0.5 and secondary air 7.5 kg/hr) was selected because the COV_{imep} was lower than Test #29. The results over 120 seconds suggest that Test #6 consumed less fuel than Test #1 but the emissions were higher. As can be seen for the discussion above, the results of the pre-catalyst temperature test had a trade-off between COV_{imep}, fuel used, total emissions and light-off time. These factors need to be considered when deciding on an appropriate strategy.

However, according to the aim of the secondary air technique, Test #1 could achieve the fastest light-off time and all emissions were converted with the lowest fuel used. The average COV_{imep} of Test #1 still gave 14.8% which need to be improved in order to make engine run smoother. Therefore, Test #1 was selected to study the mechanism of combustion variation. The closest operating condition with lean fuelling, Test #3, was used to gain knowledge of combustion variations under a wider range of circumstances.

In additional, the factors affecting pre-catalyst temperature can be optimised especially the rate of secondary air flow. In the next topic, the model based calibration (MBC) toolbox in Matlab was used to generate a pre-catalyst temperature model.

4.5 Model prediction for pre-catalyst temperature

The model for predicting pre-catalytic converter temperature was built as a one-state model using Matlab MBC. Both valid and invalid results from the experimental work were used. There are five input parameters:

SA_air	Secondary air flow. [kg/hr]
engine lambda	engine_lambda
load	Load. [bar]
spark	Spark angle. [^{o}BTDC]
speed	Engine speed. [rev/min]

The response model used the results of the pre-catalytic converter temperature as output results for the prediction model as shown in Figure 4-15. Four models were constructed, each using a different mathematical structure to represent the data. The ability of each model was used to estimate temperature based on the value of the root mean square error (RMSE[1]) and the press RMSE[2].

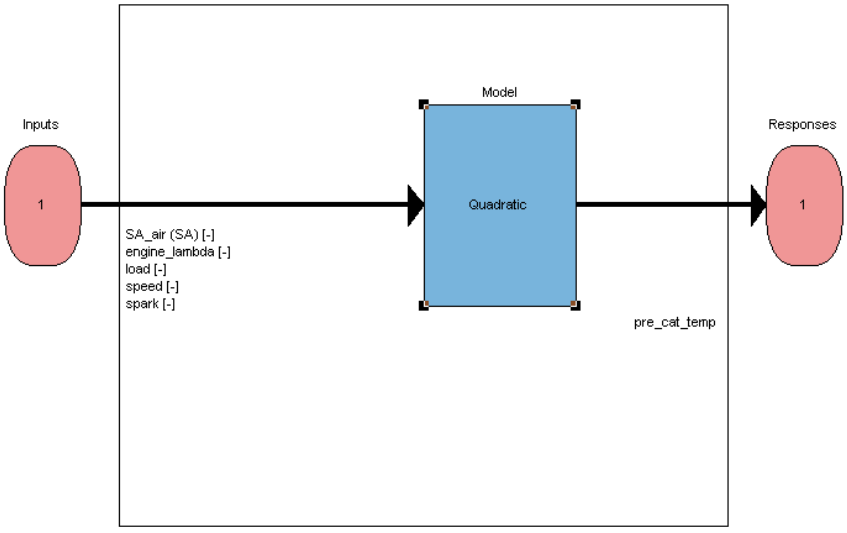

Figure 4-15: Diagram of one-state model for temperature prediction

[1] *root mean square error (*RMSE) is basic measure of how closely a model fits some data. A smaller RMSE means the model follows the data more closely (Matlab, 2008).

[2] *press RMSE* is calculated in a similar way to RMSE but a data point is removed before each value is calculated. The process is repeated for each point in the data set and the results are averaged. If the value of PRESS RMSE is much bigger than the RMSE this suggests mean the model is overfitting (Matlab, 2008).

Table 4-8 shows a comparison of press RMSE and RMSE from different model prediction. The high RMSE from the models using linear and quadratic equations shows that neither prediction can follow the experimental results. Using cubic model prediction, the model is able to predict the temperature more closely and the RMSE decrease significantly. However, the cubic model is over fitting as show in high value of press RMSE. Thus, the prediction by radial basis function (RBF) is introduced. . The RBF model is built up as a linear combination of a number of radial basis functions, each with its own distinct centre, until it achieves the minimum RMSE.

Table 4-8: Results of RMSE from different pre-catalyst gas temperature models

Models	RMSE (%)	Press RMSE (%)
Linear	62.96	65.36
Quadratic	26.84	31.71
Cubic	13.17	28.87
RBF-multiquadric-79	2.90	6.15

The model using a radial basis function (RBF) gave not only a low RMSE value but also provided a surface fit that generally followed the actual experimental data when compared subjectively. Although there are many types of RBF functions, this research only focuses on a multi-quadric function which is a default function in MBC According to the test results, the RBF used seventy nine points to build the predicted temperature model. The predicted RBF model gave not only a low RMSE value of 2.90% but also provided a surface fit that subjectively followed the actual data which is supported by a press RMSE 6.15%. However, the model still shows one test point that had an error of more than 5%, as can be seen in Figure 4-16. The model was implemented in Simulink and applied to the available test data for validation. Figure 4-17 shows the result of predicted temperature from 46 tests. The results gave a R^2 value of 0.9997 which had an error of less than 1% for all test points.

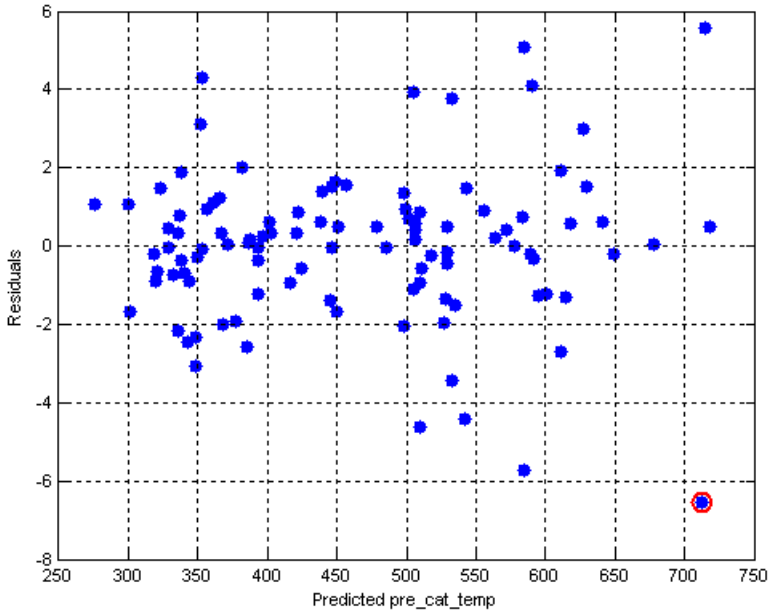

a) Residuals (^{o}C) plotted against predicted catalyst temperature (^{o}C) from RBF model from data used to train the model.

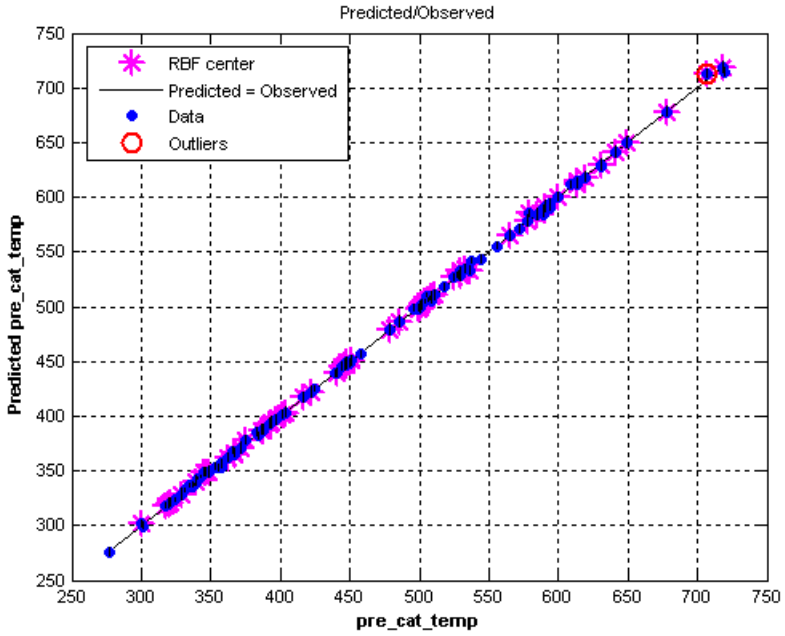

b) Plot of actual temperature against predicted temperature from data used to train the model.

Figure 4-16: Results of model created from RBF-multiquadric with 79 centres

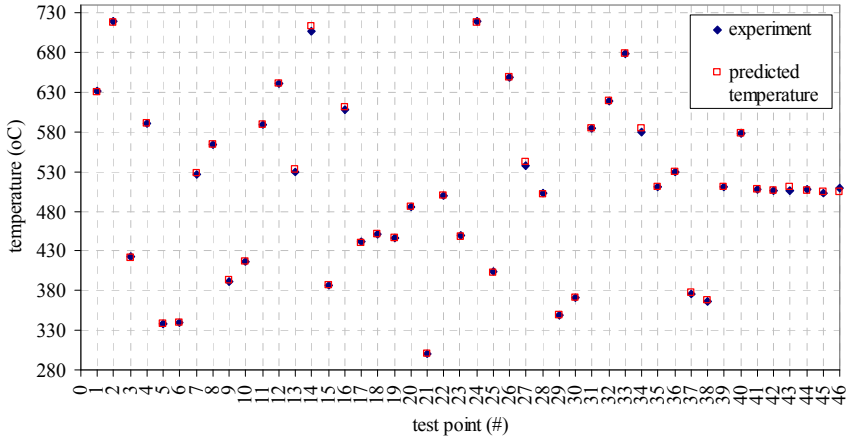

a) Comparison of actual and predicted pre-catalyst temperature from validation data.

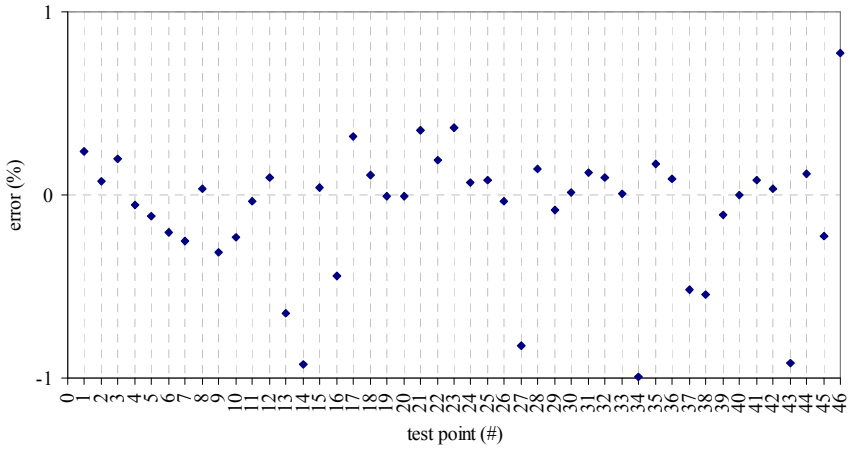

b) Error in percentage of each test point from validation data.

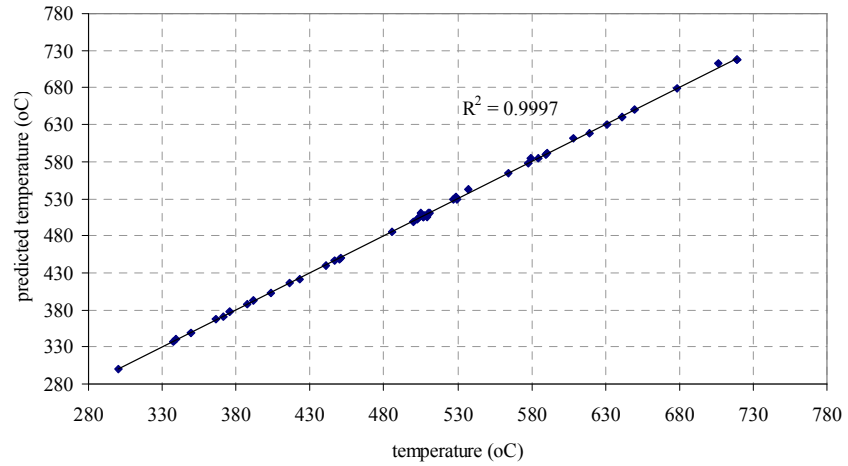

c) Plot of predicted against measured pre catalyst temperature from validation data.

Figure 4-17: Comparison of results of the model created from RBF-multiquadric with 79 centres with experimental data.

4.6 Discussion

The MBC model was used to further explore two scenarios for catalyst heating drawn from the experimental design in order to explain the effect of secondary air on the pre-catalytic temperature under rich fuelling (Test #1) and lean fuelling (Test #3). The result presents a contour plot of pre-catalytic temperature (Figure 4-18a) based on the rate of secondary air and lambda value before the secondary was introduced. Figure 4-18b shows the prediction error based on 95% confidence.

Figure 4-18c shows the contour plot for Test #1. The experimental result of pre-catalyst temperature without secondary air was 345.70 ^{o}C which is indicated by point 1A. The experimentally observed temperature increased significantly to 631.11 ^{o}C (point 1B) when secondary air was introduced at the rate of 5.87 kg/hr. Drawing a line across these two points suggests that the temperature could increase slightly higher (point 1C) if the rate of air is increased. Although, the average lambda value of 1.02, from the experimental work, shows that there was no extra fuel to be burned. However, if the flow rate increased there is a possibility for increased NO_x emission because the exhaust gases will behave as they do under lean combustion conditions. In comparison with lean combustion from Test #3, Figure 4-18d shows a contour that suggests that the results with secondary air (point 3B) dropped to 422.7 ^{o}C and there was no benefit on pre-catalytic temperature using the secondary air technique. By drawing a line across the test results, the model suggested the temperature tend to decrease even more (point 3C).

The MBC model for temperature prediction in this research aims to forecast the possible temperature under variations of the secondary air flow rate. However, the results of predicted temperature (point 1C and point 3C) had high errors as can be seen from contour of 95% confidence in Figure 4-18b. In order to increase the accuracy of the predicted temperature, the model needs more test data for different flow rates in order to predict the pre-catalytic temperature more accurately. The results, then, are targeted on the lambda of 1 which allows all emissions to be converted.

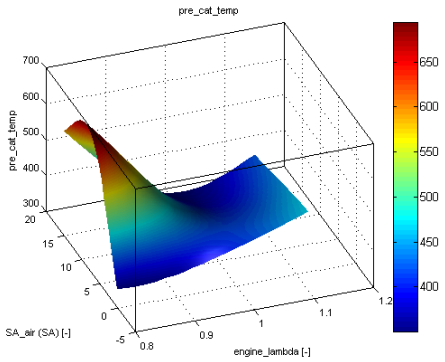

a) Overall shape of pre-catalytic temperature prediction under condition of 1225 rpm, spark at TDC, load 0.5 bar and secondary air with rate of 6 kg/hr

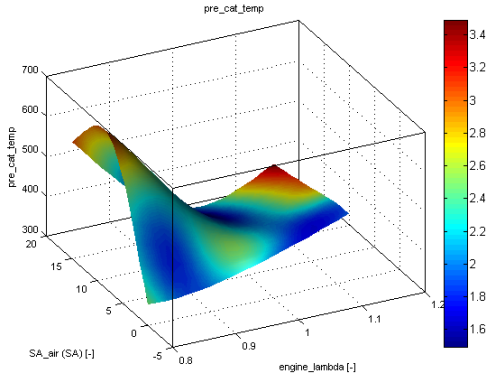

b) Prediction error shading curve base on 95% confidence.

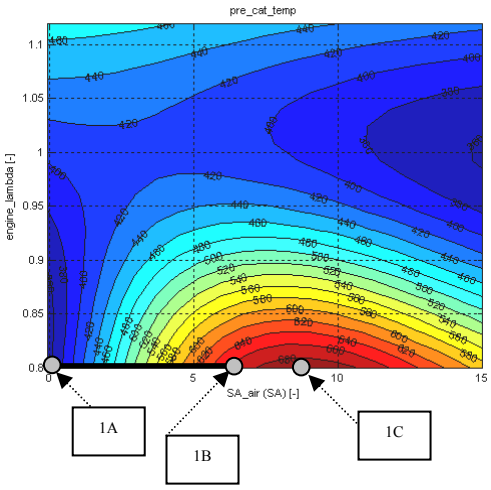

c) Contour plot showing the pre catalyst temperature increase due to secondary air under rich condition (λ =0.8)

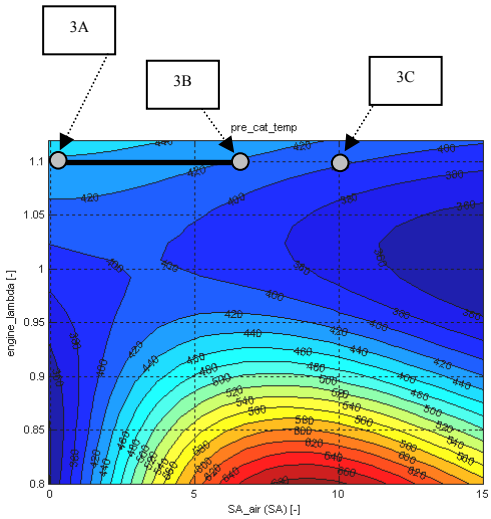

d) Contour plot showing the pre catalyst temperature increase under lean condition (λ =1.1)

Figure 4-18: Pre-catalyst gas temperature prediction bases on RBF-multiquadric with 79 centres.

4.7 Conclusion

In this chapter, the results from design test points were analysed. The raw in-cylinder pressure data that contained noise were smoothed by *rloess* method with 0.05 of span value. The problems of cylinder pressure referencing were solved by shifting an average of three measurements of pressure at inlet bottom dead centre to the average value of absolute manifold pressure value held in the ECU. The IMEPs were calculated by shifting the maximum compression pressures to TDC and heat releases were calculated with 1.25 of gamma value.

Once the data processing was completed, the results of catalyst light-off time from 5 parameters (secondary air flow, lambda, spark angle, engine speed and load) were discussed. The test that could achieve light-off time most rapidly was Test #1 which employed the secondary air technique. The maximum pre-catalyst temperature of Test #1 (rich fuelling) could achieve 631.1^{o}C with secondary air of 5.9 kg/hr but under lean fuelling (Test #3) there were no benefit from secondary air. The prediction of pre-catalyst temperature which was constructed using radial basis function (RBF) model from the MBC toolbox suggested the maximum temperature under rich fuelling could be achieved by increasing the rate of secondary air and under lean fuelling the temperature will drop. However, these prediction results need more data for validation because the errors in the model are significant.

Although the catalyst could achieve light-off for each emissions species in Test #1, the average COV_{imep} of the test was still higher than 10%. Since cyclic variation is clearly a major constraint to the further optimisation of light-off, it is important to gain an understanding of the phenomena and if possible to develop a predictive tool that can be used when assessing alternative calibration strategies. Thus, the mechanism of combustion variation of Test #1, which was run under rich fuelling conditions, is studied using an engine simulation. The study is focused on the mechanism behind these phenomena based on the effect of the air/fuel ratio and residual gas fractions. Moreover, the same engine condition with lean mixture, from Test #3, is also included in the research, in order to extend the area of cyclic variability. In the next chapter, an engine simulation model is created and validated using the data from these two test points.

Chapter 5

Engine Simulation

In this chapter, the construction of the 1D engine model is documented, along with the addition of a co-simulation element to allow the 1D simulation to be controlled from the Matlab Simulink environment. Important parameters describing the engine characteristics, including valve profiles, intake and exhaust manifold geometry have been considered and represented in the WAVE engine model. The aim of the simulation is to derive an insight into the mechanism of cyclic variability, thus the features within the model that facilitate these mechanisms, principally the simulation of fuel injection dynamics, are explained. The effect of air/fuel ratio, residual gas fractions and turbulence are known to be significant and simultaneous beyond. The measurement of small scale turbulence is the scope of this research since a methodology that could be applied within a time constrained engine calibration study without access to specialist instrumentation or three dimensions (3D) simulation tool was required. In addition, the methods used to control the combustion profile provided within in the model are discussed in order to understand the limitations of the software. Finally, the configuration of co-simulation elements to allow direct manipulation of the combustion process to facilitate the simulation of cyclic variability is presented.

5.1 Ricardo WAVE

Ricardo WAVE is a computer aided engineering software package that analyses the dynamics of pressure waves, mass flows and energy losses in ducts of various engine systems (Ricardo, 2006). WAVE is part of the software that was used in this research in order to simulate cyclic variability in gasoline engines.

An Audi 1.8-litre spark ignition engine at the University of Bath (Figure 3-1) was used to obtain data for important parameters that are needed to create an engine model. The parameters include: dimensions of the intake and exhaust manifolds, valve profiles and other engine characteristics. The schematic of the Audi engine is shown in Figure 5-1.

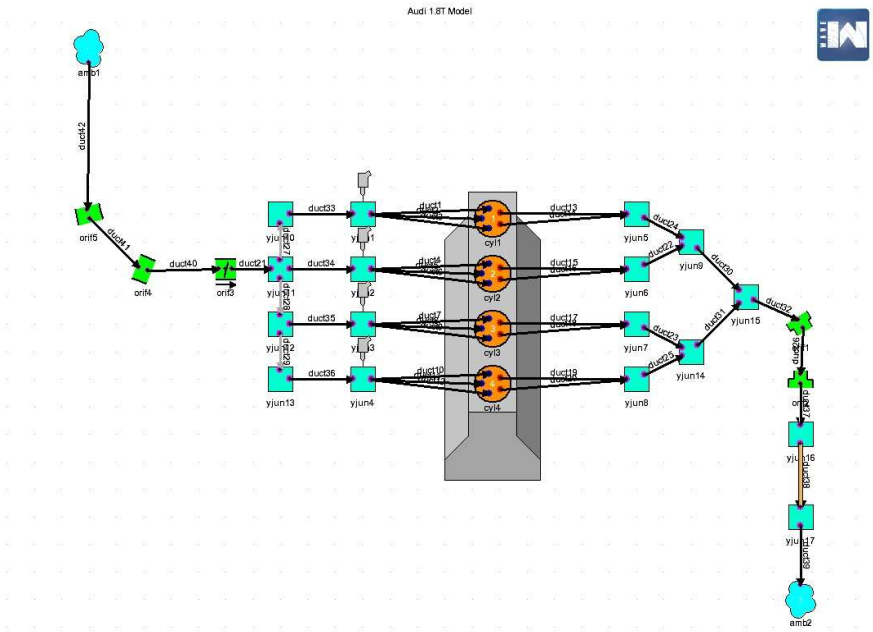

Figure 5-1: Audi 1.8-litre engine simulation schematic.

5.1.1 Engine characteristics

An important dimension that is needed in the engine model, to be implemented in WAVE, is the size of the combustion chamber. In order to obtain the exact actual value, the engine would have had to been taken apart and directly measured, to take into account any mechanical wear that might have taken place or carbon deposits that may have built up. In practice, this level of detail could be considered inappropriate and unnecessary, particularly when no complex model is ever likey to be completely accurate. Therefore, the characteristics of engine are assumed to conform to the original data from manufacture. The technical data for the Audi 1.8-litre engine were taken from Pfalzgraf et al. (2001) and are shown in Table 3-1.

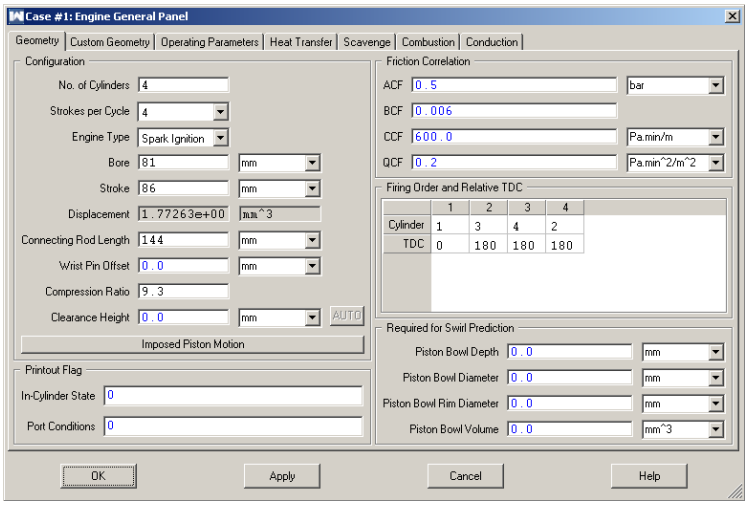

Figure 5-2: Engine general panel from WAVE

The data from Table 3-1 is added in the "engine general panel" window of the WAVE software (Figure 5-2). The friction correlations are used as a default setting since limited friction data were available for the engine and precise accuracy was not important for the proposed research.

5.1.2 Valve profile

The Audi 1.8-litre engine has three intake valves and two exhaust valves. The intake valves have a maximum lift of 7.67 mm and start to open 18 degrees ATDC. The intake valves' camshaft can be adjusted by 22 degrees of advance from its original position. The engine used a hydraulic two-point camshaft adjuster with integral chain tensioning device (Pfalzgraf et al., 2001). A hydraulically pressurised piston, energised by a solenoid valve, alters the position of the chain sliding blocks and thus the length of the chain's centre between the exhaust camshaft driven by the timing belt and the intake camshaft. The exhaust valves' camshaft is designed to open 28 degrees BBDC with 9.3 mm of lift. The opening period of the intake and exhaust valves is designed to have duration of 190 and 200 crank angle degrees respectively. These durations are measured from when valves are lifted by 1 mm. However, the valve profiles are still hard to measure, thus the default profile available in WAVE has been used in the engine model.

The intake and exhaust valve profiles from WAVE, named SI1INT and SI1EXH, were modified using interpolation. As a result, the intake and exhaust opening period profiles of the engine had another 62 and 72 crank angle degrees added respectively. In addition, the available forward and backward flow co-efficiency of both valves from WAVE were used in the engine model.

Figure 5-3 shows the profile of the exhaust cam that starts to open at 116 degrees ATDC with an opening duration of 272 degrees. For the intake profile, the starting point is 13 degrees BTDC with a 252 degree opening duration.

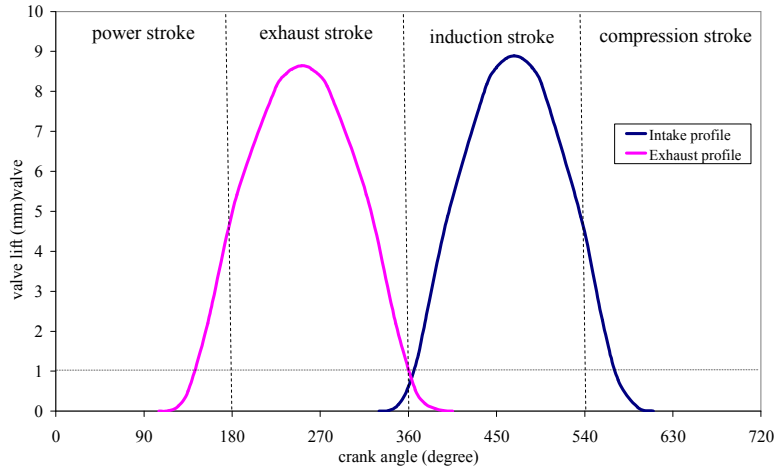

Figure 5-3: Audi 1.8-litre intake and exhaust valve lift profiles

According to the information on the valve profiles, the valves have no overlap since the measurement had started from 1 mm of lift. Considering the valve profile below 1 mm, the valves have an overlap with the centerline located after TDC. These profiles allow gas exchanges depending on the pressures differences between the cylinder and the manifold. WAVE calculates the velocity of the gases using *Equation 5-1* as shown below.

$$V = \sqrt{2\frac{\gamma}{\gamma-1}RT_o\left[1-\left(\frac{P}{P_o}\right)^{\frac{\gamma-1}{\gamma}}\right]} \quad \text{.....Equation 5-1}$$

where;

P = Upstream total pressure or manifold pressure.

P_o = Downstream total pressure or in-cylinder pressure.

By inspection of the equation, the direction of flow is controlled by the pressure from both sides. If the manifold pressure (P) is greater than the in-cylinder pressure (P_o), the flow will move to the combustion chamber. In contrast, the flow will return to the manifold as backflow if the in-cylinder pressure is higher than the manifold pressure. The volumetric flow rate (Q) is calculated by *Equation 5-2*.

$$Q = A_{eff}V \quad \text{……Equation 5-2}$$

According to *Equation 5-2*, the effective area (A_{eff}) of the valves for forward and backward flows are different and dependent on the type of flow.

The effective area of flow in the combustion chamber is considered as the gas flows from the pipe to a large area. Thus, a discharge co-efficient (C_D) is applied to the calculation as shown in *Equation 5-3*.

$$A_{eff} = C_D \pi DL \quad \text{……Equation 5-3}$$

Discharge co-efficient (C_D) in this research was set to default value that was auto. The auto value allows WAVE to calculate C_D by *Equation 5-4;*

$$\left.\begin{aligned} C_D &= 1-\left(1-\left(\frac{D}{D_1}\right)^4\right)*\left(0.2+0.2\left(1-\left(\frac{D}{D_2}\right)^4\right)\right) \text{ …….. (a)} \\ C_D &= 1-\left(1-\left(\frac{D}{D_2}\right)^4\right)*\left(0.2+0.2\left(1-\left(\frac{D}{D_1}\right)^4\right)\right) \text{ …….. (b)} \end{aligned}\right\} \text{ ……Equation 5-4}$$

Both Equation 5-4a and *Equation 5-4b* are used to obtain discharge co-efficient by using the diameter of the pipe as can be seen from Figure 5-4.

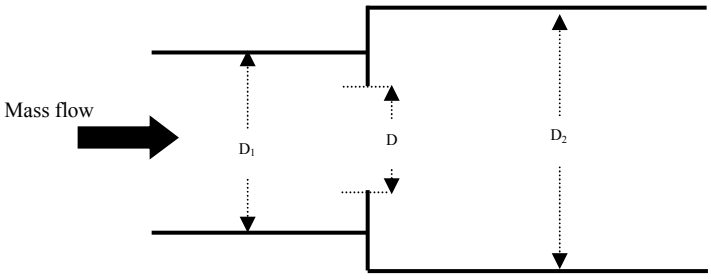

Figure 5-4: Diagram of flow in pipe for calculation of discharge co-efficient.

When the flow in the manifold is considered, the effective area is controlled by the valve flow co-efficient, which has different characteristics depending on the valve design. Therefore, the effective area under forward and reverse flow is calculated by *Equation 5-5a* and *Equation 5-5b*.

$$A_{eff} = C_F \pi \frac{D^2}{4} \quad \text{..... (a)}$$

$$A_{eff} = C_R \pi \frac{D^2}{4} \quad \text{..... (b)}$$

.....Equation 5-5

The values of C_F (forward flow co-efficient) and C_R (reverse flow co-efficient) were controlled by the ratio of valve lift (L) and valve diameter (D). Figure 5-4 shows the effect of flow co-efficient from different valve lift.

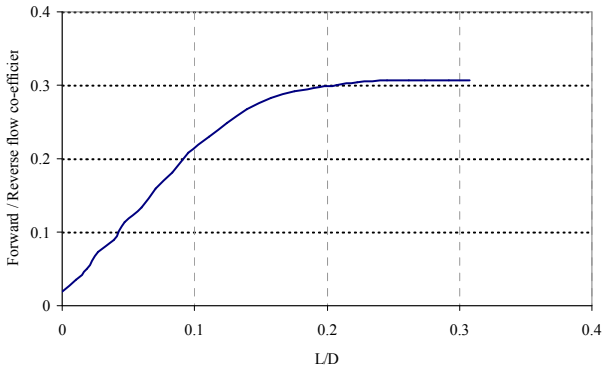

Figure 5-5: Forward and reverse flow co-efficiency profiles from WAVE.

Although, these co-efficient values are important for calculations, this research is focused on the catalytic light-off time and cyclic variability in the combustion process, based on the variations in the air/fuel ratio and the residual gases. Therefore, the available flow co-efficients for the intake and exhaust valves from WAVE have been interpolated for the engine model.

5.1.3 Intake manifold

The Audi 1.8-litre has four fuel injectors that are installed in the intake manifold near the cylinder head. The main intake manifold was designed to connect the common pipe before separating into four manifolds for delivery of fresh ambient air into the combustion chambers.

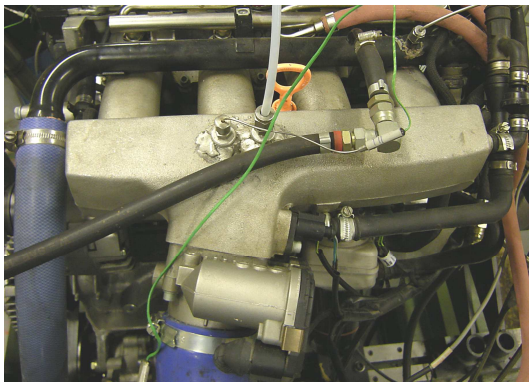

a) The intake manifold of the Audi 1.8-litre engine.

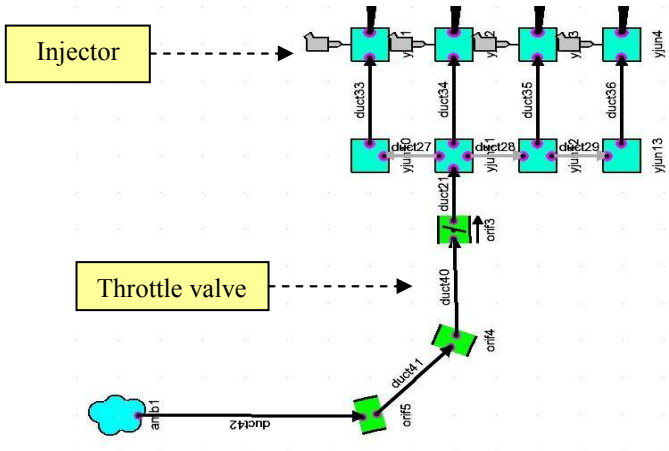

b) Model of the intake manifold.

Figure 5-6: Comparison between actual inlet manifold and model of the intake manifold from the Audi 1.8 litre engine.

The main manifold connects the common pipe near to the manifold of cylinder number 2, as shown in Figure 5-6a. The actual intake manifold dimension had been measured to build an engine model in WAVE, as shown in Figure 5-6b. The throttle valve was added before the connection of the main manifold and the common pipe. The throttle valve has a minimum opening angle of 5 degrees. The ambient air was connected to the main manifold of the engine model. The settings of manifolds and ambient air act as default settings.

5.1.4 Exhaust manifold

The exhaust manifold was based on an existing design (Bannister et al., 2007) and modified as required, as shown in Figure 5-7a. The dimensions of the modified parts had been taken from Bannister et al. (2007) and the rest of the exhaust pipe, including the catalytic converter, were measured manually. Figure 5-7b shows the catalytic converter of the engine model is located near the end of exhaust manifold before exiting to the ambient. The parameters of each component used default settings.

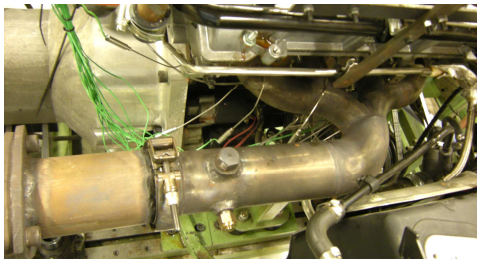

a) Exhaust manifold of Audi 1.8-litre

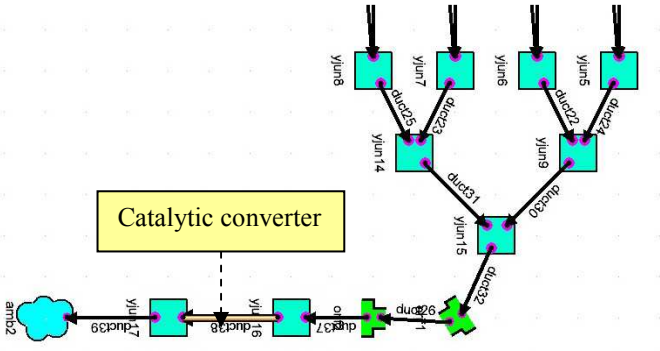

b) Model of the exhaust manifold.

Figure 5-7: Comparison between actual exhaust manifold and model of exhaust manifold from the Audi 1.8 litre engine.

5.1.5 Important sub-models in WAVE

In order to obtain realistic results from the WAVE engine simulation, there are some options that need to be understood and have to be activated before the simulation can be executed.

5.1.5.1 Fuel spray model

In the Audi engine, used in this research, some of the fuel injected into the intake manifold is lost during transportation. Although the engine model has been built by locating the injectors on the intake manifold, the simulation will consider all fuel has been induced into the combustion chamber, and that none is lost in transit. WAVE provides an option to make the engine model, with port fuel injection, obtain more realistic results by considering the fuel loss in the intake manifold. The option can be found in the "liquid fuel spray" panel as can be seen in Figure 5-8. When the option has been activated, there are another seven options to consider.

- *Mass per fuel parcel* - This option allows the user to define the mass per fuel drop parcel injected, which has 0.05 mg as a default setting. Represents the fuel spray as a series of parcels.
- *Use 5x longer time steps* - This option allows the evaporation time step to be equal to 5 times the gas flow time step which makes the simulation execute faster.
- *Activate uniform fuel film temperature* - This option considers each liquid parcel within fuel film has a uniform temperature.
- *Activate random impingement position* - Every impingement event position in this option is calculated randomly.
- *Use rosin-Rammer drop size distribution* – This option creates a uniform fuel droplet distribution by the function which suggested by Rosin-Rammler (1933, cited by Ricardo, 2006)
- *Enable fuel film model* - This option activates the full range of outcomes of the impingement including rebound, adhesion, splash and spread.
- *Enable in-cylinder fuel film model* - This option enables the fuel film formation on the cylinder wall.

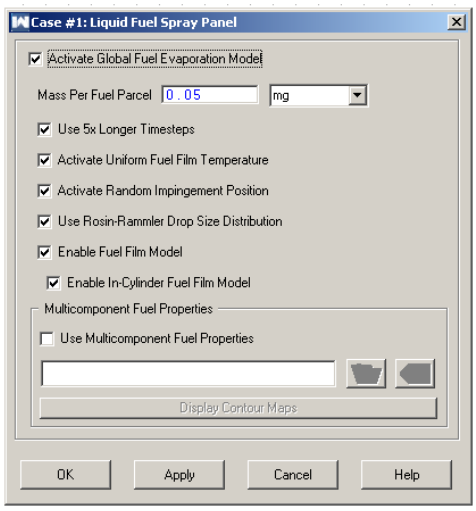

Figure 5-8: Fuel spray model control panel in WAVE

These options have been activated as a default setting in WAVE as a starting point of the simulation in this research. Moreover, the main target of this simulation is to study the mechanism of cyclic variation which is caused by variations in the air/fuel ratio and residual gases. Multi-component fuel properties are inactive because the engine is tested by using normal gasoline fuel, which is assumed to have similar properties as indolene in the WAVE software package.

The activated spray model allows WAVE to predict the liquid fuel spray motion and evaporation through the entire WAVE network, including the transportation of droplet and liquid films. WAVE (version 7.2, build 16) provides calculations for fuel evaporation in the model which are divided into two categories:

1) *In-cylinder evaporation model* - This model is activated by default which results in variations of fuel in the combustion chamber.

2) *Comprehensive evaporation model* - The model is activated when the fuel spray model is used, which predicts liquid evaporation through the entire flow network.

These two liquid fuel evaporation models are explained below.

1) In-cylinder Evaporation Model

The in-cylinder evaporation rate is active by default. The rate of liquid fuel evaporation in the combustion chamber is calculated by *Equation 5-6* as shown below.

$$\frac{dm_v}{dt} = \frac{m_l - m_v}{\tau_{evap}} \quad \text{.....Equation 5-6}$$

where;

dm_v / dt	=	rate of fuel evaporation
m_l	=	mass of liquid fuel
m_v	=	mass of the vapour fuel
τ_{evap} [1]	=	characteristic evaporation time for fuel droplet

According to *Equation 5-6*, the rate of fuel evaporation is dependent on the characteristic evaporation which is related to the temperature, the fuel droplet size, and the heat transfer. Under cold start conditions, the fuel is hard to evaporate which leads to high HC emissions compared with starting an engine under hot conditions.

2) Comprehensive Evaporation Model

A comprehensive evaporation model is used to predict the liquid fuel spray motion and evaporation, including the transportation of droplet and liquid films. There are eight parameters involved in the calculations of this model, they are:

- Mean Droplet Size and Size Distribution
- Droplet Dynamics
- Droplet Evaporation
- Spray Wall Impingement
- Film Dynamics
- Film Evaporation

---

[1] τ_{evap} (characteristic evaporation time for fuel droplet) is calculated based on the energy balance between the surrounding air and the liquid fuel with the assumption that the heat transferred is a fraction of the available energy (Ricardo, 2006)

- Liquid Film Stripping off as Droplets at Sharp Edge
- Valve-Seat Fuel Film Squeezing

Each parameter is explained below.

2.1) Mean Droplet Size and Size Distribution

The diameter of a fuel droplet is defined by the sauter mean diameter (SMD). There are two equations for the calculation of SMD based on injector pressure.

For low pressure,

$$SMD = 4.12 * d_{nozz} * \mathrm{Re}^{0.12} * We^{-0.75} * \left(\frac{\mu_f}{\mu_g}\right)^{0.54} \left(\frac{\rho_f}{\rho_g}\right)^{0.18} \quad \text{……Equation 5-7}$$

For high pressure,

$$SMD = 0.38 * d_{nozz} * \mathrm{Re}^{0.252} * We^{-0.32} * \left(\frac{\mu_f}{\mu_g}\right)^{0.37} \left(\frac{\rho_f}{\rho_g}\right)^{-0.47} \quad \text{…..Equation 5-8}$$

where

d_{nozz}	=	nozzle diameter
Re	=	Reynolds number
We	=	Weber number
ρ_f, ρ_g	=	fuel and gas density
μ_f, μ_g	=	dynamic viscosity of fuel and gas

Although the low and high pressures are not clearly defined, both *Equation 5-7* and *Equation 5-8* have similar parameters, only the constants are different. By analysis, the variation in SMD could be caused by the density and dynamics of the viscosity of the fuel and gas which are affected by temperature. The Reynolds[2] and Weber[3] numbers are mainly affected by fuel injection speed (U_{inj}), as can be seen from the equations below.

---

[2] Reynolds number (*Re*) is used to classify the state of flow. If the number is great the 4000, it is considered as turbulent flow while the number below 3000 is considered as laminar flow (Ricardo, 2006).

[3] Weber number (*We*) is a value represents the ratio of droplet kinetic energy to surface tension (Ricardo, 2006).

$$\mathrm{Re} = \frac{\rho_f U_{inj} d_{nozz}}{\mu_f} \quad \text{.....Equation 5-9}$$

$$We = \frac{\rho_f U_{inj}^2 d_{nozz}}{\sigma} \quad \text{.....Equation 5-10}$$

$$U_{inj} = \sqrt{2(P_{inj} - P_{cyl})/\rho_f} \quad \text{.....Equation 5-11}$$

where;

P_{inj}	=	injection pressure
P_{cyl}	=	cylinder pressure
σ	=	surface tension

Considering Equation 5-11, the variation in fuel speed is linked to the fuel's density, which is dependent on temperature and in-cylinder pressure. During cyclic variability in combustion, the maximum in-cylinder pressure is changed from one cycle to the next which affects fuel speed when the engine parameters are held at constant values. With a PFI system, variations in fuel speed are linked to both pressure and fuel density because the location of the injector is on the intake manifold which closes to the intake valve. Therefore, cold fresh air, which is induced into the combustion chamber, and the backflow of hot burnt gases, during intake valves opening, cause oscillations in the pressure and temperature which, in turn, cause variations in speed and size of the fuel droplets.

2.2) Droplet Dynamics

While the fuel is injected, there is a drag force exerted on the droplets from the surrounding gases which tends to decrease the relative velocity between the fuel droplets and the gas flow (Ricardo, 2006). WAVE calculates the drag force following Newton's second law with *Equation 5-12*.

$$\sum F = m_f a_f \quad \text{.....Equation 5-12}$$

The fuel's mass (m_f) and acceleration (a_f) are calculated by *Equation 5-13* and *Equation 5-14* respectively (Bird et al. 2002 cited by Ricardo 2006).

$$m_f = \frac{4}{3}\rho_f \pi d^3 \quad \text{.....Equation 5-13}$$

$$a_f = \frac{du_f}{dt} = \frac{1}{2}C_D \rho_g \left|u_g - u_f\right|\left(u_g - u_f\right)\frac{\pi d^2}{4} \quad \text{.....Equation 5-14}$$

where;

u_g, u_f = velocities of gas flow and liquid fuel droplet

C_D = drag coefficient

In order to calculate the drag coefficient, WAVE uses *Equation 5-15* which is given by Choi et al. (1992, cited by Ricardo 2006).

$$C_D = 2.3\,\mathrm{Re}^{-0.37} \quad \text{.....Equation 5-15}$$

2.3) Droplet Evaporation

The rate of fuel evaporation (ω) is defined by Bird et al. (2002, cited by Ricardo 2006) as shown in *Equation 5-16*.

$$\omega = \frac{\rho D_{AB}}{d} * Sh^* \ln\left(1 + B_M\right) \quad \text{.....Equation 5-16}$$

By inspection of *Equation 5-16*, fuel evaporation depends on the fuel droplet size and the density of fuel which are affected by temperature. However, gas diffusivity (D_{AB}), non-dimensional modified Sherwood[4] number (Sh^*) and mass transfer value (B_M) also affect the rate of evaporation.

[4] Modified Sherwood number (Sh^*) is related to the likelihood of non-vaporising droplet (Abramzo et al., 2005 cited by Ricardo, 2006).

2.4) Spray Wall Impingement

The mechanism of fuel transportation is linked to two characteristic numbers: the Weber number (*We*) and the Laplace number[5] (*La)*. The Laplace number is defined by *Equation 5-17*.

$$La = \frac{\rho_f \sigma d}{\mu_f^2} \quad \text{.....Equation 5-17}$$

These two characteristic numbers are used to define the behavior of fuel on the wall impingement model as can be seen from Figure 5-9.

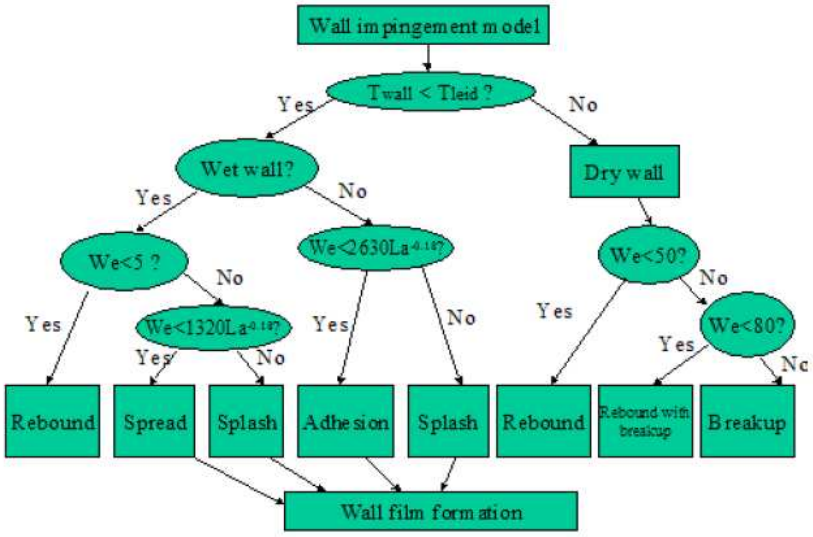

Figure 5-9: Spray Wall Impingement Regimes

When the wall temperature increases to Leidenfrost temperature (T_{leid}) which is higher than boiling temperature then the available fuel on the wall evaporates immediately and causes the incoming droplets start to evaporate before they reach the wall (1996 cited by Ricardo, 2006). Therefore, if the wall has temperature higher than T_{leid} then the wall surface will be dry otherwise the wall is considered as a wet wall. Since the wall type was addressed, the *We* and *La* number are taken into account in order to explain the

[5] Laplace number (La) is a parameter measured the relative importance of surface tension and viscous forces action on the liquid (Bai et al., 1995)

mechanism of fuel. Bai et al. (1995) explained the various impingement regimes from different condition as can be seen in Figure 5-10. There were six regimes according to Figure 5-9 including;

1) Adhesion – the impingement droplet adheres to the wall in nearly spherical form.
2) Rebound – the impingement droplet bounces off the wall after impact.
3) Spread – the droplet impacts with a moderate velocity onto a dry or wetted wall and spreads out to form a wall film on the dry wall or combines with the available liquid film on wetted wall.
4) Rebound with brake-up – the droplet bounces of a hit surface and accompanied by breakup into two or three droplets.
5) Break-up – the droplets hit the wall and form a radial film on the hot surface and cause the fragmentation of the liquid film in a random manner.
6) Splash – the droplet hit an available fuel on the wall at high impact energy and a crown shape. The jets develop on the periphery on the crown and the jets become unstable and brake up into many fragments.

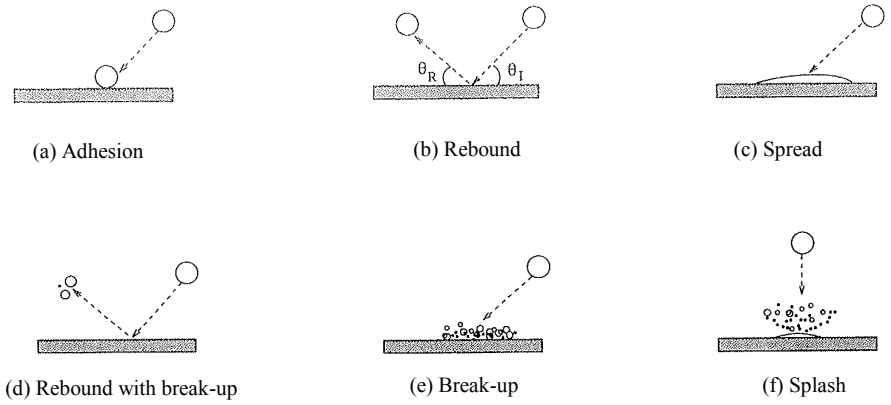

Figure 5-10: Schematic of different impact regimes (Bai et al., 1995)

2.5) Film Dynamics

According to Newton's second law, there are two different forces being exerted on a fuel film wall. The force on the gas side (τ_g), where the gas flow tends to drive the film along the same direction. The force on the wall side (τ_w), where the viscous friction tends to resist the film's movement. The balance of forces on the film (τ_{imp}) gives the equation for the film motion, as can be seen in *Equation 5-18*.

$$\rho_f \delta \frac{du_{fm}}{dt} = \tau_g - \tau_w + \tau_{imp} \quad \text{.....Equation 5-18}$$

The driving force on the gas side is calculated by *Equation 5-19*.

$$\tau_g = \frac{1}{2} f \rho_g \left(u_g - u_{fs}\right)\left|u_g - u_{fs}\right| \quad \text{.....Equation 5-19}$$

The friction force on wall side is calculated by *Equation 5-20*.

$$\tau_w = 2\mu_f \frac{u_{fm}}{\delta} \quad \text{.....Equation 5-20}$$

By inspection of *Equation 5-19*, the force on the gas side depends on the speed of gas (u_g) and fuel film (u_{fs}) which corresponds to the Reynolds number. In contrast, the force on wall, as shown in *Equation 5-20*, is affected by the fuel's viscosity (μ_f) dynamics.

2.6) Film Evaporation

The film evaporation rate (ω) is calculated as the product of the mass transfer coefficient (h_D) and the mass transfer number (B_M) as shown in *Equation 5-21*.

$$\omega = h_D B_M \quad \text{.....Equation 5-21}$$

The mass transfer coefficient (h_D) is determined by the heat transfer from the gas to the film and the heat from the wall to the film. For a PFI engine, the gases are usually fresh ambient air, which is cold, thus the evaporation rate depends on the wall's temperature. Under cold start conditions, the heat from gas and wall are relatively low, thus evaporation is low and the engine is required to inject more fuel.

2.7) Liquid Film Stripping off as Droplets at Sharp Edge

The liquid film can evaporate if the temperature is high enough but the film can also experience a stripping off of droplets at a sharp edge. As the intake gas tends to move the fuel film forwards the chamber while surface tension resists the film moving forward. However, the surface tension depends on the thickness of the film. Moreover, pressure drops across a sharp edge tend to strip the film off the edge.

Therefore, the liquid film will be stripped off an edge when the pressure drop across the edge is greater than the surface tension as shown in *Equation 5-22*.

$$\underbrace{\frac{1}{2}K_s\rho_g U_g^2}_{\text{Pressure drop across the edge}} \geq \underbrace{\frac{\sigma}{R+\delta}}_{\text{Surface tension}} \quad \text{.....Equation 5-22}$$

where;

σ = radius of the corner

K_s = loss coefficient

2.8) Valve-Seat Fuel Film Squeezing

Considering the fuel flow across moving inlet valves, the fuel film between a valve and its seat will be squeezed and forced to move in two directions.

- Forward to the cylinder.
- Back towards the inlet port.

From the conservation of mass law, the volumetric flow rates towards the cylinder and port are assumed to be equal to the rate of the volume decrease between the valve and seat. Thus, an average velocity ($u(x)$) of flow is defined by *Equation 5-23*.

$$u(x) = -\frac{\delta^2}{12\mu}\frac{\partial p}{\partial x} \quad \text{.....Equation 5-23}$$

By inspection of *Equation 5-23*, the pressure difference (∂p) is the factor that explains the direction of flow. However, the intake flow normally move forward during an intake stroke, therefore all fuel is forced to move to the combustion chamber. This could cause a problem under engine cold start conditions because the fuel has a low evaporation rate and has been induced into the chamber in the form of a liquid. As a result, the combustion energy produced is less and unwanted emissions are higher.

5.1.5.2 Two-zone combustion model

In an engine simulation, WAVE can consider a mixture as a single-zone or 2-zone model for the propose of combustion (Ricardo, 2006). For single-zone combustion, the whole cylinder is treaded as one region while 2-zone model divides the in-cylinder gases into burned and unburned regions. The 2-zone model is used to capture more detail of the combustion process. Although the combustion model can be used as either a single or 2-zone model, in order to activate the emissions model, the 2-zone mode is required. Moreover, a 2-zone model allows WAVE to calculate fuel spray, as explained earlier.

In this research of the combustion process of PFI engine, the simulation is focused on variations in the air/fuel ratio and the residual gases in the combustion chamber, before the mixture has been ignited. Thus, the 2-zone model has been activated which allows WAVE to calculate the total gas transfer during the intake and exhaust valves opening period.

5.1.5.3 Combustion control

In order to control or model the combustion profile, WAVE offers two different types of SI combustion, they are:

1) SI turbulence flame.
2) Wiebe exponent function.

These two methods of control each have different characteristics and advantages, but the most suitable method for modeling cyclic variability uses the Wiebe exponent function. This is because:

- The turbulent flame model is only available when an IRIS cylinder (IRIS is an advanced combustion module which provides more detailed analysis inside the cylinder) is used in WAVE. Moreover, WAVE allows the model to simulate only one IRIS cylinder although the engine may have more than one cylinder. These issues contribute to a pressure oscillation in the intake and exhaust manifold due to the type of cylinder that has different characteristics.
- The IRIS cylinder is good for in depth analysis of a single cylinder because the IRIS model requires more information, such as the cylinder type and the dimensions of the cylinder head and piston etc.
- There are no combustion control actuators available to the user when the IRIS cylinder model is selected. The combustion characteristics are controlled within WAVE, therefore there are no opportunities to vary combustion characteristic from cycle to cycle.

In order to control the combustion from cycle to cycle, the control of the combustion profile needs to be more flexible. Therefore, the combustion model, in this research, uses the Wiebe exponent function as shown in *Equation 5-24*.

$$W = 1 - EXP\left(- AWI\left(\frac{\Delta\theta}{BDUR} \right)^{(WEXP+1)} \right) \quad \text{.....Equation 5-24}$$

where;

W = cumulative mass fraction burnt

$\Delta\theta$ = crank degrees past start of combustion

BDUR = user-entered 10-90% burn duration in crank degrees

WEXP = user-entered Wiebe exponent

AWI = internally calculated parameter to allow BDUR to cover the range of 10-90%

The combustion is controlled by changing the 50% burn point, 10-90% duration, Wiebe exponent function and mass fraction burnt, as shown in Figure 5-11.

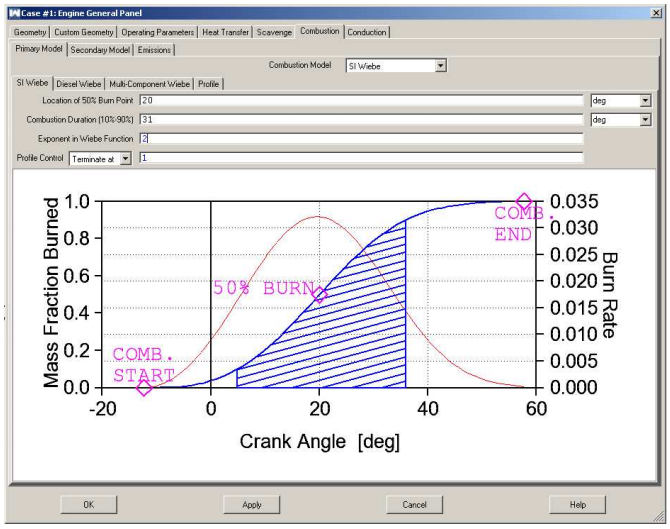

Figure 5-11: Control combustion panel in WAVE

- ***Location of the 50% burn point***

The location of the 50% burn point is the crank-angle position where 50% of the fuel has been burnt from the total amount drawn in to the chamber. The crank-angle value uses TDC as a reference point, so a positive number refers to the location after TDC. Changing the location of the 50% burn point will affect the start of combustion, which is calculated by WAVE automatically.

- ***Combustion duration***

The combustion duration value represents the time where 10% to 90% of the total mixture is burnt. The control factor for this parameter is the exponent in the Wiebe function. Changing the duration results in different burn rates. For example, reducing the duration causes the simulation to burn fuel faster. Note that the 50% burn angle is fixed, so increasing the combustion duration by the using the Wiebe exponent function has the effect of advancing the start of combustion.

- ***Exponential in Wiebe function***

The Wiebe function is used to control the start of combustion. When the function's exponent value is changed, the location of the 50% burn point and the combustion duration are kept constant, the effect is shown in Figure 5-12. Increasing the value of the Wiebe function causes faster mass fraction burns. The effects include the changing the 10% burn point and the combustion duration.

- ***Profile Control***

The percentage of the mass fraction burnt in the combustion process is controlled by the profile control option. The option has two categories to control the combustion called: *Terminate at* and *Scale by*. The maximum number allowed in the profile control option is 1, which means that 100% of the fuel is burnt. Under lean fuelling conditions, 100% refers to all the fuel in the chamber, whereas 100% in rich fuelling conditions refers to only the fuel that can be burnt with a limited amount of air. "Terminate at" means that the all fuel is treated as burnt, but the burn is terminated at the point where the number is presented. For "Scale by", the fuel is treated to burn in percentage terms. This option was used for the engine simulation in the research.

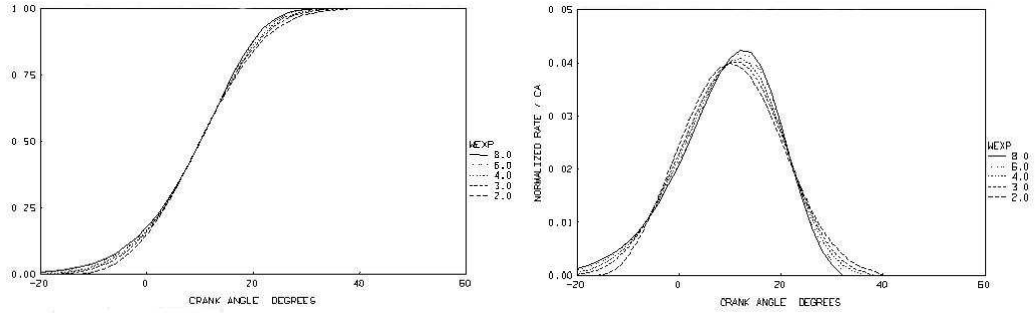

a) Cumulative burn rate b) Instantaneous burn rate

***Note** : Both case (a and b), the 10% burn point was fixed at 25^o ATDC and combustion was fixed at 25 degree*

Figure 5-12: Effect on changing Wiebe exponent function

5.2 Results from WAVE using pre-set combustion parameters

The results from WAVE are presented in two forms, which are the information within an individual cycle and the average result for each cycle. Information within the cycle shows the results for each crank angle, whilst the average results show a single value for the selected parameter.

According to the results shown in Figure 5-13, the engine model was required to run for 250 cycles under steady mode using an air/fuel ratio of 20:1. The spray model is enabled in order to see the variations in in-cylinder pressure. There are two different types of results generated by WAVE. Firstly, results for each crank angle are generated and plotted. Figure 5-13a shows a full cycle plot of in-cylinder pressure against crank angle but only one plot is generated although the simulations are run for more than one cycle. Secondly, results for each cycle are presented as an average value of the engine output as shown in Figure 5-13b. The maximum in-cylinder pressure of each cycle changed because the spray model was activated. The variations of maximum pressure from one to the next cycle are relatively low because the combustion profile can only be set for one characteristic. Those are the limitations of the result from WAVE. For cyclic variability in engine to be represented, the combustion duration, location of the 50% burn point, Wiebe function and mass fraction burnt must be changed from one cycle to

the next, as discussed in the literature review. Thus, both types of result from WAVE can be used to analyse cyclic variability in the engine and the method for control of combustion is limited. Therefore, in order to obtain details of the variations in pressure at each crank angle and allow combustion characteristics to be changed cycle-by-cycle, Matlab's Simulink was used in collaboration with WAVE to form a co-simulation package.

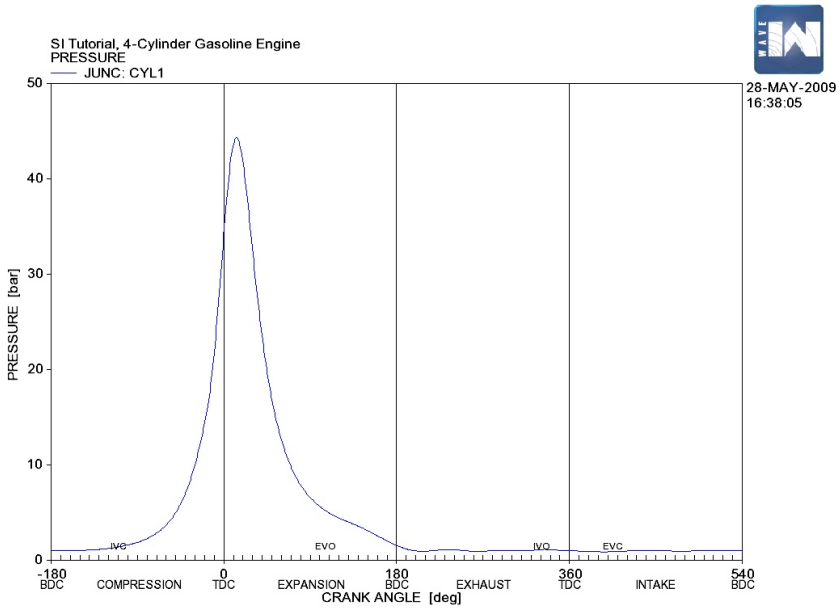

a) The only result of in-cylinder pressure that WAVE presented over 250 the cycles

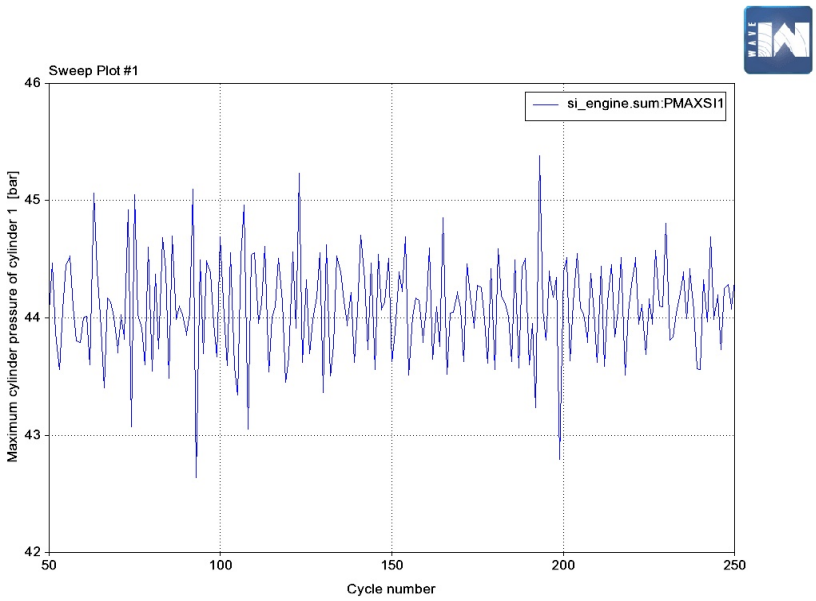

b) The results of combustion that WAVE presented over 250 cycles which shows that the results within cycle had been ignored.

Figure 5-13: Sample results of in-cylinder pressure that generated by WAVE simulation

5.3 Co-simulation between WAVE and Simulink

WAVE allows external software to communicate with it by providing actuators and sensors. Co-simulation between WAVE and Simulink enables data to be obtained for each cycle and each individual crank angle. In order to run the co-simulation, there are four important files (Table 5-1) that have to be located in the same directory folder as the engine model itself, before running the co-simulation.

Table 5-1: Important files for co-simulation

Name	*Size*	*Type*
wave	7 KB	MDL File
wavelink	11 KB	C File
wavelink.dll	72 KB	Application Extension
wavelogo	40 KB	Bitmap Image

In Simulink, WAVE will appear as a square block, as shown in Figure 5-14. In order to obtain the results, WAVE provides actuators and sensors to connect with Simulink. There are different actuators and sensors depending on the method of control for the engine model and the output required. The diagram, in Figure 5-14, shows that the actuators are used to control combustion including its efficiency, the Wiebe exponent, and the combustion duration and spark angle. The sensors are for in-cylinder pressure and in-cylinder lambda.

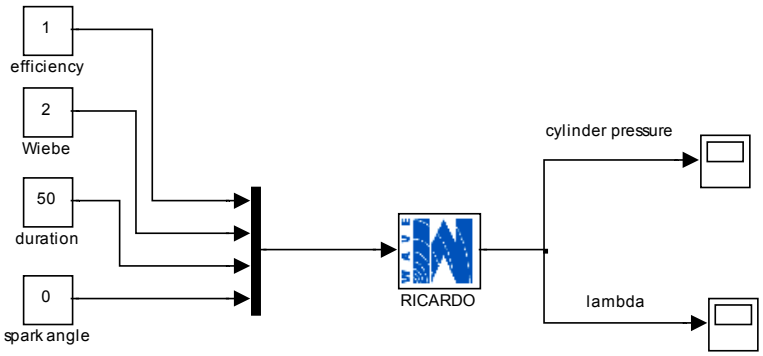

Figure 5-14: Diagram of Ricardo WAVE and Simulink in co-simulation environment.

The results in Figure 5-15 show three consecutive cycles, from the control combustion model in Figure 5-14, with a fuel amount of 12.85 mg/cycle. The results present data of the in-cylinder pressure and in-cylinder lambda for each combustion cycle over the simulation time. The simulation used information from the previous cycle for the next cycle.

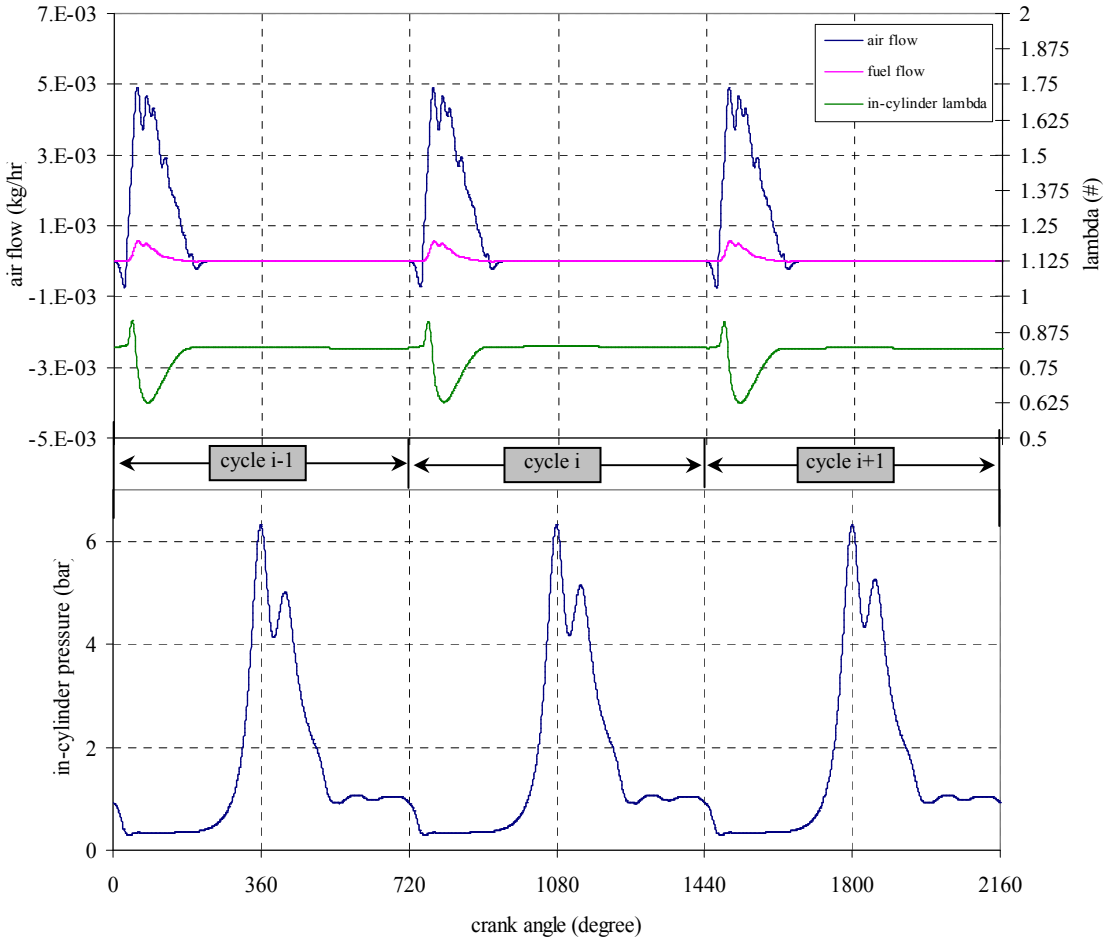

Figure 5-15: Consecutive sample results from co-simulation show air flow, fuel flow, in-cylinder lambda and in-cylinder pressure

5.4 Combustion control in co-simulation

The control of combustion in WAVE is different from the co-simulation. In the co-simulation, WAVE provides five different actuators for controlling the combustion:

1) Burn scale factor
2) Burn duration
3) Location of 50% burn point
4) Start of combustion
5) Wiebe exponent

The extra factor for control is "start of combustion". If one of these five actuators is used in the co-simulation, the characteristic of combustion is varied but the rest of the parameters are fixed by the WAVE software.

In order to have a fully controled combustion in the co-simulation, four parameters are used. There are two options for controling the combustion depending on the available information (Table 5-2).

Table 5-2: Option for control of combustion in co-simulation

Actuators	Option#1	Option#2
Burn scale factor	*	*
Burn duration	*	*
Location of 50% burn point	*	
Start of combustion		*
Wiebe exponent	*	*

Table 5-3 shows the start of combustion and the location of 50% burn point cannot be controlled at the same time. In option #1, the Wiebe exponent is used to control the profile of the fuel mass burn. Location of the 50% burn point is set using TDC as a reference point then the start of combustion is determined by WAVE. In the case of a Wiebe exponent greater than 2, location of combustion duration can be calculated by using the 50% burn angle as a reference point. The reason is that the profiles of the Wiebe function are similar during the 10% to 90% mass burn phase, but differ during

the start of combustion. Increasing the Wiebe exponent causes an increasingly distorted mass burn profile thus the start of combustion was forced to an advanced position. When Wiebe exponent was less than 2, the start of combustion (location of 1% mass fraction burnt) tended to be located at the same point, but the mass burn profile affected the combustion's duration.

Option 2 is used when the start of combustion is controlled. The location of the 50% burn has no effect on the control of the combustion. The start of combustion is at the crank-angle where the mass of fuel starts to burn and is dependent on the Wiebe function. Increasing the value of the 10% to 90% mass burn duration results in a longer combustion duration, which is achieved by interpolation while the other parameters are kept constant.

These two options have their own advantages depending on the available data. In this research, the start of combustion is fixed and the in-cylinder pressure is recorded, so that the mass fraction burnt and the combustion's duration can be calculated. Thus, option #2 is suitable for the control of the combustion in these experiments. The effects of each parameter in option #2 on combustion characteristics were shown in Figure 5-13.

Figure 5-16a shows the effect of combustion under different combustion efficiency setting. The cumulative heat release drops proportionally to the efficiency and causes the maximum heat release rate to decrease which results in a low in-cylinder pressure. By increasing the Wiebe exponent (Figure 5-16b), the cumulative heat release curves were shifted to the right closer to position of EVO which resulted in low a heat release rate since the spark ignition angle was kept constant. The same result was found on changing spark angle (Figure 5-16d). The total heat release from those cases was slightly different because the calculation used a constant gamma value. Figure 5-16c shows the effect on duration, the cumulative heat release was stretched and caused a low rate of heat release at the same angle with a shorter duration.

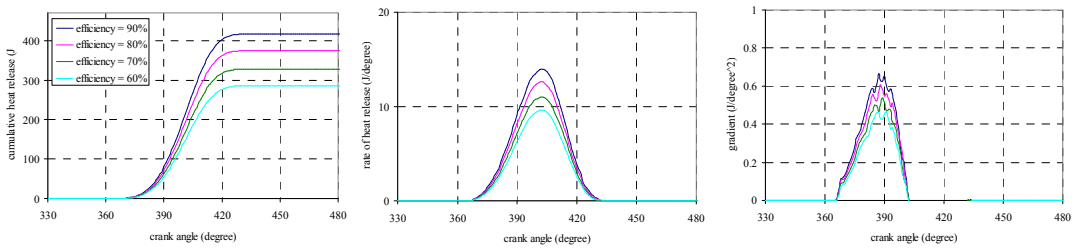

a) Effects on burning characteristics from variation in mass fraction burnt (1225 rpm, spark TDC, Wiebe exponent = 3, mass burn = 100%).

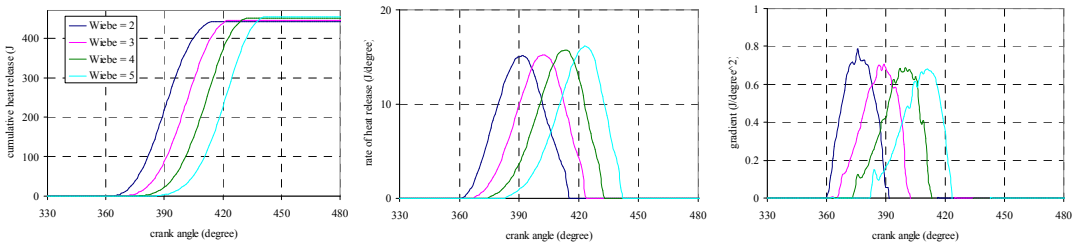

b) Effects on burning characteristics from variation in Wiebe exponent (1225 rpm, duration = 30 degrees, spark TDC, mass burn = 100%).

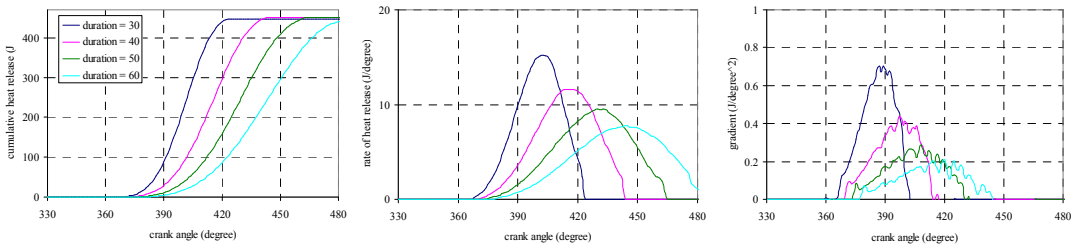

c) Effects on burning characteristics from variation in combustion duration (1225 rpm, spark TDC, Wiebe exponent = 3, mass burn = 100%).

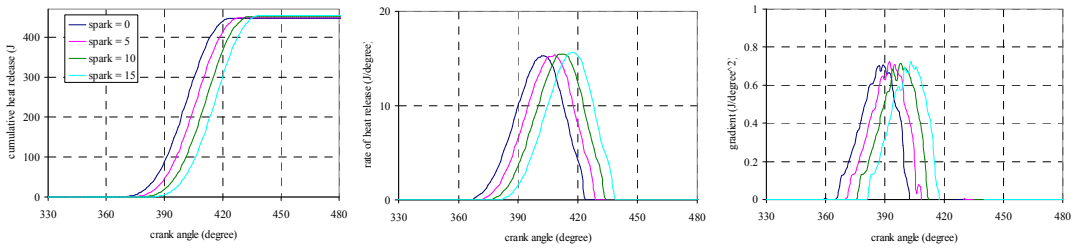

d) Effects on burning characteristics from variation in start of ignition (1225 rpm, Wiebe exponent = 3, duration = 30 degrees, mass burn = 100%).

Figure 5-16: Illustration of the effect on combustion characteristics on different efficiency, Wiebe exponent, combustion duration and spark ignition angle.

5.5 Controlling the co-simulation to represent cyclic variability

According to the literature review, the causes of cyclic variability in gasoline engines are based on two major factors including air/fuel ratio and residual gas fractions. Those two factors also affect the combustion characteristics. In order to control the combustion process, it was necessary to add features to the co-simulation that allowed direct manipulation of the combustion properties as a function of these two factors. The instantaneous values of the two factors are passed to the Simulink model using two sensors which are used to record lambda and the residual gas amount. Lambda sensors are attached to each cylinder. Residual gases, which refer to the ratio of the gas from the pervious cycle to fresh charge, are calculated from the ratio of trapped residual gases in the chamber ($trap_{residaul}$) to overall mass in the chamber ($trap_{mass}$) as shown in *Equation 5-25*.

$$RG(\%) = \frac{trap_{residaul}}{trap_{mass}} \quad \text{.....Equation 5-25}$$

Three look-up tables are used to describe the effect of air/fuel ratio and residual gas fractions on combustion and to pass this information back to WAVE as illustrated in Figure 5-17. Lambda is used to control the mass fraction burnt and feed the signal back to the input using a look-up table (see Figure 5-17). The spark angle is fixed, but the flame front starts to develop after ignition and can vary. Rousseau et al. (1999) stated that the start of combustion is considered to be at the 1% mass fraction burnt point. This delay in the start of combustion is called the ignition delay. In order to represent the ignition delay, the residual gas fractions are used to control the start of flame development by controlling Wiebe exponent and the result is then used to find the combustion duration. Look-up tables are used to predict combustion characteristics from these two signals before they are fed back to the input.

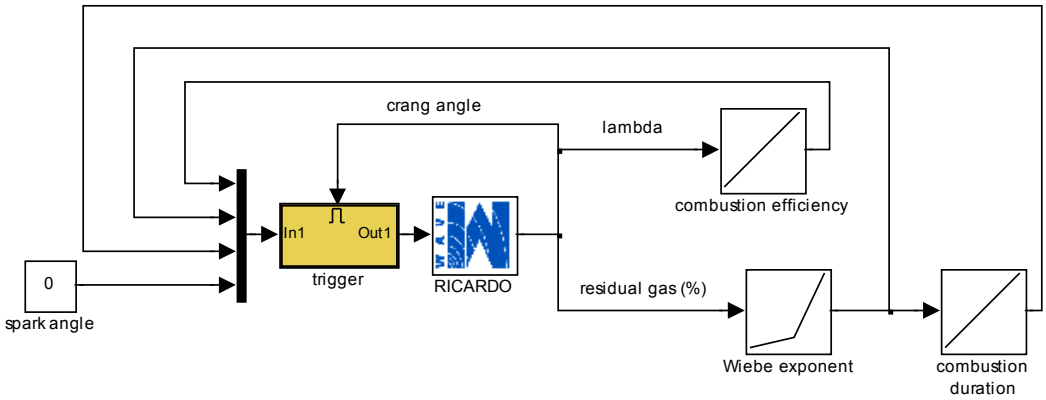

Figure 5-17: Ricardo WAVE and Simulink in co-simulation to adjust combustion profile as a function of engine operating point

As can be seen from Figure 5-17, the sensors provide signals which vary across the engine cycle. Therefore, if those signals are fed in to the model continuously, the results will be unstable. In order to solve this problem, a trigger for each cylinder is used. The triggers are set to be activated at the crank angle point where both the intake and exhaust valves are closed. When the triggers are set to activate, they allow a signal to pass through and keep its value until the new value is introduced. This process makes calculation for cycle more accurate and more stable. The trigger for each cylinder is set to active at 615, 435, 75 and 225 CA degrees for cylinder #1 to cylinder #4 respectively.

Experimental measurements detailing the residual gas fraction were not available in this work. The method developed to overcome this difficulty was to use the combustion simulation model to predict the residual gas fractions and observing how these correlate with the experimentally observed Wiebe exponent by using an average result from experimental data and applying to the simulation cycle be cycle. The next chapter explains how the experimental data was analysed and used in a look-up table by the simulation.

5.6 Conclusions

A Ricardo WAVE model has been constructed to represent the 1.8T Audi engine. The model incorporates existing engine data along with measurements of the intake and exhaust manifold geometry. The fuel spray model is activated to achieve realistic variation in the mass of fuel ingested into the cylinder. The limitations of WAVE in terms of allowing the combustion to vary realistically in response to changes in in-cylinder conditions are discussed. In order to overcome these constraints a co-simualtion with Simulink is used to allow manipulation of the heat release profile as a function of in-cylinder conditions. Specifically, the control over combustion implemented in this research is achieved by modulating four parameters - spark angle, Wiebe exponent, combustion duration and mass fraction burnt. These parameters are in reality affected by many factors, including variations in air/fuel ratio, turbulence and residual gas fraction in the chamber before combustion takes place. However, the effects from turbulence are not including because it is outside the scope of this research.

Therefore, closed-loop control of combustion is introduced by using a series of look-up tables. Air/fuel ratio and residual gas fraction were observed by sensors provided within WAVE. These two signals are fed into look-up tables, which will discussed more in the following chapter, to obtain a prediction of combustion characteristics. The resulting model is able to respond to the effects of changes in air fuel ratio and residual gas fraction and so to represent a significant proportion of the experimentally observed variability through the representation of physical effects rather than the use of stochastic methods.

Chapter 6

Analysis of experimental data for use in co-simulation

The aim of this chapter is to analyse the experimental data in order to meet the requirements for the engine simulation, specifically the values to populate the three look-up table used to control the combustion properties. Experimental data from engine Test #1, where the engine was operated under rich fuelling conditions, and from Test #3, where the engine was operated under lean fuelling conditions, are used to help calibrate the engine combustion simulation model.

6.1 Selection of simulation time

According to the cold start test experiments in this research, there are many engine parameters that vary within the 120 second test period, when the engine is initially started from a cold condition. The major variation comes from frictional engine forces, which are relatively high under cold conditions and gradually reduce, as the engine temperature increases. The engine's control strategy has to adjust the airflow rate, fuel injected per cycle and ignition timing, to overcome these frictional forces. There is also a concern with the heat transfer from the combustion chamber to liquids and engine components. In order to simulate these events, the engine model needs more information to obtain more realistic results. Therefore, there is a need to consider engine heat release.

From the experimental data, using selected test points under rich and lean fuelling conditions, the heat release has been calculated and plotted using phase lag plots. The heat release calculations from the first 100 cycles and the end of the test period have been ignored to avoid the unstable zone (i.e. after the start condition) and the transient

zone (i.e. at the end of test which changed from catalytic heating to warm-up state). Thus, the heat release data are presented from combustion cycles 200 to 1200.

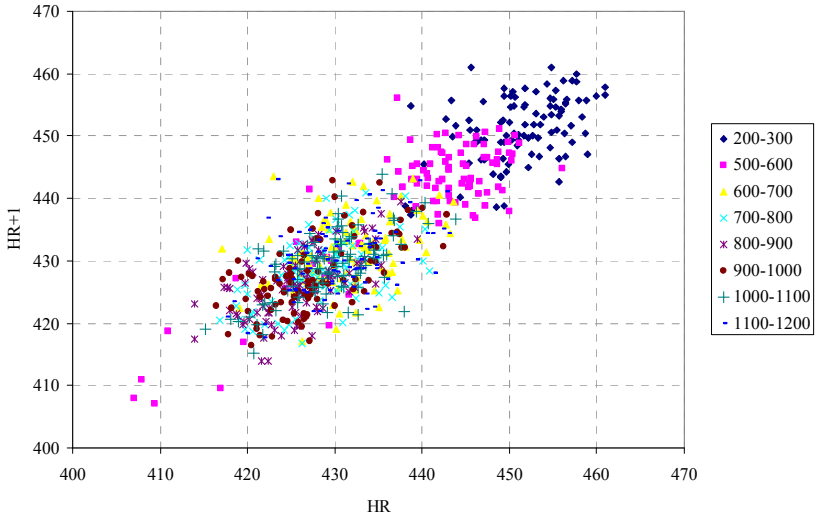

a) Phase lag plot of heat releases between cycle numbers 200 to 1200. The heat release starts to drop at cycle 200 and stops dropping at cycle 700

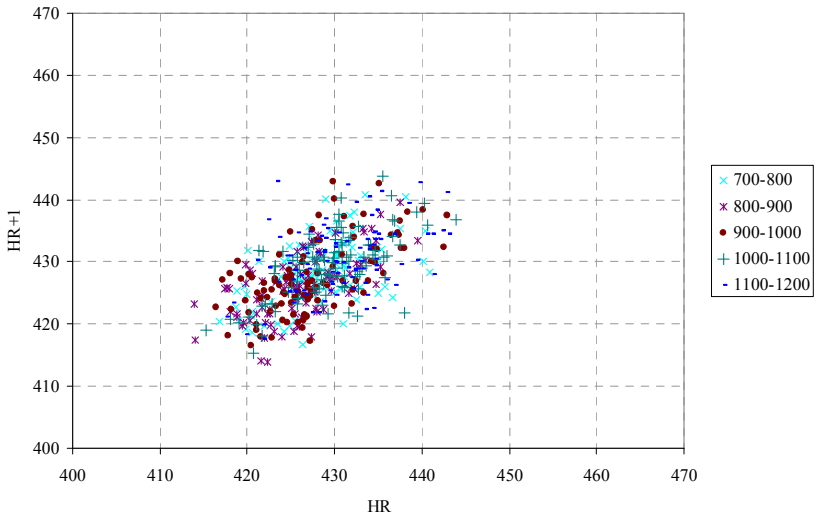

b) Phase lag plot of heat released during combustion cycles 700 to 1200. The plot shows the cyclic variability of the heat release values.

Figure 6-1: Phase lag plots of heat release showing the distribution under rich mixture fuelling from Test #1.

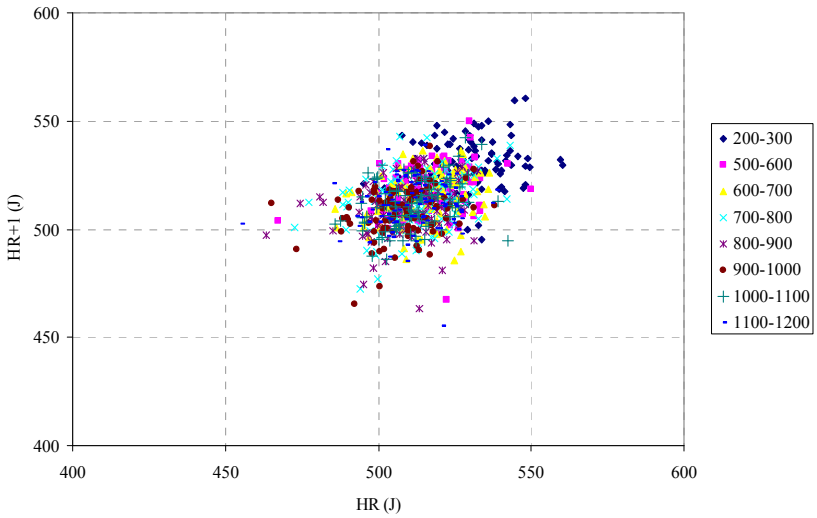

a) Phase lag plot of heat release from cycle number 200 to cycle number 1200. The heat release values from cycles 200 to 300 look slightly high. The heat release values vary from cycle to cycle.

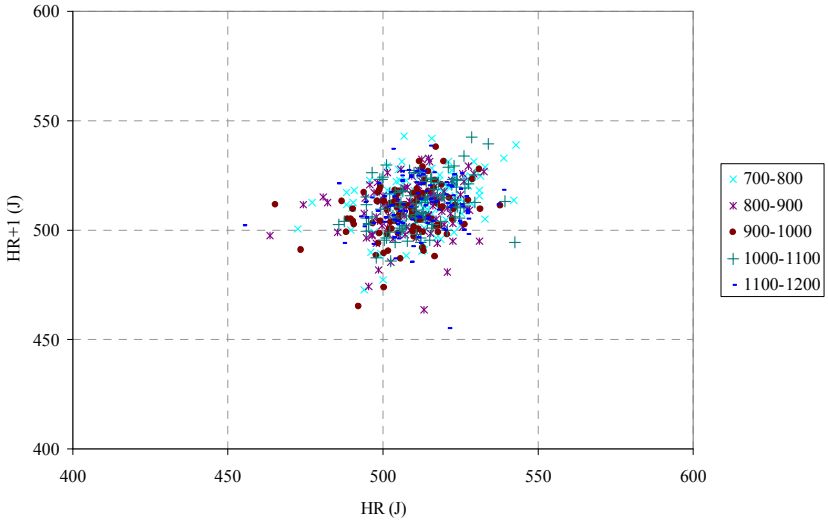

b) Phase lag plot of heat release from cycle number 700 to cycle number1200 showing the variations in heat release which start to form a triangular shape.

Figure 6-2: Phase lag plots of heat release showing the distribution under lean mixture fuelling from Test #3.

The phase lag plot for rich mixture fuelling, shown in Figure 6-1a, shows that the heat released during cycles 200 to 600 started from around 460 J and dropped to around 440 J. The heat release values from cycle numbers 700 to 1200 varied between 420 J to 440 J. The evidence suggests that the engine friction was high at the beginning and was reduced after the heat had been distributed through the components. The distribution of heat continued but remained stable from cycle 700 to 1200, which is assumed to be a stable period of Test #1. Considering the results for lean mixture fuelling, as shown in Figure 6-2a, the heat release value points trend to cluster at the same location, except for a group during cycles 200 to 300, which are of slightly higher values. The results suggest that the heat produced during lean mixture fuelling was higher, than under rich fuelling, and achieved a stable distribution in a short period. Although Test #3 shows that a stable period was established more quickly than in Test #1, the simulation required data taken from the tests where the performance was similar. Hence, data was selected from cycle numbers 700 to 1200, from both tests, for the engine simulation in this research.

6.2 Initial conditions

The co-simulation model has been built using Ricardo WAVE and Matlab Simulink. The Audi test engine has four cylinders, thus the model's combustion control blocks are separated in order to control each cylinder's combustion independently. In WAVE, signals from the sensors for lambda and residual gases, from each cylinder, are fed into a look-up table used for predicting combustion characteristics. The output signals were then fed into the combustion control blocks, as can be seen in Figure 6-3. However, there are five parameters that have been isolated from control combustion blocks which are fed as inputs into engine simulation:

- Air flow rate
- Fuel flow rate
- Engine speed
- Spark angle (located in control combustion blocks of each cylinder)
- In-cylinder temperature

These parameters are assumed to be constant values, except for the air flow rate under rich combustion.

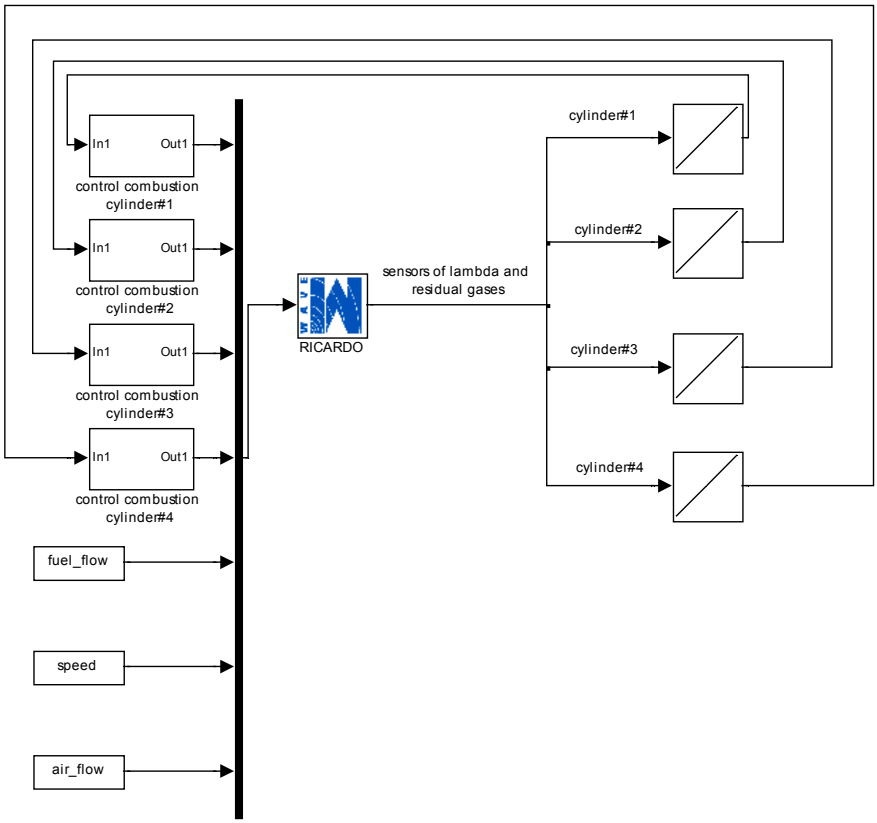

Figure 6-3: Diagram of control combustion in co-simulation environment

6.2.1 Air flow

Air flow rates affect combustion, particularly for combustion under rich mixture fuelling. Figure 6-4a shows that, during the selected simulation period of Test #1, the air flow had an affect on the heat release. Increases in the air flow rate causes increased heat release because, during rich fuelling conditions, the ratio of fuel to air is greater. In contrast, under lean mixture fuelling, as shown in Figure 6-4b, the heat release is largely independent from the air flow rate. Thus, under rich fuelling conditions, air flow rates from experimental data are feed as input to the model, while under lean fuelling an average air flow rate value is used.

Air flow cannot be set directly within WAVE because it is an output of the simulation. In order to vary the air flow rate, the model was calibrated by modelling throttle angle to achieve the target flow rate. A look-up table of flow rates with corresponding throttle angles was created by varying the percentage of the open throttle and running the simulation. Then the air flow rates from different throttle positions were used to build a look-up table. Five points were used in the simulation, as shown in Figure 6-5.

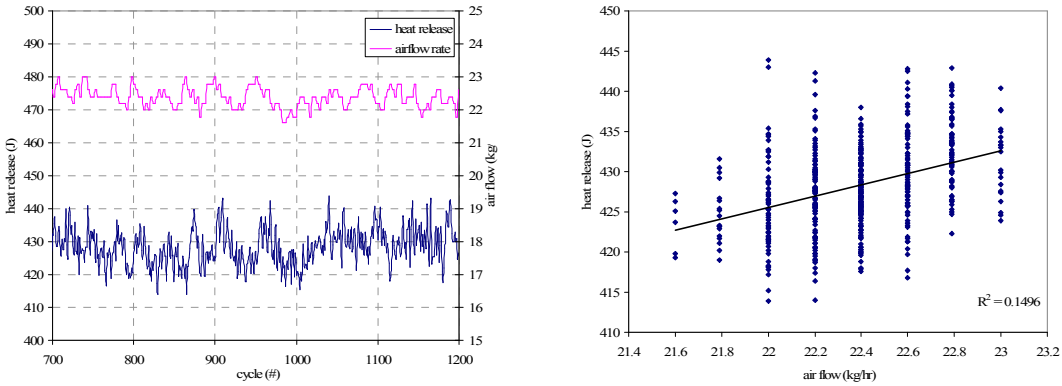

a) Experimental data from Test #1 (rich mixture) show the air flow has a weak correlation with heat release which suggests that heat release could be affected by the air flow rate.

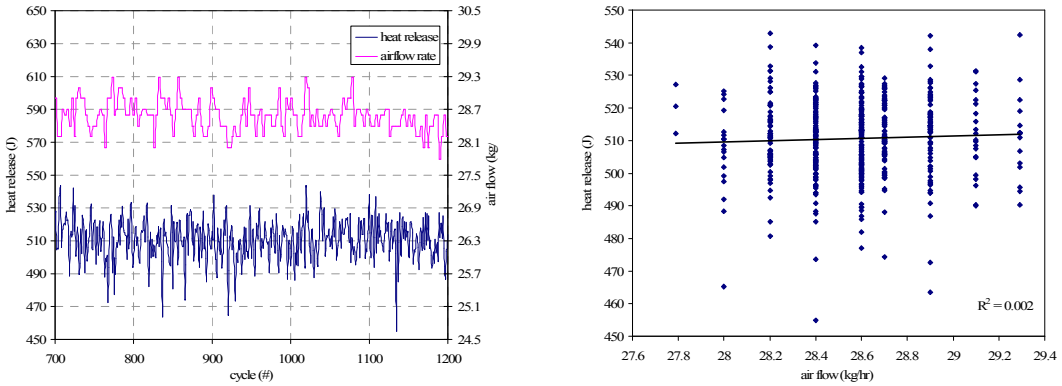

b) Experimental data from Test #3 (lean mixture) shows that the air flows have less effect on heat release compared with an engine operated under rich mixture fuelling.

Figure 6-4: Relationship between heat release and the air flow rate under rich and lean fuelling conditions.

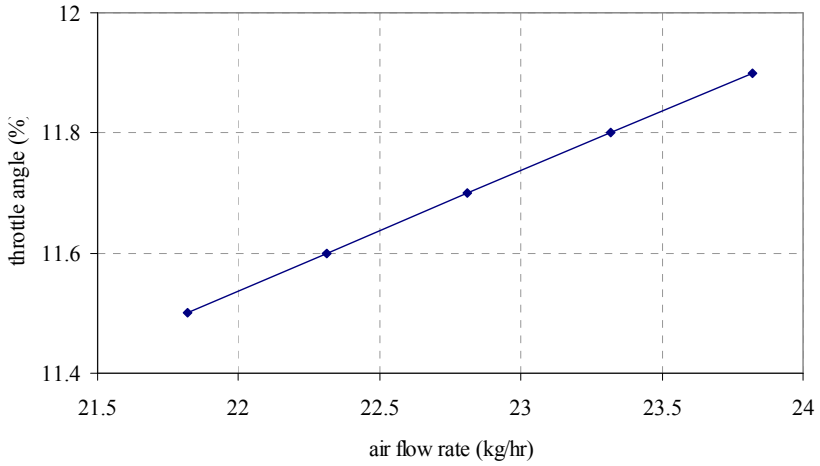

Figure 6-5: Graphical representation of the look-up table used to estimate throttle angle at engine speed of 1225 rpm for simulation on Test #1.

The air flow rate from Test #1, during the selected period, was used as an input to control the throttle in the co-simulation environment. During the simulation, the throttle of the engine was opened to achieve a target air flow. For simulation of lean combustion in Test #3, a fixed throttle position of 12.8% was used to allow 28.59 kg/hr of air flow into the system.

6.2.2 Fuel flow

In the simulation model, fuel flow rates for rich and lean combustion are held constant. The fuel flow rate from experimental data was averaged and used as an input to the simulation. Under the rich combustion operating conditions, used in Test #1, an average fuel was amount of 12.85 mg per cycle was used with the activated fuel spray model. However, the affect on combustion from the variations of fuel is less than when operating the engine under lean mixture fuelling. WAVE's spray model allows WAVE to calculate emissions which become a feedback signal for controlling combustion.

For Test #3, the fuel is used to control combustion. An average fuel amount of 11.27 mg per cycle, with the spray model activated, was used. The spray model allowed the fuel flow to vary from one cycle to the next.

6.2.3 Spark angle

The selected test for simulation had a spark angle which was controlled at zero degrees crank angle or TDC. However, the spark angles from the experimental work varied a lot over the test period, especially on Test #1, as can be seen in Figure 6-6. The spark angles of Test #1 were slightly advanced from TDC, at the beginning of the test, and slightly retarded from TDC, at the end of the test. Under lean combustion, in Test #3, the spark angle was more stable although the average spark angle was slightly advanced. However, the results show the spark angle were unstable because the engine tried to overcome the load that generated by the dynamometer which also was unstable.

An unstable spark angle will cause different combustion profiles. Normally, spark angles are advanced from TDC, to obtain maximum power output, but in this test the spark angle had been retarded to increase exhaust gas temperature. All combustion occurred during the expansion stroke, and when the piston starts to move down the cylinder the combustion chamber's volume increases. Therefore, changing start of combustion may cause the combustion to take place inside a larger volume, which will make a significant change to the engine's output.

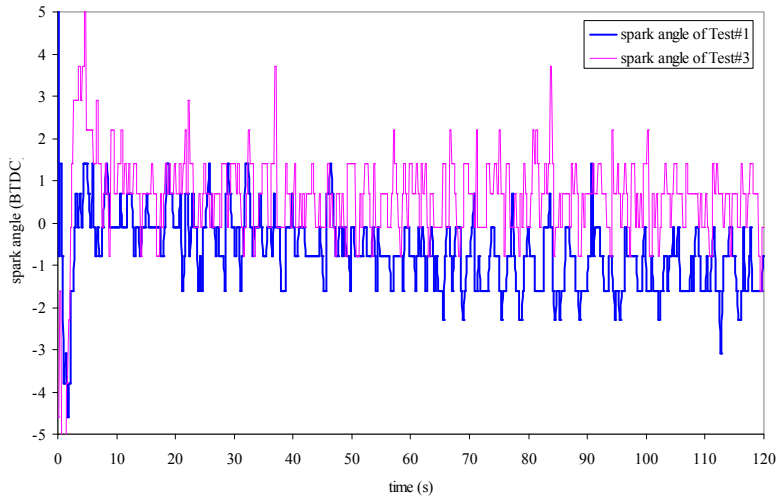

Figure 6-6: Experimental data of spark angle from rich and lean combustion

In the co-simulation, the spark angle was set to zero for both rich and lean combustion simulations, according to the test design. The variations of combustion during the selected periods are controlled by the Wiebe function's exponent which is explained later.

6.2.4 Engine speed

Engine speed is a factor that involves the air flow rate. As shown in Figure 6-7a, the engine speed in Test #1 corresponded in a similar pattern to the air flow rate, and contributed to heat release, as discussed previously in the air flow topic. The results suggest that when the throttle was opened wider, under high engine speed conditions, the air flow into the combustion chamber increased. However, when the target engine speed was set to 1225 rpm, the speed data suggested that the engine's control unit tried to regulate the speed. When the engine speed is higher or lower than the target speed, the air flow rate was adjusted by response of the throttle. The response signal in Figure 6-7a shows that the changing airflow which controlled by the throttle opening was matched with the result of engine speed which caused by oscillating throttle operation.

In contrast, Test #3 (Figure 6-7b) had no such behavioural problems, and the engine speed during the test duration had more variation than Test #1. However, part of the test period shows that the throttle still followed the engine speed. The evidence suggested that the engine's control system still tried to change the air flow rates, although they had less affect on the combustion process, because the engine was being operated under lean mixture fuelling conditions.

Although Test #1 could be controlled to achieve the target air flow rate by varying either the engine speed or the throttle angle, in the co-simulation environment, variations in the air flow rate effected by altering the throttle angle or engine speed will each cause differing variations in turbulence in the combustion chamber. Turbulence's contribution to the variation in combustion behaviour is not covered in this research. The reason for this is the limitations of the measurement suite installed on the engine, which was mainly focused on in-cylinder pressure and exhaust temperature. Accordingly, the research here was primarily concerned with cyclic variation linked to variations in the air/fuel ratio and residual gases.

In order to simplify the control of the model, and since it was possible to achieve the target air flow rate by varying the throttle angle alone, it was decided to set a fixed engine speed. The engine speed in the co-simulation environment was set to the average observed engine speed of 1225 rpm for both rich and lean combustion simulation following the test design.

6.2.5 In-cylinder temperature

In-cylinder temperature is the parameter that affects the heat transfer to the engine block and the maximum in-cylinder pressure under motoring conditions. Separate motoring pressures of the tested engine were not available but rather fortunately the very late spark timing used during all of the tests considered here allowed the motoring pressure to be observed during the working cycle. This was convenient and has the added benefit that motored pressure is available for every cycle at representative thermal and lubrication conditions. Although pressure pegging had been applied to the in-cylinder pressure data acquisition, variations in obtaining the peak compression pressure were still present. Those variations are not included in this study, thus an average peak compression pressure is used as a reference.

In order to calculate the average peak compression pressure, the maximum in-cylinder pressure at TDC of the combustion events from each test was averaged. Test #1 gives an average of 6.13 bar while Test #3 gives an average of 7.62 bar. These numbers show that more air had been induced under lean combustion. To calibrate the heat transfer sub-model (Woschni, 1967 cited by Ricardo, 2006), WAVE provides the temperature of three components that can be changed, and also allows maximum pressure to change. The components are piston top, cylinder head and cylinder liner temperature. Increasing temperature results in less heat escaping from chamber and increase in-cylinder pressure at TDC. However, each component has a different temperature depending on the combustion event, but an overall effect can be observed at maximum pressure. Calibration for the maximum pressure has been carried out by varying all three components with the same temperature until an average pressure is achieved. As a result, the simulation in Test #1 sets the component temperature to 380 ^{o}C and to 350 ^{o}C in Test #3.

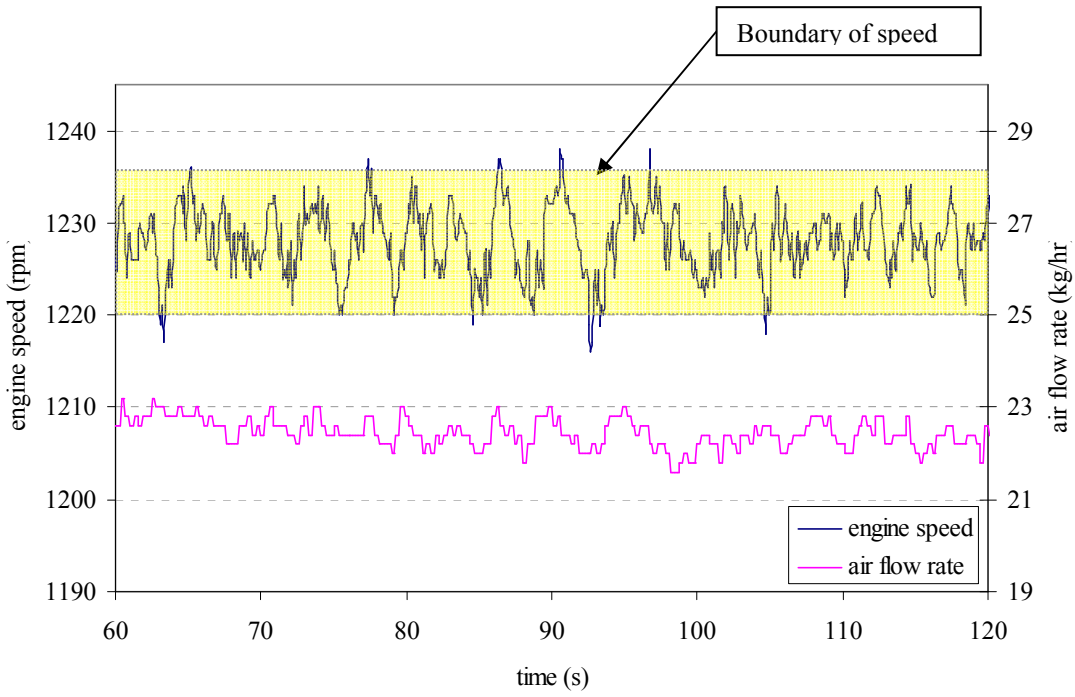

a) Experimental data from rich combustion in Test #1.

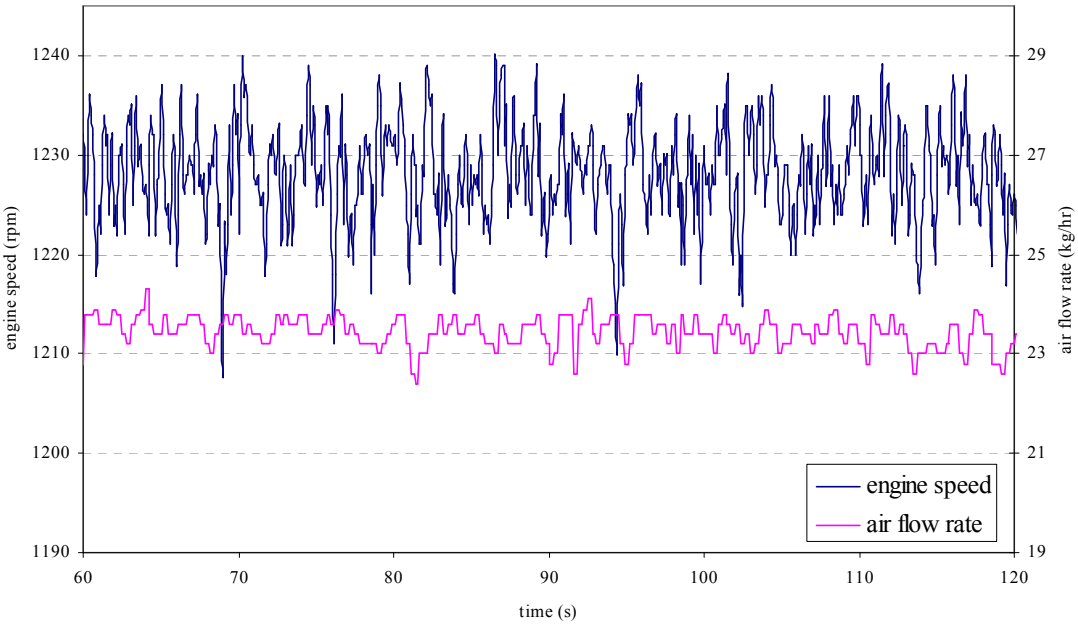

b) Experimental data from lean combustion in Test #3 shows high engine speed caused by a high air flow rate.

Figure 6-7: Comparing experimental data for engine speed and air flow rate from rich and lean combustion operations.

6.3 Control of combustion in co-simulation

In order to model the in-cylinder pressure, the combustion is controlled by three parameters, as explained in Chapter 5, they are:

- *Combustion efficiency,* which is controlled by lambda.
- *The Wiebe exponent,* which is controlled by residual gases.
- *Combustion duration,* which is controlled by the Wiebe exponent.

These three parameters were defined by analysising the experimental data and then building a look-up table to control the combustion as described in Chapter 5. However, a small amount of experimental data cannot cover all the data that is required by the simulation. Thus, the models's look-up table uses interpolation and extrapolation methods to extend its output.

The look-up table uses lambda and residual gas fraction data, as inputs from the simulation, which vary depending on the crank angle value which is unstable during the simulation. In order to prevent variations due to this instability, a trigger had been used to allow a constant to be feed into the calculation during the combustion process. Each cylinder is triggered at a different position based on the intake valve's closing position. In this simulation, the trigger for each cylinder is set to 45 degrees ABDC, which means the intake valve will be fully closed. The crank angles that are used to trigger the inputs of cylinders #1 to #4 are 615, 435, 75 and 225 degrees respectively, based on the crank angle from WAVE's sensor.

6.3.1 Analysis of combustion data for use in simulation

The analysis in this topic is targeted on the measurement of lambda and the calculation of heat release, which have been previously discussed in Chapter 4.

In regard to the control of the combustion in the engine model, lambda is the parameter which is used to control the combustion's efficiency. Measurements of lambda values in the exhaust manifold, carried out during the experimental work in this research, were

used to represent in-cylinder lambda. The lambda sensor was located near the catalytic converter and was subject to measurement errors due to noise. In order to start analysing the characteristics of the combustion, the available lambda data was compared with the heat release values using a series of histograms. The assumption here was that since combustion efficiency and hence heat release in steady state is strongly influenced by lambda, then the same will be true on a cycle by cycle basis. Therefore, if a characteristic distribution of lambda is observed, it is reasonable to assume that a similar distribution will be apparent in the heat release data. To take this assumption further, it may be assumed that the value of the observed lambda distribution is strongly related to the mean observed heat release. Furthermore, the variance in observed lambda will be responsible for a significant proportion of the observed variance in heat release. Other variations, in turbulences, for example, will also affect heat release so the two populations cannot be linked precisely. As a starting point for an adjustment mechanism, however, this seems a reasonable assumption.

Hence the mean value, standard deviation of lambda and heat release were determined and used to build an initial look-up table. This would be revised later in the calibration exercise.

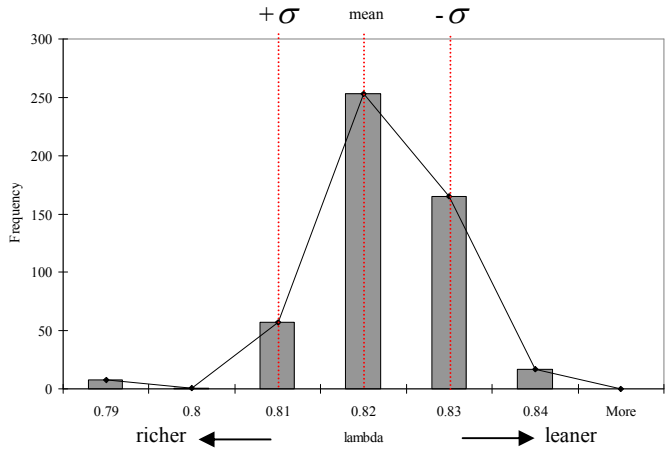

Figure 6-8: Histogram of lambda from Test #1

Figure 6-8: shows that the mean values of lambda are 0.82 and had a standard deviation of 0.01 which results in lambda distributed from 0.81 to 0.83. According to the rule of combustion efficiency used by Daw et al. (1996), a rich mixture has lower efficiency compared with a stoichiometric mixture. Therefore, the calculated heat release value will increase as lambda increases to the stoichiometric level.

Histograms were drawn showing the heat release data for all four cylinders from Test #1. Figure 6-9 shows mean value and stand deviation of heat release values for each cylinder. The distributions show that each combustion chamber had slightly different combustion behaviour, which could be caused by different amounts of fuel being injected and the effects of the air flow from unequal intake manifold lengths. All cylinders, however, had approximately normal distribution. The histograms of heat release for each cylinder were compared with the histogram for lambda in Figure 6-8. The histogram for heat release data from cylinder #4 shows the most similar distribution to the histogram for lambda.

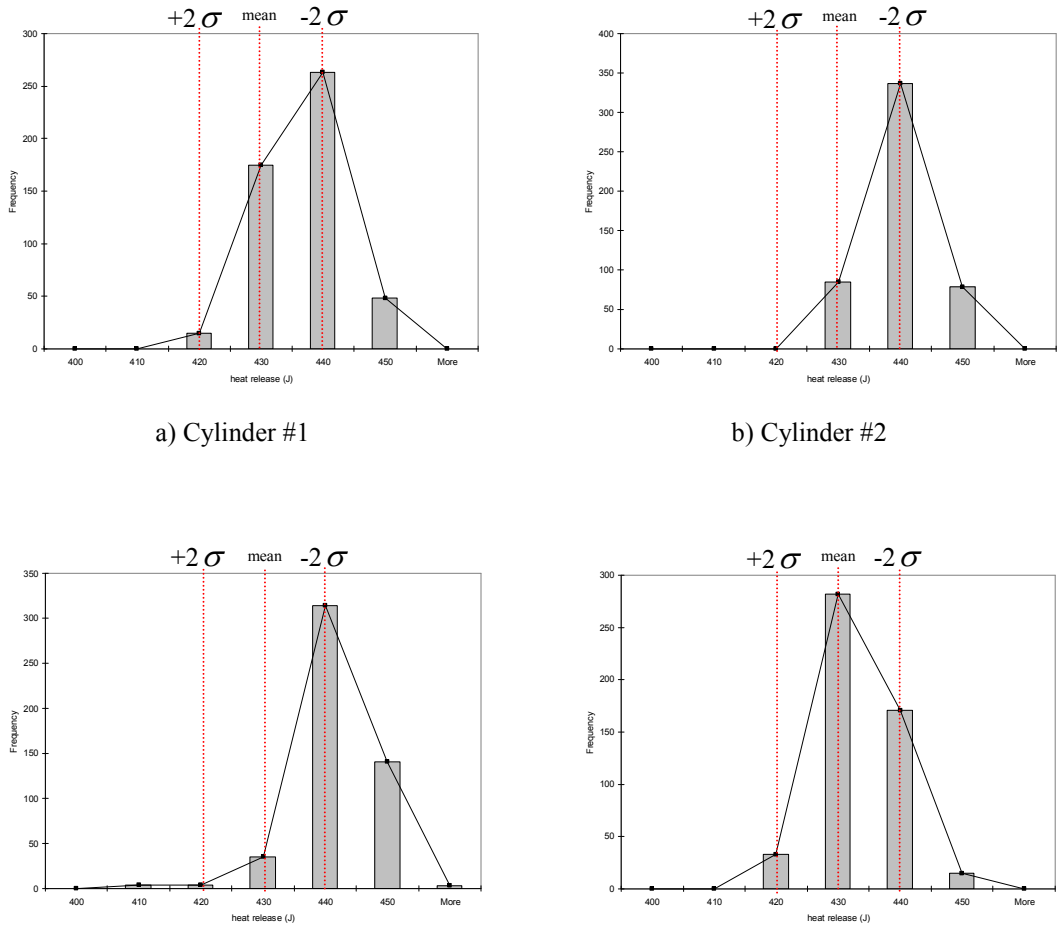

a) Cylinder #1

b) Cylinder #2

c) Cylinder #3

d) Cylinder #4

Figure 6-9: Histograms of heat release from Test #1

Under lean combustion operation in Test #3, the same analysis was used to match heat release with air/fuel ratio values. With lean combustion, the air/fuel ratio was converted to ϕ (phi is the equivalence ratio, defined as the chemically correct, stoichiometric, air/fuel ratio divided by the actual air/fuel ratio), for comparison since it was desirable to place leaner events to the left of plot to match the heat release distribution. According to the combustion efficiency model used by Daw et al. (1996), heat release increases when ϕ increases. From the same matching analysis, Figure 6-10 shows the heat release from cylinder #4 in Test #3 has a similar distribution to that of ϕ from the lambda sensor. From this point, the combustion from cylinder #4 of both tests is used for simulation and comparison.

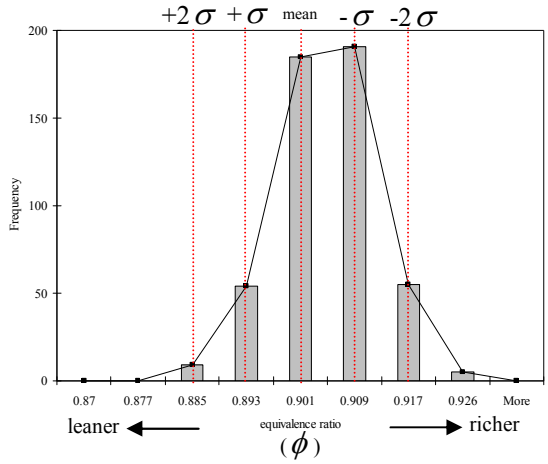

a) Equivalence ratio from Test #3

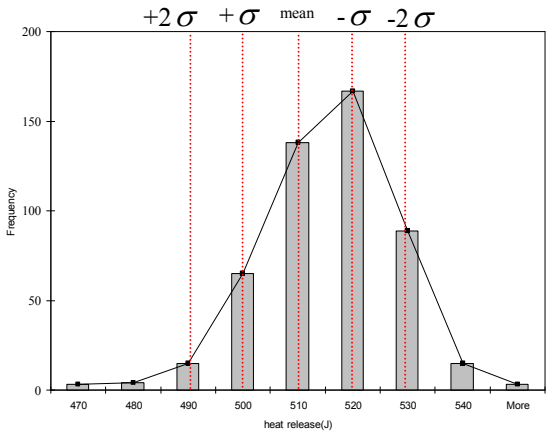

b) Heat release from cylinder #4

Figure 6-10: Histogram of equivalence ratio (ϕ) and heat release from Test #3

The analysis discussed here is used to create a look-up table for combustion efficiency. Information on lambda is not enough to form the complete combustion profiles, the Wiebe exponent and combustion's duration also have to be taken into account.

The heat release data from Test #1 and Test #3 was used to calculate the mass fraction burnt, based on the maximum heat released. The Wiebe exponent corresponds to the point where the fuel that has been burned gives 1% of heat release. That is, 1% of heat release is also used to refer to the 1% of fuel that is expected to burn in the combustion process. Rousseau et al. (1999) stated that the location of 1% heat release can be used to represent the start of combustion. However, the crank-angle corresponding to 1% of burned fuel is different from the location of the ignition spark and always occurs after it. The difference between the crank angles for ignition and 1% of fuel burnt were defined as the *ignition delay*. The combustion duration refers to the period between the crank angles corresponding to 10% and 90% of fuel burnt. Finally, the heat release is plotted against the location of 1% of heat release, and the location of 1% of heat release is plotted against the combustion duration. The two plots representing rich conditions can be seen in Figure 6-11 and those representing lean condition in Figure 6-12. Each shows all combustion events occurring during the selection period.

The plots of heat release against 1% of burned fuel (Figure 6-11a and Figure 6-12a), show that for most of the combustion events, for both conditions, the 1% of burned fuel point varys from 370 to 380 crank angle degrees. The results suggested that many combustion events resulting in the same heat release were observed even though they exhibited a wide spread of ignition delay, over 7^{o} CA. This spread is likely to be caused by the varying percentage of residual gases (Bonatesta et al., 2008). Under rich fuelling conditions, increased heat release seems to correspond to increased ignition delay, while under lean fuelling conditions the two parameters appear to have no correlation.

Considering the combustion durations in Figure 6-11b and Figure 6-12b, the plots for rich and lean fuelling conditions suggest that lengthy combustion durations are caused by large ignition delays (Lindström et al., 2005). The duration under lean conditions is longer when the point where 1% of fuel is burnt increases, which suggests that the lean mixture has a low flame speed.

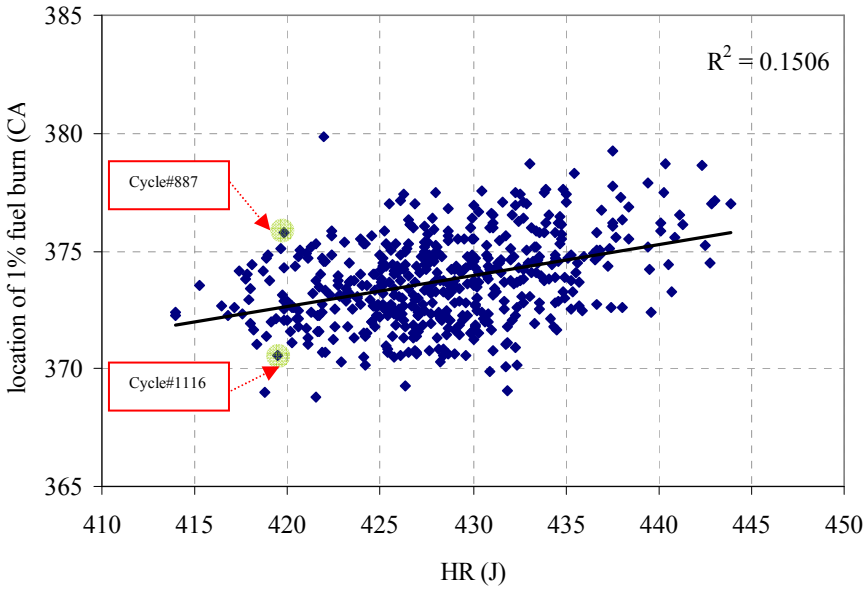

a) Relationship between start of combustion (expressed as angle of 1% burn) and total heat release for rich combustion (1228.3 rpm /0.6 bar/lambda of 0.82). It can be seen that a given heat release correlates only weakly (R^2 of 0.15) with start of combustion angle.

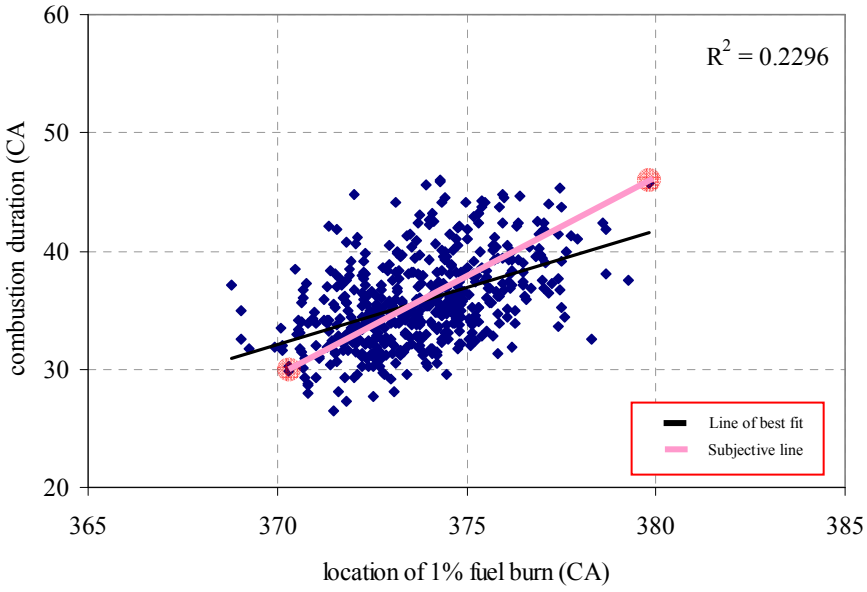

b) The relationship between combustion duration and location of start of combustion for rich combustion (1228.3 rpm /0.6 bar/lambda of 0.82). The R^2 value of 0.23 indicates a weak correlation.

Figure 6-11: Relationship of heat release, location of 1% of fuel burned and combustion duration from Test #1 operating under rich conditions.

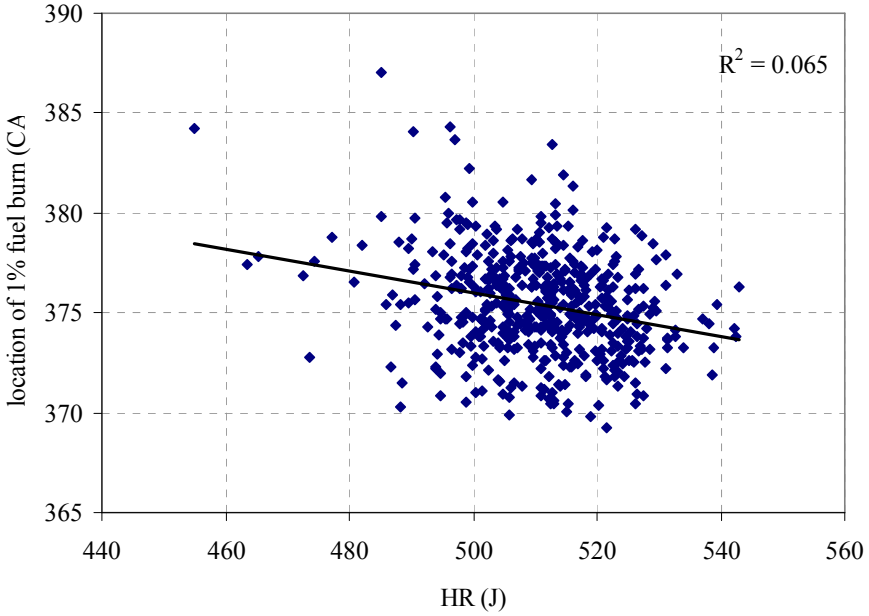

a) Relationship between start of combustion (expressed as angle of 1% burn) and total heat release for lean combustion (1228.2 rpm /0.5 bar/lambda of 1.10). It can be seen that a given heat release correlates only weakly (R^2 of 0.06) with start of combustion angle.

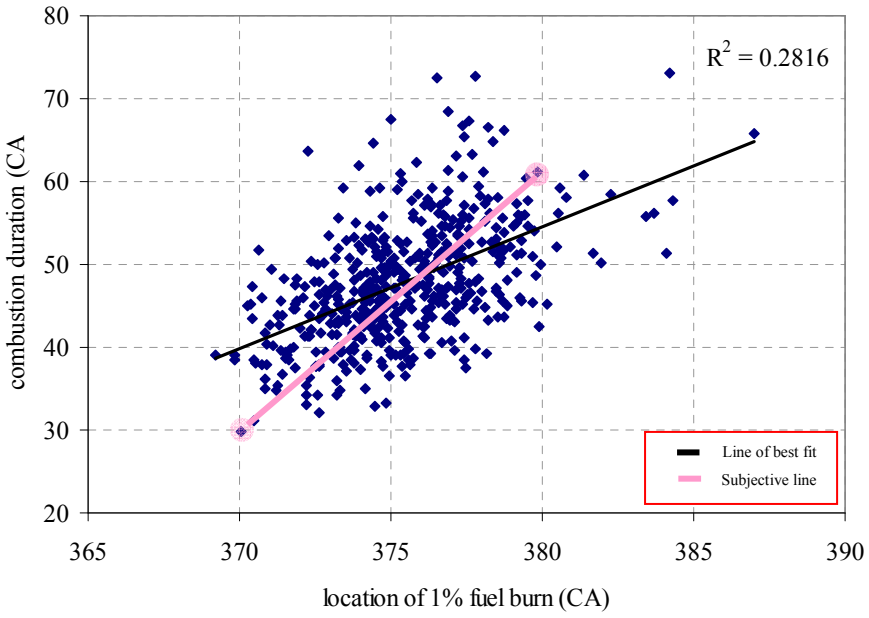

b) The relationship between combustion duration and location of start of combustion for rich combustion (1228.2 rpm /0.5 bar/lambda of 1.10). The R^2 value of 0.28 indicates a weak correlation.

Figure 6-12: Relationship of heat release, location of 1% of fuel burned and the combustion duration from Test #3 that operated under lean fuelling conditions.

6.3.2 Combustion efficiency

The heat release is assumed to be from the total mass of fuel that has been burned in one combustion event. However, the same heat could be released with different ignition delays.

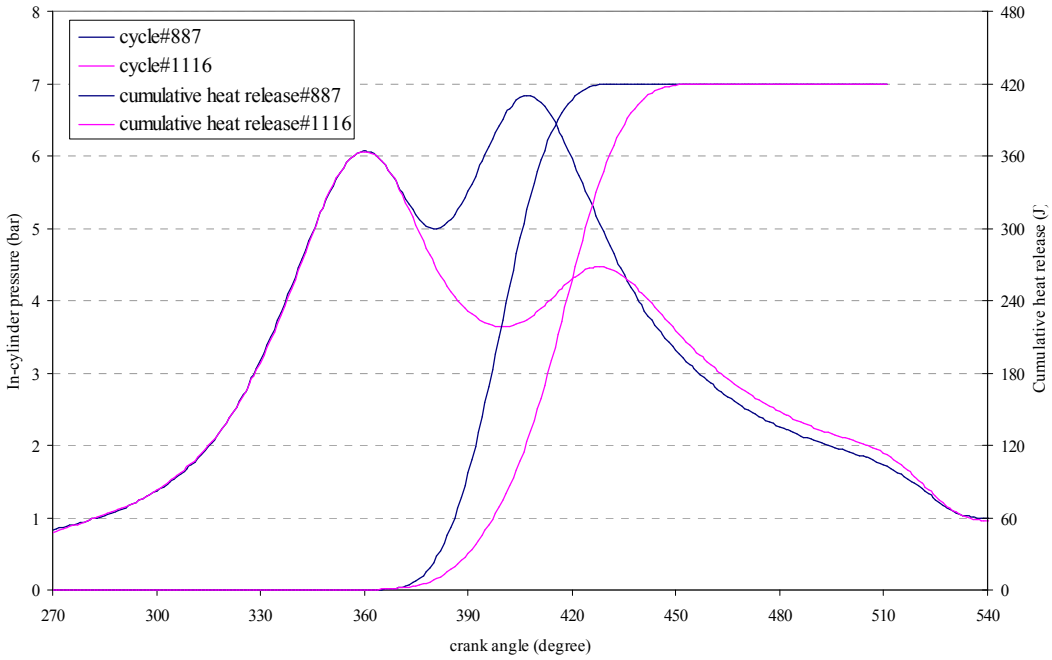

Figure 6-13: Illustration of similar heat release from different combustion characteristic

Figure 6-13, shows two different in-cylinder pressures from Test #1 that give a similar maximum heat release value of 420 J. Although, the two combustion events gave the same heat release they have different IMEP values which led to variations in engine output. The fastest burn, on Cycle #887, gave an IMEP of 5.44 bar while the slowest burn from Cycle #1116, gave only 4.25 bar. The mechanisms of ignition delay and extended combustion duration are caused by variation in residual gas fraction.

In order to calculate the combustion efficiency in Test #1, the correlation of lambda and heat release, as discussed earlier, are used to determine the combustion efficiency percentage. The air flow and fuel flow rates are taken from experimental data. Each lambda value is associated with a fast burn, although the residual gas in the combustion chamber could be either high or low. The fastest burn from Test #1 had 10 degrees CA

of ignition delay with combustion duration of approximately 30 degrees CA, as can be seen from Figure 6-11. As a starting point for the simulation, approximate initial values are used, because those values were modified later to achieve the best results.

In the co-simulation environment, the spark angle was set at top dead centre and the Wiebe exponent varied until 10 degrees CA of ignition delay was achieved. As a result of running the simulation, a Wiebe exponent value of 3.1 was found to allow combustion to start at 370 CA (10 degrees ATDC) and is used to represent a fast burn. The combustion efficiency was then varied until it achieved the target of matching the heat release. This process was repeated by changing the fuel flow rate to match other air/fuel ratios. The results for combustion efficiency are shown in Table 6-1.

The combustion efficiency for lean mixture in Test #3 also used the same methodology to obtain the look-up table. The fast burn combustion under lean fuelling had 10 degrees CA ignition delay and 30 degrees CA for the combustion duration (Figure 6-12) which are similar to those for the rich fuelling conditions. Four correspondences between lambda and heat release were taken into account, as shown in Table 6-2.

The efficiency of rich combustion dropped when the mixture's fuel quantity increased. In contrast, the efficiency of lean combustion increases when more fuel is mixed with the air. These findings agree with those of Daw et al. (1996)

Table 6-1: Fuel mass fraction burned during Test #1

Location in population	Fuel (mg)	Lambda (#)	HR (J)	Fuel mass fraction burn(%)	Residual gases (%)
$+2\sigma$	13.20	0.811	421.56	0.90	9.48
mean	13.02	0.820	431.72	0.925	9.74
-2σ	12.85	0.829	439.75	0.94	9.77

Note: Speed = 1225 rpm
Wiebe exponent = 3.1 which give fuel start burn at 370 CA
Duration = 30 CA

Table 6-2: Fuel mass fraction burned during Test #3

Location in population	Fuel (mg)	Lambda (#)	HR (J)	Fuel mass fraction burn (%)	Residual gases (%)
$+2\sigma$	12.31	1.090	529.40	0.960	8.01
$+\sigma$	12.15	1.101	519.21	0.945	8.03
mean	12.06	1.109	509.71	0.928	8.01
$-\sigma$	11.94	1.122	500.98	0.915	7.91

Note: Speed = 1225 rpm

Wiebe exponent = 3.1 which give fuel start burn at 370 CA

Duration = 30 CA

From Table 6-1 and Table 6-2, the look-up tables were created using lambda as input. The output is the fuel which is expected to be burnt, as can be seen from Figure 6-14.

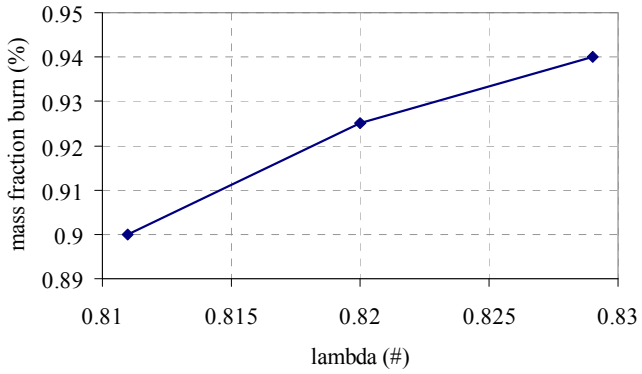

a) Combustion efficiency for rich mixture fuelling shows that the mass fraction burnt increased when lambda was increased.

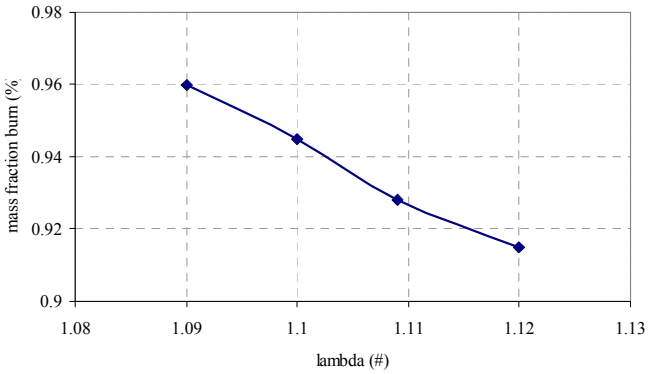

b) Combustion efficiency for lean mixture fuelling shows that the mass fraction burnt decreases when lambda increased.

Figure 6-14: Mass fraction burned presented by co-simulation.

6.3.3 Wiebe exponent and combustion duration

Under rich combustion, Figure 6-11a is used to consider the maximum and minimum ignition delay during the test period which is affected by the residual gases. When the ignition delay is plotted against the combustion duration, as shown in Figure 6-11b, the results show a weak linear relationship as can be seen in line of best fit and subjective line where a ignition delay of 10 degrees corresponded to 30 degrees of combustion duration and a ignition delay of 18 degrees had 45 degrees of duration. For lean combustion, similar analysis was carried out, with the results shown in Figure 6-12. The weak linear relationship between ignition delay and combustion duration was still present. Under lean mixture fuelling, the ignition delays were longer than with a rich mixture and contribute to a large combustion duration (Aleiferis et al., 2004).

In order to control the combustion profile, the fastest and slowest combustion events from Test #1 were chosen to calculate the Wiebe exponent. Running the co-simulation, with Wiebe exponents of 3.1 and 3.4 achieved maximum and minimum ignition delays of 10 and 18 degrees respectively. Using the relationship of the ignition delay and combustion duration, the output signals from Wiebe exponent are fed as inputs to the look-up table of combustion durations that is based on the fact that 30 and 45 degrees correspond with Wiebe exponents of 3.1 and 3.4 respectively. The look-up table's values have a linear relationship as shown in Figure 6-15a. With lean combustion, the Wiebe exponents of 3.1 and 3.8 are used to represent the minimum and maximum ignition delays of 10 and 20 degree respectively. The combustion durations were 30 and 60 degrees according to Wiebe exponent as shown in Figure 6-15a.

Considering the look-up table for the Wiebe exponent, the input is the residual gas fractions have not been measured but were estimated for these operating conditions using WAVE. The look-up table for the Wiebe exponent has a linear relationship. The maximum and minimum values of the residual gas fractions come from simulations corresponding to the cycles descried in Table 6-1 and Table 6-2. Under rich fuelling operation, the maximum and minimum residual gas fractions were estimated to be 9.77% and 9.48%, but under the spray model those values may change according to the mass transfer. Thus, the range of residual gases was set from 7% to 9% to ensure that they would cover the range of the residual gas fractions from the simulation as can be

seen in Figure 6-15b. Under lean mixture operation, the same considerations have been used and the range for the residual gases is set from 8% to 10%.

These are estimates of the effect of residual gas fraction and are used as a starting point for the simulation and will be adjusted later. The next chapter will discuss the initial results from the co-simulation and consider the results for the residual gases and heat release with the aim of improving the accuracy of the co-simulation.

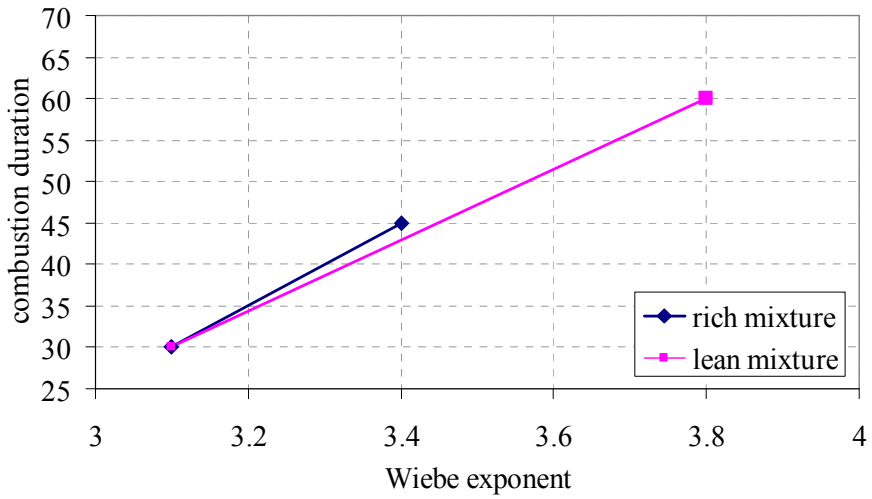

a) Combustion duration look-up table shows rich combustion had short duration while lean combustion

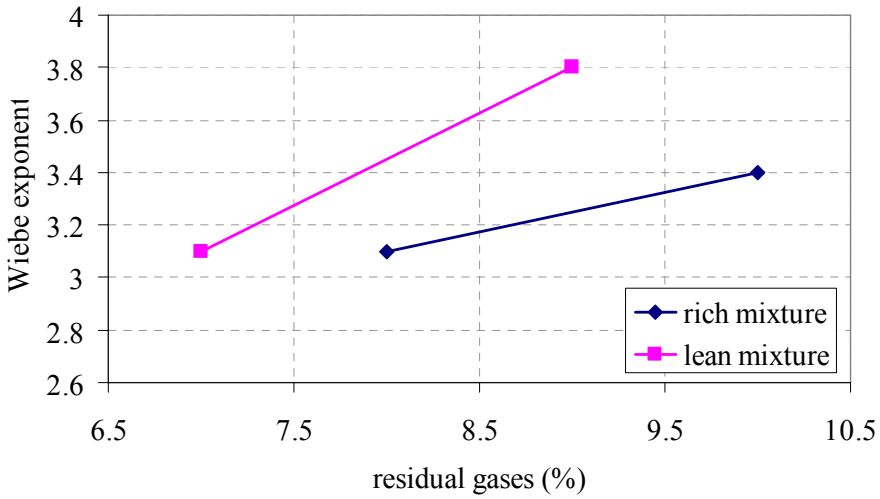

b) Wiebe exponent look-up table shows the lean combustion had potential of long ignition delay

Figure 6-15: Look-up table for controlling combustion characteristic base on estimated residual gas fraction.

6.4 Conclusion

In Chapter 5 the requirement for look-up tables to control combustion characteristics was introduced. The underlying assumption was that time averaged operating conditions could be observed and that from those average results tables describing by combustion behaviour could be constructed. Those tables could subsequently be used to control combustion on a cycle by cycle basis. This chapter presents the experimental data analysis required in order to allow the creation of these look-up tables. The stable operating period seen in the experimental data, from cycles 700 to 1200 for each test, was selected and analysed to determine combustion characteristics including the Wiebe exponent (referring to the start of combustion), combustion duration and percentage of fuel burnt in each combustion event. Those parameters were used to create look-up tables describing their variation in response to changes in air/fuel ratio and residual gas fractions. Further, the initial conditions of parameters in the simulation especially in-cylinder temperatures were calibrated to calibrate the average peak compression in-cylinder pressure. In addition, an average value of fuel flow, engine speed and spark angle were determined for use in the simulation. In the case of air flow, lean conditions were modelled using an average air flow since this is not the limiting factor in the combustion. Under rich fuelling air flow data from the experimental work was used because under such a condition air flow controls the rate of fuel that can be burnt.

The next chapter will discuss the incorporation of these relationships from experimental data into the engine model and subsequent modification of the model to achieve a better representation of cyclic variability.

Chapter 7

Simulation results using co-simulation to control combustion

In this chapter, the first results using the engine combustion co-simulation's look-up tables are presented. The prediction of residual gas fraction from the co-simulation, are used to modify the relationship of the ignition delay and the fuel mass fraction burnt. The look-up table method is also used to estimate the effect of remaining residual gases in the combustion chamber before the mixture is ignited.

7.1 Result of rich mixture simulation compared with experimental data before adjusting look-up table

The simulation was run over 500 combustion cycles. The input of engine speed was 1225 rpm, spark angle was TDC and average fuel of 12.85 mg was injected. The air flow rate was taken from the experimental data.

The first results from the simulation were used to analyse the suitability of the look-up tables that were created from the experimental data. The results were also used to develop a method to modify the look-up tables in order to achieve more accurate results. Each parameter is presented and compared with the experimental data.

7.1.1 Comparison of lambda

Sample results for exhaust lambda, from the experimental work, are taken from Test #1. The results in Figure 7-1a show that the lambda values, from the experimental data, had

a different distribution compared with those from the simulation. The fuel mixtures from the simulation had lambda values which were slightly lean and more widely distributed than the experimental data. The similar results for lambda with lean combustion are shown in Figure 7-1b. Experimental by measured lambda corresponded to a rich mixture, whilst the simulation's lambda value results were more widely distributed.

The values for lambda, in the simulation, came from the fuel flow and air flow data. The experimental work's lambda sensor was located far from the exhaust port which could cause errors, whilst the simulation's lambda was measured in the cylinder. However, the results from the experimental work and the simulation had an overlap in the ranges of lambda which are acceptable.

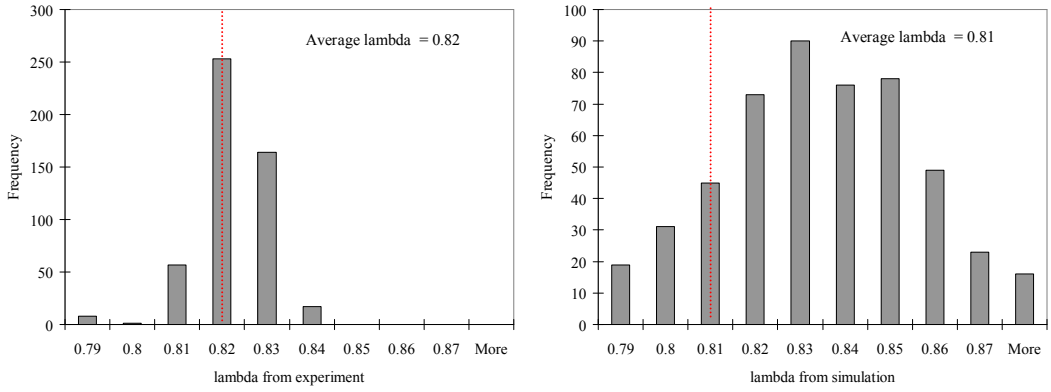

a) Lambda from rich conditions

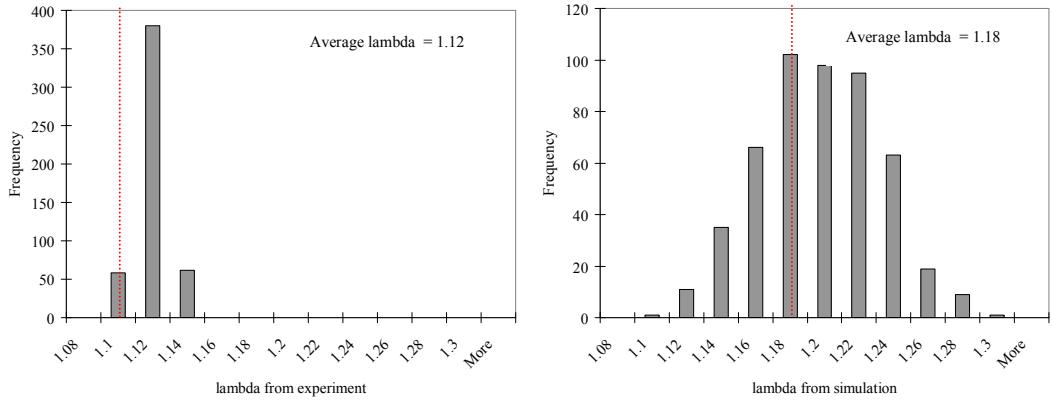

b) Lambda from lean conditions

Figure 7-1: Comparison of histograms of lambda between experimental (left) and simulation (right) results.

To examine the acceptability of the lambda results, the mechanisms affecting lambda in the exhaust are explained. Under rich combustion, the average lambda value from the simulation shows that the average lambda value at the exhaust port was slightly leaner than seen experimentally. The reasons were the location of lambda sensor and the input of simulation. The location of the lambda sensor was near the catalytic converter, which was reading the combination of lambda from all cylinders while in the simulation lambda was measured near the exhaust port, which caused different distribution of lambda values. Another error came from the input of air flow and fuel flow in the simulation, using an average value while those two values in the experimental data were varying from cycle to cycle. Therefore, the experimental results for lambda were always affected by those mechanisms which lead to either decreasing or increasing in the lambda value. Under lean combustion, the simulation shows that average lambda value near the exhaust port were slightly leaner than seen experimentally.

When using the simulation to predict the effect of combustion efficiency on the co-simulation under a wider distribution of lambdas there are some difficulties. The design of the look-up table for combustion efficiency, as discussed in the previous chapter, was created from a small range of known lambda values, recorded during the experimental work. This means that data are not available for extreme values of lambda and these must instead be estimated by extrapolation. Therefore, although the trends represented are expected to be broadly representative of actual system behaviour there will be errors in predicted combustion efficiency that will in turn lead to errors in heat release calculations.

7.1.2 Comparison of heat release

Heat release is calculated from in-cylinder pressure data and is also used to explain the fuel burn rate for each combustion cycle. Figure 7-2a shows a phase lag plot of heat release, under rich combustion, which has an approximate maximum heat release value, calculated by simulation, of 470 J, whilst the experimental results were somewhat lower. The minimum heat release value from the simulation was also lower than that calculated from the experimental data. The plot suggests that the calculation of the combustion efficiency in co-simulation needs to be adjusted.

As shown in Figure 7-2b, the consecutive combustion cycles' heat release values had similar values to those from the experimental work. The average value of heat release from the simulation was similar to the experimental value, but the range of heat release values from the simulation was a lot broader. The plot suggests that the middle combustion efficiency values were correct but that the maximum and minimum efficiency values need to be adjusted. Moreover, the range of lambda from the experimental work was wider than the range of lambda seen in the simulation. In order to ensure that each lambda value will be calculated accurately, and give results in a reasonable range, the look-up table of combustion efficiency needs to include an increased range of lambda.

In contrast, under lean combustion, the heat release values from the simulation were lower than those from the experimental data, as shown in Figure 7-3a. The distribution of the simulation results was also greater than that of the experimental results. The results suggest that the combustion efficiency table, that had been created using experimental data, was too low. The distribution also suggests that the range of lambda in the table is less than that seen experimentally, as discussed previously. These factors cause the model's look-up table to give output out of the range of the experimental data, which, in turn, directly affects the heat release calculations.

Consecutive combustion cycles' heat release values for lean combustion, shown in Figure 7-3b, show that the overall heat release from the simulation was a lot lower than that from the experimental data. Its range between maximum and minimum heat release was also larger. The results suggest that the simulation requires some adjustment to match the experimental data.

According to the discussion above, the results of the heat release calculations, from rich and lean combustion, show that the look-up table's lambda values' range needed to be modified to cover the lambda values that will occur from the calculations produced by Wave. In addition, the combustion efficiency value needed to be adjusted until it corresponded more closely to those from the experimental results. Although the look-up tables for combustion efficiency that had been created from previous data cannot achieve good results, they do provide a good starting point.

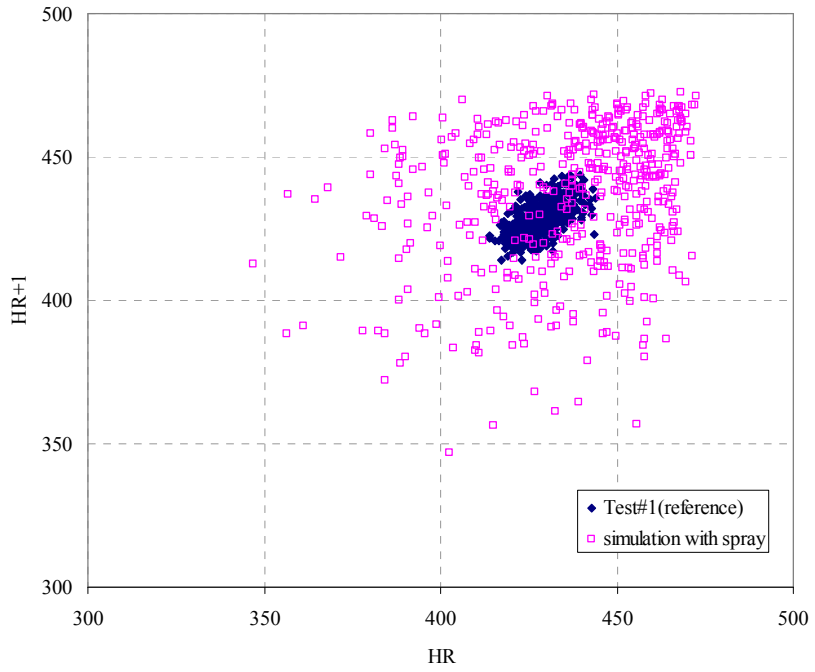

a) Simulation of rich mixture shows that the look-up table of combustion efficiency has to adjust the range to bring the high heat release down and increase the lower value

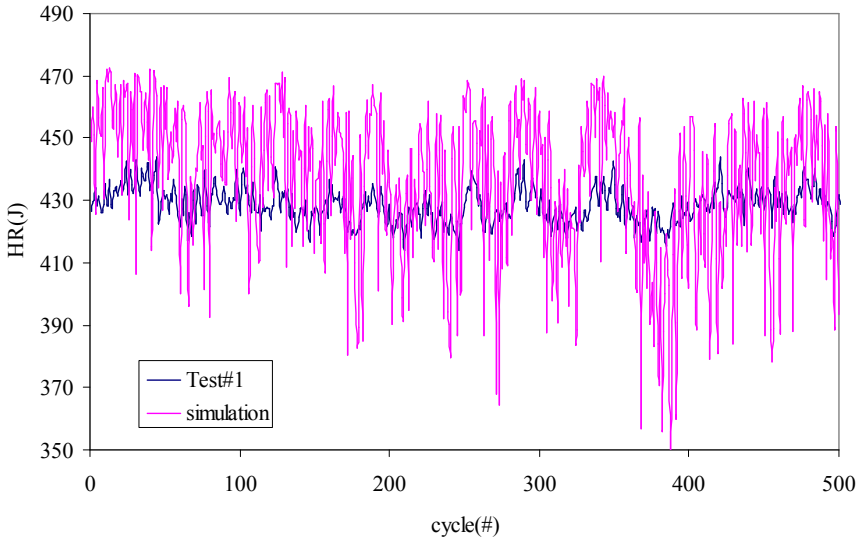

b) Consecutive heat release suggests that the middle value of look-up table of combustion efficiency is correct only the maximum and minimum need to be adjusted. Considering the consecutive cycle to cycle operation shows that the heat release from cycle to cycle behave in a similar way to the experimental data.

Figure 7-2: Comparison of heat release under rich combustion from the first results by phase lag plot (top) and consecutive plot (bottom).

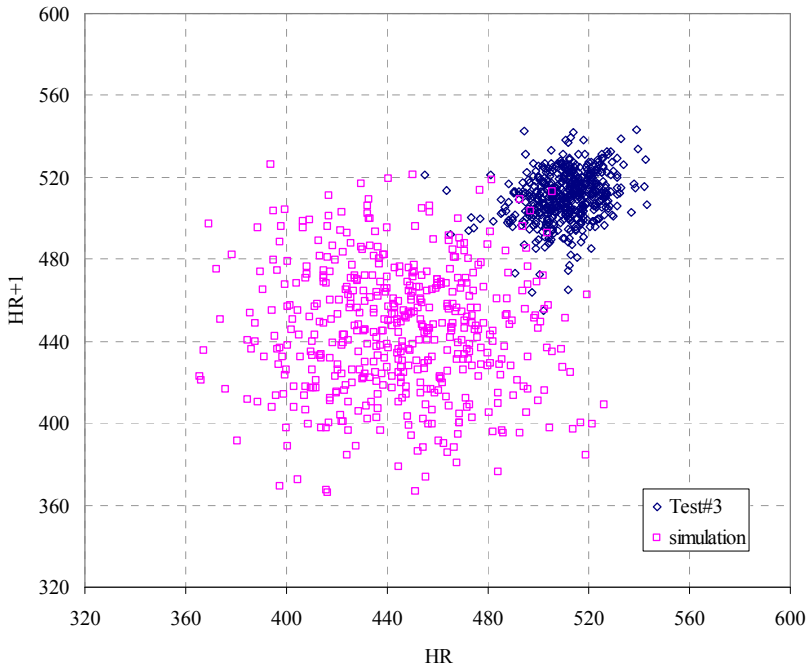

a) The simulation of lean mixture operation clearly shows that the combustion efficiency was too low and needs to increase to achieve the target heat release.

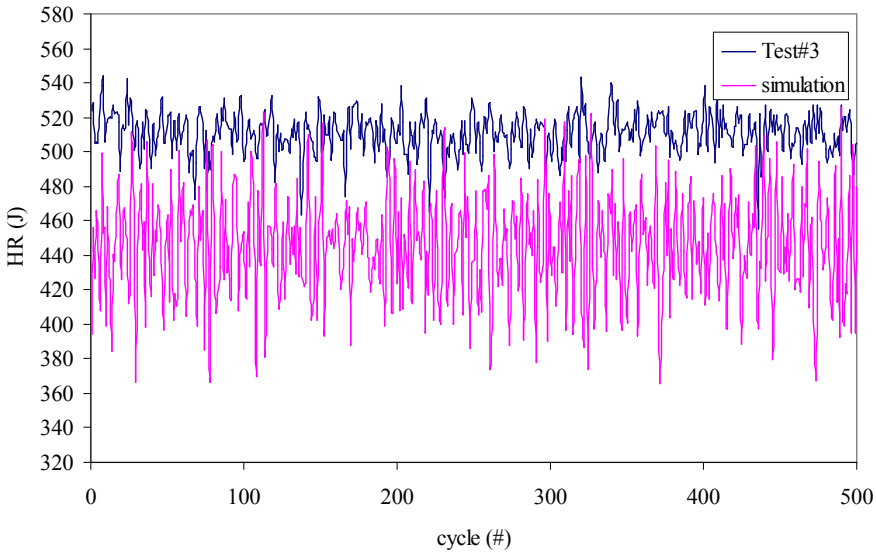

b) Consecutive heat release values confirm that the calculated combustion efficiency in the co-simulation was low and does not match experimental data so well as in the rich fuelling condition simulation.

Figure 7-3: Comparison of heat release under lean combustion from the first results by phase lag plot (top) and consecutive plot (bottom).

7.1.3 Comparison of IMEP

IMEP is determined from in-cylinder pressure. The results from the experimental work, that had high IMEP values, means that the combustion had a fast burn and a short duration. Considering the phase lag plot of IMEP, in Figure 7-4a, the calculated values of IMEP from the simulation were slightly lower compared to those from the experimental data but otherwise showed a similar beheaviour. These results were confirmed by the analysis of ignition delay, as can be seen in Figure 7-4b. The simulation had longer ignition delays which lead to longer combustion durations. However, there was some overlap in the ignition delay results, from both sources, which means the simulation's results were close but that it still needs some adjustment.

Under lean combustion, the same analysis shows that the points in the phase lag plot of IMEP values were much lower than those from the experimental work, as shown in Figure 7-5a. The simulation results show that the ignition delay was too long, as can be seen in Figure 7-5b. The simulation had no overlap in ignition delay between its results and those from the experimental work which results in low IMEP.

The results from rich and lean combustion suggest that the simulation's model for ignition delay needed to be adjusted. The ignition delay is dependent on the ratio of residual gases which, in turn, affects the combustion's duration. As a consequence, ignition delay also shows the variation in residual gases that were contained in the combustion chamber. The next topic will discuss the residual gases and the method used to adjust the ignition delay.

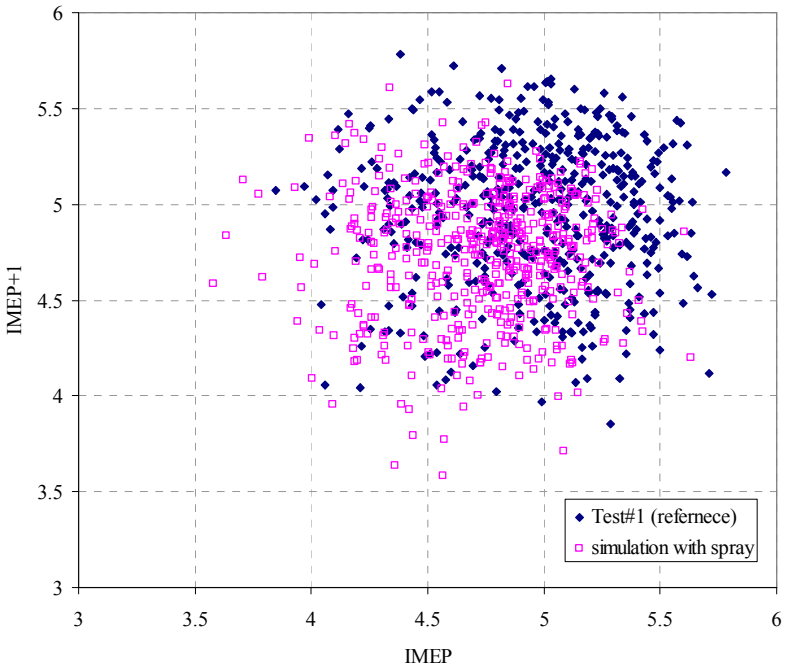

a) A phase lag plot of IMEP showing that the results of the simulation were slightly lower than the experimental IMEP data, which means the ignition delay will have to be adjusted.

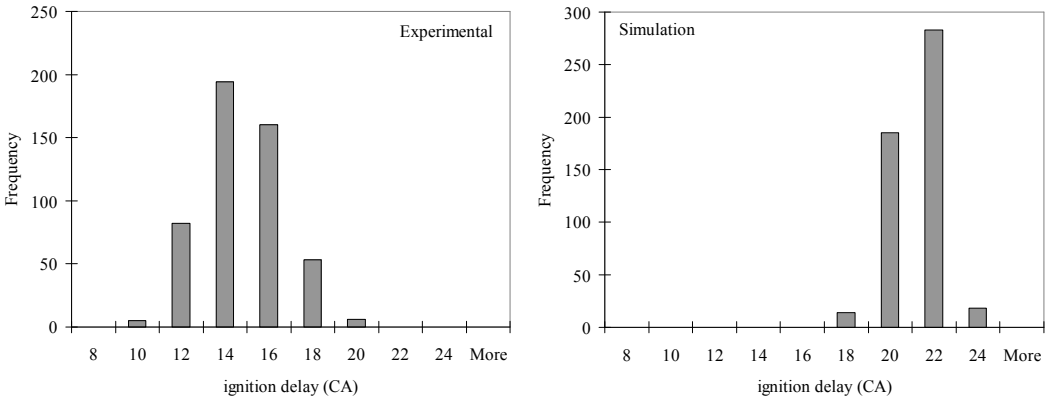

b) Ignition delay from experimental data (left) was faster than ignition delay of simulation (right), and needs to be adjusted by considering residual gases.

Figure 7-4: Comparison of IMEP from the first simulation under rich condition with experimental data

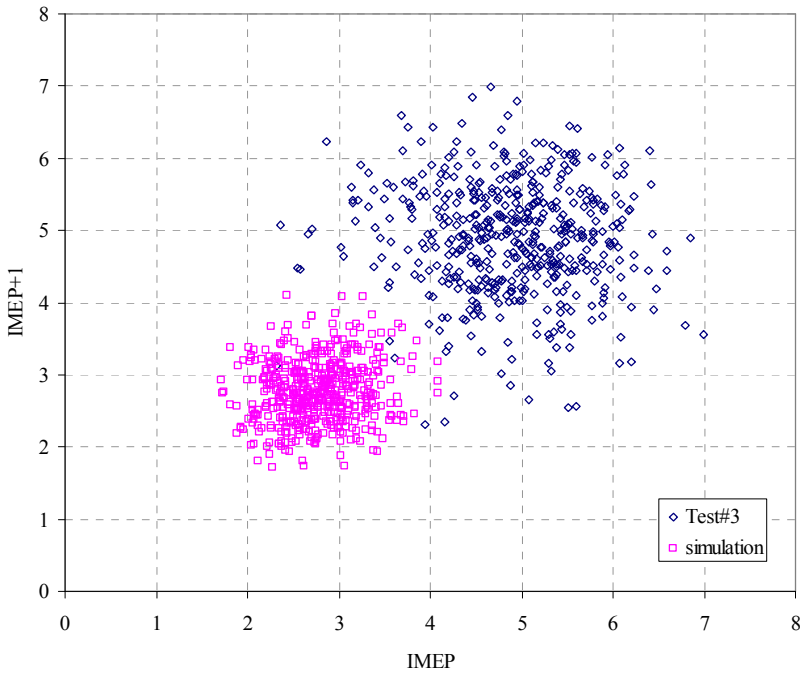

a) A phase lag plot of IMEP, under lean combustion, clearly shows that the simulation produced lower IMEP, which means the combustion control needs to be adjusted.

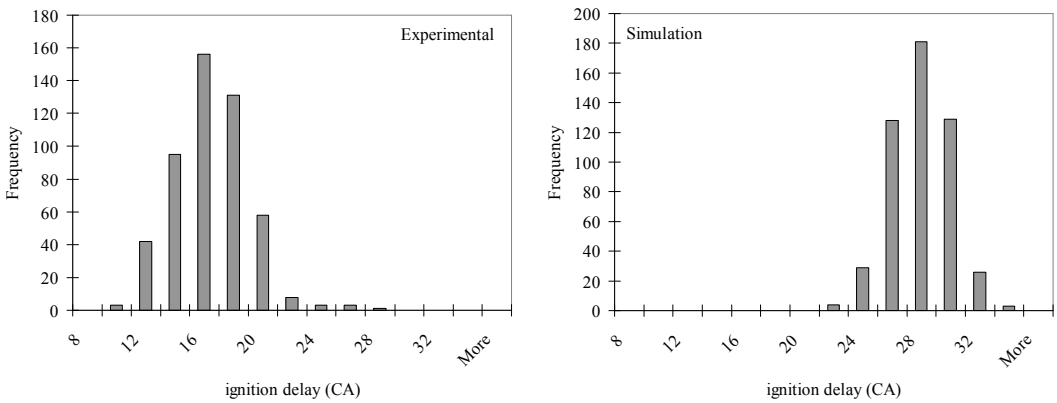

b) Analysis of the ignition delay from the simulation shows that the combustion had a long ignition delay which lead to a long combustion duration and low IMEP.

Figure 7-5: Comparison of IMEP from the first simulation under lean fuelling conditions with experimental data.

7.1.4 Residual gases

Residual gases are a major factor that control combustion characteristics. However, the residual gas amounts were not measured during the engine tests of this research, but were estimated in the co-simulation. Figure 7-6a shows the precentages of residual gases that had been calculated by the co-simulation and their effect on the Wiebe function's exponent. The average of the residual gas fraction from the two calibration points that had been used to create the look-up tables, was 9.66%, but with the simulation of the entire test period, where air flow rate and the fuel rate had been controlled, the residual gases were reduced. The results show that there were mechanisms of the gas exchange, during valve overlap, and the ratio of fresh air, that were caused by the pressure oscillations in the manifold. This results in a high value for the Wiebe exponent function. Similar results were observed under lean combustion, which used an average residual gas of 7.99% from the calibration points, whilst the co-simulation of the test cycle presents a lower value, as can be seen in Figure 7-6b.

In order to increase the IMEP, the mixture, that has low residual gas fraction in the simulation, has to burn faster by adjusting the ratio of residual gases to match with the low Wiebe exponent values to make the combustion process burn fuel faster. This is a part of residual gas estimation work, and also a part of the investigation of combustion characteristics, including ignition delay and duration.

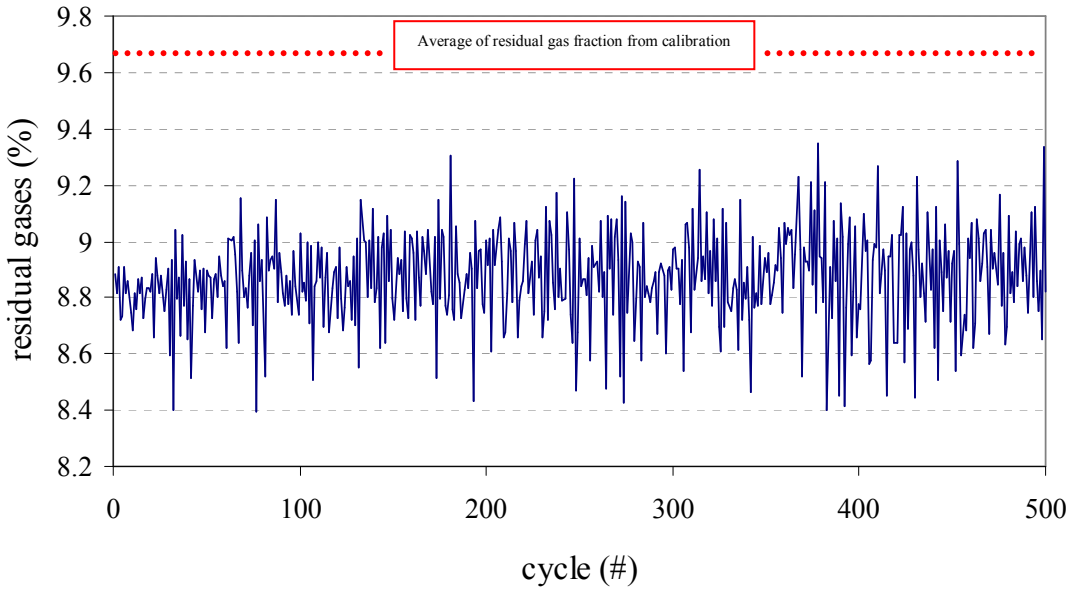

a) Residual gases under rich combustion

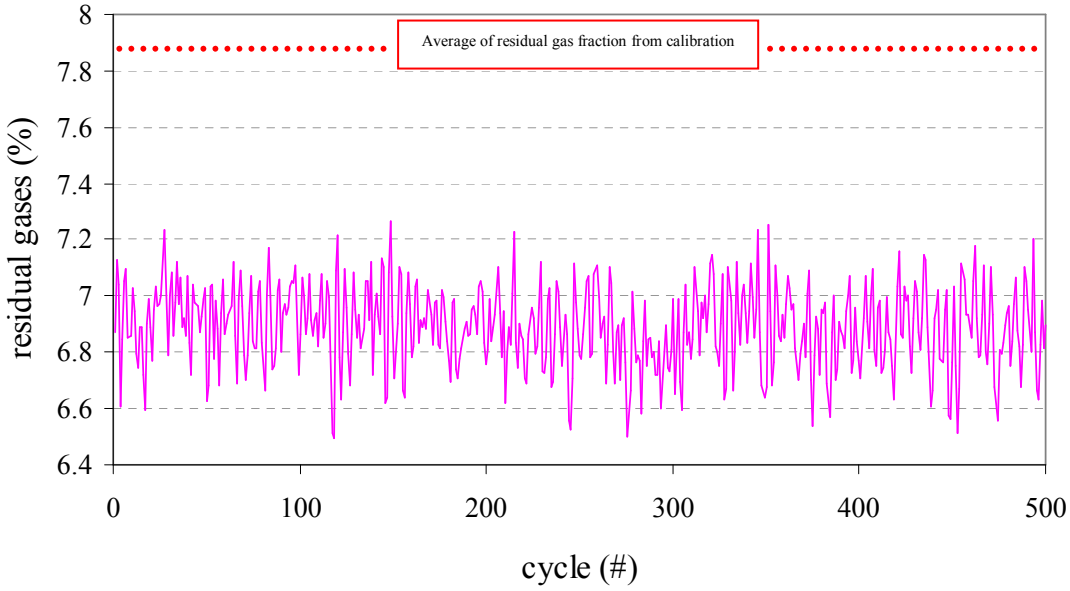

b) Residual gases under lean combustion

Figure 7-6: Residual gas fraction from the first co-simulation resulted in a high value of Wiebe exponent and exhibited excessive long combustion durations.

7.1.5 Discussion

When considering the co-simulation controlled combustion the results from the first look-up tables that were calculated from the experimental data, there are two parameters that must be calibrated to achieve a match with the test data. Those are fuel mass fraction burnt and residual gas fractions. The fuel mass fraction burnt has to be modified before adjusting the residual gas fractions, because the amounts of residual gases are affected by the fuel mass fraction burnt. In addition, in order to minimise errors associated with extrapolation, the range of estimated residual gas fractions must be large enough to cover the range observed over the test period. The extrapolation errors will manifest themselves as errors in the estimated Wiebe exponent and combustion duration which in turn will result in errors in heat release prediction.

By changing the Wiebe exponent, combustion duration and combustion efficiency under rich and lean fuelling, the combustion characteristics could be adjusted to compare well with the experimental data. However, the data analysis in Chapter 5 suggested that angle of 1% burn had a linear relationship with combustion duration thus there are only two look-up tables that can be modified in this engine model:

1) The look-up table for combustion efficiency, based on engine lambda, this will affect directly on the total of heat release of individual cycle.
2) The look-up table for Wiebe exponent which is used to control the start of combustion, based on the residual gas fraction. This will affect the IMEP since it affects the phasing of the heat release.

7.2 Result of rich mixture simulation compared with experimental data after adjusting look-up table

The look-up table that used to control the combustion's efficiency and Wiebe exponent was adjusted to obtain the best results.

There are three parameters that are used to compare and explain the results between the experimental data and the simulation's results:

- In-cylinder pressure

Maximum and minimum in-cylinder pressure from experimental data and simulation were plotted together for comparison.

- Heat release

Heat release was compared using time-series and histogram plots.

- IMEP

A phase lag plot was made of IMEP data, and calculations of COV_{imep} were used for comparison.

In the combustion efficiency table, the range of lambda values was initially small with little difference between maximum and minimum values, as can be seen in Figure 7-7a. The range of lambda was increased in order to cover the majority of expected lambda values from the simulation. The relationship agrees with the combustion efficiency under rich mixture fuelling, which shows that more fuel was burnt when the air/fuel mixture moved towards the stochiometric ratio. For the effect of residual gases, in the combustion chamber, the relationship agrees with Shayler et al. (2000) in that the residual gases affected the ignition delay only when the residuals reached a critical limit. Figure 7-7b shows that residual gases started to slow down the combustion process when a level of 8.8% of residual gases was exceeded. The Wiebe exponent increased rapidly and resulted in different amounts of heat release, although the fuel was burnt at the same rate during the combustion process. Under these limitations, the combustion had a fast burn, with the heat released dependent on the amount of fuel that had been burnt. For the combustion duration, the look-up table was similar to the pervious version because the experimental data showed that 1% fuel burnt had a linear relation with the 50% mass fraction burnt value.

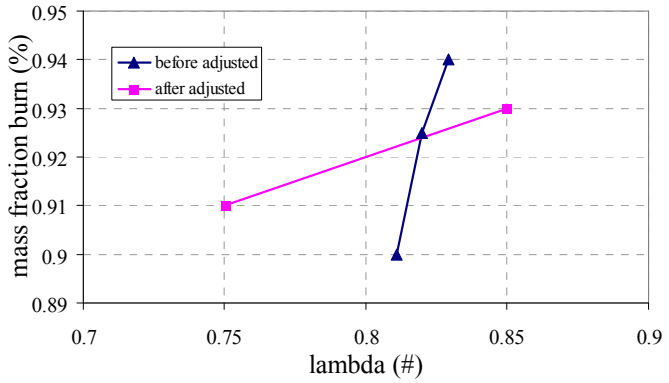

a) Look-up table for combustion efficiency

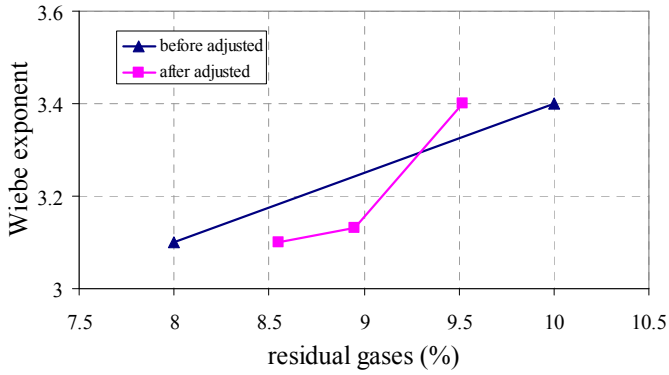

b) Look-up table for Wiebe exponent

Figure 7-7: Comparison of look-up table before and after modification for control combustion under rich mixture

7.2.1 In-cylinder pressure under simulation of rich combustion

Figure 7-8 shows a comparison of the maximum and minimum in-cylinder pressures between the experimental data and the simulation. The maximum pressure at TDC varied, because the simulation had been calibrated by using the average pressure, but the experimental results had variations in the air flow rate, which contributed to different motoring pressures. In addition, the in-cylinder heat transfer could vary because of different amounts of fresh air and therefore in-cylinder gas temperatures. The simulation used a constant component temperature. Also, fuel had been injected at the same rate but variations in air flow could result in different levels of evaporation and contribute to different amounts of heat release.

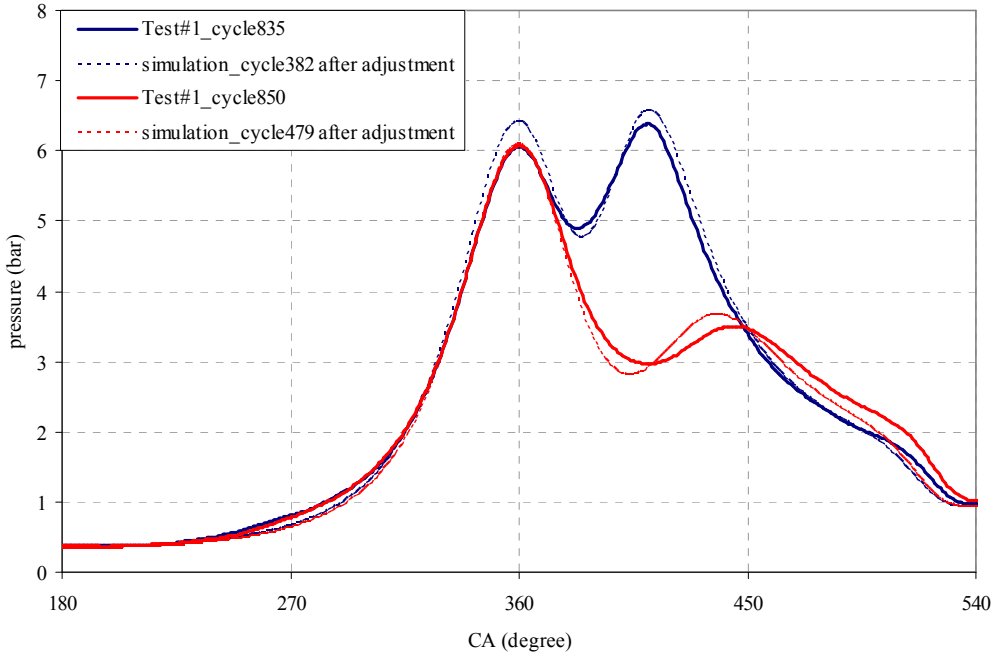

Figure 7-8: Comparison of experimental in-cylinder pressure under rich condition to simulation results after adjustment.

However, during the combustion period that occurs during the expansion stroke, the simulation cannot follow the experimental results. At high pressure (blue line in Figure 7-8), the simulation showed that the Wiebe exponent can correspond to the burn rate. Although, the combustion pressure was higher in the simulation than in the experimental data, this can be solved by adjusting the engine component temperature. Considering the simulation of low pressure in Figure 7-8, the way in which pressure increases during the combustion event in the model is different from the experimental data. Under high residual gas fractions, the combustion profiles are assumed to have a high ignition delay by way of an increased Wiebe exponent value. As a result, the Wiebe function cannot produce a similar profile to the experimental results. In order to solve these problems, the combustion control has to be changed by ignoring the ignition angle and using the 50% burnt point to control combustion, in the same manner as option #1 as discussed in Chapter 5. In this case, the Wiebe exponent can be changed to achieve the experimental results. However, the Wiebe exponents selected will result in a very early start of combustion, well in advance of the experimental observations. This will also result in errors affecting the predicted peak compression pressure at TDC. On balance these problems are more serious than the present errors introduced when using

option #2 as discussed in Chapter 5. This configuration allows the user to define the Wiebe exponent, start of combustion and combustion duration. Figure 7-8 shows the predicted pressure trace after these adjustments have been made. A slight mismatch in pressure is evident during combustion but this is considered acceptable.

7.2.2 Heat release under simulation of rich combustion with updated look-up tables.

In-cylinder pressure was used to determine the heat release and compared with experimental data within a selected period. The consecutive combustion cycles' heat release was plotted, as can be seen in Figure 7-9a. By inspection, the heat release from the simulation had a similar behaviour compare to the experimental data. Inputs which had been fed into the co-simulation suggest that under rich combustion, the air flow rate input was the most important factor in determining heat release. This is a much better match to real engine behaviour than the initial results shown in Figure 7-2.

A phase lag plot of heat release values, shown in Figure 7-9b, compares the results of the simulation to the experimental heat release data with the modified look-up tables. Each set of data has a similar distribution, but there are some heat release results located outside of the experimental data's boundary. These results are caused by a disturbance mechanism caused by the experimentally observed air flow rate oscillating in a sinusoidal manner. This is likely to be caused by the torque control feature of the rig controller causing the engine power demand to oscillate. The amplitude of the fluctuation in MAF was 0.5 kg/hr or 2.27% and the period was 5.1 sec (0.196 Hz).

In addition, Figure 7-9c shows the comparison of intake lambda and in-cylinder lambda which were calculated by Wave when the spray model was activated. The intake lambda varied according to the variation in air flow rate because the engine was simulated under rich fuelling. The results of in-cylinder lambda suggested that the fuel may loss during transport to the chamber which resulted in high lambda value. In contrast, sometime the fuel evaporated and was drawn into the chamber more than the fuel injected which resulted in low lambda value. These are the effects of spray model with default setting.

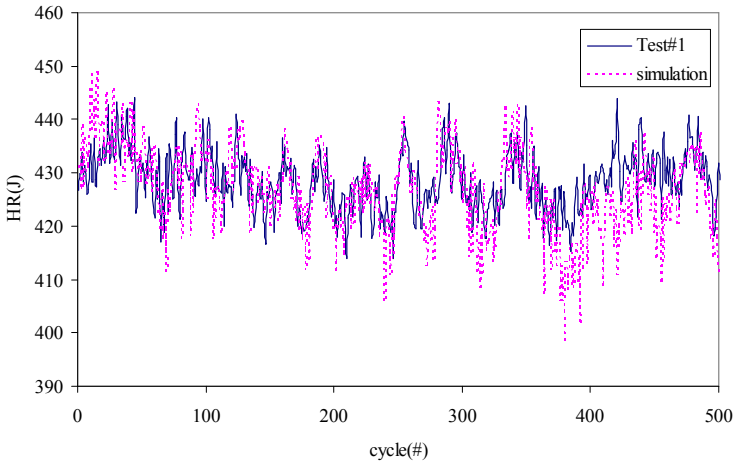

a) Cumulative heat release shows the cycle-by-cycle from experimental and simulation had similar behaviour.

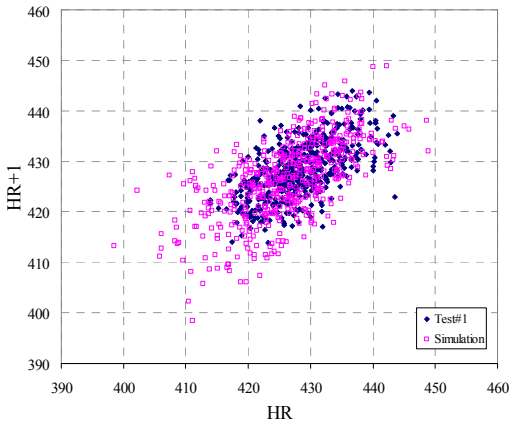

b) A phase lag plot of heat release shows that most of the simulation results were located within the boundary of the experimental results.

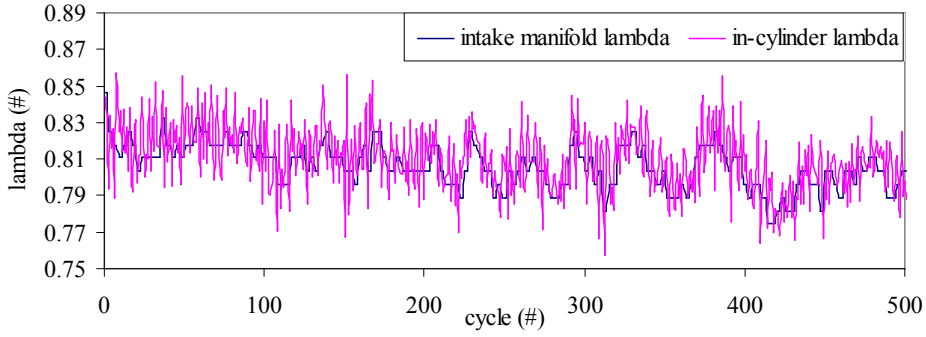

c) Comparison of intake lambda and in-cylinder lambda in the simulation when spray model is activated.

Figure 7-9: Comparison of heat release under rich condition with predicted data from the simulation using the revised look-up table

Bannister et al. (2010) suggests comparing these results by using a histogram of the probability density function, as can be seen in Figure 7-10. The percentages of error were calculated from the differences between the values of the heat release results from the experimental data and the simulation. The normal distribution explains that the overall results of the simulation were under predicted by 0.49% which is considered acceptable.

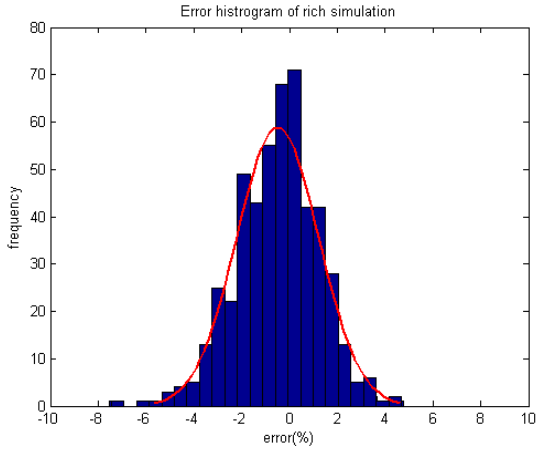

Figure 7-10: The probability density function for the heat release errors during the rich running validation cycle of rich fuelling, which are under predicted with a mean error of approximately 0.49 % by normally distributed residuals.

7.2.3 IMEP under simulation of rich combustion with updated look-up tables.

Phase lag plots were applied to IMEP data from the simulation and experimental work, for comparison, as can be seen in Figure 7-11. The results from the simulation show a triangular shape which was similar to the experimental data. However, the experimental data had a uniform distribution, within the shape, whilst most of simulation results are located near the edge of the triangular shape. The experimental data's COV_{imep} value, for the test period, was 7.6 whilst the COV_{imep} value from the simulation was 6.10, which is the best value that can be obtained during the time available. The results for the COV_{imep} show that the simulation can achieve a similar result to that of the experimental

COV_{imep}, but the cycle-by-cycle values of IMEP can be different. In all these results are a much better representation of the real engine behaviour than those obtain with the primary model shown in Figure 7-4.

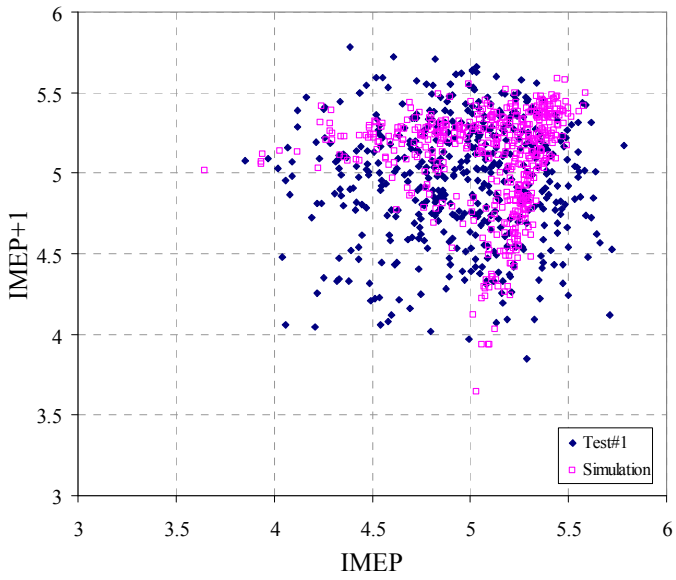

Figure 7-11: Comparison of phase lag plotted for IMEP for rich condition

7.3 Result of lean mixture simulation compared with experimental data after adjusting look-up table

The process of adjusting the look-up table described above for the rich operating regime was repeated in the lean region. The look-up table for combustion efficiency was adjusted, and is shown in Figure 7-12a. The lambda values from the experimental data had a narrow range compared to those from the simulation, as discussed previously in the first simulation results. Thus, the combustion efficiency was too low to achieve the target heat release when the fuel mixture was too lean. After the adjustment of the look-up table, the combustion efficiency was extended to cover the majority of lambda values that could give the targeted heat release. Under lean mixture fuelling, the combustion efficiency gradually drops as the mixture becomes more lean. The gradient of this relationship (decrease 0.31% / 0.1 lambda number) is significantly lower than that seen in the rich region (increase 2.19% / 0.1 lambda number).

The combustion characteristics which were controlled by the residual gases show a relationship that is similar to that for a rich combustion. The look-up table for the Wiebe exponent, in Figure 7-12b, shows that a residual gas ratio under 8.05% had little effect on the early burn, but increased in significance when its value was higher.

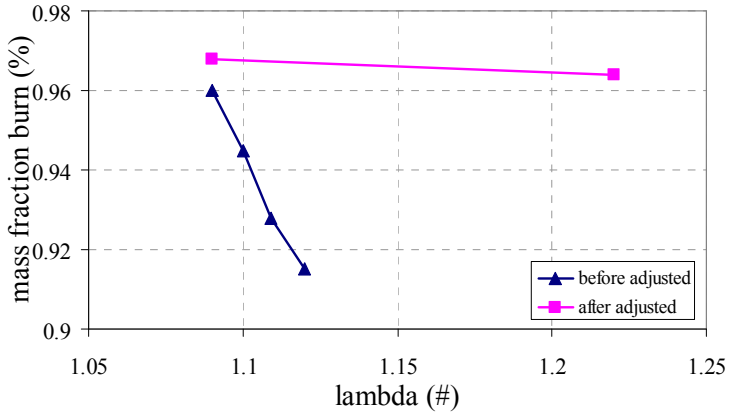

a) Look-up table for combustion efficiency

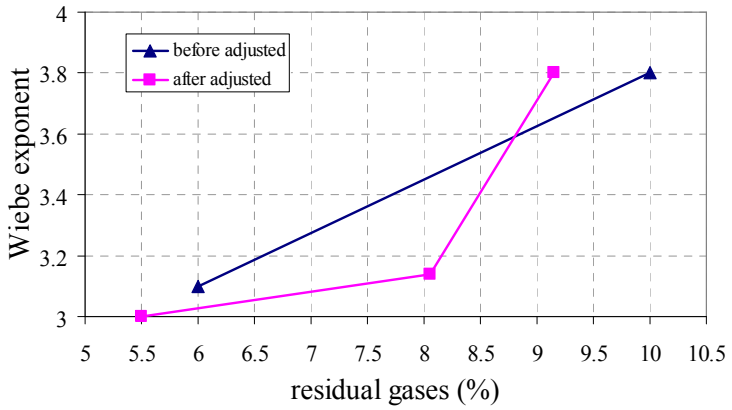

b) Look-up table for Wiebe exponent

Figure 7-12: Comparison of look-up table under lean fuelling before and after modification for control of combustion

7.3.1 In-cylinder pressure under simulation of lean combustion

Maximum and minimum in-cylinder pressure from experimental data and simulation were plotted for analysis, as can be seen in Figure 7-13. Under lean combustion simulation, the rate of air flow was kept constant which results in constant motoring pressures which had been calibrated from the engine component temperature. However, the air flow rate from the experimental data varied and resulted in a variation in the motoring pressures.

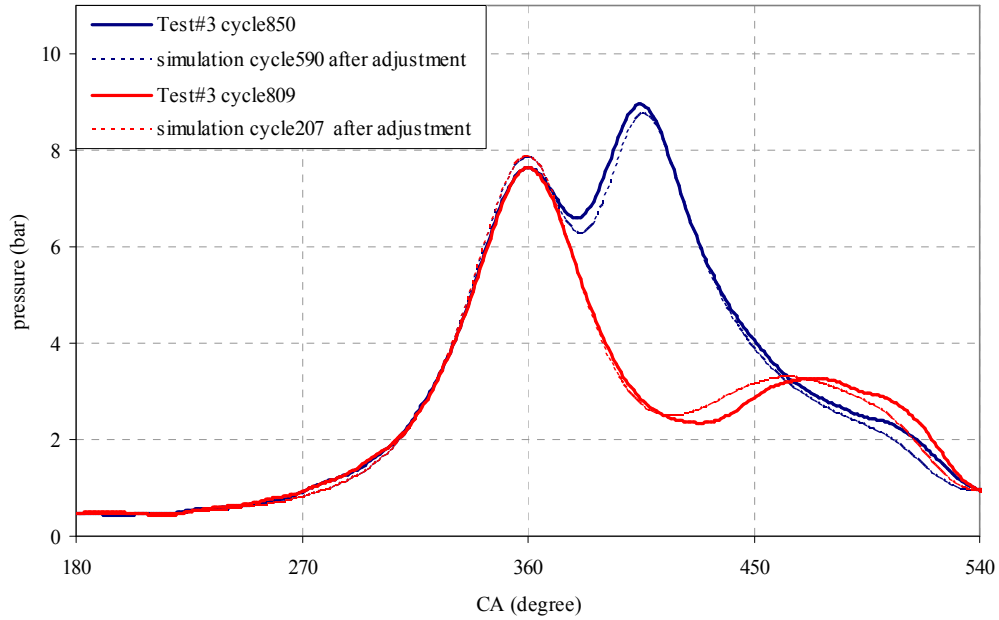

Figure 7-13: Comparison of in-cylinder pressure under lean condition with experimental data

The combustion profiles during the burning period shows that, under fast burn conditions, the simulation gives a good prediction. For long ignition delays, the simulation cannot give such a good prediction which is similar to the results observed under rich combustion, because of the limitation of the Wiebe method, that has been discussed previously.

7.3.2 Heat release under simulation of lean combustion

Consecutive combustion cycles' heat release from both the experiment and simulation are plotted in Figure 7-14a. The characteristics of the variation in lean combustion events from cycle to cycle are different than those for rich combustion. The behaviour of the combustion was variable, although the fuel was kept at constant rate. The variations are present because the spray model was activated, which allows fuel to vary from cycle by cycle. The phase lag plot, in Figure 7-14b, shows that the distribution of the heat release points from the simulation is greater than those from the experimental data, and the majority of heat release values are slightly lower than those from the experiment. The plot shows that the cycle-to-cycle behaviour, under lean combustion, is difficult to predict. However, the general characteristic of the variability are predicted well and appearing to be essentially a stochastic process.

Figure 7-14c shows the results of lambda in the intake manifold and lambda in the combustion chamber. The engine was simulated under lean fuelling with constant fuel flow and air flow. In-cylinder lambda values vary more than the lambda in the intake manifold. The reasons are the variation of fuel mass that vary by spray model. These mechanism influences to different combustion efficiency and contribute to variation in residual gas fraction for the next combustion event.

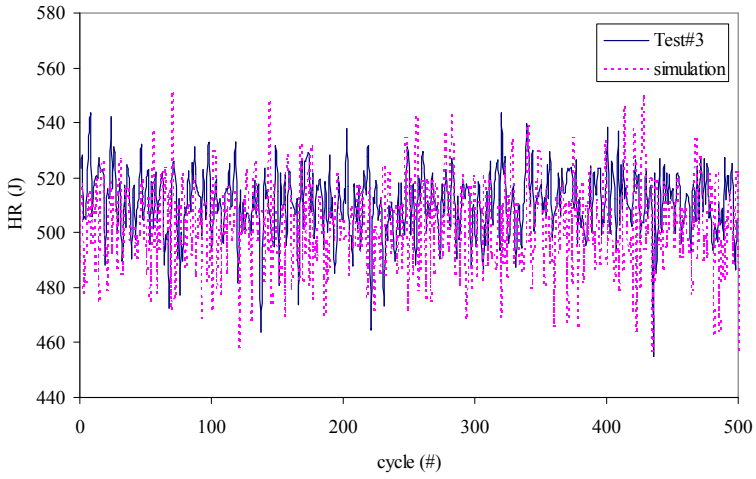

a) Comparison of heat release from consecutive combustion cycles, under lean fuelling conditions.

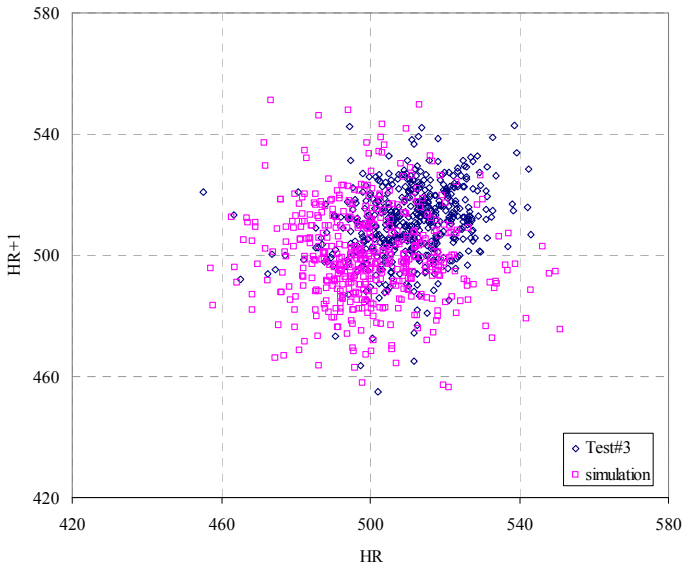

b) Phase lag plot of heat release from experiment and simulation.

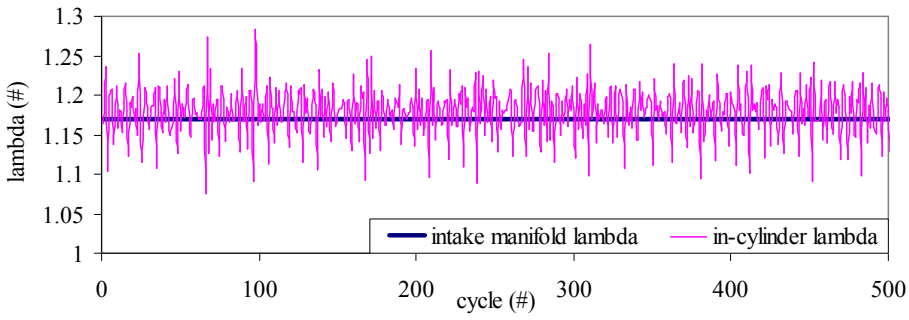

c) Comparison of intake lambda and in-cylinder lambda in the simulation when spray model is activated.

Figure 7-14: Comparison of heat released during lean fuelling operation with experimental data.

A histogram of heat release errors, under lean combustion operation, can be seen in Figure 7-15. The plot shows that the results of the simulation under predicted by 2.07% and the maximum error were up to 15.32%. In order to reduce the percentage of error, further the look-up table for combustion efficiency would need to be modified by increasing the combustion efficiency values.

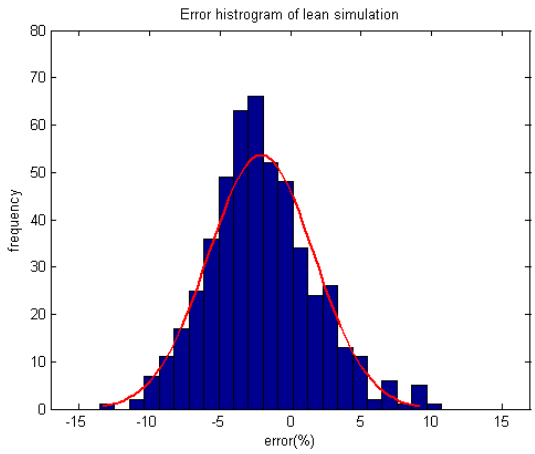

Figure 7-15: The probability density function for the heat release errors during the validation cycle of lean fuelling, which are under predicted with a mean error of approximately 2.07% by normally distributed residuals.

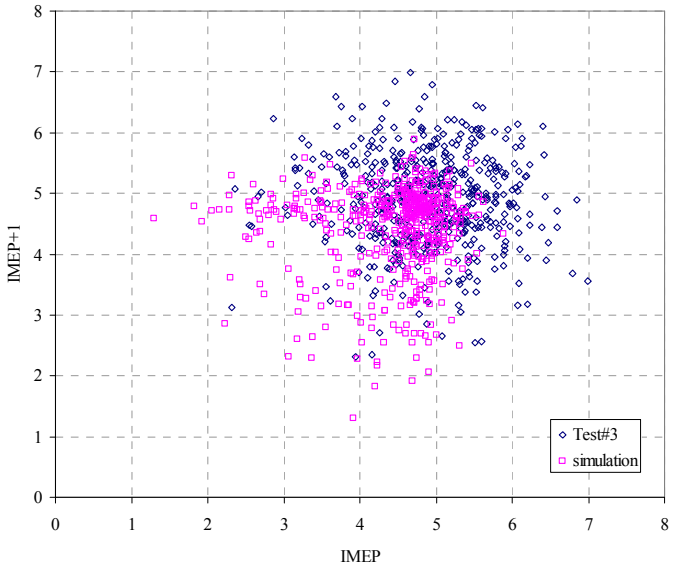

Figure 7-16: Comparison of phase lag plot of simulated IMEP under lean condition with experimental data.

7.3.3 IMEP under simulation of lean combustion

A phase lag plot was applied to the results for IMEP, from the experiment and simulation, as shown in Figure 7-16. The results for IMEP from the simulation were lower than those from the experiment, and form a triangular shape. This suggests that a degree of prior cycle dependence is present and giving a deterministic element to the combustion variability. This is combined with the stochastic elements of variability to form a loose collation of points with some suggestion of a triangular shape. In contrast, the results from the experiment are dispersed in a more irregular form suggesting more stochastic beheaviour.

The cycle-by-cycle IMEP values varied. COV_{imep} for the experiment data was 15.86% whilst COV_{imep} from the simulation was 16.56%.

7.3.4 Cycle-by-cycle comparison under simulation of lean combustion

Cycle-by-cycle combustion performance, under lean fuelling, is hard to predict, because the combustion is controlled by the amount of fuel present in the cylinder. The fuel's behaviour inside the combustion chamber is very complex. Although the engine simulation, in this research, used the spray model, which enables the simulation to model some of the behaviour of the fuel, the overall result still cannot match the experimental data. However, the subjective behaviour of the simulation is similar to the experimental data. Figure 7-17 shows the results of consecutive cycles of heat release and IMEP from cycles 485 to 497. The simulation shows that the simulation exhibits similar behaviour to the real engine.

The fuel mass flow rate has a major effect on combustion. The fuel flow into the chamber is affected by manifold pressure, flow rates and turbulence. These factors also affect fuel evaporation and cause variations in the air/fuel mixture in the combustion chamber before ignition.

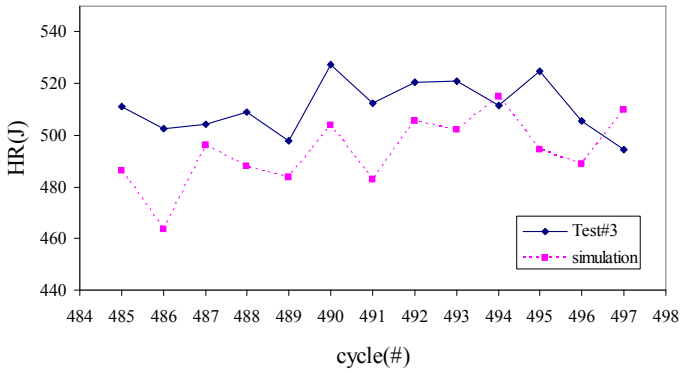

a) Heat release between combustion cycles 485 to 497

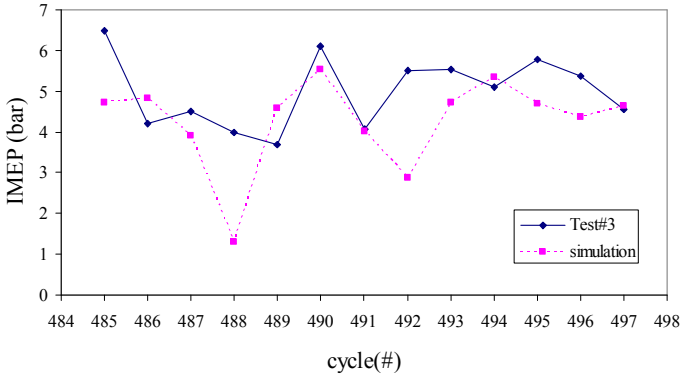

b) IMEP between combustion cycles 485 to 497

Figure 7-17: Sample of consecutive heat release shows the results from simulation can exhibit similar qualitative features to experimental data.

7.4 Conclusions

The engine model described in the previous chapter was run over a series of operating conditions and the results analysed before making further modifications in order to better represent the variability in combustion observed during the experimental work. The modifications were implemented by adjusting the look-up tables used to determine combustion efficiency and Wiebe exponent. Those two look-up tables were controlled by in-cylinder lambda and residual gas fraction respectively. The final results under rich and lean combustion suggested that the lambda values observed in the experimental data had shortcomings due to the location of the lambda sensor in the exhaust downpipe. The combustion will be influenced by in-cylinder lambda and so variations

in in-cylinder lambda caused by the gas exchange process cannot be accurately represented by the exhaust lambda measurement. This was a known limitation of the technique and was mitigated by using time averaged values for lambda from a number of test conditions spanning a range of lambda values when analysing the combustion data. For the residual gas fraction, the modifications to the look-up table from rich and lean fuelling suggested that residual gas fraction had less effect on Wiebe exponent when the residual gas fraction was below 8.8% and 8.50% respectively. The effects of residual gas fraction increase significantly when the RGF is at a higher level. For example, when running rich, an increase in RGF from 9 to 9.5% is estimated to increase the Wiebe exponent from 3.15 to 3.39, which corresponds to an increase in combustion duration from 32.68^{o} CA to 44.52^{o} CA.

The simulation results under rich conditions provided a similar pattern in cycle by cycle heat release when compared with experimental data with the mean IMEP under predicted by approximately 0.49% with an approximately normal distribution of residuals. Under lean combustion, the time series data describing cyclic variation in heat release cannot follow the experimental data as the combustion in the simulation was controlled by the fuel mass induced into the cylinder, which was was calculated using the Ricardo spray model. The governing factors for this processes were inlet port air velocity, temperature and pressure. These variables were calculated within Wave but were not measured with sufficient resolution during the experimental work to allow a cycle by cycle validation to be performed. To do so would require a highly complex instrumentation suite that was beyond the scope of the research. However, the nature of the variability observed in simulation (COV_{imep} = 16.56%) was qualitatively and quantitatively similar to that measured experimentally (COV_{imep} = 15.87%). In particular, it was noticeable that the time series of combustion data exhibited similar features in terms of heat release and IMEP. Overall, IMEP was under predicted by approximately 2.07% and the residuals were normally distributed.

In conclusion, the model gives a useful insight into cyclic variation and appears to respond to engine operating point in a realistic manner. The next chapter will investigate the potential for the use of this tool in the calibration process.

Chapter 8

Engine calibration using co-simulation

In this chapter, the potential application of the co-simulation to optimise the combustion performance and reduce cyclic variation through manipulation of the calibration of the engine is explored. In particular, will the simulation yield useful information describing the effect of changes in engine calibration on cyclic variability? Without such information it is very difficult for calibration engineers to assess the impact of their choices on engine performance until experimental data are available, much later in the development process. As a specific example, the residual gas fraction is manipulated by varying the intake and exhaust camshaft timing. The aim is to predict effect on cyclic variability using the technique described in Chapter 7 and to study the flow mechanisms responsible for the phenomena. The predicted behaviour of the combustion system when operating in rich and lean conditions is compared with the experimental measurements. The simulation is then used to predict the changes in system behaviour as camshaft timing is altered. Finally, the optimum camshaft positions to minimise cyclic variability are identified under cold start conditions, operating the engine with both rich and lean fuelling.

8.1 Effect of exhaust camshaft position

According to the review from Chapter 1, varying the exhaust camshaft position had a significant effect on the ratio of residual gases. The original exhaust camshaft position set EVC position to 8 degrees BTDC. In order to investigate the effect of camshaft timing on cyclic variability in simulation, the profile of the exhaust valve timing was shifted by advancing and retarding from its original position by 4 degrees, as shown in Figure 8-1a.

With the retarded camshaft position, the profile of the exhaust valve timing was shifted forward, which caused the valve to close later and increased the valve overlap angle. While under an advanced camshaft position, the valve overlap angle was reduced. Figure 8-1b shows that the advanced exhaust camshaft position results in the centre line of valve overlap shifting to BTDC, which could cause less residual gases to transfer to the combustion chamber.

In the Wave environment, the intake camshaft position was kept constant which allows the intake valve to open at 18 degrees ATDC. In order to change the exhaust valve closing angle, the exhaust camshaft position was shifted +4 (EVC 12 degrees BTDC) and -4 degrees (EVC 4 degrees BTDC) from its original position. These three conditions were applied to the co-simulation with the same engine settings. The results for the instantaneous gas flow that was affected by variations in the exhaust camshaft timing profile are shown in Figure 8-2.

Figure 8-2a shows that the majority of the exhaust gas flows, in the simulation, were shifted according to the position of valve opening angle which is dependent on the camshaft position. The intake gas flows were constant but may be affected by oscillations of pressure in the pipe which could affect rich combustion. Considering the flow of gases near TDC, as shown in Figure 8-2b, the back flow of the exhaust gases increased under retarded camshaft position because the EVC angle was extended to close ATDC, which caused more backflow when the piston moved to BDC. The results for heat release and IMEP, from rich and lean fuelling simulation, were calculated and plotted in the form of phase lag plots, as shown in Figure 8-3 and Figure 8-4 respectively.

Under rich fuelling, Figure 8-3a shows the phase lag plot of heat release had wide distribution and the IMEP plot started to form triangle shape when the EVC was 4 degrees BTDC. In contrast, the plot of heat release and IMEP were narrow down and provide less distribution under EVC 12 degrees BTDC (Figure 8-3c). Under lean fuelling in Figure 8-4a, the plot of heat release started to form angular shape and cause random distribution in IMEP plot when the EVC was 4 degrees BTDC. Again, the plots of those parameters become less spread under EVC 12 degrees BTDC as shown in Figure 8-4c. The mechanisms of results above were discussed more in the next topic.

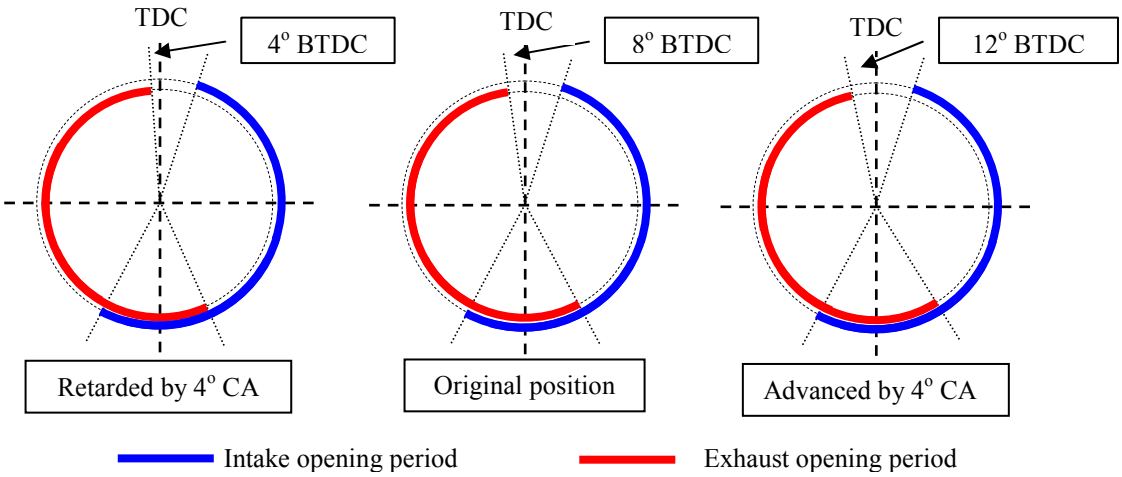

a) Diagrams camshaft opening period with varying exhaust camshaft position.

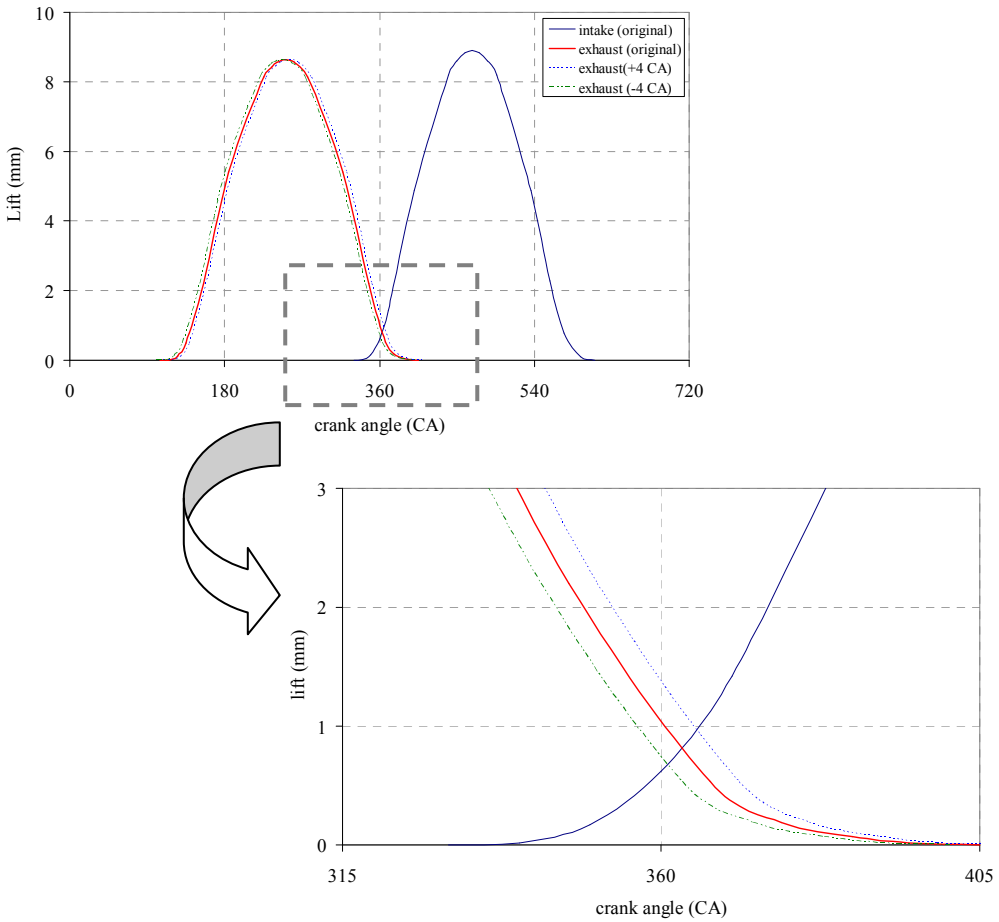

b) The valves lift profile from different exhaust camshaft positions show the overlap area near TDC increases with a retarded exhaust camshaft by 4 degree (EVC 4 degrees BTDC) and with a advanced angle of 4 degrees (EVC 12 degrees BTDC).

Figure 8-1: Exhaust valve profile with varying exhaust camshaft positions.

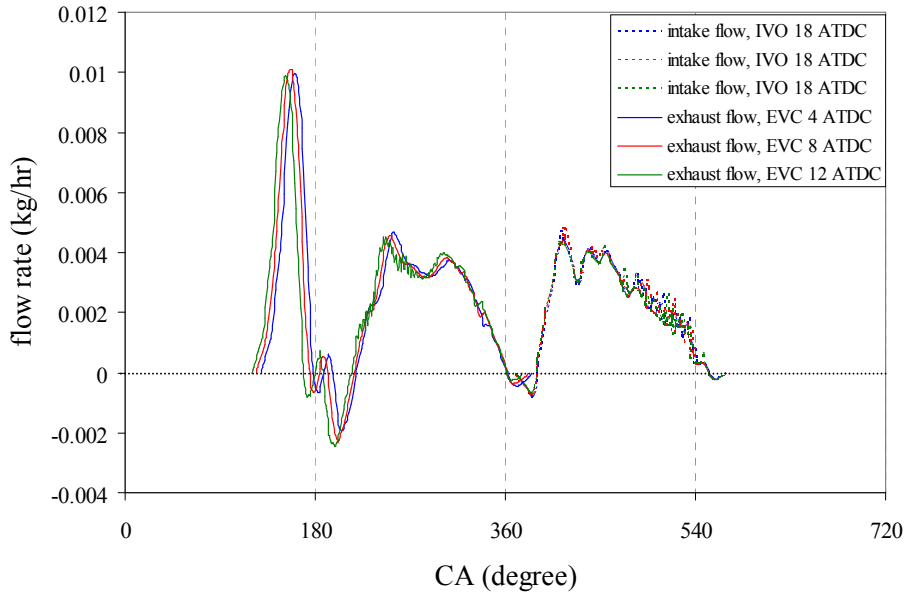

a) Overall inlet and exhaust flow under different exhaust camshaft positions.

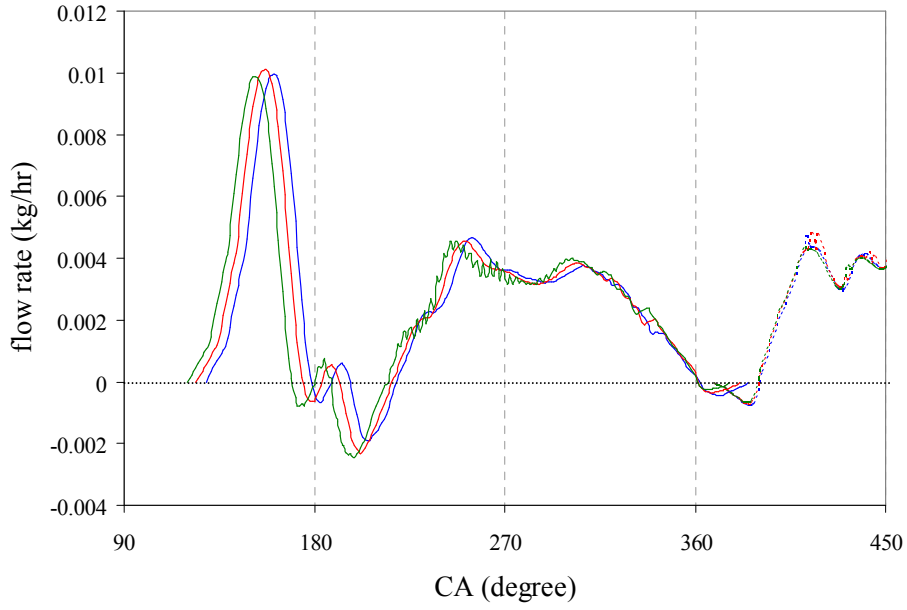

b) Large view of exhaust flow with different exhaust camshaft positions.

Figure 8-2: Gas flows with different exhaust camshaft positions.

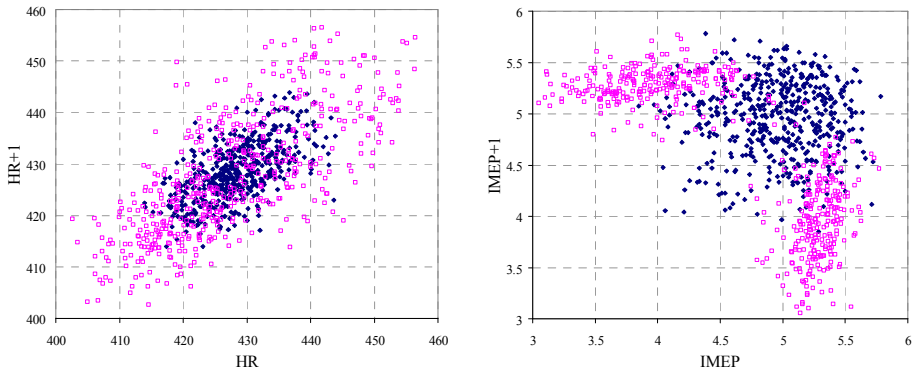

a) Retarded simulation of EVC by 4 degrees CA

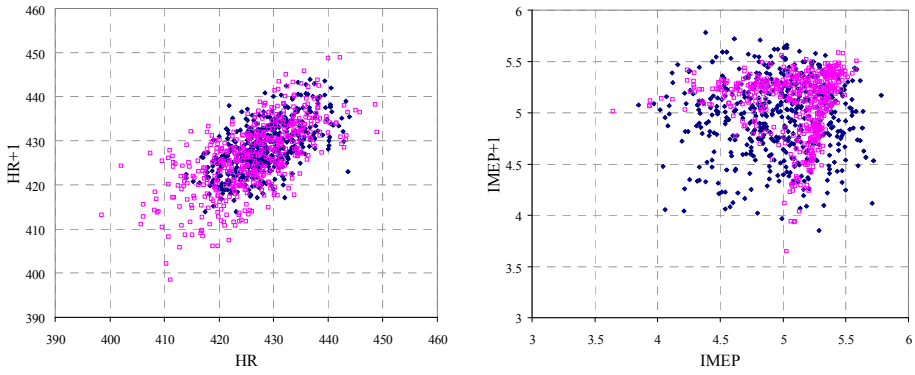

b) Reference EVC at the same position

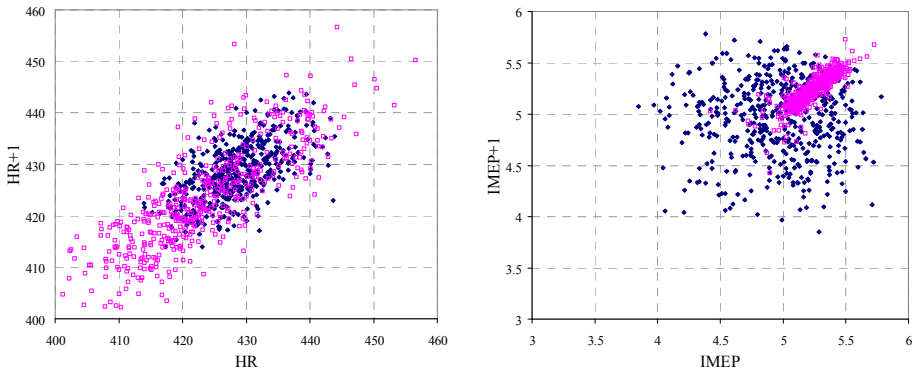

c) Advanced simulation of EVC by 4 degrees CA

Figure 8-3: Comparison of the net heat release and net IMEP from experimental data with the simulation results, under rich fuelling operation (Test #1). IVO is kept constant whilst the EVC position is altered.

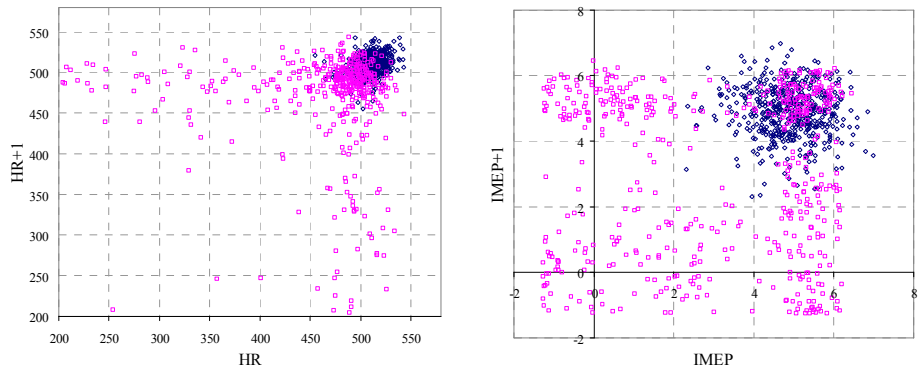

a) Retarded simulation of EVC by 4 degrees.

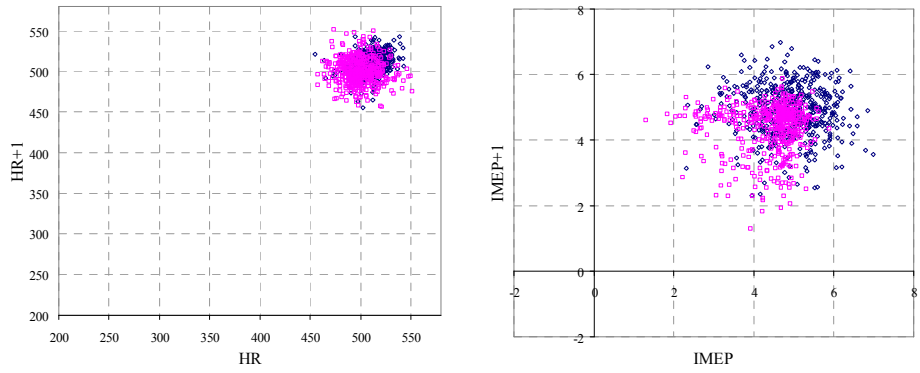

b) Reference EVC at the same position

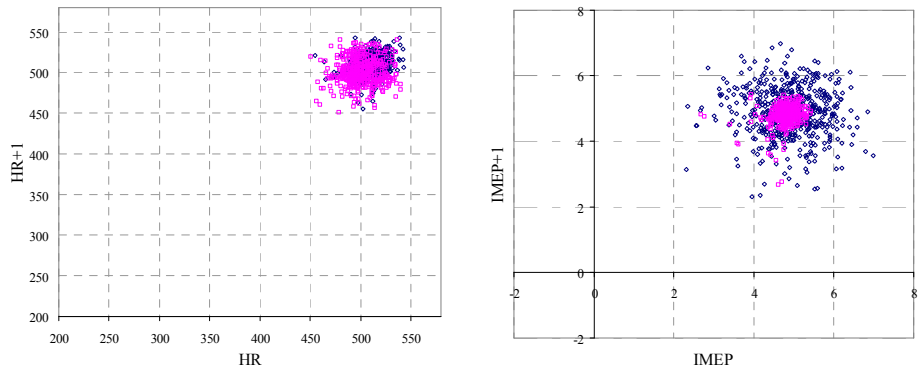

c) Advanced simulation of EVC by 4 degrees.

Figure 8-4: Comparison of the original net heat release and net IMEP from experimental data with the simulation results, under rich fuelling operation (Test #3). IVO is kept constant whilst the EVC position is altered.

8.2 Effect of intake camshaft position

Having investigated the effect of exhaust cam timing, the combustion simulation model was then used to explain the effects on combustion of different positions of the inlet valve camshaft. The original intake camshaft position, in the experiment, opened the inlet valve at 18 degrees ATDC. In order to explain the effects, the intake camshaft position was shifted to advanced and retarded positions by 8 degrees. Figure 8-5a shows a comparison of intake valve profiles from different camshaft positions. Figure 8-5b clearly shows that a retarded intake camshaft position increased the valve overlap time, which resulted in high levels of residual gases.

Figure 8-6a shows the intake gases flow with different intake camshaft positions. The exhaust camshaft timing was kept constant, but the exhaust flow rate varied. High exhaust gas flow rate was affected by the combustion that had long duration, because, at the opening angle, the pressure is higher than with fast combustion, thus the gases are forced to move faster. Considering the intake flow near TDC, an advanced intake camshaft position resulted in high backflow, which caused pressure oscillations in the pipe and reduced the air charge, in the chamber, for the next cycle. The backflow reduced, since the intake camshaft was retarded, but the total charge mixture is also reduced because of the late EVC. Figure 8-6b shows the charge mixture was pushed back during the piston's movement to TDC. However, the flow rates of the exhaust gases, from the simulation, are constant.

Under rich fuelling, Figure 8-7a shows the phase lag plot of heat release was considered to have a similar distribution to the reference condition (Figure 8-7b) and the IMEP plot started to form triangle shape more when the IVO was 9 degrees BTDC. In contrast, the plot of heat release started to spread wider and form a liner line when the IVO was 18 degrees BTDC (Figure 8-7c). Under this condition, the plot of IMEP still shows a similar distribution compared to reference position. Under lean fuelling, both heat release and MEP plot had wide distribution with no real structure the IVO was 9 degrees BTDC (Figure 8-8a). In contrast, the plots of those parameters when the IVO was 18 degrees BTDC (Figure 8-8c) were considered similar to the reference position. The results of those mechanisms were discussed more in the next topic.

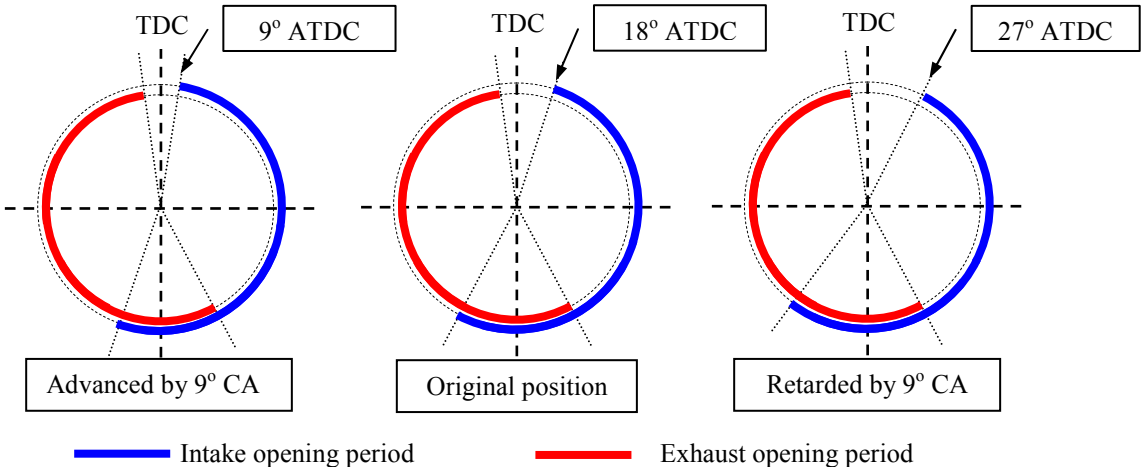

a) Diagrams camshaft opening duration with varying intake camshaft position.

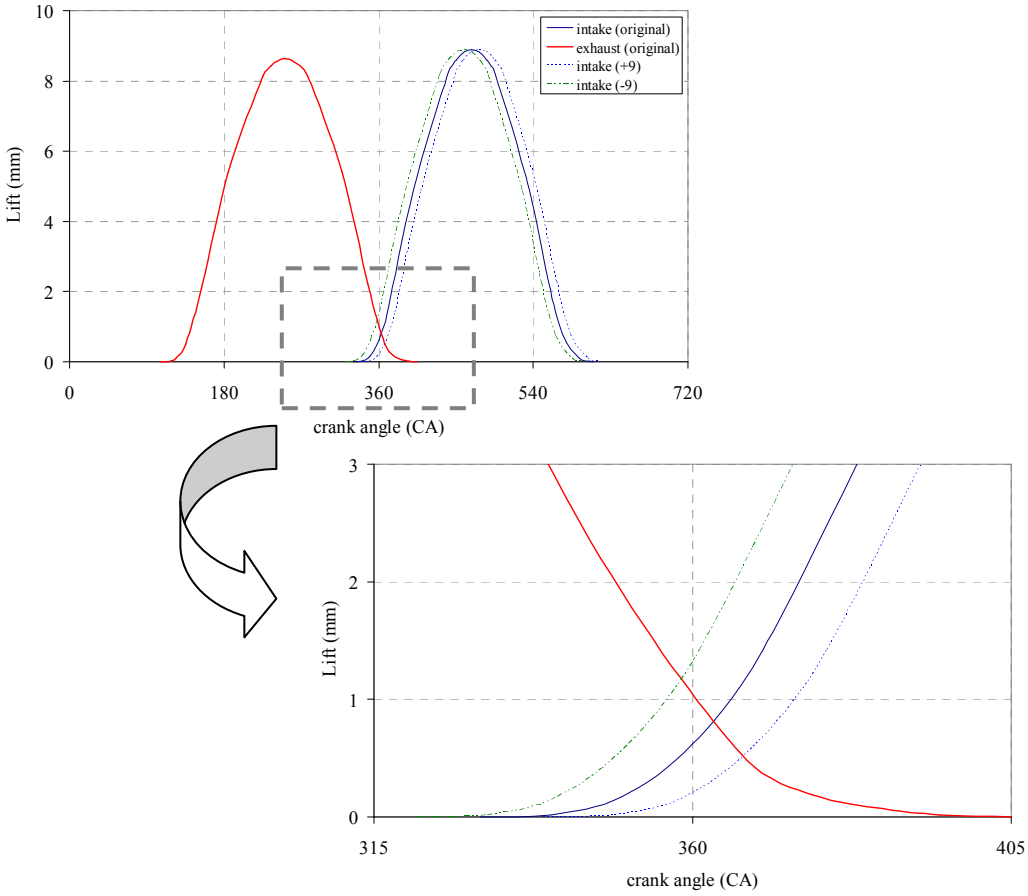

b) The valves lift profile from different intake camshaft positions show the overlap area near TDC increases with a retarded exhaust camshaft by 9 degrees (IVO 27 degrees ATDC) and reduces with a advanced angle of 9 degrees (IVO 9 degrees ATDC).

Figure 8-5: Intake valve profile with varying intake camshaft positions.

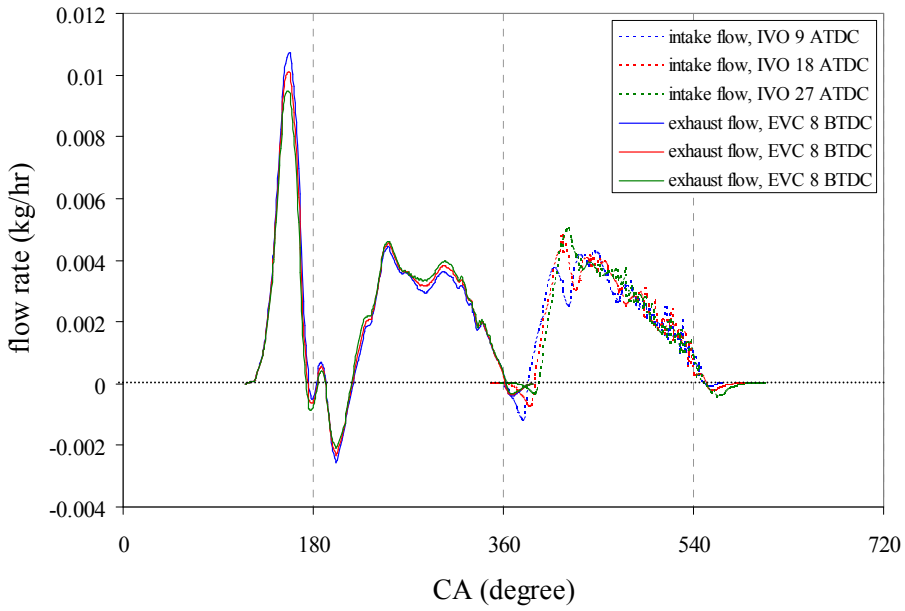

a) Inlet and exhaust gas flow under different intake camshaft positions

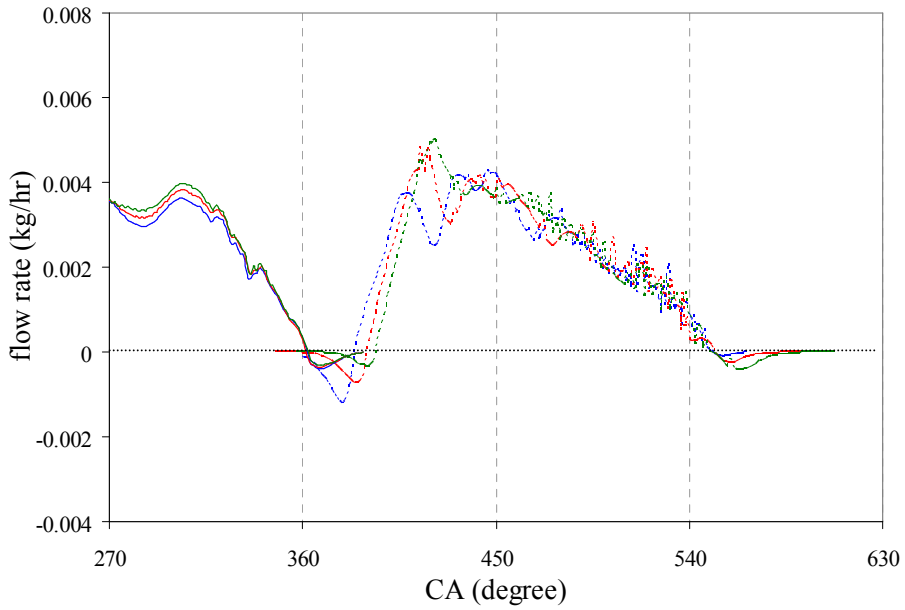

b) Intake flow from different intake camshaft positions.

Figure 8-6: Gases flows with different exhaust camshaft positions.

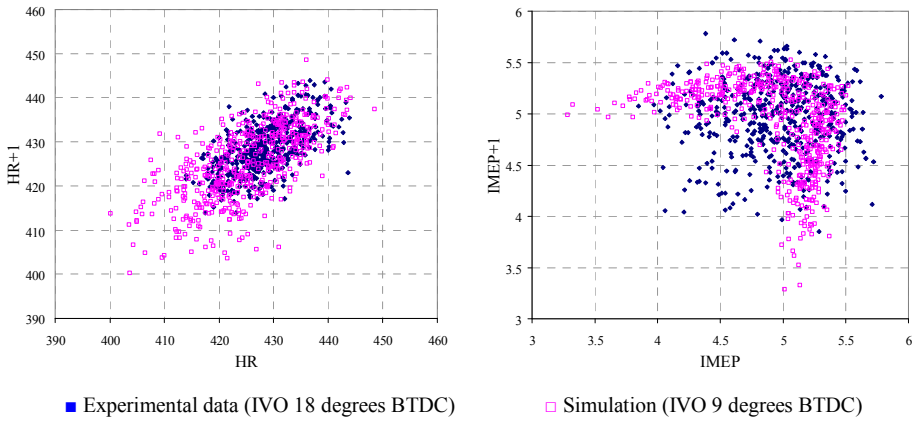

a) Advanced simulation of IVO by 9 degrees.

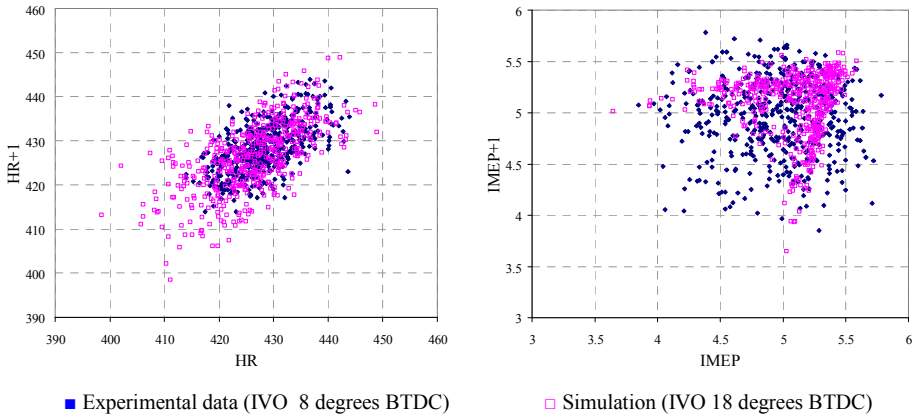

b) Reference IVO at the same position

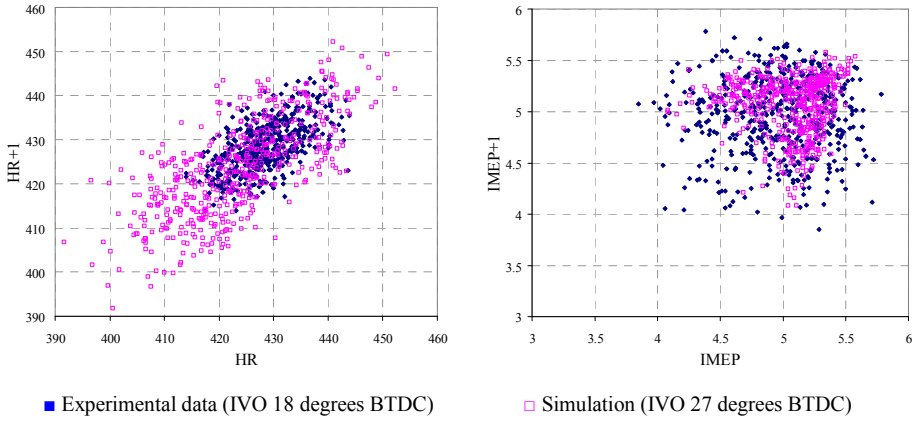

c) Retarded simulation of IVO by 9 degrees.

Figure 8-7: Comparison of the original net heat release and net IMEP data, from the experimental work of Test #1, with the simulation, under lean fuelling conditions, with different intake camshaft positions and EVC kept constant.

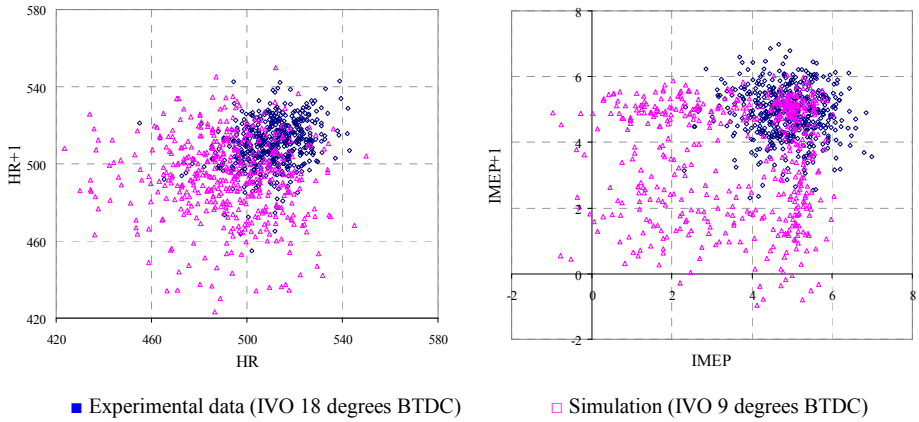

a) Advanced simulation of IVO by 9 degrees.

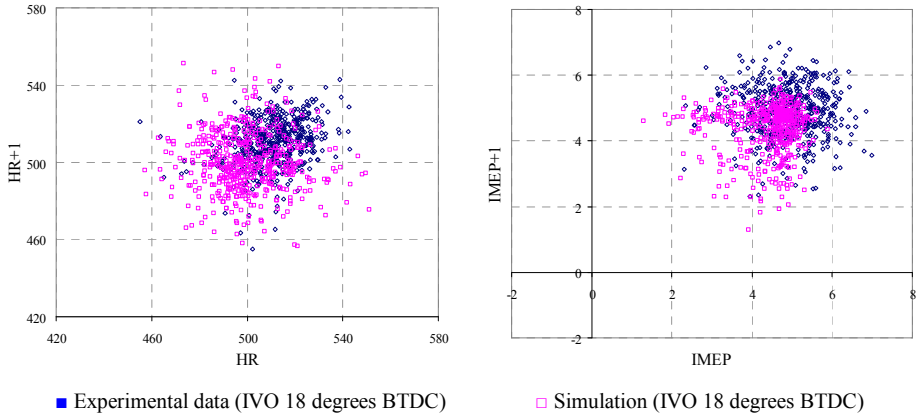

b) Reference IVO at the same position

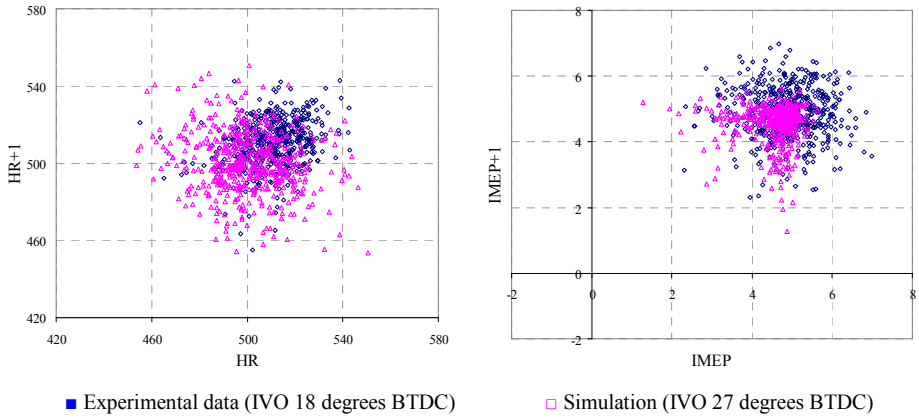

c) Retarded simulation of IVO by 9 degrees.

Figure 8-8: Comparison of the original net heat release and net IMEP data, from the experimental work of Test #3, with the simulation, under lean fuelling conditions, with different intake camshaft positions and EVC kept constant.

8.3 Discussion of camshaft optimisation position for engine smoothness

The mechanism of the camshaft position, as discussed previously, explains that high amounts of residual gases are caused by a retarded exhaust camshaft position or advanced intake camshaft position. The effects of residual gases on the Wiebe exponent, for rich and lean combustion, were different, as shown in Figure 8-9. Under rich fuelling, the limit of residual gases was 8.8%. While under lean combustion there were 8.0% of residual gases before the ignition delay started to increase rapidly and lead to long combustion durations.

The results for in-cylinder pressure, with different camshaft positions, were used to calculate heat release and IMEP for comparison and discussion. In order to compare the engine's smooth running, the COV_{imep} was calculated and plotted against the camshaft position in Figure 8-10. The residual gases from the simulation were plotted using a box plot in Figure 8-11 for additional explanation.

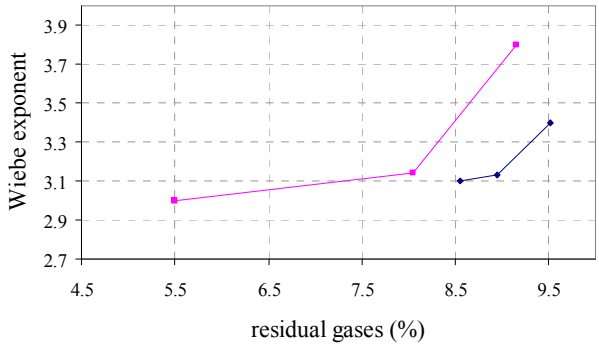

a) The Wiebe exponent shows that the variations in residual gases of rich combustion were less than those for lean combustion.

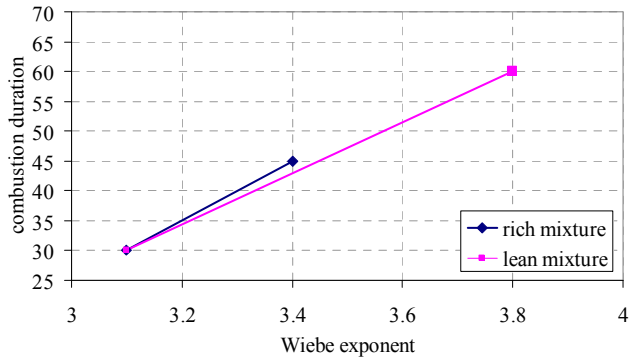

b) The combustion duration of lean combustions were a lot higher than for rich combustion.

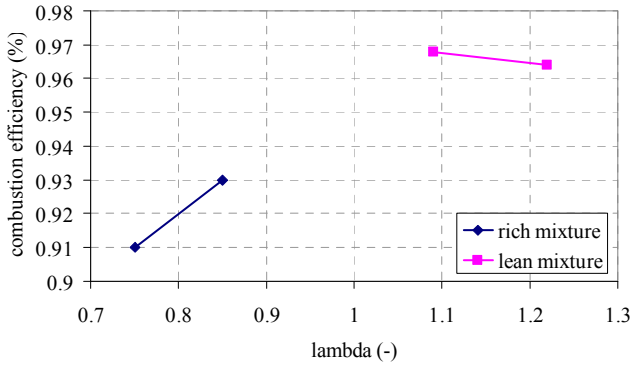

c) The combustion efficiency from rich and lean fuelling

Figure 8-9: A repeat of Figure 7-7 and Figure 7-12 showing a comparison of the look-up tables representing Wiebe exponent, combustion duration and combustion efficiency under both rich and lean conditions after modification

8.3.1 Discussion the effect of exhaust camshaft position on cyclic variability

Figure 8-10 shows the effect of exhaust camshaft positions on COV_{imep} and Figure 8-11 shows the variation in residual gases with different exhaust camshaft positions.

The original exhaust camshaft position, under rich combustion, shows that the COV_{imep}, of the selected period, is below 10% with an average residual gas amount greater than the limit boundary. Moreover, the range of the standard deviation was also above the limit boundary, but the COV_{imep} value was still low. The reason is that the width of the standard deviation is small, which results in less variation in the Wiebe exponent and a short combustion duration in the simulation. In contrast, the original exhaust camshaft position, under lean combustion, had COV_{imep} value of more than 10%. Analysis of the residual gases shows that some of the residual gases were lower than the limit but the maximum and minimum of the gases caused large variations in the Wiebe exponent. Those variations also contributed to long combustion durations and resulted in large variations in IMEP.

Under rich and lean combustion, a retarded exhaust camshaft position results in increased COV_{imep}, especially with lean combustion. The results suggested that the variations in residual gases increase when the exhaust valve closing angle was delayed, which agreed with the exhaust flow mechanism in the literature reviews chapter.

Considering the advanced exhaust camshaft position, the engine benefits from low residual gases because the overlap time was reduced. COV_{imep}, from rich and lean combustions, decreased to a minimum value when the exhaust camshaft was advanced by 4 degrees (EVC 12 degrees BTDC), and tended to be stable, although the camshaft was retarded by 8 degrees (EVC 16 degrees BTDC) from the original position. Residual gases, under rich combustion, had less variation, as can be seen in Figure 8-11. Under lean combustion, not only was standard deviation reduced but also the maximum and minimum residual gases were reduced too, which resulted in more stable combustion.

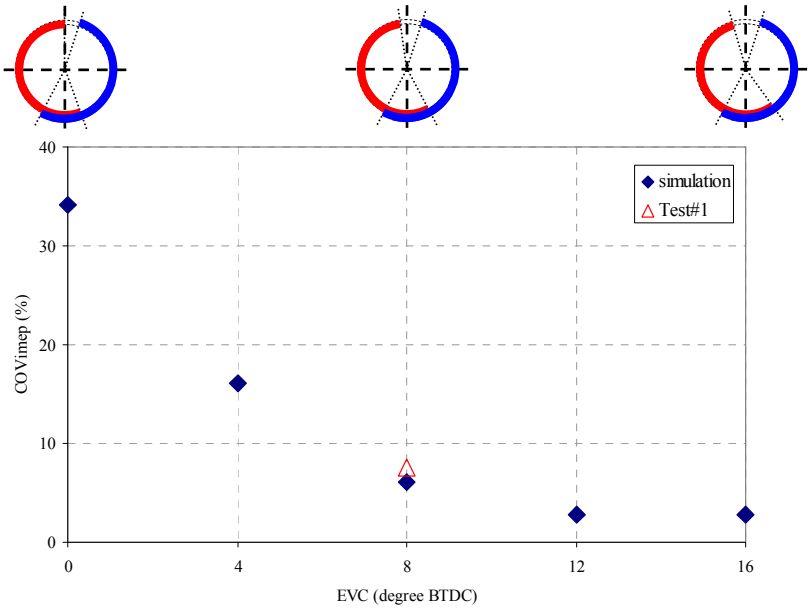

a) COV_{imep} of simulation under rich combustion

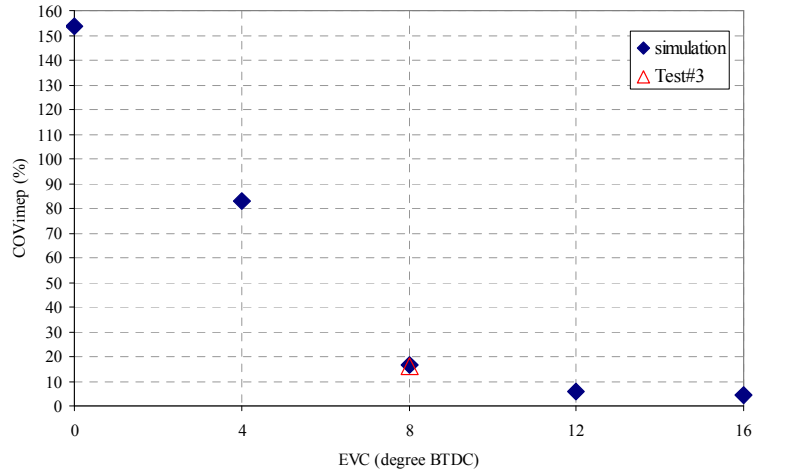

b) COV_{imep} of simulation under lean combustion

Figure 8-10: Comparison of simulated COV_{imep} from different exhaust camshaft positions, under rich and lean combustion conditions showing experimental data for comparison.

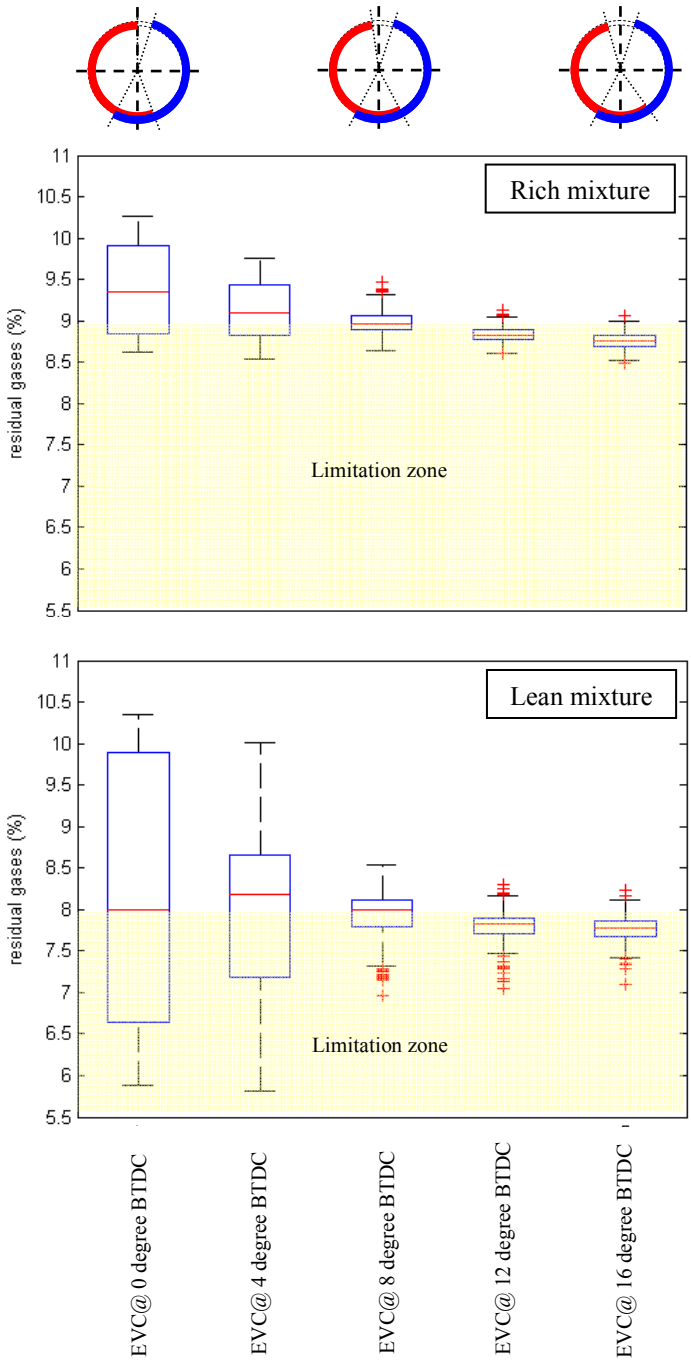

Figure 8-11: Box plot of residual gas fraction from simulation, under rich and lean combustion, with varying exhaust camshaft positions.

8.3.2 Discussion the effect of intake camshaft position on cyclic variability

The original intake camshaft position had been set to allow the intake valve to open at 18 degrees ATDC. A task in this research is to understand the impact on combustion stability from different intake camshaft positions. Thus, the intake camshaft position in the simulation was advanced by 9 degrees (IVO 9 degrees ATDC) and retarded by 9 and 18 degrees, which set IVO at 27 and 36 degrees ATDC respectively, in order to see the effect on COV_{imep}.

Figure 8-12 shows that the COV_{imep} under rich combustion increased when the intake camshaft position was advanced. This allowed the intake valve to open earlier and increased valve overlap, which meant that more residual gases were induced into the chamber. Figure 8-13 shows that the average of the residual gases was similar to that with the original camshaft position, but the variation in standard deviation increased, along with variations in the combustion profiles.

When using a retarded intake camshaft position, the intake valve opened ATDC and less residual gases were induced into the chamber by the flow mechanism. Rich combustion benefited from a retarded intake camshaft of 9 degrees (IVO 27 degrees ATDC) but started to increase when the camshaft was retarded by 18 degrees (IVO 36 degrees ATDC) from its standard setting. Under rich combustion, the experimentally measured air flow rate varied in a sinusoidal pattern, these boundary conditions were imposed on the simulation and so the quality of combustion also varied from cycle to cycle. In fact, the variation of intake air flow air and its effect on the dilution of residual gases is small enough to have no significant impact on combustion when running rich when the intake camshaft was retarded anything up to 18 degrees. Beyond this the increased residual begins to have an effect on total oxygen availability and with 27 degree retarded intake camshaft angle the high ratio of residual gases caused very high combustion variation. Under rich combustion, the air flow rate was kept constant and the combustion cycles were more stable than they were with a rich mixture coupled with variations in the air flow. However, retarding the intake camshaft by 18 degrees (IVO 36 degrees ATDC), under lean combustion operation, resulted in the variations in

residual gases decreasing slightly, although their mean value remained similar to those from the original camshaft setting.

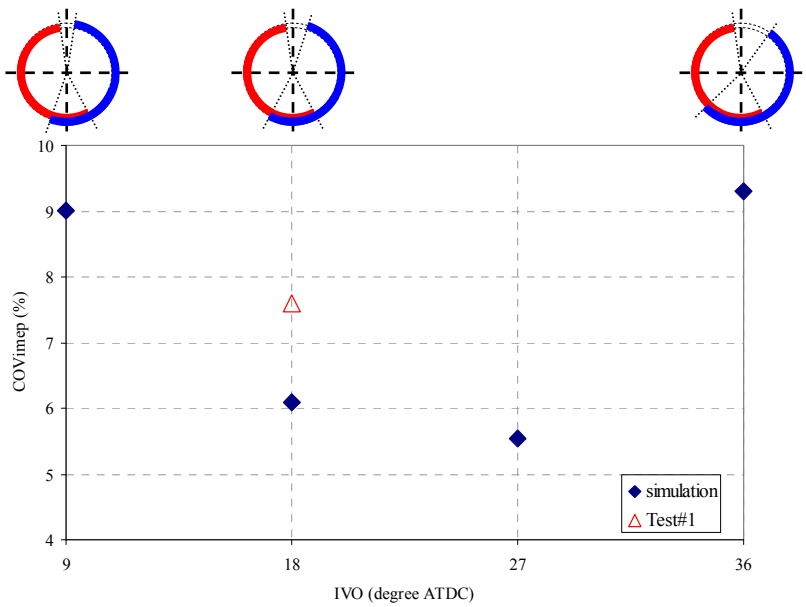

a) COV_{imep} *of simulation under rich combustion*

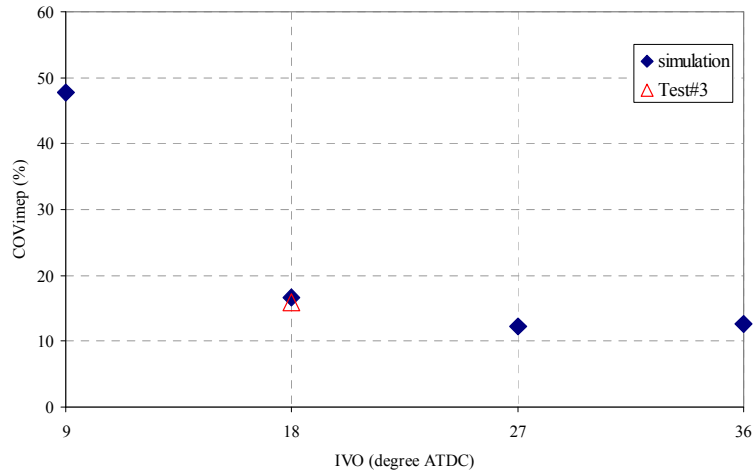

b) COV_{imep} *of simulation under lean combustion*

Figure 8-12: Comparison of simulated COV_{imep} with different intake camshaft positions under rich and lean combustion conditions showing experimental data for comparison.

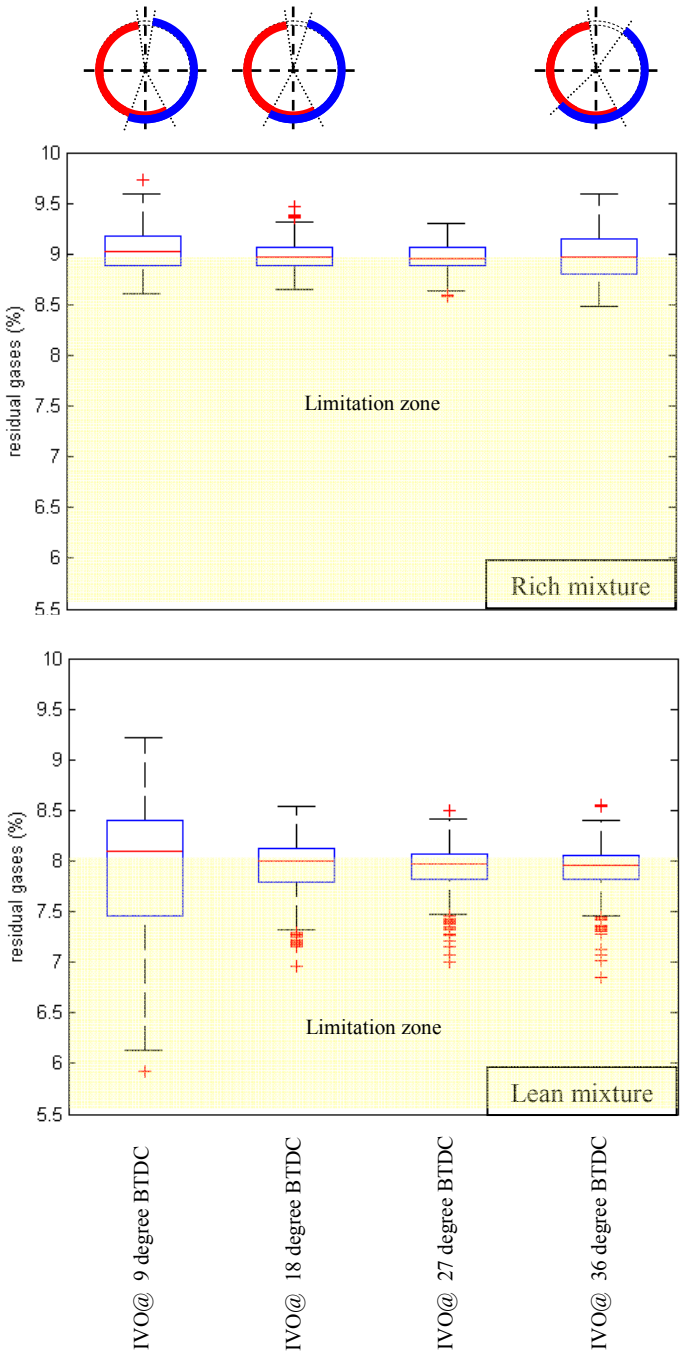

Figure 8-13: Box plot of residual gases from simulation of lean fuelling, with varying intake camshaft positions.

8.4 Conclusion

In this chapter, the engine simulation under rich and lean fuelling that were calibrated from Chapter 7 were used to predict variation of COV_{imep} with different camshaft position. Varying the camshaft position in the engine simulation will affect to pumping load (Jung et al., 2004) which require a recalibration of inputs such as air flow and fuel flow rates. These will result in different heat release and IMEP outputs. Due to the limitations of the experimental data available within this research, the optimisation has been based on a restricted number of operating points although the technique could readily be extended to cover a wider operating range.

8.4.1 Conclusion of optimising camshaft position during rich combustion

Although the rich combustion, from the experimental work, had a low COV_{imep} during the selected period, the study showed that retarding the exhaust camshaft position by 4 degrees (EVC 12 degrees BTDC) could reduce COV_{imep} by 62.3% (Figure 8-10a). However, a retarded exhaust camshaft, and hence valve timing, could cause an increase in the pumping load (Jung et al., 2004), thus the engine has to increase the amount of air and fuel to be burned. Therefore, the unburnt fuel fraction could increase which, in turn, increases the burning process in the exhaust manifold. Using the secondary air technique, increases the air flow rate to ensure the fuel can be burned. A lambda value of 1 will make the pre-catalytic converter temperature increase faster. Advancing the intake camshaft position by 9 degrees (IVO 27 degrees ATDC) can reduce COV_{imep} by 27.1% (Figure 8-11a). By varying intake camshaft position caused high pumping load more than by varying the exhaust camshaft position (Jung et al., 2004) and need more test results for validation which are not included in this research.

8.4.2 Conclusion of optimising camshaft position during lean combustion

The simulation of the engine under lean combustion is an extension of this study. The original camshaft position gives a COV_{imep} value higher than 10%. Retarding the exhaust camshaft position by 8 degrees (EVC 16 degrees BTDC) could reduce the

variation in combustion cycles by 71.5% (Figure 8-12a) and achieve a COV_{imep} value of less than 10%. The pumping load increased with retarded valve timing (Jung et al., 2004) but the pre-catalytic temperature will benefit from the increased load because the engine has to produce more energy which results in a higher temperature at the exhaust port. Considering the intake camshaft position, the minimum COV_{imep} reduced by 22.6% (Figure 8-12b) by advancing the camshaft by 9 degrees (IVO 27 degrees ATDC), but COV_{imep} was still higher than 10%. The pumping load was also increased too (Jung et al., 2004). These factors also lead to higher fuel consumption, which suggests that the original intake camshaft position is best, and only the exhaust camshaft should be adjusted, as discussed above.

Chapter 9

Conclusions and future work

The research in this thesis is focused understanding the cyclic variability of combustion under cold start conditions in a gasoline engine. the research had a large experimental component which was designed to gain on understanding of the effect of engine calibration on catalyst warm-up. The result showed that use secondary air could achieve high catalyst temperature but the COV_{imep} of the engine was higher than the accepted limited of 10%. Thus an engine simulation was used in this research in order to understanding the mechanism of cyclic variability in gasoline engine under rich and lean fuelling. In addition, a method for the optimisation of the calibration with reference to cyclic variability was introduced by varying camshaft timing within the simulation.

9.1 Conclusion

The research was achieved through a number of objectives and the concluding remarks are arranged around each of these objectives.

1) Conduct a review of previous research.

A review of previous research which related to the work in this research conducted. The reviews included the knowledge on cold start condition and the techniques of reducing emissions. Furthermore, the review of cyclic variability including causes and effects were conduced. Finally, the engine simulation was introduced. These reviews were used to explain the mechanism of combustion under cold start condition in this research and were used to construct an engine model to represent the real engine behaviour.

2) Carry out an experimental design to determine the influence of key calibration factors on the cold start.

- The *Box-Behnken design* was used to design as there are only a small number of studied factors. The 46 test points were generated by varying five interested parameters including engine speed, lambda, spark angle, load and rate of air which is pumped into the exhaust manifold by secondary air pumps.
- According to the technique of increasing exhaust temperature in this research, the pre-catalytic temperature increased up to 631.11°C while all emissions including NO_x, CO and HC emissions achieved their light-off temperature within 5.3, 11.9 and 17.2 seconds respectively. To obtain those results, the engine was operated under rich fuelling (Test #1) with lambda of 0.82, engine speed of 1228.29 rpm, 0.57 bar of load, spark was ignited at TDC and the secondary was pumped into exhaust manifold at 5.87 kg/hr.
- The available test data (include valid and invalid test data) were used to generated a pre-catalyst temperature prediction using the Matlab model based calibration toolbox (MBC). The studied methods for pre-catalytic temperature prediction suggested that RBF-multiquadric with 79 centres could perform adequately without over fitting giving a value 2.90% of RMSE and value 6.15% of press RMSE.
- According to the pre-catalytic model prediction, the results suggested that under rich conditions (Test #1), the temperature can be made to increase slightly higher and faster by increasing secondary air flow rate. In contrast, under lean fuelling, there are no benefits from secondary technique as the fresh air became cooling air when it was pumped in the exhaust manifold.
- With the secondary air technique, the air flow rates have to be just enough to cause the remaining fuel in the exhaust manifold to burn as observed by lambda value of 1 from measurement. If the flow rate is too high or too low, the emissions will increase and affect the pre-catalytic temperature.
- For cyclic variability, the experimental results suggest that the cyclic variability is not affected by secondary air flow rate in the exhaust manifold. Under rich fuelling, the variations are lower than lean fuelling and also give a benefit through high pre-catalytic temperature since the air was introduced. In the case

of retarded spark angle and increased engine speed, high exhaust port temperature was observed but the combustion variation also increases. The variation decreased when the engine load increases.

3) Construct an engine model using the Ricardo Wave engine simulation software in combination with Matlab Simulink.

- An engine model was created in Ricardo Wave by using the engine specification from the factory augmented by measurements of the intake and exhaust manifolds. Target of this research was to describe the mechanism of cyclic variability thus the combustion events have to be varied cycle by cycle. In order to control the individual combustion profiles, Wave has a limitation on varying combustion from cycle to cycle as the burn characteristics in Wave are fixed, therefore Matlab Simulink was introduces as a co-simulation. As a result, the combustion profiles can be manipulated from cycle to cycle.
- The literature review determined that the characteristic of combustion was controlled by air/fuel ratio and residual gas fraction. The alternative methods of combustion control with Wave were introduced. However, the method that was best suited to this research was to control by using mass fraction burn. The experimental data were analysed and look-up tables created to control combustion events based on those two parameters. Analysis was conducted into appropriate cylinder pressure smoothing methods, pressure pegging, real top dead centre determination and gamma value estimates.

4) Describe some of the key mechanisms causing variation in SI engines by using the Wave and Simulink modelling environments.

- The experimental data that were used to generate look-up tables, for the combustion efficiency from rich and lean combustion, follows the theory of combustion efficiency described in the literature which is based on the lambda value.

- Under rich combustion, the mass of air in the mixture is an important factor that controls combustion. Thus, the air flow rates from the experiment work were used as an input to the co-simulation.
- The engine runs under 2 modes during pre-catalytic heating period including after start and pre-catalytic heating mode. In the first mode, the engine increases air and fuel flow rate automatically which produce high emission because the mixtures have to be rich enough to ensure the combustion process. The second mode is pre-catalytic heating which was extended to 120 seconds. For the engine simulation in this research, the first mode was ignored because the data was unstable and need more sensors to measured information. In order to start the simulation, the stable period was selected which include cycles 700 to 1200.

5) Calibrate the engine model to a level where it is capable of representing cyclic variability in a similar manner to a real engine.

- The result of heat release under rich operation shows a similar pattern to the experimental data while the pattern under lean fuelling is difficult to predict. Overall, predicted IMEP of rich and lean operations are under predicted giving an error of approximately 0.49% and 2.07% respectively and have normally distributed residuals. These results suggest that cyclic variability of combustion can be simulated by using information describing the effect of air/fuel and residual gas fraction to control combustion characteristics
- According to the results of the simulation, residual gas fractions have a limiting value under both rich and lean mixtures. If the residual gas fractions are higher than the limit of 8.8% (under rich fuelling) or 8.0% (under lean fuelling), the ignition delay will increase significantly as can be seen in Figure 8-9a. Those results in long combustion duration (Figure 8-9b) and contribute to high cyclic variability.
- The cyclic variability of the engine, under rich mixture fuelling, is predictable to some degree. Whilst under lean mixture fuelling, the combustion cycles are less predictable, but the mechanisms of combustion are understandable.

6) Use the simulation to attempt a calibration task with represented to cyclic variability

- A calibration study was conducted to explore the use of the engine model to allow decisions regarding engine calibration to be taken with the benefit of some insight into cyclic variability effects. In order to minimise the cyclic variability of the combustion of the engine, the simulation suggests that varying the exhaust valve timing by 4 degrees (EVC 12 degrees BTDC) can reduce variation better than varying the inlet valve timing. This is because the exhaust valve timing has a direct effect on residual gases and has less effect on pumping losses.

9.2 Future work

The methods explored in this research could be improved to obtain better results. Moreover, the benefits of this research can be used to assist with the development of production engines. The details of future work are discussed below.

9.2.1 Experimental work

Design of test points

The pre-catalyst temperature models that were generated by the design test point of *Box-Behnken designs* are subject to error since only 2 levels of each calibration parameter were tested. For further work, a design that provides more than 2 levels for each parameter (when the other parameters were kept constant) could be considered as the results will give an improved accuracy of the predicted model including a better representation of interactions between parameters and better representation of highly non-linear effects.

Lambda sensors

The engine tests performed in this research used only one lambda sensor. The lambda sensor was located near the catalytic converter which was used to represent the engine overall lambda value. As the results, the errors of lambda values were presented because the gases had to move along a distance before reach the sensor. Therefore, individual lambda sensors, installed near the exhaust port of each cylinder, would provide more detailed information which could eliminate all the error and can be used to represent in-cylinder lambda.

Fuel flow sensors

The engine has four fuel injectors, but the injection rate, used in the analysis, came from the average fuel flow. The results of heat release, from each cylinder, shows that the injectors may inject fuel at slightly different rates for each cylinder. Testing could be improved by installing a measurement unit that can give information of fuel that has been injected into each cylinder or measure the fuel that has been injected per cycle. This could be achieved by monitoring injection operating times and developing a model to relate these to mass of fuel injected.

Fuel injection timing

Fuel injection timing is important information for an engine simulation. According to the experimental results, each cylinder shows different heat release distributions which could be related to the fuel injection timing. In order to obtain more accurate results, the sensor that can gives the information of injection time need to be installed. Again this could be achieved by monitoring injector operating time.

Dynamometer response time

According to the method for setting torque, the results for engine torque readings show that the dynamometer has a slow response. The engine ECU is also involved in the control system which is trying to achieve the required load and may be contributing to the variations in torque. This could be improved by developing a more efficient response of either the dynamometer or the ECU.

Ion current sensors

According to the literature review, ion current sensors have a capability to measure activity around the start of combustion. Therefore, understanding of the signal from an ion current sensor could be useful for the prediction of start of combustion.

In-cylinder gas fraction measurement

According to the cause of cyclic variability, air/fuel ratios residual gas fractions are the factor control combustion. In order to determine trapped air/fuel ratio and residual gas fraction, fast emission analysers would need to be combined with a gas sampling valve to measure in-cylinder gas composition.

9.2.2 Engine simulation

Calibration of engine model

Not all of the critical parameters describing the engine were available. Therefore some parameters such as co-efficient of flow past intake and exhaust valves and friction in the manifold came from the default setting of the software. These parameters should be determined in order to obtain a more precise result. However, the general behaviour of the engine is well represented even with these assumptions.

Control combustion separately for each cylinder

The model has access to limited information for building the look-up table for controlling combustion. The different results for heat release show that each cylinder has a different combustion characteristic. In addition, the lengths of the intake manifolds from throttle valve to each cylinder are not equal. The variation in lengths causes variations in the manifold pressure oscillations and contributes to variations in the air flow. This could be accounted by calibrating a set of look-up tables for each cylinder once cycle specific data were available.

Look-up table modification

The look-up tables that have been created for the co-simulation, in this research, can only give an approximation of the relationship between the input and output variables. A simple linear relationship was used in the research. In order to obtain more accurate results, the look-up tables require more data points, to which, for example, a higher order polynomial could be fitted to establish a more accurate model.

Extending the simulation period

In this research, the simulation time was selected from a stable period of operating in the experimental study. Potentially, an extension of the simulation period to cover the whole test period could be achieved by calibrating the engine model under unstable zone that was observed when the after-start condition finished. These periods need more data on air flow and fuel flow for further analysis. Also, the peak in-cylinder pressure in simulation would need to be re-calibrated based on air flow rate to obtain a more precise result.

9.2.3 Real time simulation

Real time simulation is the next step for the validation of the engine model. Under rich combustion, the air flow rate, crank angle and spark angle from engine have to be fed in to the engine model as input signals. Under lean combustion, the crank angle and spark angle can be used as inputs to the engine model. By running the engine and the engine model in parallel, the result of net heat release and IMEP calculation have to be compared for modification of the look-up tables. The next step is to study an optimisation of cyclic variability that could either vary camshaft angle or create a control algorithm for the engine during cold start condition. For example, if a poor combustion event were expected the spark angle could be advanced or the fuel flow increased to mitigate this effect.

References

Adomeit, P., Lang, O., Pischinger, S., Aymanns, R., Graf, M., and Stapf, G., "*Analysis of Cyclic Fluctuations of Charge Motion and Mixture Formation in a DISI Engine in Stratified Operation*", 2007-01-1412, SAE, 2007

Aleiferis, P.G., Taylor, A.M.K.P., Whitelaw, J.H., Ishii, K., and Urata, Y., "*Cyclic Variations of Initial Flame Kernel Growth in a Honda VTEC-E Lean-Burn Spark-Ignition Engine*", 2000-01-1207, SAE, 2000

Aleiferis, P.G., Taylor, A.M.K.P., Ishii, K. and Urata, Y., "*The relative effects of fuel concentration, residual-gas fraction, gas motion, spark energy and heat losses to the electrodes on flame-kernel development in a lean burn spark ignition engine*", IMechE Part D, Vol 218, p. 411-425, 2004

Bai, C. and Gosman, A.D., "*Development of Methodology for Spray Impingment Simulation*", 950283, SAE, 1995

Bannister, C.D., Brace, C.J., Taylor, J., Brooks, T. and Fraser, N., "*An empirical approach to predicting heat transfer within single- and twin-skin automotive exhaust systems*", IMechE Part D, Journal of Automotive Engineering, Vol 225, p. 913-929, 2011

Bannister, C.D., Taylor, J. and Brooks, T., *"Exhaust Line Thermal Model for Prediction of Catalyst Inlet Gas Temperature"*, Mahle Powertrain, 2007

Batteh J.J. and Curtis, E.W., "*Modeling Transient Fuel Effects with Variable Cam Timing*", 2003-01-3126, SAE, 2003

Batteh, J.J. and Eric W. Curtis, E.W., "*Modeling Transient Fuel Effects with Alternative Fuels*", 2005-01-1127, SAE, 2005

Bonatesta, F. and Shayler, P.J., *"Factors influencing the burn rate characteristics of a spark ignition engine with variable valve timing"*, IMechE Part D, Vol 222, p. 2147-2158, 2008

Borland, M. and Zhao, F., "Application of Secondary Air Injection for Simultaneously Reducing Converter-In Emissions and Improving Catalyst Light-Off Performance", 2002-01-2803, SAE, 2002

Chen, R., Milovanovic, N.,Turner, J. and Blundell, D., *"The Thermal Effect of Internal Exhaust Gas Recirculation on Controlled Auto Ignition",* 2003-01-0751, SAE, 2003

Cheng, Y., Wang, J.X., Zhuang, R.J. and Wu, N., "*Analysis of Combustion Beheaviour During Cold-Start and Warm-Up Process of SI Gasoline Engine*", 2001-01-3557, SAE, 2001

Dai, W., Trigui, N., and Lu, Y., "*Modeling of cyclic Variations in Spark-Ignition Engines*", 2000-01-2036, SAE, 2000

Daw, C.S., Finney, C.E.A., Green, J.B., Kennel, M.B., Thomas, J.F. and Connolly, F.T., *"A Simple Model for Cyclic Variations in a Spark-Ignition Engine*", 962086, SAE, 1996

Eriksson, L., *"Spark Advance Modelling and Control",* Dissertations No.580, Linköping University, Sweden, 1999

Fox, J.W., Cheng, W.K. and Heywood, J.B., "*A Model for Predicting Residual Gas Fraction in Spark-Ignition Engines*", 931025, SAE, 1993

Ghauri,A., Richardson, S.H. and Nightingale C.J.E.,"*Variation of Both Symmetric and Asymmetric Valve Events on a 4-Valve SI Engine and the Effects on Emissions and Fuel Economy*", 2000-01-1222, SAE, 2000

Jeong, S.J. and Kim, W.S., "*A Numerical Approach to Investigate Transient Thermal and Conversion Characteristics of Automotive Catalytic Converter*", 980881, SAE, 1998

Jung, H.H., Stein, R.A. and Leone, T.G., "*Comparison of Dual Retard VCT to Continuously Variable Event Valvetrain*", 2004-01-1268, SAE, 2004

Kramer, U. and Phlips, P. "*Phasing Strategy for an Engine with Twin Variable Cam Timing*", 2002-01-1101, SAE, 2002

Kulzer, A., Lejsek, D., Kiefer, A. and Hettinger, A., "*Pressure Trace Analysis Methods to Analyze Combustion Features and Cyclic Variability of Different Gasoline Combustion Concepts*", 2009-01-0501, SAE, 2009

Lapuerta, M., Armas, O., and Molina, S., *"Study of the compression cycle of a reciprocating engine through the polytropic coefficient"*, Applied Thermal Engineering, volume 23*,* 2003, p. 313-323

Lee, T., Bae, C., Bohac, S.V. and Assanis, D.N., "*Estimation of Air Fuel Ratio of a SI Engine from Exhaust Gas Temperature at Cold Start Condition*", 2002-01-1667, SAE, 2002

Leroy, T., Alix, G., Chauvin, J., Duparchy, A., and Le Berr, F.L., "*Modeling Fresh Air Charge and Residual Gas Fraction on a Dual Independent Variable Valve Timing SI Engine*", 2008-01-0983, SAE, 2008

Lindström, F., Ångström, H.E., Kalghatgi, G. and Möller, C.E., "*An Empirical SI Combustion Model Using Laminar Burning Velocity Correlations*", 2005-01-0204, SAE, 2005

Maftouni, N., Ebrahimi, R. and Siamac Hossein. S., "*The effect of Intake Manifold Runners Length on the Volumetric Efficiency by 3-D CFD Model*", 2006-32-0118, SAE, 2006

Maloney, P.J., "*Embedded Torque Estimator for Diesel Engine Control Application*", 2004-01-1371, SAE, 2004

Miller, J.M., "*Propulsion Systems for Hybrid Vehicles*", 2nd edition, Institution of Engineering and Technology, 2010

Moon, S., Choi, J., Abo-Serie, E. and Bae, C., "*The Effects of Injector Temperature on Spray and Combustion Characteristics in a Single Cylinder DISI Engine*", 2005-01-0101, SAE, 2005

Ozdor, N., Dulger, M. and Sher, E., "*Cyclic Variability in Spark Ignition Engines: A Literature Survey*", 940987, SAE, 1994

Peron, L., Charlet, A., Higelin, P., Moreau, B. and Burq, J.F., *"Limitations of Ionization Current Sensors and Comparison with Cylinder Pressure Sensors",* 2000-01-2830, SAE, 2000

Pfalzgraf, B., Fitzen, M., Siebler, J., and Erdmann, H.D., *"First ULEV Turbo Gasoline Engine – The Audi 1.8L 125kW 5-valve Turbo",* 2001-01-1350, SAE, 2001

Pipitone, E., Beccari, A., and Beccari, S., "*Reliable TDC Position Determination: a Comparison of Different Thermodynamic Methods Through Experimental Data and Simulations*", 2008-36-0059, SAE, 2008

Prucka, R.G., Filipi, Z.S., Assanis, D.N., Kramer, D.M., and Gregory L. Ohl, G.L., "*An Evaluation of Residual Gas Fraction Measurement Techniques in a High Degree of Freedom Spark Ignition Engine*", 2008-01-0094, SAE, 2008

Randplph, A.L., "*Methods of Processing Cylinder-Pressure Transducer Signals to Maximize Data Accuracy*", 900170, SAE, 1990

Rousseau, S., Lemoult, B. and Tazerout, M., "Combustion characterization of the natural gas in lean burn spark-ignition engine", IMechE., 1999, p. 481-489

Russ, S., Lavoie, G., and Dai, W., "*SI Engine Operation with Retarded Ignition: Part 1 – Cyclic Variations*", 1999-01-3506, SAE, 1999

Scharrer, O., Heinrich, C., Heinrich, M., Gebhard, P. and Pucher, H., "*Predictive Engine Part Load Modeling for the Development of a Double Variable Cam Phasing (DVCP) Strategy*", 2004-01-0614, SAE, 2004

Scholl, D. and Russ, S., "*Air-Fuel Ratio Dependence of Random and Deterministic Cyclic Variability in a Spark-Ignited Engine*", 1999-01-3513, SAE, 1999

Schwarz, F. and Spicher, U., "*Determination of Residual Gas Fraction in IC Engines*", 2003-01-3148, SAE, 2003

Sendilvelan, S., Jeyachandran, K. and Bhaskar, K., "*Thermal Analysis of Electrically Heated Catalyst to reduce Cold Start Emission from Gasoline engine*", 2001-01-1845, SAE, 2001

Shayler, P.J., Winborn, L. D., Hill, M. J. and Eade, D., "*The Influence of Gas/Fuel Ratio on Combustion Stability and Misfire Limits of Spark Ignition Engines*", 2000-01-1208, SAE, 2000

Shayler, P.J., Wing-Cheung Lai, W.C., Brown, N. and Harbor, N., "*Limits on Charge Dilution, Fuel and Air Proportions for Stable Combustion in Spark Ignition Engines*", 2004-01-1533, SAE, 2004

Soltau, J.P., "*Cylinder Pressure Variations in Petrol Engines*", I.Mech.E., 1960, p. 96-116

Sung, N.W., Song, J.W., Jeong, Y., and Kim, C.S., "*Flow Modeling for the Branched Intake Monifold Engine*", 960079, SAE, 1996

Taraza, D., "*A Faster Algorithm for the Calculation of the IMEP*", 2000-01-2916, SAE, 2000

Tily, R., "*The application of sonification and time series analysis to cyclic variability in internal combustion engines*", PhD Thesis, University of Bath, Bath, UK, 2009

Tily, R. and Brace, C.J., "*Cyclic combustion variability in gasoline engines*", Institution of Mechanical Engineers: Combustion Engines and Fuels Group - Internal Combustion Engines: Performance, Fuel Economy and Emissions, 2008, p. 111-120

Tinaut, F.V., Gimenez, B., Horrillo, A.J. and Cabaco, G., "*Use of multizone combustion models to analyze and predict the effect of cyclic variations on SI engines*", 2000-01-0961, SAE, 2000

Upadhyay, D., and Rizzoni, G., *"AFR Control on a Single Cylinder Engine Using the Ionization Current*", 980203, SAE, 1998

Wang, Y., and Zhou, L., "*Investigation of the detection of knock and misfire of a spark ignition engine with the ionic current method*", IMechE Part D, Vol 217, p. 617-621, 2003

Wilstermann, H., Greiner A., Hohner, P., Kemmler, R., Maly, R.R. and Schenk, J., *"Ignition System Integrated AC Ion Current Sensing for Robust and Reliable Online Engine Control",* 2000-01-0553, SAE, 2000

Zhong, L., Henein, N.A. and Bryzik, W., "*Effect of Smoothing the Pressure Trace on the Interpretation of Experimental Data for Combustion in Diesel Engines*", 2004-01-0931, SAE, 2004

Bibliography

Bedford, J., Brereton, G., Schock, H. and Herrin, R., "*Measurements of Cycle to Cycle Variability of the Inlet Flow of Fuel Injectors Using LDA*", 2006-01-3314, SAE, 2006

Bauer, H., "*Automotive Handbook*", Stuttgart, Bosch, 2000

Bird, R. B. Stewart, W. E. and Lightfoot, E. N., "*Transport Phenomena*," 2nd edition, Wiley, 2002

Cho, H., Lee, J. and Lee, K., *"Measurements of cycle resolved air/fuel ratio near the spark plug in a spark ignition engine***",** I.Mech.E., 2000, p. 421-434

Choi, K.J. and Lee, H. J. *"Experimental Study on the Dynamics and Evaporation of Tandem Liquid Droplets in a Hot Gas Flow*", International Journal of Heat and Mass Transfer, Vol. 35, pp. 2921-2929, 1992

Davis, P.W. and Peckham, M.S., *"Measurement of Cycle-by-Cycle AFR using a Fast Response NDIR Analyzer for Cold Start Fuelling Calibration Applications"*, 2006-01-1515, SAE, 2006

Davis, P.W. and Peckham, M.S., *"Cycle-by-Cycle Gasoline Engine Cold Start Measurement of Residual Gas and AFR Using a Fast Response CO&CO_2 Analyzer"*, 2008-01-1649, SAE, 2008

Ferguson, C.R. and Kirkpatrick, A.T., "*Internal Combustion Engines: Applied Thermosciences*", 2nd Edition, John Wiley & Sons, 2000

Förster, J., Günther, A., Ketterer, M. and Wald, K.J., *"Ion Current Sensing for Spark Ignition Engines"*, 1999-01-0204, SAE, 1999

Gazis, A., Panousakis, D., Chen, R. and Chen, W.H., "*Computationally inexpensive methods of ion current signal manipulation for predicting the characteristics of engine in-cylinder pressure*", International Journal of Engine Research, volume 7, p. 271-282, 2006

Heywood, J. B., "*Internal Combustion Engine Fundamentals*", McGraw-Hill, 1988

Holub, A., and Jie Liu, J., ***"****Recognizing Combustion Variability for Control of Gasoline Engine Exhaust Gas Recirculation using Information from the Ion Current"***,** Master's degree project report, 2005

Maloney, P.J., "*Embedded Torque Estimator for Diesel Engine Control Application*", 2004-01-1371, SAE, 2004

Matlab, Matlab version 7.7.0.471 (R2008b), September, 2008

Pulkrabek, W.W., "*Engineering Fundamental of Internal Combustion Engine*", Prentice-Hall, Inc., 1997

Ricardo Wave Help, WaveBuild 7.2 Build 16, 2006

Sendilvelan, S., Jeyachandran, K. and Bhaskar, K., "*Thermal Analysis of Electrically Heated Catalyst to reduce Cold Start Emission from Gasoline engine*", 2001-01-1845, SAE, 2001

Shayler, P.J., and Alger, L., "*Experimental Investigations of Intake and Exhaust Valve Timing Effects on Charge Dilution by Residuals, Fuel Consumption and Emission at Part Load*", 2007-01-0478, SAE, 2007

Shigarkanthi, V.M., Porpatham, E. and Ramesh, A., *"Experimental Investigation and Modeling of Cycle by Cycle Variations in a Gas Fuelled S.I. Engine"*, 2005-01-3480, SAE, 2005

Simmonds, S.M., Bassett, M.D., Blaxill, H. and Schneider, F., "*Study of fuel economy improvements available vai valvetrain optimization of a SOHC engine with fully independent inlet and exhaust cam timing control*", Internal Combustion Engines : Performance, Fuel Economy and Emissions Conference, 11-12 December 2007, session 3 – Gasoline, IMechE, London

Stone, R., "*Introduction to Internal Combustion Engines"*, 3rd Edition, Macmillan Press Ltd., 1999

Taylor, C.F., "*The Internal Combustion Engine in Theory and Practice, Volume 1: Thermodynamics, fluid flow, performance*", Revised Edition, U.S.A., The M.I.T. Press, 1985

Taylor, C.F., "*The Internal Combustion Engine in Theory and Practice, Volume 2: Combustion, Fuels, Materials, Design*", Revised Edition, U.S.A., The M.I.T. Press, 1985

Tomoda, T., Kawauchi, M., Kubota, M., Nomura, Y. and Senda, J., "*Modeling of Wall Impinging Behavior with a Fan Shaped Spray*", 2003-01-1841, SAE, 2003

Ozdor, N., Dulger, M. and Sher, E., *"An Experimental Study of the Cyclic Variability in Spark Ignition Engines",* 960611, SAE, 1996

Winterbone, D.E. and Pearson, R.J., "*Theory of Engine Manifold Design, Wave action method for IC engines*", Professional Engineering Publishing Limited, 2000